2006-11-20

A New Spectroscopic Method for the Non-Destructive Characterization of Weathering Damage in Plastics

Andrew Robert George
Brigham Young University - Provo

A NEW SPECTROSCOPIC METHOD FOR THE NON-DESTRUCTIVE CHARACTERIZATION OF WEATHERING DAMAGE IN PLASTICS

by

Andrew R. George

A thesis submitted to the faculty of

Brigham Young University

in partial fulfillment of the requirements for the degree of

Master of Science

School of Technology

Brigham Young University

December 2006

BRIGHAM YOUNG UNIVERSITY

GRADUATE COMMITTEE APPROVAL

of a thesis submitted by

Andrew R. George

This thesis has been read by each member of the following graduate committee and by majority vote has been found to be satisfactory.

Date	A. Brent Strong, Chair
Date	Val D. Hawks
Date	Kent Kohkonen

BRIGHAM YOUNG UNIVERSITY

As chair of the candidate's graduate committee, I have read the thesis of Andrew R. George in its final form and have found that (1) its format, citations, and bibliographical style are consistent and acceptable and fulfill university and department style requirements; (2) its illustrative materials including figures, tables, and charts are in place; and (3) the final manuscript is satisfactory to the graduate committee and is ready for submission to the university library.

Date

A. Brent Strong
Chair, Graduate Committee

Accepted for the School

Val D. Hawks
Director, School of Technology

Accepted for the College

Alan R. Parkinson
Dean, Ira A. Fulton College of Engineering and Technology

ABSTRACT

A NEW SPECTROSCOPIC METHOD FOR THE NON-DESTRUCTIVE CHARACTERIZATION OF WEATHERING DAMAGE IN PLASTICS

Andrew R. George

School of Technology

Master of Science

The weathering of plastics and composites is a problem because of the loss of both physical and mechanical properties that it causes in these materials. But this weathering effect has been difficult, and in some cases, impossible to characterize without the destruction of the plastic or composite part. Clearly a rapid, reliable, and non-destructive test for the extent of the weathering damage is critically needed.

A recent problem that arose at Superyacht Solutions, a boat repair company in Australia, required a solution to just this problem. Such a test was developed for Superyacht Solutions, and is being applied across a wide range of plastic materials. The chemical foundation upon which this solution rests is also being confirmed.

The Superyacht Solutions problem was that a boat was brought in for repair which was yellowing dramatically. Surface erosion was confirmed by scanning electron microscope (SEM) surface studies. A loss of mechanical properties was also suspected. A new spectroscopic method of analysis was developed that not only identified the problem as extensive oxidation, but was able to quantify the extent of damage that occurred through a non-destructive technique. This method has also been applied to other plastics with encouraging initial results. The method used and its theoretical basis are included in this thesis.

ACKNOWLEDGMENTS

I wish to express my sincere gratitude to Dr. Brent Strong, who has been my mentor in all things related to my education since I first met him. He has provided me with so many opportunities for education and personal growth through research and teaching, that I owe a significant portion of my character to his mentorship, and consider him as a guiding influence for the rest of my life.

I would also like to express my appreciation to the other members of my committee, Val Hawks and Kent Kohkonen, who have been so patient with me and willing to help. I am grateful to Jonathan Zari and Suvud Udtamadilok, of the City of Los Angeles Sanitation Engineering Department, for their constant support and willingness to share the fruits of their research, thus saving me the task of considerable time of experimentation that I would have had to do myself. I am also grateful to Phillip Swindler, of Mity-Lite, for his sponsorship of this research and willingness to share even somewhat-proprietary information to assist in this study.

I am most grateful to my wife, Jennifer, for her confidence in me, her much-needed support, and her patience with her new husband throughout the writing of this paper. I am equally grateful to my Heavenly Father who is the source of all my talents and whose blessings were continually requisite to the accomplishment of this study.

TABLE OF CONTENTS

LIST OF TABLES

LIST OF FIGURES

1 Introduction

Almost all products made from plastics are meant to be of service in our oxygen-rich atmosphere. With time, the mechanical integrity of any plastic will slowly degrade if exposed to the air we breathe (Hrdlovic 2000). This mechanical degradation process, called oxidation, comes from various chemical reactions between the polymer itself and the atmosphere's oxygen.

Some environments, such as exposure to oxidizing chemicals (chemical-induced oxidation) or sunlight (photooxidation), accelerate the oxidation process in plastics. The physical manifestations of this degradation include loss of transmissivity and discoloration, loss of mechanical and thermal properties, especially embrittlement and crazing, and evolution of gaseous by-products (Strong 2006). Loss of transmissivity will result in a lowering of the efficiency of a collector or drier window, or the clouding of a lit-sign. Crazing or embrittlement will render the plastic more prone to damage by wind and rain or any other force. This is due to the accompanying decrease in elongation-to-break, flexural strength, and other mechanical properties (Schoolenberg 1988a).

Much research has been done to study the mechanisms behind oxidative degradation and which materials are more resistant to oxidation (Hrdlovic 2000; Gijsman, Meijers and Vitarelli 1999; Lemaire and others, 1996; O'Donnell, White and Holding 1994). Many additives have been developed to combat oxidation (Bataillard, Evangelista

and Thomas 2001; Scoponi, Cimmino and Kaci 2000). We can comparatively and generally say which materials work better, and which anti-oxidant additives are better, but the comparisons are not defined well and oxidation rate predictions are rare. There's too much guesswork involved in predicting the lifetime of storage tanks, pipes, structural parts, etc., when exposed to either the sun or strong oxidizing chemicals (Strong 2002).

Part of this problem is that there is no standardized method to quantify the degree of oxidation in a material. Recently, a boat repair company approached Brigham Young University (BYU) with a problem. Their client had purchased a boat, which began to lose its white, glossy sheen within less than a year's time after the purchase. The boat manufacturer claimed that the yellowing was normal and only required cleaning to restore it to white. The boat-repair company guessed that it was actually an oxidation problem (it was non-cleanable), but had no way to measure the oxidative damage. Clearly a rapid, reliable, and non-destructive test for the extent of the weathering damage was critically needed.

Traditionally used methods of oxidation characterization involve looking for particular oxidation products using transmission spectroscopy. But these methods have proved to be time-consuming, expensive, and difficult to operate (Küpper and others, 2004; Bruijn 1996). X-ray photoelectron spectroscopy (XPS) has been used to simply quantify oxidation by monitoring the atomic percent of oxygen on the surface, but is limited to a very shallow depth of examination (Onyiriuka 1993). Energy dispersive x-ray spectroscopy (EDS) can also examine the atomic percentage of oxygen on a surface, but has a greater range of depth of analysis. EDS has been used to qualitatively monitor

impurity appearance in degradation samples (Gulmine and others, 2003), but never as a means to monitor the extent of oxidation in photooxidative degradation.

EDS was used to successfully characterize the oxidation in the boat-repair problem and proved to be a quick and easy way to quantify the oxidation. This prompted further research to evaluate the application of this method to a wide variety of resin formulations and degrees of oxidation to determine its efficacy as a metric in all studies of plastic-weathering.

The primary purpose of this research is to establish EDS analysis as a method to characterize the oxidation in plastic materials. This evaluation consists of two requirements:

1. Quantification of the extent of oxidation in a weathered plastic should yield clear profiles of increasing oxidation.
2. The profile of increasing oxidation should be able to be systematically correlated (matched up and agree) to the corresponding profiles of the mechanical properties of the weathered plastic.

The secondary purpose of this research is to establish a method to predict the service lifetime of plastic materials in an outdoor environment.

The Sanitation Engineering Department of the City of Los Angeles has conducted a thorough study of the weathering, both natural and accelerated, of polyethylene (PE) trash carts for curbside sanitation service. Weathering and characterization of the degradation of the mechanical properties was conducted in accordance to consultation with Dr. Brent Strong at BYU. They agreed to send both the test data of the mechanical property profiles and the exposed samples (thick PE) for EDS analysis, thus enabling not

only the correlation of the mechanical changes to the chemical changes (primary purpose), but also to compare the changes in plastic when under natural weathering to the changes under accelerated weathering. This latter comparison has been the aim of many recent studies as the applicability of accelerated weathering devices to plastic-weathering studies has been in question. The evaluation of accelerated weathering devices is not an objective of this study, but will be commented on for the purposes of further research into this area.

Mity-Lite (Orem, Utah) approached BYU with a similar request – they desired the comparison in weathering sensitivity of various formulations of acrylonitrile butadiene styrene (ABS) in hopes of developing an outdoor table-top solution. ABS has proven to degrade rapidly in outdoor environments, thus requiring the thorough characterization of possible candidates. The samples from the various candidate-formulations were artificially aged over a period of 252 days and the impact strength and EDS oxygen content were profiled over the exposure duration and correlated (primary purpose).

The applicability of EDS analysis to oxidation measurement was evaluated according to the above-mentioned primary purpose of this study. The test of applicability was applied across and compared between both materials (PE and ABS), showing its ability to monitor degradation in both moderately UV-sensitive materials and highly sensitive ones. These results agreed with and further quantified the earlier results from the boat repair study (a cross-linked, fiberglass reinforced polyester).

2 Literature Review

Polymer degradation is a series of chemical reactions affecting the resin's microstructure, leading to changes in the polymer's physical properties and/or appearance. These reactions can occur at anytime, from the polymerization of the polymer, through its palletizing, storage, shipment, and fabrication, up to its end use application. Sometimes the degradation comes from a combination of different reactions, such as the case of UHMWPE used for biomedical joints, where degradation is not only produced by radiation (gamma-ray sterilization) but also from oxidation by the chemical environment (hemoglobin and/or synovial fluids) (Jahan and others, 1991).

2.1 The Environment

A particularly susceptible phase is when the plastic part is exposed to sunlight. In any outdoor application, all polymers degrade (Hrdlovic 2000). Weathering of plastics is due to many different chemical reactions that can occur between the many different environments a part can serve in and the functional character of the polymer itself. The most commonly damaging form of weathering on plastics is the combination of effects from both UV-induced photochemical degradation and oxidative degradation inherent in the oxidizing atmosphere.

2.1.1 Sunlight

Photodegradation involves basic photochemistry relationships. The wavelength (λ) and the cyclic frequency (ω_c, measured in hertz) of light are inversely related to each other by their product, the speed of light (3.00 x 10^8 m/s):

$$\lambda \cdot \omega_c = c \qquad \textbf{(2-1)}$$

This relationship allows the definition of a further relationship between the energy associated with one photon of energy (the smallest unit of radiant energy) E, with Plank's constant h:

$$E = h \cdot \omega_c = \frac{h \cdot c}{\lambda} \qquad \textbf{(2-2)}$$

Where h (Plank's constant) is equal to 6.62 x 10^{-34} J·s. This equation shows the inverse relationship between wavelength and energy: lower wavelengths have higher energy. Multiplying this energy E by Avogadro's number (6.02 x 10^{23}) gives the total radiant heat available through absorption of one mole of photons (Rodriguez 1989).

Since the average bond energy of the carbon-carbon bonds along a polymer-backbone is 351 kJ/mol (Ranby and Rabek 1975), a calculation proves that 350 nanometers is the threshold wavelength where the energy is sufficient to cause photolytic degradation (chain scission/ free radicalization) of the C-C backbone. Any radiant light with lower wavelengths (higher energy) will have sufficient energy to cause degradation. Visible light, on the other hand, with wavelengths from 400 to 700 nm has too little energy to cause many problems.

The portion of the sunlight-spectrum that reaches the earth's surface is limited. Most of the higher energy X-rays, gamma rays, and cosmic rays never make it through the atmosphere due to their absorption by ozone, leaving only UV, visible, and IR rays. The radiation spectrum of light in the UV to IR region is given in Table 2-1 with the corresponding wavelengths (nm).

Table 2-1 Light radiation spectrum (nm): UV to IR

UVC	UVB	UVA	Visible	IRA	IRB	IRC
200-280	280-315	315-400	400-800	-1400	-3000	-1000000

Ozone absorption even takes care of the highest energy UV radiation, blocking anything up to about 290 nm. The solar energy that reaches the surface is limited to the UVB to IRA region (290 to 2450 nm). The total radiant solar energy consists of (in order of decreasing energy): 37.8% IR (800-2450 nm), 55.4% visible light (400-800 nm), and 6.8% UV light (290-400 nm) (Ranby and Rabek 1975). As will be shown, the ultraviolet regions are especially damaging to polymeric molecules.

2.1.2 Indoor Weathering

Although often under-appreciated, UV-induced photooxidation can happen indoors as well as it does outdoors (Zielnik 2004). An example is furniture discoloration from short exposure to sunlight entering through nearby window glass. Another example is the chalky and brittle qualities imbued in PP light fixtures during aging from long-term indirect UV exposure combined with the heat from the adjacent light bulbs. "Light-

fastness" refers to a products resistance to indoor degradation, behind glass or interior artificial lighting.

2.2 UV Radiation

The photolysis of a polymer occurs because the energy of the UV region of light has the right amount of energy to dissociate the typical bonds in most polymers. Table 2-2 lists the photon energy in kJ/mol of electrons in various wavelengths of the UVB/UVA spectrum along with the bond dissociation energies of matched polymer chemical bonds.

Table 2-2 Photon energy of light and equivalent bond dissociation energies (Ranby and Rabek 1975)

Wavelength (nm)	Photon Energy (kJ/mol)	**Chemical Bond**	Photon Energy (kJ/mol)
		C = C	502
280	428	O - H	426
		C - H (primary)	414
300	399	C - H (secondary)	393
320	374	C - O	372
340	352	C - C	351
		N - H	339
360	333	C - N	330
380	315	C - Cl	326
400	299	O - O	213

Since 351 kJ/mol is the energy threshold for photolysis of the C-C bonds in the backbone chain of a polymer, 340 nm is the equivalent threshold in wavelength. It is thus UV radiation in the range of 290 nm (ozone absorption limit) to 340 nm (equivalent wavelength for that dissociation energy) that needs to be addressed as the cause of initial backbone bond cleavage.

2.2.1 Measurement

In photooxidation, the quantity of light is just as important as the quality of light (spectrum described above). Radiation exposure is reported in J/m^2 for either the total spectrum of exposure or only the UV range. Any energy passed in the form of electromagnetic radiation such as heat, radio, and light is referred to as radiant energy. Irradiance, measured in W/ m^2, is the radiant flux incident of the radiation per unit area of surface. Spectral irradiance, measured in $W/m^2/nm$, is the irradiance measured as a function of λ (wavelength). The radiant exposure, sometimes referred to as irradiation, is measured as the time integral of the irradiance over the exposure duration.

Diurnal and seasonal effects

The natural solar irradiance varies greatly on both a daily basis and a seasonal basis. The day/night cycle of natural sunlight exposure is referred to as the diurnal cycle. It was reported that no appreciable natural degradation occurred in either fall or winter when PE was naturally exposed in Geleen, The Netherlands (Gijsman, Hennekens and Janssen 1996). This is due to the combined effects of the shortened length of sunlight exposure and lower average temperatures.

Another source of long-term variation is due to the depletion of the atmosphere's ozone layer. The accelerated rate of ozone depletion in the atmosphere due to environmental factors is expected to raise the level of UV-B radiation (290-320 nm), thus adding severity to the problem of degradation and urgency to the need for solutions (Motyakin, Gerlock and Schlick 1999).

Effect of location

This brings up the importance of location. Significant degradation may have occurred during fall and winter in the previously mentioned study if it had been carried out in a location with greater irradiance. Generally accepted values for the average annual UV radiation come from averaging as many exposure variables as possible by long-term testing. These values for some locations are:

- Arizona desert: 350 MJ/m^2
- California: 300 MJ/m^2 (although Los Angeles has been listed as slight lower, 270 MJ/m^2, probably due to the high amount of smog)
- Florida: 280 MJ/m^2

The differences between degradation at different locations was illustrated in a study where the degradation of HDPE exposed in Florida showed a maximum depth of degradation (depth profiles will be discussed in Section 2-5), but the maximum depth of degradation continued to increase for similar exposure in Delft, The Netherlands (Bruijn 1996). The author supposed this to be due to the longer dark periods (at night) and hence longer periods without the UV-induction of photooxidation. This allows for oxygen diffusion to carry oxygen to deeper layers instead of the reactive consumption of all the available oxygen at a certain depth.

2.3 Weathering Trials

The incidence of weathering-related failures of plastic products is on the rise (Zielnik 2004). There are usually a limited number of predictable variables that affect the service life of a plastic product. Therefore, most material producers and processors have

conducted designed experiments to simulate the expected outdoor exposure, in order to gauge the sensitivity of the product to the environment (Strong 2002). This usually pays for itself by decreasing warranty costs and allowing processors to optimize formulations and processing methods without having to worry about any unknown imparted instability to weathering (Zielnik 2004).

ASTM D1435 defines the practice for outdoor weathering of plastics ("ASTM Reference Manual" 2001). This test is used to evaluate color measurements, gloss measurements, transmission haze and clarity and visual assessment of naturally exposed plastic samples. Further characterization can be accomplished according to the methods laid out in Section 2-6.

2.3.1 Trial Aspects

The challenge to outdoor weathering testing is answering two questions (Ranby and Rabek 1975):

3. What should the experimental conditions be to replicate the desired exposure?
4. How can the changes that occur to the sample be best characterized, i.e., how should the chemical/mechanical changes be evaluated?

The first question deals with the complex evaluation of the many variables in outdoor exposure to simulate a predicted service environment. The second question will be treated later in Section 2-6.

There are a host of variables affecting outdoor UV-exposure that must be considered when designing a weathering test. The variables specific to the UV irradiance include:

- The light quality (spectrum) and quantity (irradiance)
- The length of day/night in the diurnal cycle
- The angle of direct light exposure

Meteorology

Many outdoor meteorological variables can also influence the amount of radiation a product is exposed to or the rate of the subsequent oxidative reaction (Tidjani 1997). These include:

- Location dependent variables: average temperature of the climate (affects rate kinetics), light (amount of daylight), pollutants, water (average rain fall, humidity)
- Seasonal variation of temperature
- Long term variables: atmospheric contamination by corrosive agents (smog), volcanoes (ash reduces UV transmission), hurricanes, variations in the ozone layer (changes the light spectrum portion reaching the surface)
- Surface reflectance variation around the sample (explained below)

Surface reflectance variation

The radiation that reaches a sample can be both direct and indirect (reflected) light. Only a portion of the light exposure of a product comes from direct light. The rest of the exposure comes from the reflective nature of the surroundings. While grass, soil, and asphalt are only minimally reflective, concrete, cement, or snow are highly reflective and can contribute high amounts of indirect exposure to a sample surface.

Accelerated outdoor weathering

In order to exaggerate the effects of weathering on the degradation of a product's mechanical properties, the natural exposure under sunlight is "accelerated" by either employing a sun-concentrating device, or applying a load (stress) during the exposure. Solar concentrators employ reflective surfaces to apply high amounts of indirect (reflected) light onto the surface, thus increasing the irradiance. Applying a stress during irradiation has been proven to accelerate the degradation rate ("Railway Gazette International" 1994).

Weathering environment correlation

With the complexity of all the outdoor variables involved in selecting a weathering environment, using multiple sites of exposure can make the sampled data more representative of a universal average environment and provide a greater macro-scale understanding of the effects of weathering (Bruijn 1996).

2.4 Artificial Weathering

Artificial weathering refers to the accelerated weathering consisting of increasing the irradiance by means of a manufacture light source. It is sometimes labeled as incorrect nomenclature as the photooxidation is similar to that of natural exposure, suggesting that it is still "natural" weathering, but on an accelerated time scale. But the term, "accelerated weathering" can also be confused with the accelerated outdoor weathering methods (sunlight concentrators or tests under load) mentioned above. Therefore, neither term has become universally accepted.

The study of natural degradation in polymers can take years to accumulate any substantial data. Often the deleterious effects are not immediately detected but develop over longer periods (Motyakin, Gerlock and Schlick 1999). UV degradation simulation testing with artificial weathering has become a popular way to speed up the degradation process in the laboratory. Its advantages are: repeatability, independent control over stress fractures, and that it is faster than real time (Strong 2002). The most common forms of oxidation acceleration are UV, thermal, and chemical-induction (Strong 2006). But other forms of radiation apart from UV have been used as well, such as γ (gamma) rays (Shintani and Nakamura 1991).

Artificial weathering has assisted researchers with a good comprehension of the photo-oxidation process in polymers as well as assisting in the prediction of service life for those polymers under natural conditions. These predictions are something more of an art than a science, though, due to the many varied combinations of the aforementioned environmental conditions that a plastic may be exposed to (Tidjani 1997). Further inaccuracies in laboratory simulation experiments result from the difficulty of matching impurity concentrations existent in the natural application of plastics. Random types and amounts of impurities are introduced through processing steps and create "hot-spots" for UV-induced photolysis (Celina, George and Billingham 1996).

Because of this difficulty in acquiring data on degradation results from experimentation, other sources of rate predictions have been sought through detailed studies into the mechanisms of photo-oxidative degradation in plastics to make predictions of service life. These studies of reaction mechanisms are presented in Section 2-5.

ASTM G-90 defines the standardized test for accelerated weathering ("ASTM Reference Manual" 2001). This test ensures water quality (silica ppb<200), mirror reflectance, type and direction of airflow, and the measure of UV irradiance.

Artificial weathering has been used not only for testing purposes, but also as a value-added step in processing to increase the functionality of a product. An example is the common intended induction of cross-linking in parts by UV radiation. Another example was a study where UV exposure was used to increase the polar component (in the photooxidation products) of a plastic surface to increase its biocompatibility. This study reported complications of this process: the oxidation products leaked into the biological fluids, changing them into differently behaving liquids, and the wettability of the surface changed with time because of the initial degradation from this surface modification (Lee and Ruckenstein 1987). This proves the importance of testing to understand the all of the possible effects of weathering.

2.4.1 Artificial Light Sources

The research shows a number of different light sources used to increase the irradiance. Artificial light sources must be carefully evaluated as to magnitude of the increase in irradiance. A general rule applies: the greater the increase in irradiance over that of natural exposure, the greater the probability of causing different reaction mechanisms. Also, the filtered spectrum of light by a light source must be considered – some sources more closely match the spectrum intensities of natural light than others.

Mercury borosilicate lamps have been used to increase the irradiance by a moderate amount (Kaczmarek 1996; Scoponi, Cimmino and Kaci 2000). But the two most common artificial light sources are fluorescent UV lamps and xenon-arc sources.

Fluorescent UV lamps are used in the QUV machines manufactured by Q-Panel (Cleveland, Ohio). Xenon-arc sources are used in the Weather-Ometer (WOM) equipment from ATLAS (Chicago, USA).

The QUV spectral irradiance (irradiance, accounting the wavelength of the incident light) is practically two-fold the irradiance in WOM (Andrady 1997). The typical wavelength of UV light for both QUV and WOM is 340 nm, but higher energy (lower wavelengths) bulbs or sources can be acquired and employed. In comparing the degradation induced by the two light sources, WOM showed the initiation of surface cracks in one direction, while QUV showed more severe damage, with cracks in all directions (Gulmine and others, 2003). The authors of this report theorized that WOM favors cross-linking during exposure, while oxidation is favored in the exposure by QUV.

2.4.2 Application of Weathering Devices

By comparing natural to accelerated-weathering testing methods, a good understanding of degradation from UV-radiation accelerated weathering has been obtained (Ranby and Rabek 1975). Accelerated weathering testing can provide useful data for comparison of multiple materials' weathering sensitivity, as well as service life prediction of a material (Strong 2002).

The ability of accelerated weathering to produce results that agree with real-time outdoor service environment is referred to as the "correlation" of the weathering method. Correlation studies often report acceleration factors as the exposure time by outdoor weathering, divided by the exposure time in accelerated weathering, to produce a similar change of some critical property (elongation, discoloration, oxidation) in the tested

material. As mentioned above, greater irradiance produces different mechanisms of reaction. Therefore, greater acceleration factors usually imply worse correlation.

Service life prediction usually consists of exposing the product to accelerated weathering until it fails, and then multiplying the time to failure by the acceleration factor to predict how long it has in service before failure by photodegradation. But the high variability of outside weather, especially over short time periods, has made acceleration factors and service-life predictions to often be considered unreliable (Kurtz and others, 2001). Polymer manufacturers are extremely hesitant to claim acceleration factors, service-life predictions, or other aging predictions for their materials due to the wide range of operating environments and the use of inaccurate aging models (Lewis 2004). The automobile industry has been the greatest promoter of correlation studies and their reporting due to the extreme environmental conditions and expected service life of plastic parts used (Maher and Bank 1992; Strong 2002).

It is also considered inaccurate to apply acceleration factors and aging predictions across multiple resin types, or even across different additive formulations or part thickness of the same resin (Strong 2002). Furthermore, acceleration factors have been repeatedly shown to vary between the profiled properties in a degradation experiment, even for the exact same material and exposure (Gijsman, Hennekens and Janssen 1996).

With these caveats, the literature has reported the following experimentally determined acceleration factors (the characterizing properties listed will be explained in Section 2-6):

- LDPE films by mercury borosilicate lamps: 7.5x, carbonyl or vinyl absorbance (Scoponi, Cimmino and Kaci 2000).

- Thick HDPE by WOM and Xenotest (another xenon arc accelerator): 5x (WOM), 12x (Xenotest), time to failure in micro tensile strip testing ("MFTT"); 4x (WOM), 5x (Xenotest), irradiation (Bruijn 1996).
- PE films by WOM: 2.5x, oxygen uptake; 7-10x, carbonyl or vinyl absorbance; 6-8x, elongation (Gijsman, Hennekens and Janssen 1996).
- PP films by Xenotest: 14x, irradiation (not tested, but manufacturer claim referenced in Schoolenberg 1988a).

But the assumption of these acceleration factors as industry standards was not intended. Even these authors understand that there will never be a universal acceleration factor – the acceleration sources and materials introduce too many variables. The need for experimentation of a variety of simulations is apparent, but is time consuming and frequently involves factors that are difficult to control and even to record (Tidjani 2000).

After simulating a given environment for a particular resin formulation and part type, an acceleration factor can be determined that should apply to any future cases. And real-time aging by itself to predict aging patterns is too slow to economically be considered as a viable business solution (Küpper and others, 2004).

2.5 Photooxidation and Stabilization

The combined effect of UV-induced photolysis and oxidative degradation has been the topic of much recent literature. The last ten years have seen the proposal and testing of many different mechanisms for UV-induced damage of polymers. The degradation mechanisms and their controlling factors of some polymers, like PE and PP,

are well established (Allen and others, 1996; Rabello and White 1997; Fechine and others, 2004).

2.5.1 Photooxidation Mechanism

Photodegradation and oxidation work together, in what's called photooxidative degradation, to bring about chemical changes in the properties of the plastic. As already mentioned, certain UV wavelengths are particularly damaging to plastics because their energy equivalent closely matches the bond energy between many neighboring atoms common to plastics (Strong 2006). This causes the formation of free radicals across the exposed surface by dissociative (cleavage) processes. The supply of free radicals as well as the thermal heating effect of UV radiation both serve to greatly increase the oxidation rate over that of a similar part in an indoor environment. Oxidation causes a host of different reactions that cause degradation (Wu and others, 2000; Rabek 1990; Pospíšil 1995), including:

- The formation of peroxides along the polymer chains, which further induces more free radicalization and promotes chain-scission and cross-linking reactions
- Scission of polymer chains into various oxidation byproduct segments (ketones, alcohols, CO_2, CO) thus lowering the molecular weight and changing the material's properties.
- Conversion of polymer chain end-groups into acids that promote more UV susceptibility.

The physical manifestations of photooxidative degradation include loss of transmissivity and discoloration, loss of mechanical and thermal properties, especially embrittlement and crazing, and evolution of gaseous by-products (Strong 2006).

Photochemistry

The energy imparted to a polymer through UV exposure excites electrons shared across the covalent bonds, raising them to a higher energy level (Strong 2006). This excited state causes weaker bonds and easier scission of bonds than in a ground-state polymer through two basic phenomena. First, it promotes the population of an anti-bonding orbital in the excited state [($\pi \rightarrow \pi^*$) or ($n \rightarrow \pi^*$)], which allows the occurrence of chemical transformations that are electronically not available to ground state species.

Secondly, excited states can promote reactions that normally would be highly endothermic because of the energy transfer that occurs (Carey and Sundberg 1990).

2.5.2 Chromophores

The basic photochemistry relationships presented in Section 2-2 show that UV radiation in the range of 290 nm to 340 nm is the critical portion of sunlight polymer degradation. Even though wavelengths of 340 nm have sufficient available energy to match the bond energy in an average carbon-carbon bond, the threshold wavelength at which significant photolysis occurs in experimentation has been shown to be lower than this. Some additional force holds the bonds together.

Most commodity polymers contain only C-C, C-H, C-O, C-N, or C-Cl bonds, which were reported to require a wavelength of below 190 nm for appreciable amounts of photolysis (Hrdlovic 2000). This is most likely due to steric effects of nearby chains,

which assist in holding the bonds together by the close packing in a solid polymer, thus decreasing the rate of free radical formation. Regardless, the wavelengths required for polymer backbone photolysis never make it through the earth's atmosphere.

Several authors conclude that UV-absorbing impurities in a polymer are what enable photolysis with wavelengths greater than 290 nm (Hrdlovic 2000; Gijsman, Meijers and Vitarelli 1999). These chromophores have lesser bond energies than those of a commodity plastic and are all that is needed for the initiation of photooxidative degradation. Much research has recently been done to determine the initiation mechanism of photooxidation. Because so many different mechanisms have been proposed and substantiated, initiation seems to be accomplished by a variety of different paths, dependent on the polymer molecular structure and concentration of the chromophores involved in each mechanism. The chromophores suspected to easily absorb UV rays in polymers are:

- Internal in-chain impurities (hydroperoxides/carbonyls) formed during storage, processing, or weathering (Hackett and Dillenbeck 1993).
- External impurities as polymerization catalyst residues, additives (pigments, dies, or antioxidants), pollutants from the atmosphere or metal traces from processing equipment (Gijsman, Meijers and Vitarelli 1999).
- Charge transfer complexes (CTC's) between oxygen and the polymer chain (Karlsson, Hakkarainen and Albertsson 1997).
- Parts of the natural molecular structure of the polymer (Rodriguez 1989).

Chromophore absorption of UV light and the resulting dissociation creates free radicals in the polymer, which cause further dissociation (cleavage). The free-radical dissociation of the polymer usually begins at carbon-hydrogen bonds.

Chromophores have been found to be the initiation site of other deleterious reactions as well. Nitrous oxides in the exhaust gases from burning hydrocarbons react with chromophores in polymers commonly causing "gas fading", especially associated with industrial facilities or traffic jams (Makowsik, Samuels and Wagner 1995).

2.5.3 Pathway Mapping

Photolysis by itself (in an inert atmosphere) provides a much slower rate of degradation than when combined with an oxidative environment (Davis and Sims 1983). The two work together in a synergistic relation. Oxidation reaction rates are increased by the higher temperature and higher free radical concentration provided by photodegradation. In turn, oxidation reactions create more UV-susceptible chromophores for photodegradation.

Many authors have proposed mechanisms for the different individual reactions in this degradation system. It has been the subject of much recent research, but various aspects of the mechanisms involved remain unclear (especially in the initiation mechanisms). One proposed scheme of the photooxidation process plausibly seemed to encompass the entire system. It has been mapped out as a cyclical radical-based autooxidative process (Figure 2-1), which can be divided into four stages.

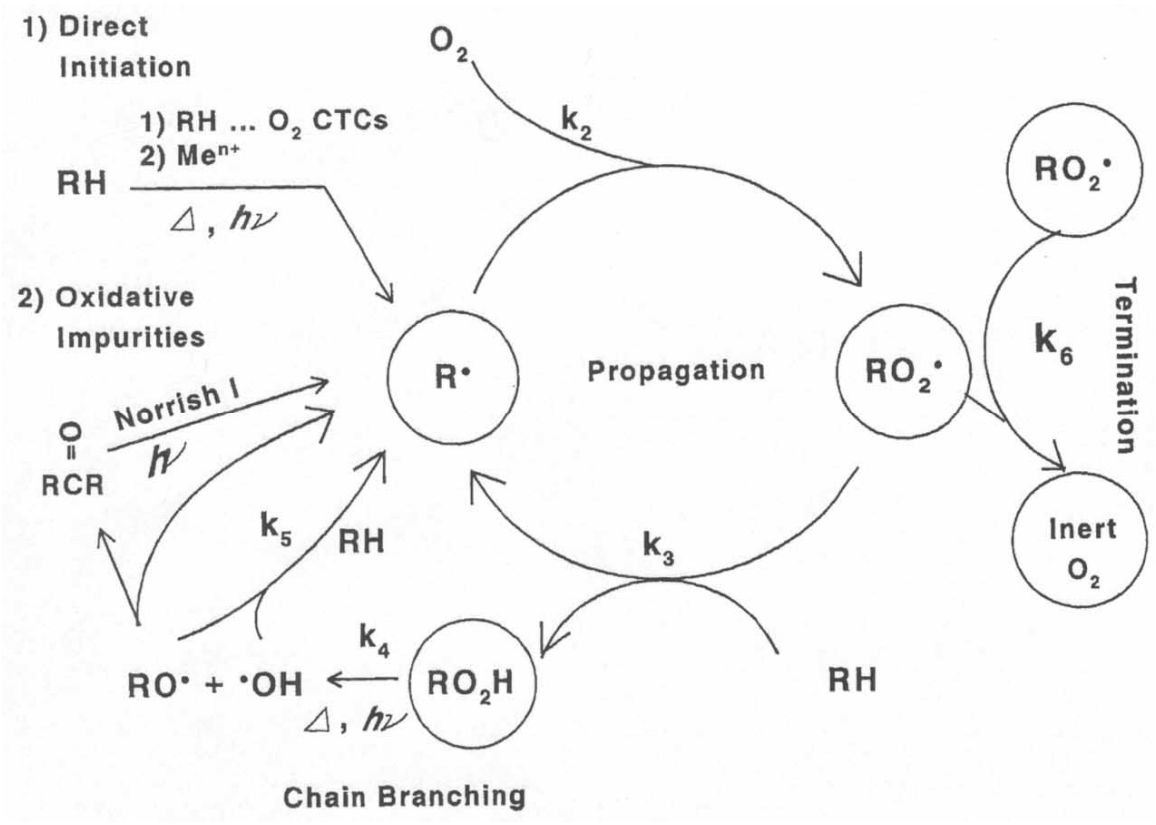

Figure 2-1 Photooxidation: autooxidation mechanism for almost all polymers. Key: R, polymer chain; H, most liable hydrogen; k_i, reaction rate) (Gijsman, Meijers and Vitarelli 1999)

In the first stage (initiation), photolysis reaction of chromophores creates free radicals (k_1) as discussed earlier in this paper. The particular mechanism responsible for this step probably depends on the type and concentration of chromophores present. In any case, it usually involves the breaking of a C-H bond to form a radical along the chain, or the formation of a CTC between the polymer and oxygen and the subsequent chain scission and CO_2/CO evolution. The latter process, CTC-induced degradation, is presented in Figure 2-2.

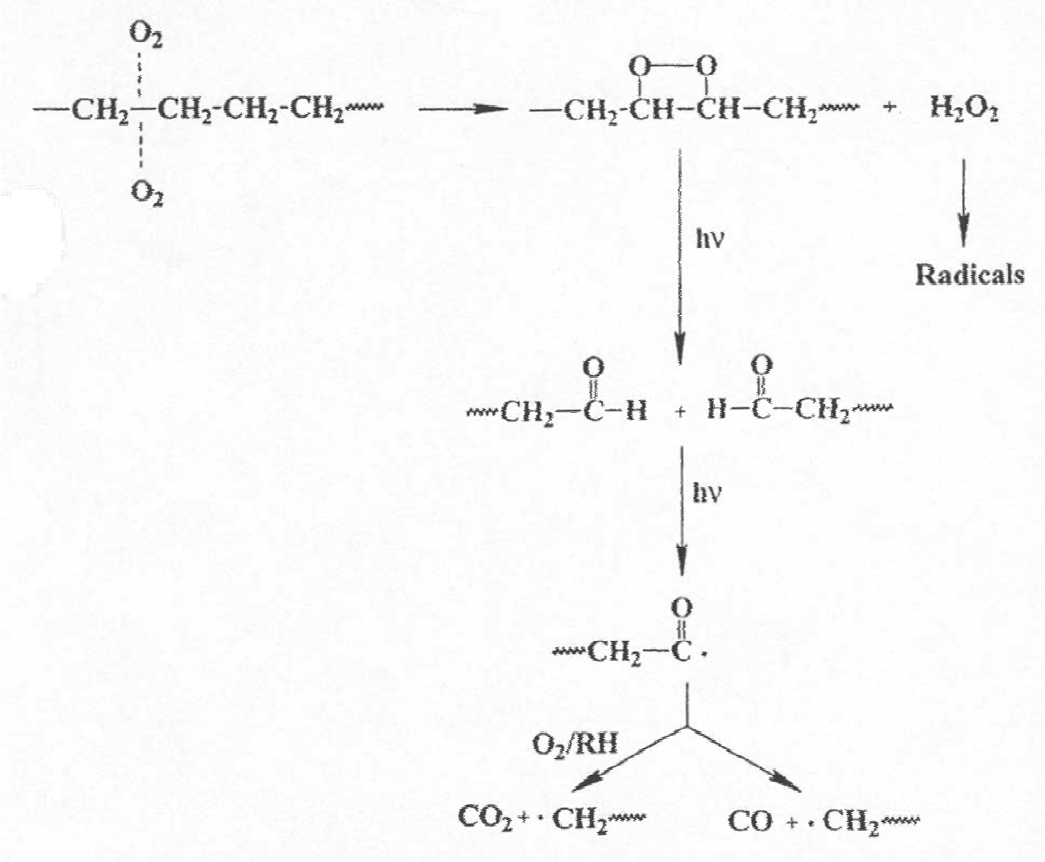

Figure 2-2 CTC-induced degradation of PE and subsequent chain scission (Hrdlovic 2000)

The second stage (propagation) consists of two major thermal reactions, which have been studied in detail. The first reaction is the oxidation of any radicals present (k_2). Oxygen reacts with the free electron on a molecule to make an alkyl peroxide. The rate of this oxidation reaction is enhanced by the free-radicalization caused by the peroxides already present. The second reaction (k_3) occurs between additional C-H bonds and the peroxide radicals from the first reaction. This is called hydrogen abstraction, as it is the transfer of a hydrogen atom to the peroxide to form a hydroperoxide, and the formation of another free radical (Karlsson, Hakkarainen and Albertsson 1997). These new free radicals also undergo oxidation, hence the propagation of free radicals along the polymer

chains and hydroperoxide formation. The oxidation rate of reaction in this stage is much faster than the hydrogen abstraction reaction, so the rate of propagation is determined by the abstraction rate.

The third stage (termination) controls the rate of reaction. Throughout the propagation stage, some peroxide radicals will react with each other (k_6) to yield oxygen and an organic product based on the degree of steric hindrance. In the case of a tertiary peroxide, dialkylperoxides are produced, whereas secondary peroxides yield an alcohol and a ketone (Tidjani 1997).

It is still unclear as to what happens to the hydroperoxides formed during propagation in the fourth stage. The hydroperoxide decomposition stage has been suggested to be the photochemical decomposition (k_4) into alkoxy and hydroxyl radicals, which can initiate another propagation cycle (k_5). This and several other decomposition mechanisms have been proposed, leading to radical formation, chain scission, or neither of these. One plausible decomposition method is the further oxidation of the hydroperoxides formed producing gaseous byproducts, especially CO_2 and CO.

By studying the amount of each type of byproduct from the degradation of each common polymer (oxidation profiling), researchers have assembled pathways for many of these decomposition reactions. For example, the proposed mechanism for formation of CO_2 and CO and new free radicals from the hydroperoxide derivatives (suggested in preceding paragraph) of many polymers is given in Figure 2-3.

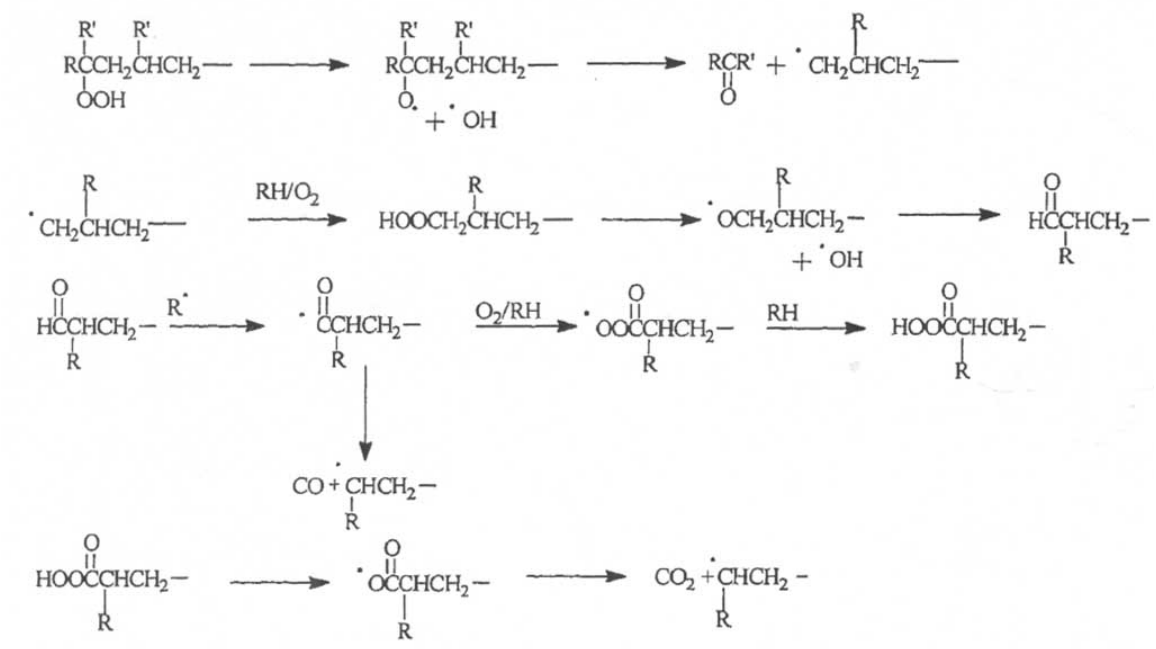

Figure 2-3 Hydroperoxide formation of CO2 and CO. Key: R, CH3 (PP) or H (PE, PBT, PA6) (Gijsman, Meijers and Vitarelli 1999)

Karlsson, Hakkarainen and Albertsson (1997) proposed a mechanism for the degradation of polyethylene that illustrates well the cycle presented in Figure 2-1. It is based on zip depolymerization of the PE chain through a cyclical transition sate and is presented in Figure 2-4.

In this scheme, UV photolysis occurs on carboxyl end-groups of the polymer chains. A mechanism of intramolecular hydrogen abstraction via a cyclic transition state produces a free radical on the carbon backbone. Peroxide and hydroperoxide formation occur via propagation, and the hydroperoxides decompose by various methods to form more radicals and dicarboxylic acid/ketoacid oxidation products. The authors of this mechanism proved that after long times of exposure, these two acids indeed dominate the products of indeed degradation.

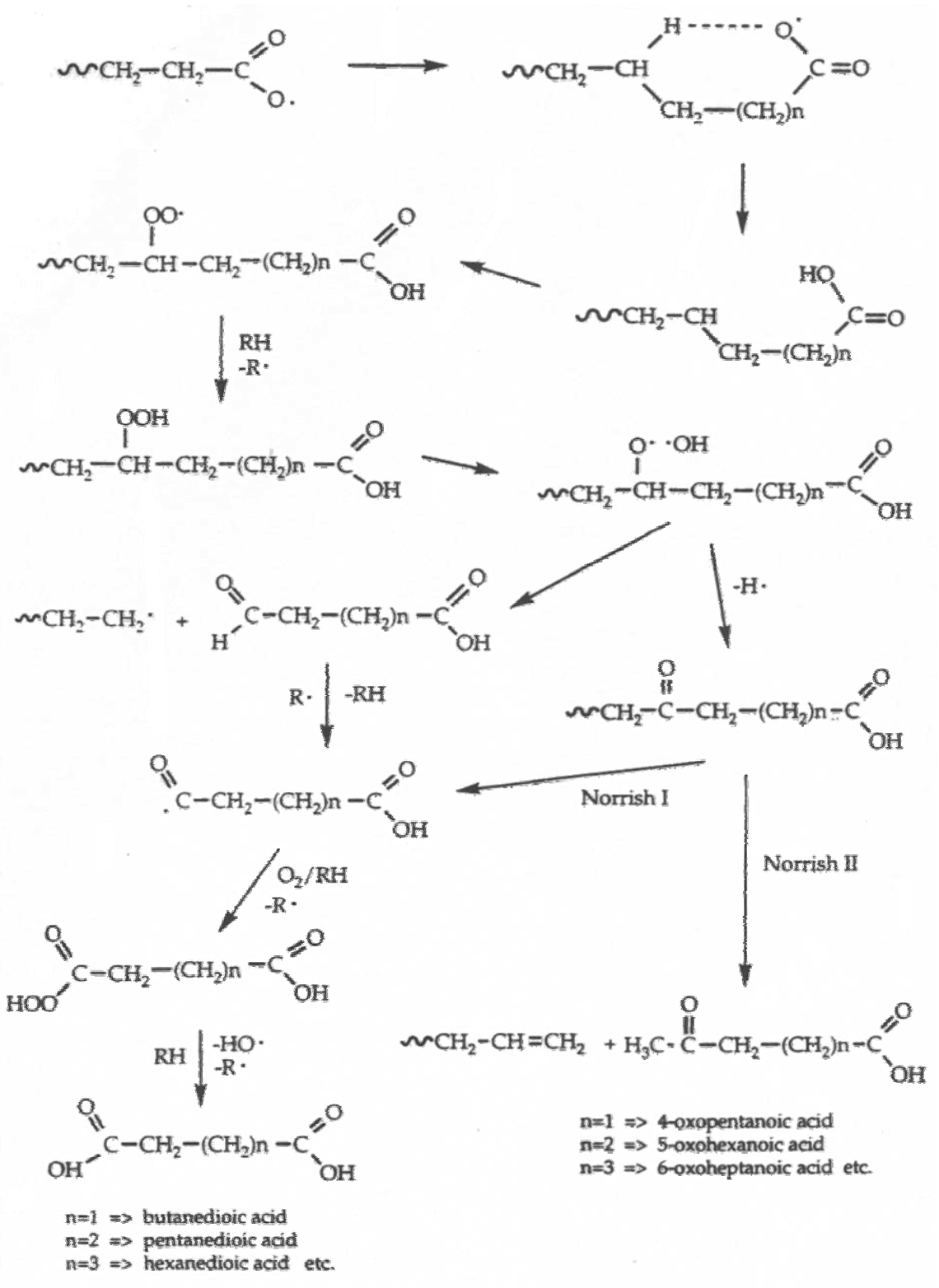

Figure 2-4 Formation of low molecular weight oxidation products through zip depolymerization

Degradation end results

As free radicals are formed and peroxides are introduced, two main types of molecular rearrangements occur in a polymer chain: chain scission and cross-linking.

Chain scission is the dominant method of backbone-degradation under UV radiation for highly substituted carbons along the backbone (tertiary or quaternary). Thus, most polypropylenes, polyacrylates, and polymethacrylates will favor chain scission over any other degradation method (Rodriguez 1989). A commonly accepted pathway for chain scission at tertiary carbons based upon dissociation of the pendant C-H bonds is presented in Figure 2-5.

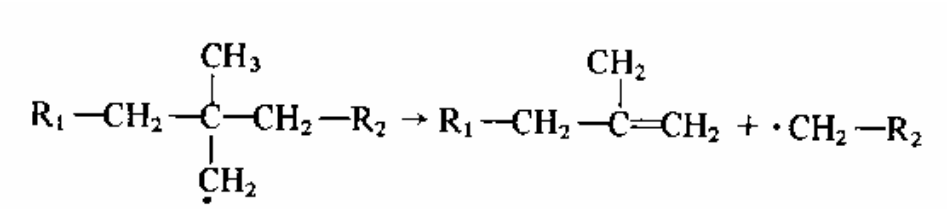

Figure 2-5 Chain scission of polyisobutylene (Rodriguez 1989)

Another common pathway for chain scission is the CTC-induced one presented previously in Figure 2-2.

Chain scission makes smaller chains from larger ones, decreasing the average molecular weight and the corresponding structural properties. Another effect scission has is more freedom of chains in amorphous regions to line up (less viscous) and become more crystalline (Allen, Edge and Mohammadian 1993). The increase in crystallinity competes with some of the effects of decreasing molecular weight (tensile strength, elongation-to-break, etc.). But the loss of structural properties from photooxidative

degradation has been highly reported, so the effects of greater crystallinity are probably insignificant in comparison. Widely reported, however, are evidences of embrittlement in aged plastics and this may reflect some increase in crystallinity. The reported increase in density during photooxidative degradation, however, is probably due to this increase in crystallinity, as well as the oxygen uptake (Hrdlovic 2000).

Although cross-linking is a useful reaction in making thermally stable rubbery materials, it can sometimes be very undesirable when occurring within a polymer in service. The tensile modulus increases with cross-linking, but the energy-absorbing capacity goes through a maximum and decreases thereafter (embrittlement). Cross-linking can also cause incompatibility problems in some polymers, like the exudation of plasticizers, shrinkage of systems, and delamination (Rodriguez 1989).

In the intentional cross-linking of a thermoset, heat and peroxide initiator work to initiate the reactions. With the absorbed energy from UV radiation and the peroxides formed during photooxidative degradation, addition polymerization cross-linking is initiated in UV-exposed plastics. An interesting study noted that by heating (pre-conditioning) a plastic product, one can deactivate the peroxides already present and substantially decrease UV degradation by hindering the initiation step (Allen, Edge and Mohammadian 1993).

Although many researchers have focused on chain scission as the leading factor to a plastic's changes in properties, it seems that cross-linking can offset many of these changes or even reverse their effects (Tidjani 1997). Chain scission decreases the average molecular weight, thus decreasing most structural properties including the modulus. Cross-linking, on the other hand, causes an increase in the molecular weight, and thus

increases the modulus. The rate of change in tensile modulus E_t has been quantified by Rodriguez (1989) as the difference in the rates of cross-linking (dN_C/dt) and chain breaking (dN_S/dt):

$$\frac{dE_t}{dt} = K\left(\frac{dN_C}{dt} - \frac{dN_S}{dt}\right) \quad \textbf{(2-3)}$$

The conditions under which degradation occurs determine the weighting of each of these rates and the outcome of these two competing rearrangement processes. As an example, high and low crystallinity PP (polypropylene) films were tested for the retention of physical properties after exposure times. It was shown that high crystallinity PP became useless after short exposure, but low crystallinity PP retained its physical properties for a longer period of time. The author of this study proposed that this is due to a greater probability of cross-linking than of chain scission in the low-crystallinity material (Rodriguez 1989). This is due to a larger amorphous region where the chains are free to move and line up in optimum conformations for cross-linking.

This relates to the spherulite conformation in polymers. When a crystallizable polymer is cooled from the liquid state during processing, the long polymer chains fold up like an accordion forming a regular, repeating structure, which constitutes a crystal. Polymers are never 100% crystalline. A semicrystalline polymer is characterized by crystalline lamellae interspersed by amorphous regions. The lamellae are shaped into spherical structures, called spherulite, by the amorphous regions (Budinski and Budinski 1999).

The dependence of degradation rates on crystallinity and spherulite size have been studied by varying the manufacturing methods of PP samples. Schoolenberg (1988a)

theorized that compression molded samples should be used in degradation studies because this eliminates the shear stresses and morphology transitions as much as possible to give equally sized spherulites and no skin morphology changes, thus causing regular degradation. This was based on the susceptibility to degradation induced by the rapid cooling in injection molding (Kagiya and others, 1985).

In a later study, Schoolenberg and Vink (1991) directly compared the degradation profiles of compression-molded to injection-molded samples. The injection molding samples exhibited the "skin-core effect": a stretched outer skin from the rapid cooling and shear deformation on surface during processing (Sandilands and White 1985). This produced a measure of orientation in the surface – stretching and lining up of the polymer chains imparted crystallinity. Although the absence of outside stresses allows regular and large spherulites to be formed in compression molded PP, the crystallinity proved to be lower than in the injection-molded samples. Orientation reduces mobility, and thereby oxygen diffusivity and degradation sensitivity. The higher degree of orientation/ crystallinity in the injection-molded samples did indeed prove to cause slower degradation than with the compression-molded samples.

Discoloration

Another end-result of oxidative degradation is discoloration of the surface. The changes in crystallinity will have an effect on the light-transmission character of a plastic part's surface. Many times, a yellow color is observed at sites of degradation. The unsaturated products of the degradation reactions cause this discoloration: conjugated

polyenes, various oxygenated species (like dihydroxy-benzophenones), or products of ring-opening reactions (Ranby and Rabek 1975; Thomson and Klemchuk 1996).

2.5.4 Functional Groups

From an understanding of the mechanisms involved in photooxidative degradation, predictions can and have been made concerning the effects of functional groups present on the susceptibility of a polymer to this type of degradation. Many rules of thumb have been collected and are presented here, grouped by three families of functionality factors: tertiary versus secondary carbons, aromaticity, and active bases for free radicalization.

Tertiary versus secondary carbons

It has been proven that pendant methyl groups considerably promote photodegradation rates. Tertiary carbons are very active sites for chain scission based on Norrish II type reactions forming vinyl and carboxyl end groups (Fujimoto and Fujimaki 1999). This is due to the acceleration of both peroxide formation and radicalization of hydroperoxides. This explains the lower UV stability of PP when compared to PE (Gijsman, Meijers and Vitarelli 1999) in terms of concentration of tertiary carbons – while PE has some tertiary carbons from branching and cross-linking, PP has them at every other carbon along the back-bone.

Peroxide-forming oxidation of free radicals occurs much faster at tertiary free radicals along a polymer chain than at secondary ones (Tidjani 1997). Therefore, the propagation step of the scheme in Figure 2-1 is accelerated by the presence of tertiary

carbons on the polymer chain. This agrees with Hrdlovic (2000) who proved peroxide formation to be faster for PP than for PE and PA6.

Cross-linking is also accelerated by the presence of tertiary carbons. Tertiary hydroperoxides become radicals faster than secondary ones, thus aiding in the preparation of linking of chains (Gijsman, Meijers and Vitarelli 1999).

Aromaticity

It has been shown that of all the possible pathways for oxidative degradation of PS, scission of the phenyl ring C-C bonds is the most dominant (Onyiriuka 1993). The resonant character of an aromatic group causes high UV absorption due to delocalization of electrons in adjacent orbitals along the ring (Hrdlovic 2000). The jump from a bonding orbital to an anti-bonding orbital ($\pi \rightarrow \pi^*$) is lower energy due to this "see-through" effect of the electrons. If the aromatic groups are pendant groups, and not part of the backbone chain, then they may act like traps for the UV rays, causing either degradation on an area less critical than the backbone, or stabilization of the free radical allowing for molecular rearrangement and therefore scission.

Active bases for free radicalization

Active bases for free radicalization are functional groups that serve as good sites for hydrogen abstraction due to low bond energies. Active bases include carboxylic/ aldehyde end groups, ketones, esters, etc. Carbonyl groups have sensitivity to wavelengths of up to 350 nm, and therefore easily undergo photolysis. The jump of an electron from a non-bonding orbital to an anti-bonding orbital ($n \rightarrow \pi^*$) is about half as

much of an energy gap as a $\pi \rightarrow \pi^*$ jump, so carbonyl groups (with the pairs of non-bonding electrons on the oxygen atom) are much easier to sensitize. Sometimes, large pendant groups can interfere with the free radical-accessibility to active bases thus decreasing degradation rates (Allen, Edge and Mohammadian 1993). A polymer with many sterically-free active bases would be initiated fast and degrade quickly.

An example of this is the degradation of PS. The homopolymer PS by itself degrades very slowly (Piton and Rivaton 1997), possibly due to the effects of aromaticity described above. But PS degrades rapidly in an outdoor environment (Strong 2006). This is probably due to a high accumulation of, or affinity to impurity-chromophores in the PS material. When combined with BR (butadiene rubber) (easily photo-degraded due to the double bond), as in ABS, the material degrades much faster than the homopolymer PS. As soon as PS material has an active base introduced to initiate degradation by the introduction of free radicals, the oxidation rate of PS is greatly increased (Piton and Rivaton 1997).

Photooxidative degradation of plastics requires initiation by either hydrogen abstraction or CTC's. When a polymer has few active bases for hydrogen abstraction, photooxidation will be driven more by the CTC-induced pathway. As seen in Figure 2-2, the CTC-induced pathway to chain scission seems more direct and quicker to scission than a hydrogen abstraction mechanism like that in Figure 2-4. Perhaps this is why polymers such as PP and PE degrade so fast in comparison with other commodity plastics: no active bases make degradation happen by the faster CTC pathway. In comparison, PA6 (Polyamide-6) and PBT (polybutene terephthalate) would degrade in

the slower, direct photolysis of the amide bond and ester bond respectively (Hrdlovic 2000).

A couple of last rules, which do not fit well under any of the above topics are included here. First, although any C-H bond can be attacked, positions especially vulnerable to hydrogen abstraction are those next to a double bond, an ether linkage, or on a tertiary carbon (in order of decreasing vulnerability)(Rodriguez 1989). Any of these functionalities will increase photooxidative susceptibility. This is because of the stability of the resultant free radical caused by dissociation of these functionalities.

Second, polymers such as polymethylmethacrylate (PMMA) and polytetrafluoroethylene (PTFE) are popular for outdoor application because of their excellent resistance to weathering. This is attributed to their low diffusion rates (Allen 1983) and high transmission (as opposed to absorbance) of UV radiation when compared to other commodity plastics (Ranby and Rabek 1975).

2.5.5 Heterogeneous Depth Profiles

Much research has been done concerning the depth to which substantial photooxidation occurs. All reports claim that the greatest degradation for any material is limited to the first 500-600 μm next to the surface, owing to oxygen diffusion limits (Küpper and others, 2004; Schoolenberg and Vink 1991). Although some transmission of UV radiation occurs from the exposed surface to the center, oxygen diffusion limits the reaction (Davis and Sims 1983). Photooxidative degradation rates (measured by losses in average molecular weight) are much less in the center than at the surface, due to oxygen-diffusion limitations restricting oxidation's role in the synergistic degradation described

earlier (Schoolenberg 1988a). The diffusion of PE at 25 ºC was reported to be $1.7x10^{-11}$ m^2/s (Stannet 1968).

On unexposed surfaces of polyolefins, the degradation rates are slightly higher than in the center of a plastic part, due to the availability of oxygen combined with UV radiation transmitted through the bulk (O'Donnell, White and Holding 1994; Gijsman, Meijers and Vitarelli 1999). Polyolefins do not absorb UV light with wavelengths greater than 290 nm. Therefore, the UV light will pass through the substance and degrade both the front and backsides of PE and PP, being limited by oxygen diffusion on either side. The transmission is of course limited by the thickness of the sample – the two studies referenced above demonstrated this phenomenon with thin (250 μm) films.

In contrast to the low absorbance of polyolefins, PBT showed degradation only on the exposed side, and not on the backside (Gijsman, Meijers and Vitarelli 1999). This was attributed to the strong absorbance of UV in PBT by its chromophore functional groups. Absorbance is thus ascribed as the limiting factor (penetration depth of UV light) in polymers such as PBT with high amounts of chromophores, instead of oxygen diffusion.

A degradation profile can be observed over the thickness of the part, to compare the effects of oxidation versus photolysis, and to show the transmission capability of the polymer. For example, O'Donnell, White and Holding (1994) showed the profiles for PP and GFPP (glass fiber-reinforced polypropylene). A molecular weight profile across the thickness of the part (depth) is presented for both the control sample (before exposure) and after five weeks of exposure (Figure 2-6).

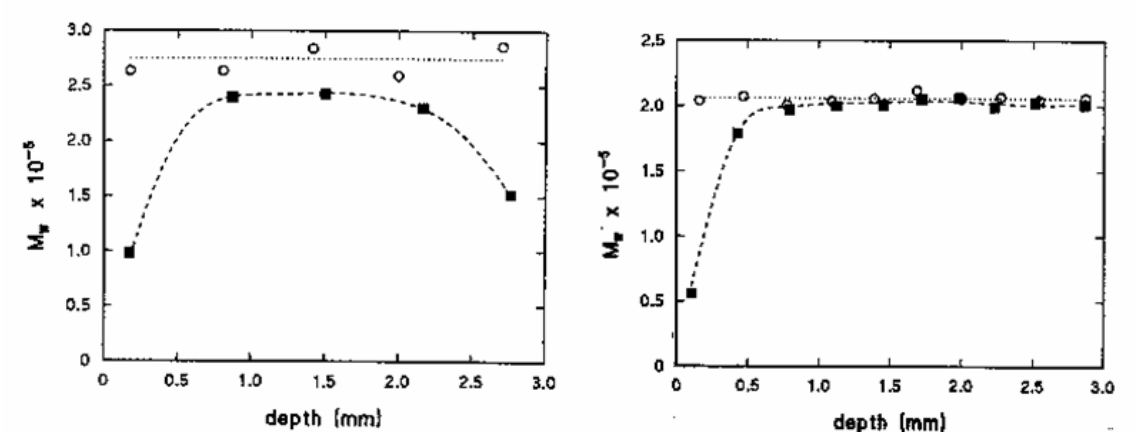

Figure 2-6 Mw vs. depth for an un-exposed bar (○) and for a similar bar after 5 weeks exposure to UV irradiation (■): PP (left) and GFPP (right)

As one can see, GFPP had slightly higher degradation than PP at the exposed surface, but almost no degradation anywhere else in the part, whereas PP has significant degradation at both the center and unexposed surfaces. This shows that GFPP is more susceptible to photooxidative degradation than PP where UV and oxygen are plentiful, but has much less UV-transmission than PP The greater susceptibility of the fiber-reinforced plastic (FRP) could do with the reported phenomenon of greater susceptibility at phase boundaries in plastics (Kaczmarek and Decker 1995).

The maximum degradation depth is proportional to the oxygen diffusion coefficient (which decreases with increasing crystallinity), and inversely proportional to the square root of the oxidation rate (Bruijn 1996). The max degradation depth has been shown correlated to the time to failure (Schoolenberg 1988b; Bruijn 1996).

Oxygen diffusion has been related to the diurnal cycle of sunlight. Bruijn (1996) compared the degradation depth profiles for Delft (The Netherlands) (natural sunlight), Florida (natural sunlight), Xenotest, and WOM. It was found that for Delft the maximum depth of degradation kept going deeper with time whereas the other three modes of UV

exposure reached a limit of maximum depth of oxidation. Bruijn suggested that this is because of the longer dark periods (at night) and hence longer periods without UV-induction of photooxidation. This allows for oxygen diffusion to carry oxygen to deeper layers instead of the reactive consumption of all the available oxygen at a certain depth (zero-order reaction-rate).

The degree of oxygen depletion in the center differs between polymers as well. A similar comparison was made in the same study (O'Donnell, White and Holding 1994) comparing the molecular weight change profiles for PP versus PS (polystyrene). Oxidation depletion in the center was reported to be more of a factor for PP than PS, and UV penetration is much greater in PS than in PP. This is probably due to the differences in functionalities present. Aromatic groups, like those in styrene, could promote light transmission through resonance. Oxygen diffusion is probably limited in PP because of the tighter packing of chains over PS (steric hindrance of the benzene group). Therefore, it is proposed that the greatest effect on depth-degradation profiles is the transmission and oxygen diffusion capabilities of the functionalities present.

2.5.6 Product Failure

The effect of photooxidation on service life must be kept in the context that this is only one possible means of failure in a plastic product. Lewis (2004) mentioned environmental factors as being only one of four factors leading to failure in polymers, the others being: the manufacturing process, the assembly process, and assembly loading or design considerations.

Also, failure of a product oftentimes depends on the designer's understanding of the environmental effects. This is why so much research has been devoted to the subject

of UV-induced photooxidation. While the environmental effects may cause failure of a plastic part at a particular time, it may only because of engineering error. Zielnik (2004) stated that the premature failure of plastics, including photooxidation-associated failure, can happen from:

- Bad design, including improper material formulation for the end-use environment
- Using the product outside of design criteria
- Changes to processes or materials that affect performance

The many concurrent chemical processes taking place in polymers exposed to UV radiation result in several different modes of degradation, each progressing at a different rate. It is usually the critical first-observed damage process that determines the useful service life of the product. For instance, a PVC part exposed to sunlight undergoes discoloration, chalking, loss of impact strength, and a reduction in tensile properties as well as a host of other chemical changes (Ranby and Rabek 1975).

It is, however, the discoloration (uneven yellowing) of the part that generally determines its service life. The consumer may demand its replacement based on this criterion alone. In less developed areas, however, these products often continue to be used despite changes in appearance or even after stages of damage become apparent. With continued use, however, other damage such as chalking and eventually loss of impact resistance (leading to cracking) can occur making the product even more unacceptable. Service-life is determined by both the customer's tolerance for degradation, and the relative rates of chain scission, cross-linking, and yellowing. In the end, it is the

customer who defines when failure occurs, and customers want it to both perform and look good through its expected service life.

Most polymers become stiffer and embrittled during UV exposure. The polymer no longer maintains its ductile qualities as it ages, which means that instead of recovering from local yielding, the part exhibits an unexpected brittle failure (Sandilands and White 1985; Lewis 2004). Küpper and others (2004) reported that weathering leads to brittle-failure in otherwise ductile plastic products, which results in a considerable reduction of their service life. Plastics exposed to outdoor conditions thus fracture easily, especially on impact.

Tensile properties have been shown to change only slightly with degradation - Carrasco and others (2001) showed an elongation decrease of 3020% in HDPE and a decrease of only 26% in tensile strength over the same period of exposure. Therefore, the increase in stiffness (modulus) is mainly due to the significant decrease in elongation. This embrittlement is reported to occur from two means: the breaking of bonds and subsequent reactions with oxygen, thus lowering the molecular weight (Ranby and Rabek 1975), and the initiation and propagation of surface cracks (Schoolenberg 1988a).

As discussed above, most degradation only affects a very thin surface layer and sometimes degradation only happens on that exposed surface. But even so small a depth of degradation compared to the whole wall thickness, a brittle-fracture of the product can occur (Küpper and others, 2004). Some might wonder how this endangers an entire part apart from surface cosmetic changes.

The answer to this question lies in the already mentioned development of surface cracks. The oxidized surface layer fractures at low loads or even spontaneously during

oxidative degradation. The result is a surface defect, from which final fracture appears easily through crack propagation, thus significantly lowering its impact resistance (Schoolenberg 1988a). Surface cracks also increase oxygen diffusion to the bulk, causing further degradation (Schoolenberg and Vink 1991).

The science of fracture mechanics can explain the strength of a product with a surface defect, as long as the size of the defect is known, as well as the fracture resistance of the material and the influence of the geometry. By measuring the lengths of the surface cracks on a degraded sample, Schoolenberg (1988a) was able to attempt application of fracture mechanics analysis to the degraded polypropylene. Both degraded and single-edge notched specimens (with simulated cracks created by razor blades) were compared with this analysis. Results showed that different fracture mechanisms occur at different periods of exposure, thus invalidating the comparison to simple fracture mechanics.

2.5.7 Stabilization

The resistance of polymers to UV degradation can be improved by the use of additives that absorb the UV radiation, or by coating them with another polymer that is opaque to UV radiation (Ranby and Rabek 1975). UV stabilizers work by either dissipating the absorbed energy by transferring it as heat to the surroundings, or by reemitting it at longer, safer, wavelengths through phosphorescence, fluorescence, or IR radiation (Rodriguez 1989). Use of a combination system of these two is often most effective. The two major producers of stabilizer packages are Ciba Specialty Chemicals (Tarrytown, N.Y.) and Cytec Industries (West Patterson, N.J.).

UV stabilizers include both UV absorbers and excited state quenchers. UV absorbers, like carbon black or titanium oxide, benzophenones, benzotriazoles, or

hydroxyphenyltriazines, function by competitively absorbing UV light and dissipate it through non-destructive pathways (heat/light)(regenerable). Carbon black is a frequently used stabilizer because of its low cost and efficiency at absorbing these wavelengths. However, it is hard to clean from molds and limited cosmetically. So other, more expensive additives like titanium dioxide and benzophenones are also commonly used (Strong 2006). Excited state quenchers accept the energy from sensitized chromophores (making them non-sensitized) and also dissipate it through non-destructive pathways (also regenerable).

Oxidation quenchers are used in many stages of a polymer's life to stabilize it in our earth's atmosphere. Radical scavengers, like hydroquinones, find hydroperoxy or alkyl radicals and readily quench them by giving up hydrogen atoms (non-regenerable).

HALS (hindered amine light stabilizers) are multi-purpose chemicals that act as radical scavengers, alkyl hydroperoxide decomposers, and excited state quenchers. They cannot be used in many applications, however, because of their alkaline reactive nature, making them initiation sites for oxidation reactions (Makowsik, Samuels and Wagner 1995). This demonstrates the importance of careful testing of the additives chosen for a product.

This reactivity hazard of some stabilizers, along with the multitude of selection criteria to evaluate, makes choosing the right stabilizer a difficult task. To choose a UV absorber, activation spectra maxima data must be examined to find out what wavelengths the material is most sensitive to. In general, the lower the wavelength, the more sensitive. But there are nodes along a graph of this relationship, showing wavelengths where it is particularly sensitive.

Other absorber selection criteria (Bonekamp and Maecker 1994) include:

- Thickness of the polymer substrate (should it be a coating or mixed through?)
- Solubility/migration (controlled by molecular weight - higher weight for harder parts)
- Permanence of the UV absorber (how long will it work?)
- Chemical reactivity of the absorber in the polymer degradation process

Complications and problems of stabilizers

The physical loss of the stabilizer has been shown to occur by photochemical reactions and degradation (Bell and others, 1994). Loss of the stabilizer can also occur by diffusion to the polymer surface during exposure (Billingham 1990), particularly often in products with high surface-to-volume ratios, i.e. fibers, thin films, coatings, etc. This loss accelerates the ageing of polymers more than thermal-oxidation or photo-oxidation (Scoponi, Cimmino and Kaci 2000).

Characterizing the amount and type of stabilizers in a plastic has been a big business in the last few years. The trend seems to be that more and more companies make claims of UV-stability without understanding the true performance of their product against weathering. This oftentimes leaves the responsibility of accurate service life prediction with the buyer. Furthermore, the rapid loss of many stabilizers through degradation time necessitates characterization to understand how stabilized the product will be.

Many of the chemical analysis methods described in Section 2-6 have been used to follow or determine the concentration of stabilizers. UV spectroscopy after extraction

(Vandenburg and others, 1997) and FTIR-ATR (Scoponi, Cimmino and Kaci 2000) are the most commonly used methods.

2.6 Characterization of Degraded Polymers

As mentioned in Section 2-3, Ranby and Rabek (1975) stated that the challenge to outdoor weathering testing is answering the two questions:

1. What should the experimental conditions be to replicate the desired exposure?
2. How can the changes that occur to the sample be best characterized, i.e., how should the chemical/mechanical changes be evaluated?

The literature is full of attempts at answering these questions. The first deals with simulation of the environment and the second, how to monitor the effects of the weathering. The former question has been discussed in detail above. The latter question, characterization of degradation, is the subject of this section. The need to answer this question has prompted the application of many standard mechanical properties tests to plastics, induced the creation of new tests to better monitor a specific change, and driven technology to create new monitoring equipment.

That which is to be characterized, the changes to a plastic during degradation, can be summarized by the combination of physical, mechanical property, and chemical changes. As already mentioned: the physical manifestations of photooxidative degradation include loss of transmissivity and discoloration (Strong 2006). The loss of mechanical properties usually involves embrittlement and stiffening (Schoolenberg 1988a). Chemical property changes include crystallinity and molecular weight changes, and evolution of oxidation products (Gulmine and others, 2003).

2.6.1 Physical Properties

As mentioned in Section 2-5, one result of oxidative degradation is the discoloration or "yellowing" of the surface. This is the easiest way to detect degradation in a plastic – it can be done with a simple visual glance at the surface. Inexpensive spectrophotometers are available, which can quantify the discoloration and measure the color shift on sample surfaces over time of degradation to show a profile of "yellowness". This is called a "Yellowness" Index Test when seen in the literature (Makowsik, Samuels and Wagner 1995). This only applies, however, to white or other similarly bright colors of material as the yellowness is overwhelmed by any dark colorants.

The other physical property change during degradation able to be characterized by the naked eye is surface cracking. This is usually described in the literature as length and concentration of cracks, which are determined through the aid of simple light microscopy or scanning electron microscopy.

2.6.2 Mechanical Properties

Elongation

Tensile elongation-to-break has been found to be the most sensitive mechanical property to weathering in PE and has thus been used extensively as the property to monitor throughout UV-induced photooxidation of a variety of polymers (Bruijn 1996; Gijsman, Hennekens and Janssen 1996; Gillen and Clough 1991; Yakimets, Lai and Guigon, 2004; Carrasco and others, 2001).

Testing is usually done according to ASTM D 638 ("ASTM Reference Manual" 2001). Failure of a sample is usually considered as the "half-time" of the property, i.e. the

degradation time at which a 50% decrease of some property is observed. This half-time rule is frequently applied to elongation profiles to compute a t_{fail} (time to failure) (Schoolenberg 1988a; Strong 2002).

Impact strength

Although elongation is the most sensitive property in monitoring oxidation degradation, and therefore the most widely used, it isn't critical in determining service life, as long as the yield point doesn't change. As already mentioned, failure of a plastic product is more often determined by its decrease in impact strength (higher deformation rates) as its behavior changes from ductile to brittle (Schoolenberg 1988a). Therefore, impact strength testing is considered the principle mode of failure and a good property-candidate to monitor (Strong 2002). This is usually either done by ASTM D 256 ("Izod" or "Charpy" methods) or ASTM D 3763 (with a "Dynatup" tester).

Molecular weight

Molecular weight (MW) is the most direct measure of the loss of mechanical properties (Strong 2002). High MW materials exhibit high mechanical properties, and vice-versa. Chain scission during degradation will cause a general trend of decreasing MW that has been reported (Lemaire and others, 1996; Karlsson, Hakkarainen and Albertsson 1997; Srinivasan, Braren and Casey 1990; O'Donnell, White and Holding 1994).

Molecular weight can be measured by a variety of instruments. A simple method yet effective method of measurement is through a melt index test (ASTM D 1238), where

the sample is heated and the rate of melting extrude falling from the solid is inversely proportional to the MW, as the melting point is a direct consequence of MW.

The degradation monitoring of MW causes confusion sometimes, however, because although it usually decreases over time (chain scission), it can also increase due to cross-linking or other reaction mechanisms (Onyiriuka 1993; Osawa and others, 1996). Thus, it can show different profiles with different mechanisms of degradation.

Density

Density has been monitored through photooxidation in the literature (Bruijn 1996; Gulmine and others, 2003). During photooxidation, density has been reported to increase because of a phenomenon known as "chemi-crystallization" (Winslow 1979), the increase in polar groups (Reich and Stivala 1971), and oxygen uptake (Bruijn 1996). Chemi-crystallization is when molecular chain scissions in the amorphous phase at the sample surface (chemical degradation) initiate the process of rearranging of cut molecular chains into a crystalline phase (Winslow 1979). It has been attributed to account for a portion of the acceleration phase in the property profiles during photooxidative degradation (Yakimets, Lai and Guigon, 2004).

The monitoring of density has been carried out through a variety of methods including ASTM D 792 or ASTM C 693. Density profiling has been reported to mirror the changes in crystallinity during degradation (Gulmine and others, 2003), thus making difficult and expensive differential scanning calorimetry (DSC) measurements of crystallinity unnecessary.

Tensile Strength

The tensile strength has been profiled through degradation but has frequently proven to not show good trends (Gillen, Clough and Wise 1996). Slight, linear decreases in tensile strength have been reported (Yakimets, Lai and Guigon, 2004), but so have slight increases at first followed by slight decreases (Carrasco and others, 2001). Tensile strength depends on the integrated strength of the entire bulk more than the surface-dependence in elongation failure. And the mechanisms behind its profile are different with time (either cross-linking or chain-scission), causing both increases and decreases in the property. Therefore, it is not a recommended property to profile with degradation.

Modulus

The tensile modulus, or Young's modulus, is a direct measure of stiffness. It is simply the slope of the stress-strain curve in tensile property testing according to ASTM D 638. Modulus can be inferred from the changes in elongation and tensile strength. AS mentioned in Section 2-5, most polymers undergo rapid changes in elongation and slight changes in tensile strength during photooxidation, which infers an increase in the slope of the stress-strain curve and an increase in modulus. The stiffening of polymers has been substantiated by a number of studies (Tavares and others, 2003; Carrasco and others, 2001; Gillen, Clough, and Wise 1996).

Hardness

Measurements of plastic hardness are made using a simple Shore D Durometer by ASTM D 2240. The surface hardness of a sample is directly related to the modulus.

Oxidation of plastics has been shown to cause an increase in hardness similar to that of the modulus (Gulmine and others, 2003). Tavares and others (2003) reported a 3x increase in surface hardness in LDPE and a 5x increase in modulus after the same duration of UV exposure, a comparable change.

2.6.3 Chemical Properties

The analysis of the chemical changes in a substance is far less standardized than mechanical testing. This is due to the continual advancement in technology that continues to enable better analysis and characterization of chemical changes (Bataillard, Evangelista and Thomas 2001). To understand what methods have been used in the literature, the technologies are presented here in order of complexity and chronology of development.

Chromatography

Chromatography refers to a family of tests to separate mixtures. A mixture containing the analyte is passed through a stationary phase that separates and isolates the analyte from the rest of the mixture. All chromatography methods require an extraction method specifically chosen for a particular functionality chosen as a "target" for analysis (Vandenburg and others, 1997). For polymers, this usually implies dissolving or swelling the polymer in an organic solvent and then precipitating it, leaving the specific compounds with particular chemical functionalities. This requires an understanding of the probable degradation mechanisms to choose what reaction products to look for, and becomes more difficult as the number of examined products increases.

In thin layer chromatography (TLC), the material is chromatographed on a glass plate coated with a stationary phase. When the edge of this plate is placed in a solvent, each compound present migrates up the plate a distance known as the R_f value. The distance migrated by a particular compound depends upon its chemical functionality and therefore can differentiate between compound types. This method uses inexpensive equipment and is easy to analyze, but sample preparation can take a long time, and the analysis produces very low resolution. It is difficult to differentiate between the oxidized products of the same family (Bataillard, Evangelista and Thomas 2001). TLC is not used anymore as a quantification tool by itself (Airaudo and others, 1988).

High performance liquid chromatography (HPLC) is the most common technique for additive analysis (Bataillard, Evangelista and Thomas 2001). A solvent system is pumped through a column packed with a stationary phase. The compounds are separated according to their affinity/partition between the mobile phase and the stationary phase. HPLC is a commonly used analytic in profiling the molecular weight changes in photooxidation (Piton and Rivaton 1997). HPLC is more expensive and more difficult to analyze then TLC (Dorsey and others, 1996). And like TLC, HPLC is not well suited for quantification.

Reverse phase, normal phase, and gel permeation chromatography (GPC) are all types of HPLC. In GPC, the column packing has pores in it, and the separation mechanism is by the molecular weight or apparent size of the analytes (Marcato, Fantazzini and Sevini 1991). Therefore, GPC has also commonly been used to monitor changes in MW (Karlsson, Hakkarainen and Albertsson 1997). O'Donnell, White and Holding (1994) describe GPC as “the simplest and most effective way to monitor MW

during artificial weathering, but with inherent shortcomings to reproducibility." GPC has also been used to monitor oxygen uptake during degradation (Gijsman, Meijers and Vitarelli 1999; Gillen, Clough and Wise 1996). A disadvantage in GPC profiling, like all chromatography methods, is that the extraction required before analysis makes it a very slow test compared to other characterization methods. Unless the samples are very clean and free from oligomeric material or soluble polymeric material, GC can prove to be expensive and frustrating (Bataillard, Evangelista and Thomas 2001).

Spectroscopy

Spectroscopic analysis involves the interactions between energy and the analyzed matter. The reported interactions are compared to published standards to determine the characterization of the sample. Spectroscopic characterization includes chemical structure, molecular environment, polymer tacticity and conformation, and to monitor changes in these properties following external perturbations (Ghiggino 1989). Spectroscopic testing methods are more specialized and expensive than the commonly used chromatography methods. An advantage of spectroscopy is its ability to not only quantify chemical changes with good resolution, but also to provide qualitative or structural analysis of all compounds contained in the sample (Bataillard, Evangelista and Thomas 2001). Another advantage over other means of polymer characterization is that spectroscopic measurements are non-destructive and generally quicker to perform (Ghiggino 1989).

Ultraviolet spectroscopy (UVS)

Because the basic polymer structures in polyolefins are mostly transparent in the UV region, the UV absorbance of other functional groups can be easily detected without substrate interference. UVS relies on relatively broad band spectra to show the existence of chemical functionalities. This makes it more of a quantitative tool than a qualitative one, due to the lower resolution when compared to other spectroscopic methods, causing the overlaps of many similar functionalities. UVS is the cheapest and easiest to operate of all the spectroscopic methods (Bataillard, Evangelista and Thomas 2001).

Fourier transform infrared spectroscopy (FTIRS)

In contrast to UVS, FTIRS has a very detailed spectral analysis and is useful for the characterization (quantitative and qualitative) of samples with much different functionality. Its high resolution has made FTIRS a frequently used tool in profiling the effects of polymer degradation (McKelvy and others, 1996; Ghiggino 1989). The extent of oxidation is usually expressed as the absorbance of carbonyl end-groups, and is reported as the carbonyl index: the ratio of carbonyl-E_{1720} absorbance to methylene-E_{2020} absorbance. The comparison of absorbances across time has been expressed as the profile of crystallinity in the degradation of PP (Yakimets, Lai and Guigon 2004).

Sample preparation is minimal compared to all previously described methods of characterization. A thin layer of material is required for transmission. Polymer pellets can be flattened into thin films to be analyzed by the variety of IR and "Raman" microscopes that employ FTIRS (Bataillard, Evangelista and Thomas 2001). A disadvantage of FTIRS is that samples containing very strong absorbing chromophores, such as carbon black or

other pigments, are not suitable for direct IR analysis as the absorbance of the matrix overcomes any absorbance from the additive (Bataillard, Evangelista and Thomas 2001). Another disadvantage is the time requirement to do the microtoming and readings for depth profiles (Schoolenberg and Vink 1991).

Attenuated total reflectance (FTIRS-ATR)

FTIRS can be modified to pay particular attention to the surface of a sample through the use of attenuated total reflectance (ATR) cells. When using ATR, the IR light penetrates only into the top 20 microns of the sample. So while characterization resolution is higher than for any other of the methods described, it is not employed to characterize the bulk of any non-film sample. IR signals acquired with an ATR can measure very small levels of chemical functional groups on the surface of a sample with low noise and relatively good resolution (Bataillard, Evangelista and Thomas 2001).

The problem with this method is the expense of the machine, the required peak-identification knowledge, and the rigidity of plastics. FTIR works best when you can spread the material over the viewing crystal for high contact area. Most products made from the commodity plastics are rigid enough to cause problems with repeatability with this method. This often becomes the challenge in ATR and requires some time and creativity (Küpper and others, 2004).

Despite these challenges, FTIRS-ATR is the most common tool in polymer oxidation degradation studies because of the surface-limited nature of oxidation as diffusivity hinders UV and oxygen from causing changes deeper into the bulk (as described in Section 2-5). The indication of oxidative degradation of polymers in FTIRS-

ATR, like FTIR, is usually the observation of carboxyl end-groups. A comparison can be made between the relative intensity of the carbonyl absorption band (1715 cm^{-1}), and then for vinyl groups and any other groups associated with the end products of oxidative reactions. In this way, the degradation profiling is not limited to the detection of one particular chemical reaction mechanism (Küpper and others, 2004; Fechine and others, 2004).

There are also techniques in the literature describing ways to isolate particular groups to assist in quantitative and qualitative studies. One such (Tidjani 2000) study describes chemical treatments to:

- Make the detection of something easier: NO gas reacts with hydroperoxides and alcohols to make a more easily detected compound
- Pull something out of a band to see what and how much of other related compounds are in the remainder: acid groups react with SF_4, so the residual carbonyl band only shows ketone and ester species

One advantage of FTIR-ATR is the ease with which it can do profiling by depth or some other sample. By varying the angle of incidence in ATR, it is possible to detect variations in composition of distinct layers from the surface down to a depth of 1.2 μm. Deeper layers can be analyzed only by microtoming the sample (Gulmine and others, 2003).

A disadvantage to all transmission spectroscopy methods is that analysis relies on an understanding of the reaction mechanism, enough so to predict which functionalities to look for. The carbonyl index has been shown to monitor degradation with suitable correlation to accompanying mechanical property changes, but this relies on the

assumption that all mechanisms of degradation that occur will be equally represented by carbonyl formation. Perhaps the reason why it sometimes does not show resolution or clear trends when profiling degradation (Bruijn 1996) is that the mechanism is producing a different reactive product.

Mass spectroscopy (MS)

In MS, molecules in the sample are ionized with energy and then separated according to each of their mass to charge ratios. Molecules fragment under this ionization in reproducible patterns, thus allowing determination of the original structure of the molecule from the spectrum of the fragment ions (Bataillard, Evangelista and Thomas 2001). MS is mostly a quantitative tool, but has advantages in quantification as it requires very little sample and has low detection limits. Direct analysis of stabilized polymers may be achieved by electron impact mass spectroscopy (EI/MS). Static secondary ion mass spectroscopy (SIMS) has been used to monitor the extent of oxidation (Onyiriuka 1993).

X-ray photoelectron spectroscopy (XPS)

In XPS, the ratio of oxygen atoms to carbon atoms for a microscopic area on the sample surface can be reported as the extent of oxidation (Onyiriuka 1993). The problem with this method is that XPS can only report the oxygen number corresponding to the top 100 angstroms of the sample, and no deeper (even shallower than ATR). The resolution may be better than with FTIRS-ATR, but XPS may not be able to look deep enough to see the majority of the oxidation products (Favez and others, 2002; Wu and others, 2000; Brewis, Dahm and Mathieson 2000). An advantage of XPS over FTIR-ATR is that its

analysis incorporates all possible functional groups of oxidative products at once – the accompanying disadvantage is that without the separation of functionalities, no analysis of reaction mechanisms based on particular end-products can be made.

Energy dispersive x-ray spectroscopy (EDS)

Scanning electron microscopes function by "scanning" an electron beam across the sample. This produces a signal that can be detected and processed into an image. Several types of detectors can be installed on the microscope to detect the different available signals. One such detector is the energy dispersive x-ray spectroscopy (EDS) detector. EDS looks at the characteristic x-rays being fluoresced from the sample and determines the elements in the sample based on the energy of each of the x-ray lines produced. Chemical analysis (microanalysis) is performed by measuring the wavelength and intensity distribution of the X-ray signal generated by a focused electron beam on the specimen. Like XPS, the surface is mapped to see relative concentrations of atomic elements (Gulmine and others, 2003). The ratio of oxygen atoms to carbon atoms for a microscopic area on the sample surface can thus be reported for oxidation characterization. EDS, however, can report the oxygen number for deeper areas than XPS by simply increasing the voltage of the electron beam. This enables relatively easy depth profiling as well. EDS has the same advantage/disadvantage of looking at all the atoms at once, thus incorporating all functional groups, but losing the ability to individually analyze particular functionalities.

EDS is also a powerful tool for qualitative x-ray microanalysis. The fact that the total spectrum of interest, from 0.1 to the beam energy (e.g. 29 kV) can be acquired in a

short time (10-100 s) allows for a rapid evaluation of the specimen constituents (Goldstein 2003). The resultant spectra can be easily analyzed with computer programs for other trace elements from impurities or additives. Surface mapping by Gulmine and others (Goldstein 2003) of PE samples deduced the presence of sodium chloride (NaCl), silicon oxide (SiO_2), and aluminum oxide (Al_2O_3), all salts from the water sprayed on the samples in the WOM, showing the need for thorough sample cleaning (Gulmine and others, 2003).

A typical EDS spectrum for a lightly oxidized PE sample from the City of Los Angeles' trash cart study is presented in Figure 2-7. The large peak represents the high concentration of carbon, and the only other significant peak is represented by the small amount of oxygen present.

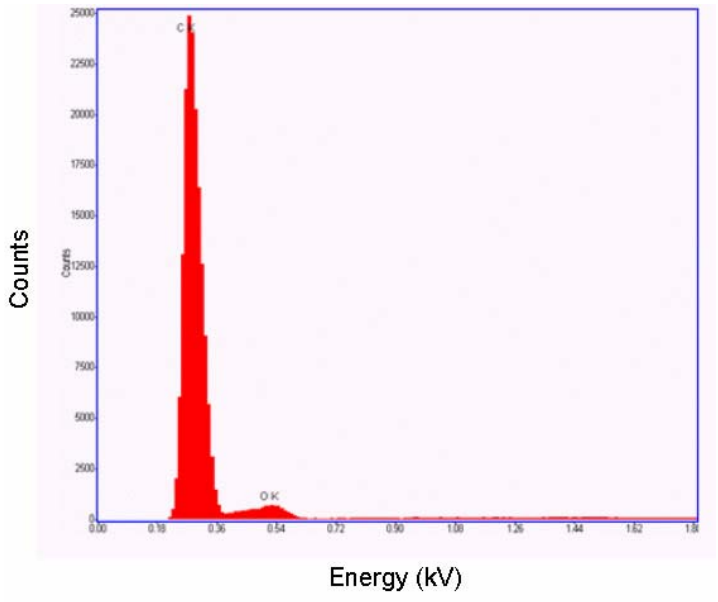

Figure 2-7 Typical EDS Spectrum

Environmental scanning electron microscopy (SEM)

To understand the value of EDS analysis, the recent development of environmental scanning electron microscopy (ESEM) must be understood. Three usual challenges to the SEM analysis of polymers are: bond breakage, mass loss, and a decrease in crystallinity. All of these changes are incident to the ionizing radiation and thermal effects of the high vacuum electron bombardment (Sawyer and Grubb 1996). ESEM minimizes these problems by only allowing the incident beam to affect a very small area of the sample and by leaving the environment in the sample chamber similar to the ambient. Both of these differences from traditional SEM's are allowed by the use of a pressure-limiting aperture (PLA): a very thin hole at the end of the column that constricts passage of the incident beam (focus of beam on small area). The PLA is so small that the pressure above it, in the incident beam generation column, can be kept at a low pressure to minimize gaseous deterrence of the beam, even when the sample chamber (on the other side of the PLA) has a much higher pressure (Goldstein and others, 2003).

The high pressure of the sample chamber allows water to be kept as mist in chamber. This is impossible in traditional SEM's because the high vacuum makes pressures that always are below the triple point of the water phase chart - no liquid phase, only solid to gaseous. Allowance of a water mist in the chamber helps prevent drying of the sample during the pumping of the chamber (Goldstein and others, 2003).

This suggests that the hydrogen and oxygen of the water vapor might adversely affect elemental analysis of the sample surface, especially when small amounts of oxygen are being profiled. But the amount of water vapor is small (insignificant), and in profiling studies the relative change in oxygen concentration is examined, not the absolute

quantification. As long as the concentration of water vapor in the chamber remains constant, this will not affect oxygen content profiles during degradation.

Polyethylene, as well as most other commodity-resins, is a poor/non-conductor. Traditional SEM beam electrons therefore impinge on the surface and cannot be re-transmitted from the surface, creating a differential charge in relation to the chamber environment vacuum, thus distorting the image. This is why SEM studies of polymers usually require the time and resources of sputter coating a thin layer of conductive material (gold/silver/copper) on the sample. EDS analysis in this manner for one study thus had to explain the presence of a strong gold (Au) peak due this sputter coating (Gulmine and others, 2003).

The ESEM allows good surface analysis of polymers without needing to make them more conductive because of the gas that is left in the chamber (low vacuum). Electrons ionize some of the gas particles in the chamber, helping maintain the charge balance at the surface during electron impingement from the incident beam (Goldstein and others, 2003). This is a tremendous development as it minimizes the time and resources needed for sample preparation.

2.6.4 Shape of Degradation Profiles

The monitoring of photodegradation provides resultant data according to the characterization methods listed above, which when profiled against time, often show recognizable trends. The data can oftentimes be fit well (with low residual error) to a function of the property change versus time. This is done to understand this relationship over all times – in between the data points measured, as well as before (early performance) and after the exposure duration (future performance). With such a function,

a prediction can be made as to how much time of exposure will lead to a certain degree of change in a property.

The most widely accepted standard for a property change amount representing time to failure of a plastic part is the "half-time", or degradation time at which a 50% decrease of some property is observed (Schoolenberg 1988a; Strong 2002). As already mentioned, the "half-time" of degradation is usually applied to elongation, but has been applied to many other mechanical and chemical property profiles.

Some studies have reported linear profiles in degradation studies. The polymers studied, and properties with reported linear profiles (against time) for some of these studies are:

- PP: decrease tensile, decrease limit of viscosity (Yakimets, Lai and Guigon 2004)
- LDPE: carbonyl and vinyl absorbances (Scoponi, Cimmino and Kaci 2000)
- PE: carbonyl absorbance (Karlsson, Hakkarainen and Albertsson 1997)
- PE, PP, PBT: oxygen uptake (Gijsman, Meijers and Vitarelli 1999)
- PS: oxygen/carbon ratio (Onyiriuka 1993)

Other studies have reported non-linear behavior and fit the data to theoretical models based on known chemical relationships. Many of the non-linear profiles have been shown to follow a three-step pattern:

1. Slow change or no change initially (incubation)
2. Followed by a sharp and dramatic change (acceleration)
3. Until a limit is reached whereupon the property does not show any further change (stabilization)

This agrees with the 4-stage auto-oxidative mechanism (Gijsman, Meijers and Vitarelli 1999) mentioned in Section 2-5 (Figure 2-1):

1. Incubation is the initiation stage of free radical generation
2. Acceleration is the 2nd stage of oxidation-propagation and the simultaneous 4th stage of hydroperoxide decomposition stage, with rate determined by the 3rd stage (termination)
3. Stabilization is a point where the 2nd and 4th stages can proceed no further due to oxygen saturation, where the 3rd stage (termination) dominates

There are many studies in the literature exhibiting this 3-part pattern of behavior. In a study of the photo-degradation of PP, the lowering of Young's modulus was split into four stages: incubation period (3–5 days), period of decrease of Young's modulus caused by surface cracks (5 days–3 weeks), period of decrease of Young's modulus caused by surface cracks and chemi-crystallization (3–5 weeks) and period of stabilization (5–7 weeks) (Yakimets, Lai and Guigon, 2004). In another study, FTIR-ATR analysis showed the profiles during oxidation of ketones, aldehydes, acids, and alcohols to exhibit an induction period before a rapid increase in concentration to a steady increase with time, which was interpreted as the limiting oxidation rate of the polymer (Vink 1979).

Reports showing parts of this pattern are even more numerous:

- For times of 200 h and lower (WOM and QUV) the variations in surface mechanical properties of LDPE were small and restricted to a thin layer. A significant increase in modulus, surface hardness, and depth of oxidation followed this incubation time (Tavares and others, 2003).

- The elongation of HDPE strongly decreased at 120 days of exposure – from 231% to 7.4 % (relative decrease of 3020%), with a remarkable drop off at 60 days. This fall in elongation corresponded to a notable increase at the same time in carbonyl absorbance (Carrasco and others, 2001).
- Elongation at break (for LDPE) in accelerated weathering stayed at desirable levels until a certain carbonyl absorbance (0.075) and then fell dramatically to its lowest value (Tidjani 2000)
- The degradation of elongation due to UV irradiation was divided into two periods, i.e., the degradation-incubation period and degradation development period. The elongation did not change in the first period, and gradually decreased with increase of the integrated UV irradiation energy ("Railway Gazette International" 1994).
- Thermooxidation showed an incubation time in oxygen uptake for PP (Gijsman, Meijers and Vitarelli 1999)
- The oxidation of PP showed an incubation period followed by a sudden increase in rate (Celina, George and Billingham 1996).
- The incubation period and later increase in oxidation rate with time was shown in HDPE (Bruijn 1996).
- Carbonyl absorbance of PP leveled off at about 450 hours on the surface, and did not go any higher (Schoolenberg 1988a).

The initiation stage was described attributed to localized "hot-spots" by Celina, George and Billingham (1996). The oxidation of PP was initiated in localized centers, possibly associated with catalyst residues or other defects. Stabilizers were unable to

prevent this, but limited the spreading. The induction period is when oxidation is still limited to these centers and begins to spread between them, after which oxidation happens across the surface and moves to the acceleration phase.

Yakimets, Lai and Guigon (2004) explained the acceleration stage in elongation decrease as a two-part process. For the first half of acceleration, surface crack propagation causes the sudden decrease in elongation. For the second half, the surface crack propagation effect on elongation is supplemented by the "chemi-crystallization" already described.

The stabilization stage of oxidation after a certain duration of exposure is characterized by no appearance of new cracks on the surface and exposed surfaces are completely photo-oxidized. There is no access of O_2 to further depths in the sample because of diffusion limits; so ageing is saturated on the surface.

2.6.5 Arrhenius Modeling

The 3-step oxidation and degradation profiles described above have oftentimes been fit to the Arrhenius equation (Gillen, Clough and Wise 1996; Bruijn 1996). The rate of a chemical reaction was first shown formally to be an exponential function of temperature in 1886 by Savante Arrhenius. This function has since been called the Arrhenius equation, shown in Equation 2-4.

$$K = A \cdot e^{(-E_a / R \cdot T)} \qquad \textbf{(2-4)}$$

K is the chemical reaction rate coefficient, A is a constant, E_a is the activation energy of the compound, R is the universal gas constant [0.008314 kJ/(mol·K)], and T is the temperature in degrees Kelvin. The constant A represents the effectiveness of

collisions between the reacting species ("collision factor") (Strong 2006). According to this model, the rate of the reaction approximately doubles with every 10 K (or 10°C) rise in temperature.

The activation energy of a compound is dependent on the energy required to break the bonds that are split in the reaction. Bond dissociation energies of three typical bonds broken in oxidation are (Ranby and Rabek 1975):

- C-C: 351 (kJ/mol)
- C-H: 414
- O-O: 213

Predicting the complex reaction mechanisms that occur to quantify how much bond energy will be required is difficult. The activation energy of plastics in UV-induced oxidation has been inferred from measurements of reaction rates and reported as ~56 kJ/mole (Vincent, Jansen and Nijsten 1982) and 92 kJ/mol for thermal oxidation (Gillen, Clough and Wise 1996).

The Arrhenius equation has also been applied to many other profiles not involving chemical reactions, such as diffusion, viscous flow, and electrolytic conduction (Strong 2006). For example, diffusion at different temperatures has been described with a modified form of the Arrhenius equation:

$$D = D_0 \cdot e^{(-A/R \cdot \Delta T)} \qquad \textbf{(2-5)}$$

D represents the diffusion rate at a new temperature when compared to the standard diffusion rate, D_0, at a standard temperature. The difference between the

standard and new temperatures is ΔT. A represents the energy required for gas or liquid to pass through the molecules of the material (Strong 2006).

Bruijn (1996) proposed a version of the Arrhenius prediction of reaction rate that accounts for UV intensity:

$$K = k_0 \cdot e^{(-E_a / R \cdot T)} \cdot I^{\alpha} \quad \textbf{(2-6)}$$

K is the reaction rate as a function of the activation energy, temperature, and UV intensity (I). I is the cumulative radiant exposure at the time to failure divided by the time to failure, thus normalizing the irradiance by time to predict a constant intensity of radiation. The standard reaction rate, k_0, and the degree of stabilization, α, are also constants.

Bruijn exposed HDPE to two natural environments and two accelerated environments and then correlated oxidation reaction rates to elongation profiles and found that all environments reached time to failure of the part (50% decrease in elongation) at the same critical reaction rate. A profile of the reaction rate could thus be used to predict the service life of a plastic part.

In fitting oxidation profiles to this equation, Bruijn also reported no appreciable difference in reaction rate with small changes in temperature (27-35 ˚C), and that the modeling fit the data better when the differences in temperature were not accounted for.

Another example of Arrhenius fitting is Gillen, Clough and Wise (1996), where thermal oxidation acceleration (not UV-induced) of nitrile, SBR, and neoprene rubber was monitored by elongation, tensile strength and oxygen consumption. Oxygen consumption was shown to be linear with exposure time. Elongation showed good

Arrhenius behavior, but the tensile data did not show either a linear profile or a profile that could be fit to the Arrhenius equation. They proposed this difference to result from the test failure mode. Elongation to break in oxidated samples results from crack initiation and propagation of cracks throughout cross-section Tensile strength is the integrated strength over entire cross-section at failure, and is not as dependent on surface defects as elongation, due to spatially non-uniform degradation, or the depth profiles discussed in Section 2-5.

The Arrhenius profile of the elongation data was successfully expressed as a linear relationship in this same study by graphing the log of the time to a certain elongation change (25%, 50% and 75%) against the inverse of the temperature. To correlate this thermal degradation relationship to photodegradation, the equivalent of the temperature change for photodegradation must be selected. The irradiance is proposed as a possible equivalent to the temperature change for such a relationship. Theoretically, by doing the same comparison with a number of different degradation environments with different irradiances, the elongation profile could be similarly expressed.

2.6.6 Correlation

Two reported successful correlations have just been mentioned (Bruijn 1996; Gillen, Clough and Wise 1996), between the mechanical and chemical property profiles. Such correlations have tremendous potential, as they can predict mechanical property profiles after only relatively quick, non-destructive measurements of the chemical property changes (Gijsman, Hennekens and Janssen 1996).

Other correlations preformed in the literature include:

- The carbonyl absorbance (CA; representing the extent of oxidation) of HDPE is linear when plotted against the percent change in elongation (Carrasco and others, 2001). This came from agreement of the sharp increase in elongation during the acceleration phase with a corresponding sharp increase in the carbonyl index at the same time
- The CA in LDPE was correlated to modulus (Tavares and others, 2003).
- The CA's of LDPE, LLDPE, and HDPE were correlated to density (Gulmine and others, 2003).
- The vinyl absorbance of HDPE was correlated to density and elongation (Bruijn 1996).
- The CA of PP was correlated to elongation (Schoolenberg and Vink 1991).

All of these correlations are based on similar times of acceleration in both mechanical property changes and oxidation. This implies Arrhenius fitting based on the typical 3-step pattern of oxidation. But the application of the Arrhenius equation to the reaction rates of oxidation in UV-induced degradation of plastics has been shown to be hindered by the changes in behavior of the oxidation at low temperatures (Miller and Maguire 1995). The activation energy cannot be assumed to be constant. Thus, the prediction of oxidation behavior for a particular system remains dependent on rigorous sampling of the behavior of the system before being able to model it. The challenge however, then returns to the questions posed by Ranby and Rabek: how to, first, simulate the environment, and second, characterize the changes.

3 Methodology

3.1 Sample Preparation

3.1.1 Polyethylene

Rehrig Pacific manufactured injection molded polyethylene trash carts for the City of Los Angeles in 3 sizes: 35, 65 and 95 gallons. The carts came in four colors: black, green, blue, and brown. All the carts have UV-screeners (HALS) and no absorbers (besides 1.2% carbon black in the black carts). Specimens were cut from standard carts taken from the field or straight from natural production after delivery to the City.

Some 95 gallon green carts were obtained with the designation 'FA', denoting "fully automated". These carts were injection molded in a fully automated process of injection molding as opposed to the semi-automatic injection molding used in all the other carts.

Sample sets were designated as follows:

- W: Weather-Ometer (accelerated UV exposure)
- C: Control (placed in darkroom)
- SC: Special-control (wrapped in foil and placed in a freezer)
- N: No-Load (outdoor-exposed carts obtained from the field at test intervals)

- L: Loaded (outdoor-exposed carts with the actual applied load that home owner put in the trash cart on the street during exposure)

The 'W' samples were placed in the Weather-Ometer and pulled out at time intervals specified in Table 3-1. Control samples (C) were left in a darkroom, and special-control samples (SC) were wrapped in foil and placed in a freezer, both to be taken out and tested at the same time as the 'W' samples. For 'N' and 'L' samples, trash carts were taken from the field for longer periods of time because of the slower oxidation associated with natural sunlight when compared to the Weather-Ometer. Short period testing was performed on the 'W', 'C', and 'SC' samples at the beginning to watch for early trends and failures in the accelerated degradation profiles.

Table 3-1 Los Angeles testing schedule

Time	Period for W, C, and SC	Period for N, L
1	3 Months	6 Months
2	6 Months	1 Year
3	1 Year	1 Year, 6 Months
4	1 Year, 6 Months	2 Years
5	2 Years	2 Years, 6 Months
6	3 Years	3 Years

For each sample set, three tensile samples (each from a different size cart) for each color of black, green, and blue, as well as one sample of green "FA", and 1 sample of brown, were cut from the carts. The samples were numbered by color and size according to Table 3-2. This was repeated to cut out izod impact samples as well.

Table 3-2 Los Angeles sample cart color and size

Sample Number	Description
1	Black 65 Gallon
2	Black 95 Gallon
3	Green 65 Gallon
4	Green 95 Gallon
5	Green 95 Gallon FA
6	Blue 65 Gallon
7	Blue 95 Gallon
8	Black 35 Gallon
9	Green 35 Gallon
10	Blue 35 Gallon
11	Brown 65 Gallon

Samples were each assigned an ID based upon the following key: (Letter denoting sample set)(sample number – color/size) – (time period). For example: W3-2 denotes the Weather-Ometer-exposed ('W'), Green 65 Gallon sample ('3'), with 6 months of exposure ('- 2').

Most of the tensile- and impact-tested samples were sent to Brigham Young University by the City of Los Angeles for the purpose of EDS analysis and correlation to their mechanical property testing. All samples provided are listed in Table 3-3.

3.1.2 ABS

All samples came from ABS extruded sheets of different formulations (by color and additive package). The sheets were all specified to be 0.06 inches thick, and have one side flat and one side the same grainy surface typically applied to plastic tabletops. Five of these sheets, labeled 'A', 'B', 'C', 'D', and 'E', were purchased by Mity-Lite and passed on to Brigham Young University. Two additional ABS sheets with similar

Table 3-3 Trash cart samples provided by Los Angeles

Type	Time Period	Labels	Sample Type
Initial	0		11 Izods
Weather-Ometer ('W')	2	W1-2 to W7-2	7 Tensiles, 7 Izods
Weather-Ometer ('W')	3	W1-3 to W7-3	7 Tensiles, 7 Izods
Weather-Ometer ('W')	4	W1,2,4,5,7-4	5 Tensiles
Weather-Ometer ('W')	5	W1-5 to W7-5	7 Tensiles, 7 Izods
Weather-Ometer ('W')	6	W1-6 to W7-6	7 Tensiles, 7 Izods
No-Load ('N')	1	N1-1 to N11-1	11 Izods
No-Load ('N')	2	N1-2 to N11-2	11 Tensiles, 11 Izods
No-Load ('N')	3	N1-3 to N11-3	11 Tensiles, 11 Izods
No-Load ('N')	4	N1-4 to N11-4	11 Tensiles, 9 Izods
No-Load ('N')	5	N1-5 to N11-5	11 Tensiles, 11 Izods
No-Load ('N')	6	N1-6 to N11-6	11 Tensiles, 11 Izods
Loaded ('L')	1	L1-1, L4-1	2 Izods
Loaded ('L')	2	L1-2, L4-2	2 Tensiles, 2 Izods
Loaded ('L')	3	L1-3, L4-3	2 Tensiles, 2 Izods
Loaded ('L')	4	L1-4, L4-4	2 Tensiles
Loaded ('L')	5	L1-5, L4-5	2 Tensiles, 2 Izods
Loaded ('L')	6	L1-6, L4-6	2 Tensiles, 2 Izods
Control ('C')	2	C1-2 to C7-2	13 Tensiles, 7 Izods
Control ('C')	3	C1-3 to C7-3	7 Tensiles
Control ('C')	4	C1-4 to C7-4	7 Tensiles
Control ('C')	5	C1-5 to C7-5	7 Tensiles, 7 Izods
Control ('C')	6	C1-6 to C7-6	7 Tensiles, 7 Izods
Special-Control ('SC')	2	SC1-2 to SC7-2	7 Tensiles, 7 Izods
Special-Control ('SC')	3	SC1-3 to SC7-3	7 Tensiles
Special-Control ('SC')	4	SC1-4 to SC7-4	7 Tensiles
Special-Control ('SC')	5	SC1-5 to SC7-5	7 Tensiles, 7 Izods
Special-Control ('SC')	6	SC1-6 to SC7-6	7 Tensiles, 7 Izods

thickness and surfaces, labeled 'F' and 'G', were also provided by Mity-Lite from competitor outdoor-tables. Half way through the total exposure duration, another 3 sheets purchased by Mity-Lite, labeled 'O', 'P', and 'Q', were sent to Brigham Young University to be tested in the same fashion as the other sheets.

The ABS sheets of formulations ‘A’ and ‘B’ were both Mity-Lite’s standard ABS material for indoor tabletops and contain no UV-stabilizer additives. The other formulations have some combination of UV-stabilizer additives, which were to be evaluated against the non-UV-stabilized ABS as well as against each other. Information on the actual additive package of each sheet is proprietary to Mity-Lite and the sheet manufacturers, so an abbreviation for each additive package as well as the color of each formulation is listed in Table 3-4.

Table 3-4 Formulations of ABS sheets

Formulation	Color	Additive Package
A	white	Standard non-UV
B	black	Standard non-UV
C	white	UV2
D	black	UV1
E	black	UV2
F	gray	V
G	brown	M
O	white	T
P	white	T-C
Q	black	T

Ten samples were cut from each formulation for controls, and six more samples were cut from each formulation for each of six time periods of exposure, as illustrated in Table 3-5.

‘A’, ‘B’, ‘F’, and ‘G’ formulations were only scheduled to be tested through three time periods of exposure (126 days). All samples were cut as 2” squares using a sheer press. The non-control samples were all mounted for radiation exposure with the grainy side facing out to simulate actual sunlight exposure of the tabletop.

Table 3-5 ABS exposure times and sample size

Time period	Exposure time (days)	N
0	0	10
1	42	6
2	84	6
3	126	6
4	168	6
5	210	6
6	252	6

Eventually, when the importance of chemical changes in the white ABS samples at exposure times less than 42 days became apparent, six new samples of 'A' were exposed for 10 days, six more for 21 days, and 6 samples of 'O' were exposed for 21 days.

3.2 Sample Aging

3.2.1 Polyethylene

The polyethylene 'W' samples were aged by the City of Los Angeles using the Weather-Ometer (WOM) equipment from ATLAS (Chicago, USA). This instrument employs a xenon arc lamp of 6500 W, providing an irradiance 0.35 ±0.03 W/m^2/nm (at 340 nm). Exposure was set at cycles of 3.8 hours of light and 1 hour of dark on a continuous basis. This cycle arrangement is suggested to maximize the period of exposure, while allowing contraction in the dark, thus accelerating the weathering effects (Strong 2002). Although a typical supplement in accelerated laboratory weathering, no water spray was employed in this aging setup. The two-part explanation was that:

1. Water has no effect on the polyethylene plastic and negatively affects the weathering cycle because the water lowers the heat and screens the UV radiation.
2. Water spray is prone to mechanical and clogging problems (Strong 2002).

The individual tests lasted for 3 months, 6 months, 1 year, 1.5 years, 2 years, and 3 years, respectively. The naturally exposed samples ('N' and 'L') were exposed in the natural service environment of the Los Angeles metropolitan area. The average annual radiation for Los Angeles was listed in Section 2-2 as 270 MJ/m^2 (Strong 2002). The sampling time periods were 6 months, 1 year, 1.5 years, 2 years, 2.5 years, and 3 years, respectively.

3.2.2 ABS

The ABS samples were aged using the Weathering Tester (QUV), model QUV-50 from Q-Panel (Cleveland, Ohio), according to ASTM G154 ("ASTM Reference Manual" 2001). UVA-340 fluorescent bulbs were used, with an irradiance of 0.68 $W/m^2/nm$ at 340 nm, and which produce ultraviolet light that matches reasonably well with sunlight (Fechine 2304). New bulbs were given a 100-hour burn-in time, and rotated every 400 hours. The QUV was set at constant exposure, at a temperature of 45 °C, for durations of 42, 84, 126, 168, 210, 252 days, respectively.

3.3 Analytical Methods

3.3.1 Polyethylene Mechanical Testing

The property changes of all polyethylene samples were monitored by the City of Los Angeles according to each of the tests presented in Table 3-6. ASTM standards were followed according to the indicated tests ("ASTM Reference Manual" 2001).

Table 3-6 Tests performed on polyethylene samples

Property to Monitor	Test	ASTM Equivalent
Tensile elongation (to break)	Tensile test	ASTM D 638
Tensile strength	Tensile test	ASTM D 638
Impact toughness	Izod impact	ASTM D 256 (test method A)
Loss of molecular weight	Melt Index	ASTM D 1238
Changes in polymer structure	Density	ASTM C 693
Presence of residual non-polymerics	Ash Content	ASTM D 5630 or 2584

The resultant data was provided to Brigham Young University, along with the remains of the tested impact and tensile specimens (Refer Table 3-3), for EDS analysis. The data provided is somewhat incomplete, as the impact strength data at time periods 1 and 4 for 'W', 'C', and 'SC' was not included.

The control (C) and special-control (SC) samples were tested at the same time as the WOM samples (W) to determine the property changes due to any degradation not associated with UV irradiation. This serves two purposes:

1. To show what portion of all the degradation is specifically due to UV-induced photooxidation by comparing the property changes to the 'W' samples.

2. To counteract any time-dependent experimental bias in the testing (in the case of skewed data on a particular day) by profiling the difference in observed properties between the control samples and the weathered samples.

3.3.2 ABS Impact Strength Testing

The impact strength of every ABS sample was measured by a variation of ASTM D 3763 for multiaxial impact testing ("ASTM Reference Manual" 2001). Sample size (2"x2"x0.06" squares), was the key difference from the ASTM standards. A Dynatup Mini-Tower with hammer weight of 13.9 lbs and drop velocity of 11 ft/sec was used. The parameters were set as follows:

- Load Range: 500 lbs
- Tup Calibration Factor: 2231 lb
- Max Tup Load: 3500 lbs
- Time Range: 25 milliseconds
- Hammer Weight: 13.9 lbs
- Data Points: 2048

Measured data for each sample included the energy to maximum load (ft-lbs), the total energy (ft-lbs), and the maximum load (lbs). The relation between these data categories is illustrated in Figure 3-1, representing a typical graph of impact failure of a plastic sample.

Thickness of the samples was measured using a micrometer with a friction thimble and the data was then normalized for thickness.

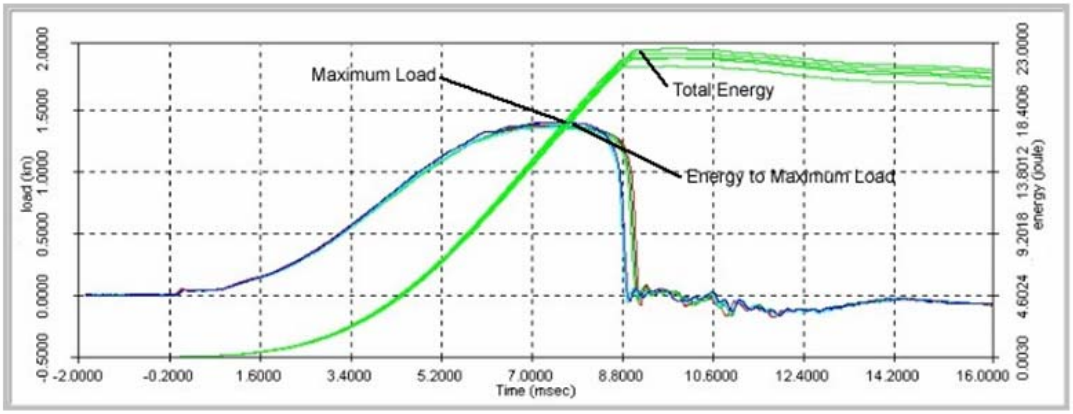

Figure 3-1 Typical Dynatup impact test result: load (left axis) and energy (right axis) vs. time

3.3.3 Scanning Electron Microscopy (SEM)

The polyethylene SEM samples were cut from the corners of each of the actual test specimens (tested remains) sent by the City of Los Angeles by means of a hacksaw. The Charpy impact specimens were used preferentially because of the clean squared corners (without tensile grip marks) whenever they were available (Refer Table 3-3). When only tensile samples were sent for a particular sample, a corner was cut from the tensile specimen near the point of failure (middle of the dog-bone). The samples were cleaned of skin oils and other contaminants by an ethanol bath, and then mounted onto SEM stubs using double-sided carbon tape.

Visual inspection was required to determine which side to mount for SEM analysis, as it was not indicated on the samples sent which side had been exposed to radiation (not necessary for impact or tensile testing). In the case where visual inspection was inadequate to determine which side was exposed (as was the case for any samples with little oxidation such as the control samples), a duplicate sample was prepared from

the same specimen, and both sides were tested by SEM and EDS, later disregarding whichever side showed the least oxidation.

The ABS samples were cut from the corners of the Dynatup Impact test specimens after impact testing by means of cutting pliers. These samples were then bathed in ethanol and mounted with double-sided carbon tape, the degraded side facing up.

All samples were analyzed using a Philips (Hillsboro, USA) XL30 environmental scanning electron microscope (ESEM) with a field emission electron gun (FEG). Signal detection was by gaseous secondary electron detector (GSE). The sample chamber was maintained at a constant pressure of 1.0 torr of water vapor. Images were made at a working distance of 10 mm and 15 kV for high contrast; the high energy causes less scattering of electrons by collisions with gas particles in the sample chamber (Goldstein and others, 2003).

3.3.4 Energy Dispersive Spectroscopy (EDS)

Sample prep was the same as for SEM analysis. The importance of the sample ethanol bath is illustrated by the detection of unusually high ratios of oxygen to carbon in oxidized PE (10:1) in a previous study, which could be from salts accumulated on the surface from water spraying in the exposure chamber (Gulmine and others, 2003).

EDS microanalysis was performed with GSE on each sample in the ESEM chamber directly after SEM imaging. EDS data was collected at a lower voltage, 5 kV, to lower electron beam penetration of the sample, thus focusing on the surface and accentuating the oxygen component of the substance. Magnification was generally kept at

100x (scanned area of ~ 700x1000 μm), but was increased to avoid large defects or to avoid the sample edges in the case of small surface areas.

The EDS data was collected by an EDAX SAPPHIRE Si (Li) detector and qualified and quantified through EDAX GENESIS software using standardless quantification (thus needing no spectra library consultation or constant calibration to a standard) and ZAF correction factors. The voltage (5 kV) resulted in 800-1200 counts/second (CPS). The clock was set at 100 μs resulting in a dead time percentage range of 20-35%. Data sampling was run for 30 seconds (live time) for each spectrum.

Elemental analysis reported the atomic percentage of oxygen on the surface of each sample, with carbon as the only other element measured in the peak quantification. This simplifies the data analysis by only having to record one value for each test. The oxygen-percent (O-percent) is therefore the metric used in this paper to monitor the extent of oxidation. The carbon-oxygen ratio can easily be extrapolated from the O-percent because of the two-element basis of quantification as will be discussed in its application to the results.

Other elements are of course present in all samples, both ABS (from impurities and monomer structure) and PE (from impurities only), but only in small concentrations compared to carbon and oxygen. The focus of this study is the profile of oxygen concentration with time, so attention to the other elements can be minimized when solely examining the percent change in oxygen concentration.

3.3.5 Exclusions

EDS analysis was not performed on the polyethylene (Los Angeles) control and special control samples. Microanalysis of these samples was deemed unnecessary for the following reasons:

- Time purposes
- Since most samples were analyzed on both the exposed and unexposed sides (unable to visually distinguish them in many cases), and EDS data showed which side was more oxidized, the remaining (unoxidized) side's EDS analysis would indicate the O-percent of an unexposed sample at the same time period. The 'C'/'SC' samples were suspected to have been oxidized to the same minimal extent, making repeat EDS readings of the same values superfluous.
- The EDS testing occurred over a short period of time (all within a few weeks) and was closely monitored to minimize experimental/instrumental bias. The initial samples should yield equal O-percent as equivalent control and special-control samples, regardless of the time period they were meant as standards for.
- The output O-percent profiles are reported as percentage decreases and are therefore already on a relevant scale, and not absolute.
- The objective of this study is to enable better prediction of the service life of plastic parts, which implies actual time to a percentage change in properties; comparing the drop to control standards only takes away from the correlation of the testing to service in the field.

Neither was EDS analysis performed on the ABS samples of formulations ‘B’, ‘C’, ‘D’, ‘P’, or ‘Q’. SEM and EDS analysis was only performed on formulas ‘A’, ‘E’, ‘F’, ‘G’, and ‘O’, due to the lack of statistical difference in the property profiles of some of the formulations. The statistical basis of this will be explained in Section 4.

4 Results

4.1 Surface Morphology Changes

The two monitored physical changes to surface morphology were surface crack development and discoloration.

4.1.1 Surface Cracks

Surface cracks on the PE sample surfaces were an easily identifiable sign of oxidation. Surface cracking of a photo-degraded surface is assumed to be the cause of impact-associated failures in plastic parts (Schoolenberg 1988a). Monitoring the development of surface cracks associated with oxidation allows the inspector to note when oxidation has made a product readily susceptible to impact failure.

The PE samples show visible surface defects after only 6 months of WOM exposure. The concentration and magnitude of these surface defects can be visually seen to continue to increase throughout the three years of WOM exposure. The naturally exposed and control samples (‘N’, ‘L’, ‘C’, and ‘SC’) do not ever show visible surface defects attributable to weathering – only scratches from handling, testing, etc.

Surface cracking was much harder to visually detect in the ABS samples without the aid of SEM magnification due to their grainy surface.

4.1.2 Discoloration

The polyethylene samples showed no visible yellowing because of the dark colorants. Evidence of rapid oxidation in the white ABS samples, however, can easily be detected visually by the yellow-discoloration of the exposed samples. Even after 42 days of exposure, 'A' had been significantly yellowed, and 'C' had yellowed as well, although to a lesser degree. Mity-Lite's initial color shift requirement for the ABS white material was no yellowing through five years of exposure. Discussion of the quick discoloration of the 'C' formulation with the manufacturer prompted new candidates to be tested; the formulations 'O' and 'P' were then purchased. In this same discussion, the manufacturer claimed the caveat that no discoloration would be impossible, only its minimization. The formulations 'O' and 'P' showed similar discoloration rates as 'C'.

This shows that the UV-stabilizer additives in 'C', 'O', and 'P' do indeed stabilize the UV-induced degradation to an extent. But the discoloration after such short of an exposure duration hints that none of these additive packages would meet usual customer expectations in the cosmetics of an outdoor table.

To quantify this, Mity-Lite used a spectrophotometer as described in Section 2-6 to show the amount of "yellowness" in some of the white samples. Accepting the manufacturer's claim that some yellowing would have to be allowed for, a slightly yellowed color plaque was first measured with the limit of yellowness that was deemed cosmetically acceptable for service in the field. The spectrophotometer measured a yellowness of 12.8 for this plaque. This yellowness was then compared to the measured yellowness of the 'A' samples for the control, 42, and 84-day samples. Results showed an average yellowness of 0.5 for the controls (nearly perfect white), which increased to 39.2

after 42 days of exposure, and then 50.9 after 84 days. The yellowness of 'C' at 84 days of exposure was measured at 42.4, showing a 17% decrease in yellowing due to the UV-stabilizer additives. But both 'A' and 'C' had proven to pass the accepted limit of discoloration, and 'O' and 'P' exhibited similar visual yellowing to the 'C' samples, so it was assumed that they would all fail this test after a short period of exposure as well. Mity-Lite did not bother to perform any more yellowness testing because of these failures.

Even though the profile of the yellowness of 'A' consists of only three data points, it shows an initially high rate of increase, followed by a lower rate. This later stabilization of property changes will be seen in nearly all properties measured and denotes a limit to the oxidation extent. This suggests that simple spectrophotometry color-shifts could be another insightful property that correlates to chemical changes along with the other mechanical and physical property profiles. This only applies, however, to white or other similarly bright colors of material. The black, gray, and brown samples showed very little or no visual discoloration. Because yellowness is overwhelmed by these darker colorants, spectrophotometer yellowness for such colors is not applicable to such a study.

4.1.3 Scanning Electron Microscopy (SEM)

Many previous studies have used SEM to microanalyze the surface morphology, especially the evolution of cracks, in degraded polymer surfaces. The spontaneous initiation of cracks (without an applied load) during photooxidation has been detected according to the following studies:

- Crack initiation detected at 5 days of UV exposure (xenon lamp) in thick PP (Yakimets, Lai and Guigon 2004).
- Comparison of WOM and QUV exposure of PE: after 1600 hrs of WOM exposure, the surface was covered with microcracks in one direction. After only 800 hrs of QUV exposure, the photographed damage was much more severe, showing a mosaic pattern with no preferential propagation tendency (Gulmine and others, 2003).
- Comparison of the surface cracking in PE and PP, where failure in PP was reported to be more influenced by cracking of the photo-degraded surface layer than in PE (Kelly and White 1997).
- In the WOM exposure of compression-molded PP, cracks became visible in the surface between 250 and 300 hours, and at 1300 hours the surface was completely crumbled and powdery (Schoolenberg 1988a).
- Only small fissure-cracks were observed in similar WOM exposure of PP using injection-molded samples (Qayyum and White 1986).

SEM images were taken from a variety of samples for this study. All images taken are presented in Appendix A.

The photomicrographs of the unexposed samples for both PE and ABS show new, non-degraded material (Figure 4-1). It is smooth, without cracks, holes, and free of any defects (the ABS sheets' grainy surface finish is the cause of the large pits).

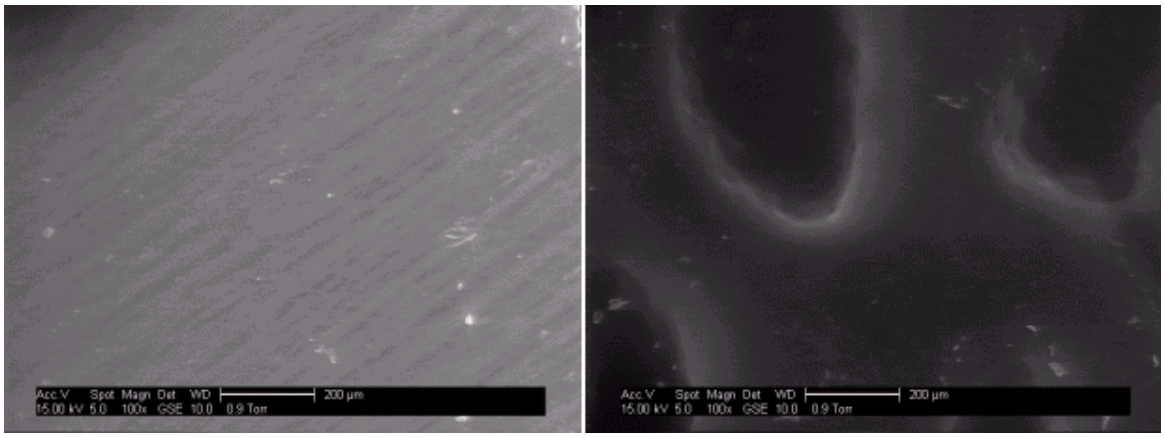

Figure 4-1 Control samples for PE (left) and ABS (right)

Polyethylene

The polyethylene 'W' samples (samples exposed to WOM) showed little degradation in SEM images up until one year of exposure. After that, all the green and blue 'W' samples show a sharp increase in surface cracks, with apparent continual increase throughout the duration of exposure. This trend is illustrated in Figure 4-2, where the images at 100x are presented of green 'W' samples for times 4, 5, and 6. These cracks follow the same random mosaic pattern for PE reported by Gulmine and others (2003). The "induction" time shown in crack initiation (time after initiation of exposure until evidence of oxidation begins) agrees with the many studies' incubation period mentioned in Section 2-6 and provides evidence of a chemical reaction occurring on the surface.

The blue samples at time period 6 (3 years exposure) show a high extent of degradation and visual signs of surface delamination. Figure 4-3 shows the border of the delamination. The original, heavily oxidized surface is seen on the left, and the newly exposed surface is seen on the right. Cracks are already seen forming perpendicular to the

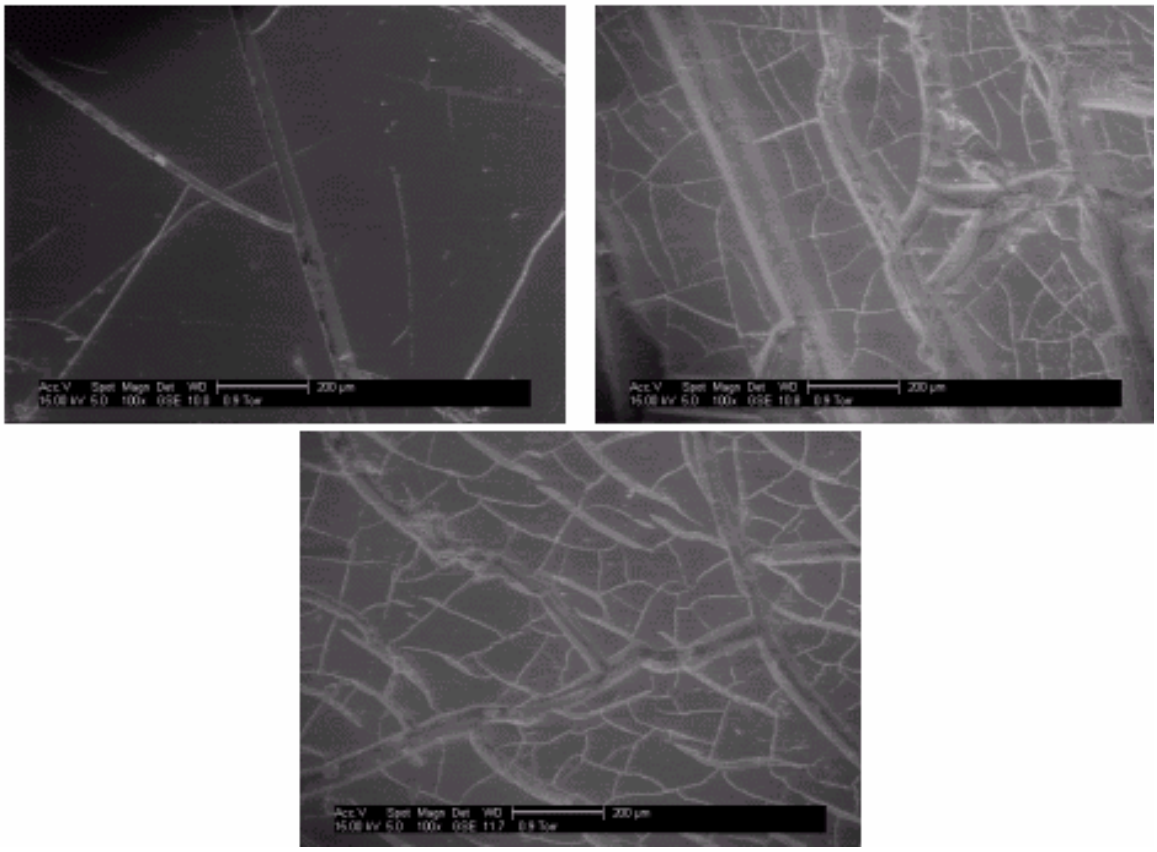

Figure 4-2 Crack propagation for 'W': 18 mos. (top-L), 24 mos. (top-R), 36 mos. (bottom)

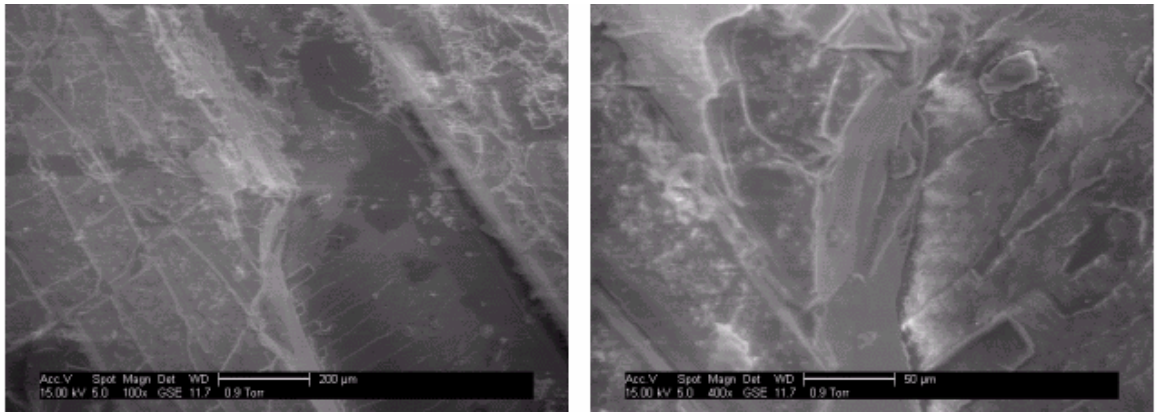

Figure 4-3 Surface delamination of blue 'W' at 36 mos.: 100x (left), 400x (right)

border on the new surface. The 400x image shows a detail of the "cliff" separating the two surfaces. The crack initiation by the boundary on the new surface illustrates the previously mentioned phenomenon reported by Kaczmarek and Decker (1995), who reported that the boundary between phases in polymer blends (copolymers) was always more sensitive to photooxidation than the pure polymers, thus making copolymers difficult to protect against UV degradation.

The black 'W' samples showed small amounts of crack propagation, but the cracks seen are not guaranteed to be from UV-degradation; they could be from handling of the samples through testing. The limited amount of oxidation (inherent to the carbon black absorber) made it a confusing task to determine the exposed side from the unexposed side of each sample, even for the most exposed samples. Figure 4-4 shows the images of the most mottled side of two different black samples at 3 years of exposure (W1-6 and W2-6). The left sample showed short cracks, but that appeared very different to the cracks in the more oxidized samples. The right sample should have comparable degradation, but appears very different and shows few surface cracks.

This confusion could be caused by the unequal exposure across the PE surfaces. It is obvious on the highly oxidized samples that one side was exposed to the WOM and one wasn't. But even on the exposed sides, the extent of oxidation seemed to be higher or lower for different locations on the surface. This could be caused by sample clamps holding down the specimens in the WOM, or some other obstruction of the radiation. Therefore, not only was it difficult to determine in some cases which side to test, but where on the exposed side to test as well.

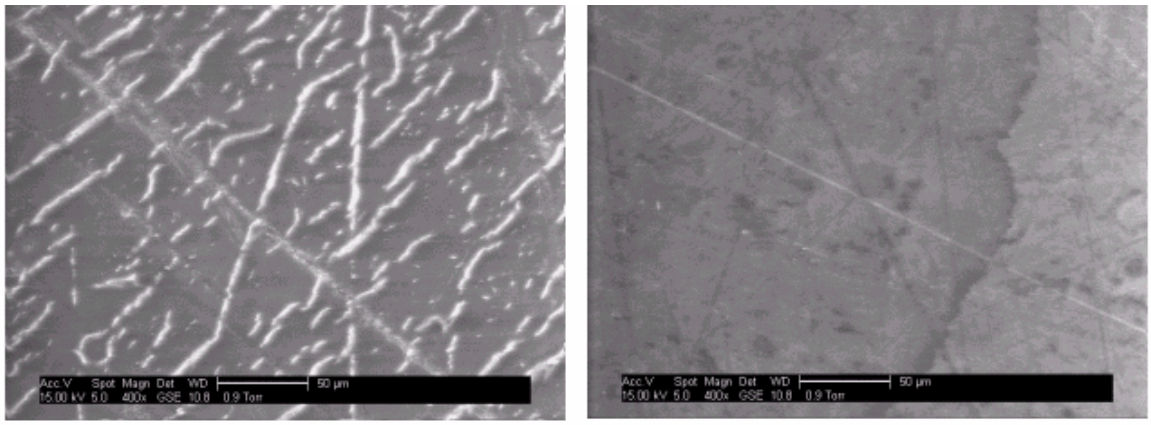

Figure 4-4 Most mottled side - black samples at 36 mos.: W1-6 (left), W2-6 (right)

All 'L' and 'N' samples were very difficult to differentiate exposed areas from non-exposed areas. The SEM images of these samples show very little cracks throughout the exposure duration.

ABS

All ABS samples exhibited the formation of surface cracks by the first time period (42 days of exposure). The surface cracks of the ABS samples are generally characterized by more geometrical order than those on the PE surfaces. Long, linear longitudinal cracks are the first to appear, with perpendicular transverse cracks appearing between the longitudinal cracks at higher extents of degradation. The transverse cracks had already appeared after only 42 days of exposure for all samples except 'F', in which they eventually appeared after 84 days. An example of this typical crack-geometry ('E' after 168 days, at 400x) is presented in Figure 4-5.

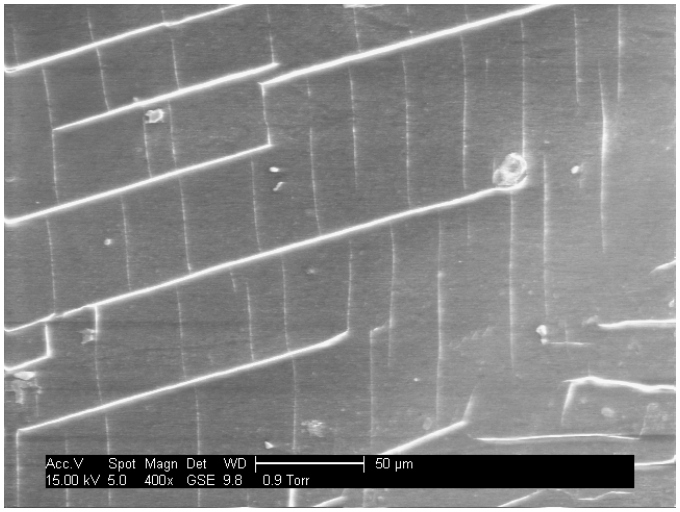

Figure 4-5 Typical degraded ABS crack geometry

Unusually high amounts of surface cracks were noticed on the ABS samples near the boundary where the SEM sample was cut from the impact test specimen. The additional cracks were larger and perpendicular to the direction of the cut. These are attributed to stress cracking associated with the applied mechanical stress from the cutting pliers. This agrees with Gulmine and others, where the same additional cracks not associated with aging were found by the cut boundary (2003). This also agrees with Schoolenberg's findings that a significant increase in the surface cracks of degraded samples followed fracture testing with applied mechanical stress (1988a). These stress-cracks were not seen in the PE samples, most likely due to the more localized stresses associate with the hacksaw-cuts performed on them.

With the short-time period samples of the white ABS formulations, the early initiation of the surface cracks as short versions of the longitudinal cracks was seen at the shortest exposure time analyzed (10 days for 'A' and 21 days for 'O')(Figure 4-6).

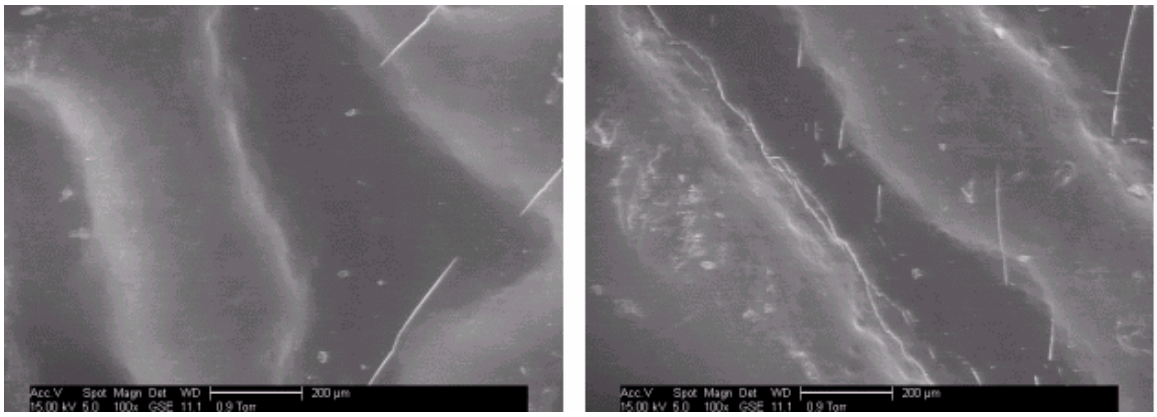

Figure 4-6 Initiation of surface cracks: 'A' after 10 days (left), 'O' after 21 days (right)

In the later exposure times of 'E', the samples showed continued cracking in the "wells" of the grainy surface, but at the same time a disappearance of the cracks on the ridges. The cause of this "well effect" is suspected to relate to the applied stresses to create the grainy finish – acting as a load-accelerated version of laboratory weathering to cause more photosensitivity in the wells. Why the ridge-cracks are present up through 168 days, but then disappear after 210 days is not yet answered. An example of the "well effect" from time period 5 (210 days of exposure) is shown in Figure 4-7.

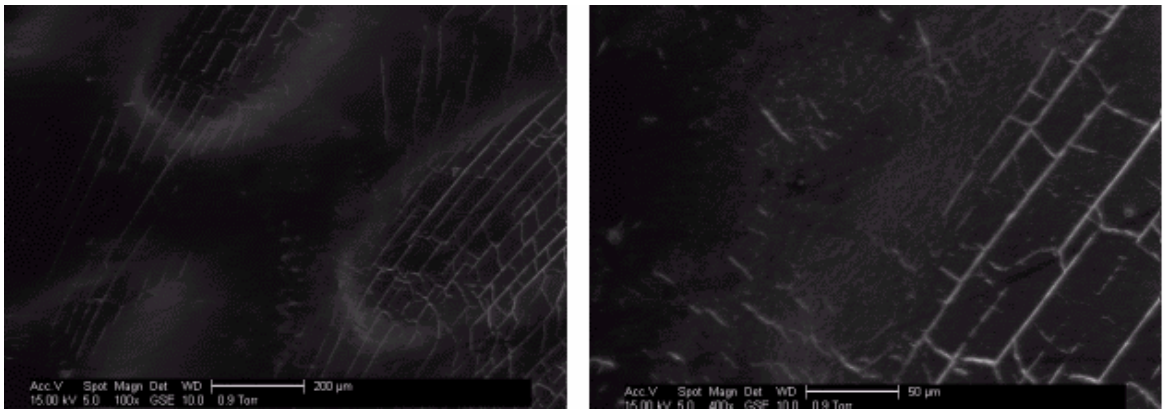

Figure 4-7 "Well effect" at 210 days in 'E': 100x (left), 400x (right)

Another noteworthy disappearance of cracks is the high concentration of cracks in the 'G' samples at 42 days, followed by a decrease in cracks over the next two time periods (Figure 4-8). EDS measurements (reported below) show that for the time period three samples have less oxygen than for time period 1 and 2 (1 and 2 being nearly equal).

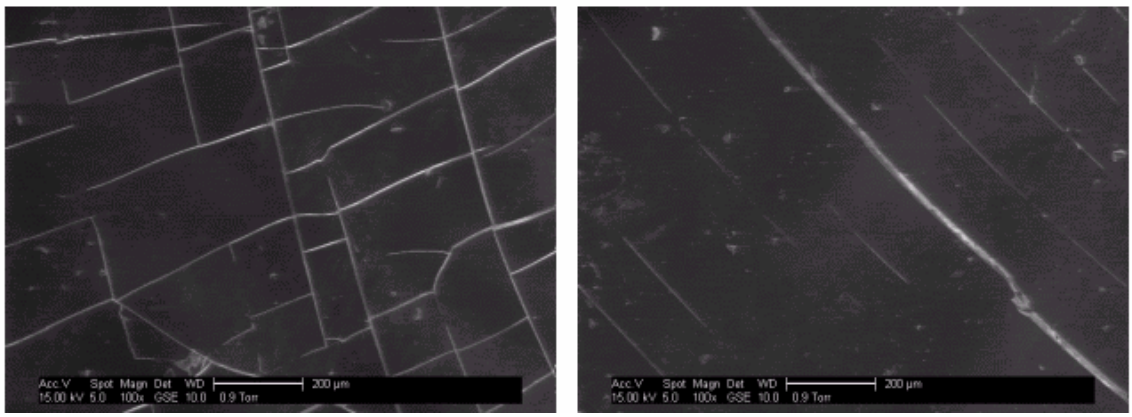

Figure 4-8 Decrease in cracks for 'G': 42 days (left), 126 days (right)

A similar disappearance of cracks appears in the 'O' samples, where the most cracks are observed at 84 days of exposure, followed by a decrease over each subsequent time period (Figure 4-9). The transverse cracks even disappear at 210 days exposure, leaving only longitudinal cracks at 210 and 252 days. EDS data confirms this as well; the highest O-percent was measured at time period 2, followed by a steady decrease in oxygen concentration over the remaining time periods.

The 'G' sample data suggests that the order in which the samples were mounted on the SEM stub may have been recorded incorrectly causing attribution of images and EDS data to the wrong time periods. But the regular decrease over four time periods of

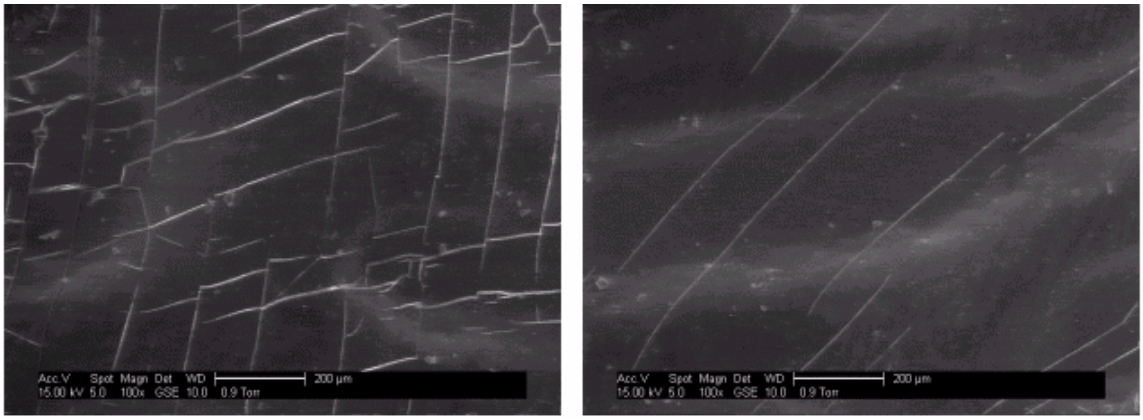

Figure 4-9 Decrease in cracks for 'O': 84 days (left), 210 days (right)

sampling for 'O' does not show chance and refutes the possibility of incorrect record keeping.

The disappearance of cracks over long periods of exposure (samples 'E' and 'O') and the accompanying decrease in oxygen percentage suggest a mechanism of degradation not yet understood. The author's only theory for this is the "peeling off" of oxidized functional groups from the surface (delamination) at long periods of UV radiation, leaving either a clean surface not yet through the induction period for significant oxidation, or a chromophore-free surface after chromophore-saturation with oxygen. This could explain the "well effect" in 'E' as the ridges would be most prone to auto-delamination (more exposure), leaving a crack-free surface on the ridge-tops. But the "well effect" is not seen in the 'O' samples; cracks still appear across both wells and ridges even after the decrease in crack amount. Another problem with this theory is that the visual evidence of delamination seen in the heavily oxidized PE samples (Refer Figure 4-3) is not seen in the ABS samples. Delamination in ABS could occur in a more

uniform manner, however, with less of the powdery residual matter seen in the delamination of PE.

Other authors have observed a similar "peeling off" effect for PVC (Qayyum and White 1987) and PC (Sherman, Ram and Kenig 1982), but not in PP (Schoolenberg 1988a). This phenomenon has been described as the spontaneous delamination of outer surface layers upon extensive degradation and is suggested to cause regeneration of ductility (Sherman, Ram and Kenig 1982). The ABS impact properties for the present study (reported below), however, only show either decreasing profiles (embrittlement) or no change (limits); increases in ductility are not seen for this exposure duration.

4.2 Mechanical Properties: Polyethylene

The data from the tests performed on PE by the City of Los Angeles (presented in Appendix B) was provided to Brigham Young University with a few exceptions: no izod impact data was provided for the 'W', 'C', and 'SC' samples for time periods 1 (three months) and 4 (18 months). The data was first profiled against exposure time for each cart. Each of these profiles was then converted from the original data to percentage changes across time. This prepared each profile for general comparison against other properties including EDS by making a universal base of property changes. It also cleared up the trends in many instances. For example, the melt index changes in 'W' originally showed a gap between the black carts of different sizes. This can be due to a host of processing differences in the two carts. But converting the data to percentage changes brings the black profiles together to illustrate that they are alike in their minimal decreases with exposure time (Figure 4-10).

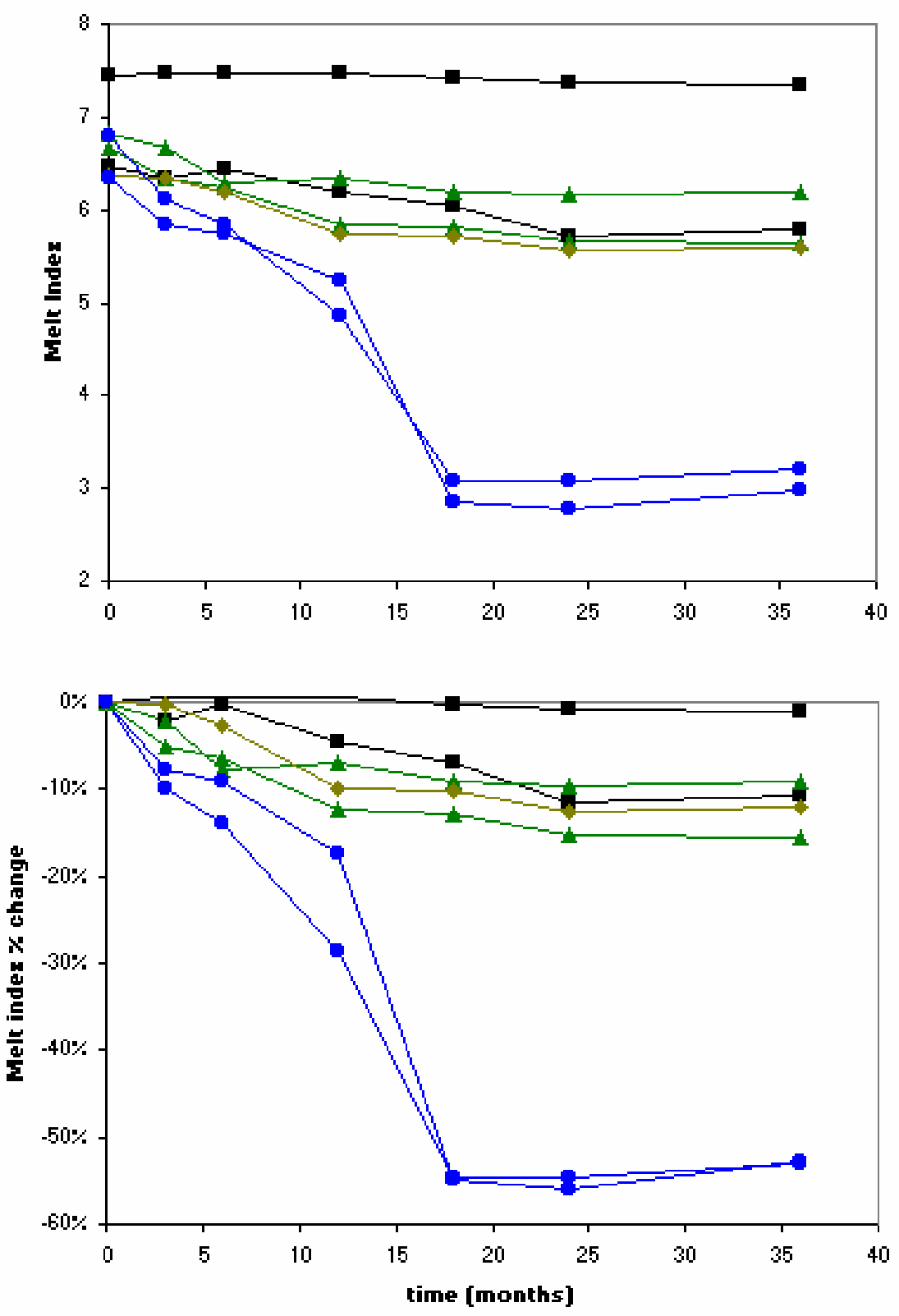

Figure 4-10 Conversion to percent-change: 'W' PE samples. Key: □, black; Δ, green; ◊, green 'FA'; ○, blue

Two key observations are made on inspection of the resultant data. First, the 'W' samples all show clearer trends and color matching of data in all profiles when compared to 'N' or 'L'. This can be assumed to be from the both the exaggeration of the degradation effects caused by the accelerated oxidation reactions in the 'W' samples. In every case, only a fraction of the property changes seen in 'W' were seen in 'N' or 'L'. Also contributing to this is the variation inherent to random selection of naturally exposed carts from the field ('N' and 'L'). Control over the oxidative environment is impossible for these samples.

Also, the tensile strength data (Figure 4-11) shows no clear trends in any of the sample sets. The maximum percent change for all tensile data over this period of exposure was only about 10%. With such small changes, variation masks any trends. The small degree of change in tensile strength is not surprising. As photooxidation is surface-intensive, properties that depend on surface fracture mechanics like elongation will naturally show more change during exposure than will a property that focuses on the integrated strength of the sample bulk like tensile strength. The slight changes in the tensile strength of PE have been previously reported by Bruijn (1996) when compared to density, and Carrasco and others (2001) when compared to elongation and modulus. Gillen, Clough and Wise (1996) reported good fits of elongation data to the Arrhenius equation, but were not able to use it to model their tensile data, and explained this in terms of the above-mentioned difference in failure modes.

Another suspected reason for the absence of clear trends in photooxidation/tensile strength studies is that there may be complex differing mechanisms behind oxidative tensile failure. Crosslinking and accompanying stiffening (Lewis 2004) may compete

against chain scission and the resultant loss in molecular weight. Carrasco and others (2001) reported this to be the case: initial increase (6% in 60 days) in tensile strength, followed by a decrease (30% over the next 60 days) with the explanation that structural and molecular reorganization dominated during the first period of irradiation whereas the chemical changes become dominant afterwards. This increase followed by a decrease can be seen in the tensile strength profile of 'W' (Figure 4-11), and the application of this theory is supported by the lack of any accompanying increase in tensile strength of any of the control samples at time period 2 (6 months).

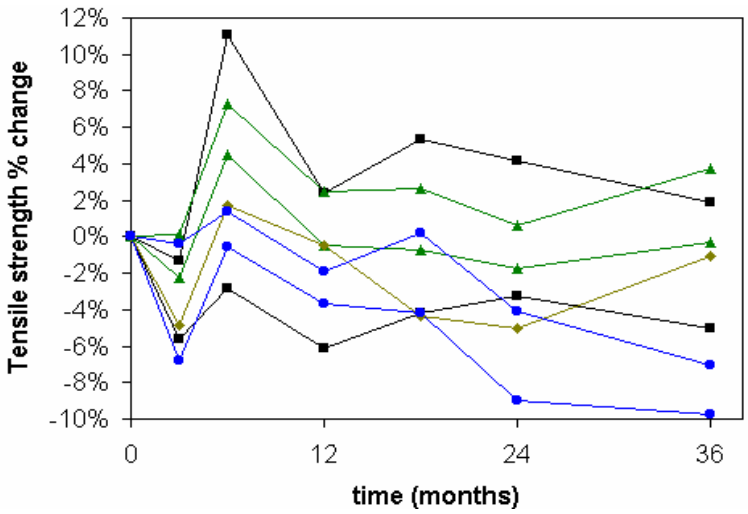

Figure 4-11 Tensile strength % change: 'W'. Key: □, black; Δ, green; ◊, green 'FA'; ○, blue

4.2.1 Control and Special-Control Samples

As mentioned in Section 3, the city of Los Angeles tested separate control (C) and special-control (SC) samples at the same time as each sample exposed to accelerated weathering ('W' samples) was tested for two purposes:

1. To show what portion of all the degradation is specifically due to UV-induced photooxidation by comparing the property changes to the 'W' samples.
2. To counteract any time-dependent experimental bias in the testing (in the case of skewed data on a particular day) by profiling the difference in observed properties between the control samples and the weathered samples.

Analysis of the 'C' and 'SC' mechanical/physical property profiles shows minimal observable trends. This suggests that without UV acceleration, little chemical change occurs.

Because of the lack of non-UV-associated degradation (degradation by other means) to compare to, the property profiles for the WOM samples are generally not presented as a comparison to the control or special-control samples. Looking at the 'W' sample data independent of the 'C'/'SC' data thus shows trends attributable to UV-induced photooxidation. Furthermore, the 'C'/'SC' data variation only contributes more "noise" to the 'W' data, muddying the observable trends. Besides, the focus of this study is to predict the service life of plastic parts in outdoor environments. A customer won't care if the product failure can only be partly attributed to UV-associated photooxidation. All that matters is when it actually fails. Because the property changes are minimal without UV exposure, this study's focus on modeling the UV-photooxidation effects on property degradation is acceptable.

In one case, however, the WOM data was compared to the average of the control and special-control data. The secondary purpose of the 'C'/'SC' sample testing proved to be a wise decision as the impact testing data is uniformly skewed high at time period 3 (1 year of exposure) for the 'W', 'C', and 'SC' samples (Figure 4-12).

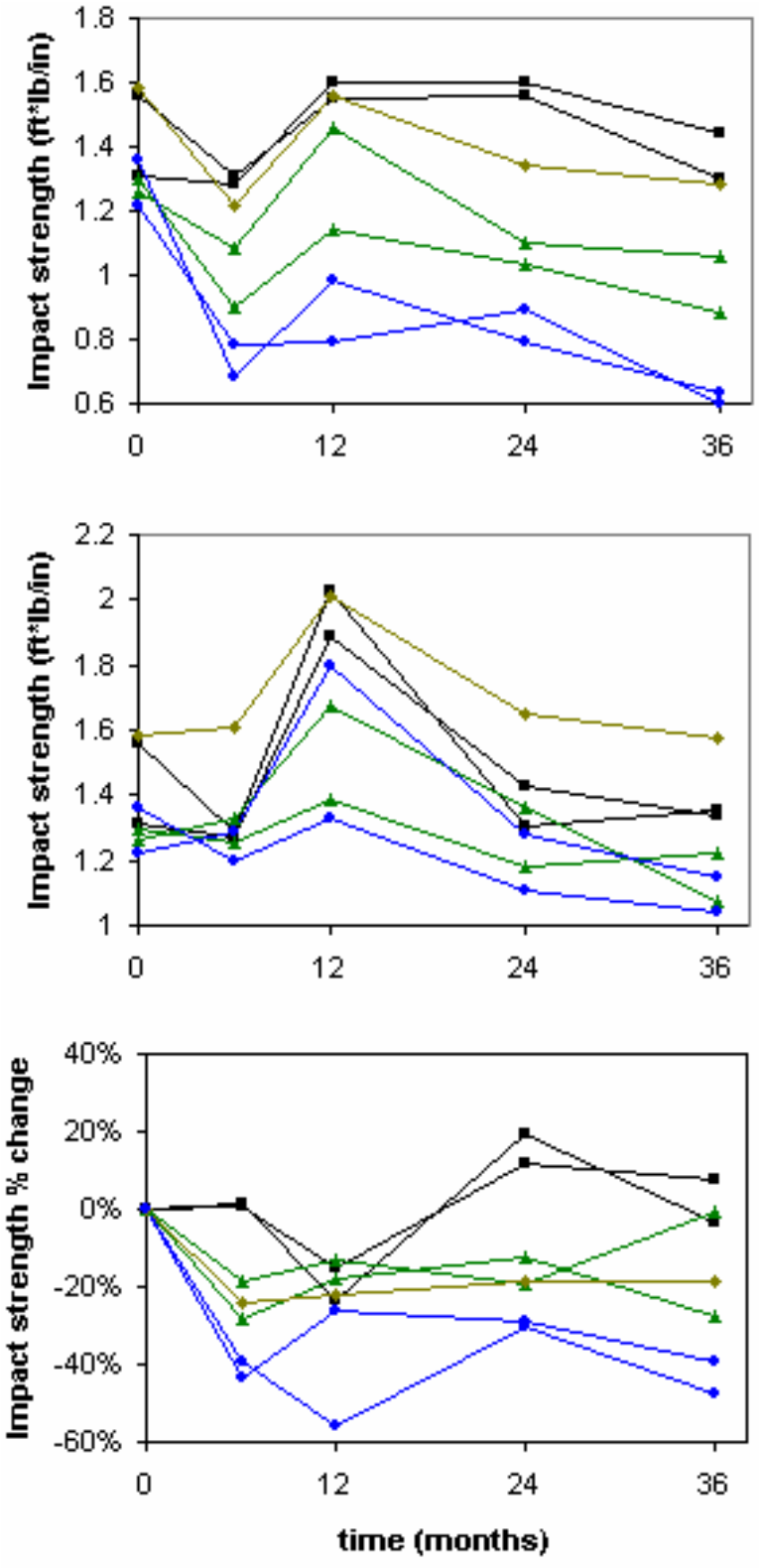

Figure 4-12 Impact strength for 'W': 'W' data (top), 'C'/'SC' average (middle), 'W' profile when compared to controls (bottom)

When the ‘W’ impact data is looked at as a percentage change and compared to its corresponding control points, the degradation profile becomes clearer.

Other bias trends were observed:

- High impact strength at time period 4 for “N” and “L”
- High EDS O-percent at time period 5 for “N” and time period 2 for “L”.

But because there were no control or special-control samples tested at the same time as the “N” and “L” samples (only “W”), these other bias trends were left untreated. There was no need to present any other property profiles as a comparison to the control/special control samples as no significant bias was noticed in the remainder of the data.

4.2.2 Combination of Data by Color

Without any repeat measurements for each PE sample (only one test specimen was analyzed for each cart and test), statistical analysis of the data would be powerless. The need for repeats and the appeal of simplification prompted the combination of data for each color. That is, the data for the ‘W’ black trash carts was combined and averaged as a n=2 sample set, and the ‘N’ black carts were averaged as a n=3 sample set, and the same was done for the green carts, as well as the blue carts. Theoretically, the only difference between the combined data is the size of the cart from which samples were taken. This combination relies on the assumption that the degradation profiles for all properties will not change with cart size.

To test this assumption, a statistical method was needed to test for a significant difference in the mean of the paired data observations of the two matched cart sample sets. A paired samples t-test is generally used for this purpose, but the t-test is based on normally distributed, or parametric data. With sample subset sizes of only 1, 2, or 3

observations to test from, and a quick glance over the data showing a significant amount of variation in each of those subsets, the data is assumed to not be normally distributed (non-parametric).

The Wilcoxon signed-ranks test is the non-parametric alternative to the paired samples t-test. Like the t-test, it formally tests for a difference between the medians of 2 related samples. It is similar to the signed-ranks test except that it takes account of the magnitude of the observations, whereas the signed-ranks test only takes account of the sign, or direction, of the difference between each pair of observations. When precise quantitative measurements can be made the Wilcoxon signed-ranks test is more powerful (Conover 1980).

The sample testing data for melt index, elongation, impact strength, density, and tensile strength, for all time periods, was listed as a complete sample set and paired against the equivalent sample set of the same color. Analysis was based on the confidence that there exists no significant difference in the medians between sets. The alternative hypothesis (H1) is therefore that there is a significant difference in the medians of the two sample sets. With 95% confidence, any paired set with a null hypothesis confidence percentage over 95% is said to have differing medians and therefore the cart size has actually caused a significant difference in the data.

The Wilcoxon signed-rank test results are presented in Table 4-1 as the percent confidence that the null hypothesis is true. The ‘N’ confidence percentages are presented as the average of the test between carts 1 and 2 (65 and 95 gallons), carts 1 and 3 (65 and 35 gallons), and carts 2 and 3 (95 and 35 gallons). The data showed highly significant differences between the sample sets for the colors. But as mentioned above, tensile

strength data does not show any clear trends or color matching, so the tests were performed again after exclusion of the tensile strength. The resultant data shows much lower significance of difference for the 'W' samples, but does not affect the difference shown for the 'N' samples. As with the tensile strength data, t the absence of clear trends or color matching in the 'N' samples makes the resolution too low to show clear matches in the pairings. For simplicity's sake, the cart sizes were then all combined by color, with the understanding that the 'W' sample tensile strength data, and all the 'N' sample data will continue to not represent any clear trends in degradation.

Table 4-1 Wilcoxon null hypothesis confidence (%) for PE color combination

	All data			W/o tensile strength		
Set	black	green	blue	black	green	blue
W	83	94	96	5	78	71
N	91	82	85	97	81	96

After the colors were combined, the resulting profiles were graphed over time. These graphs were quickly "eyeballed" to determine a kind of acceleration factor by comparing the maximum percent property change. For instance, the melt index profiles for 'W' and 'N' are shown in Figure 4-13. The 'W' blue carts' data shows a maximum change of nearly 50%, whereas the 'N' blue carts only show a maximum change of about 12%, giving roughly a 4:1 ratio. In similar fashion, the elongation and impact strength both show ~5:2 (2.5x) and density shows ~8:5 (1.6x). The tensile data shows no comparable trends. This does not show the typical acceleration factor however, which is based on the ratio of time to a certain change in a property. But it is a quick method to determine which properties will change the most.

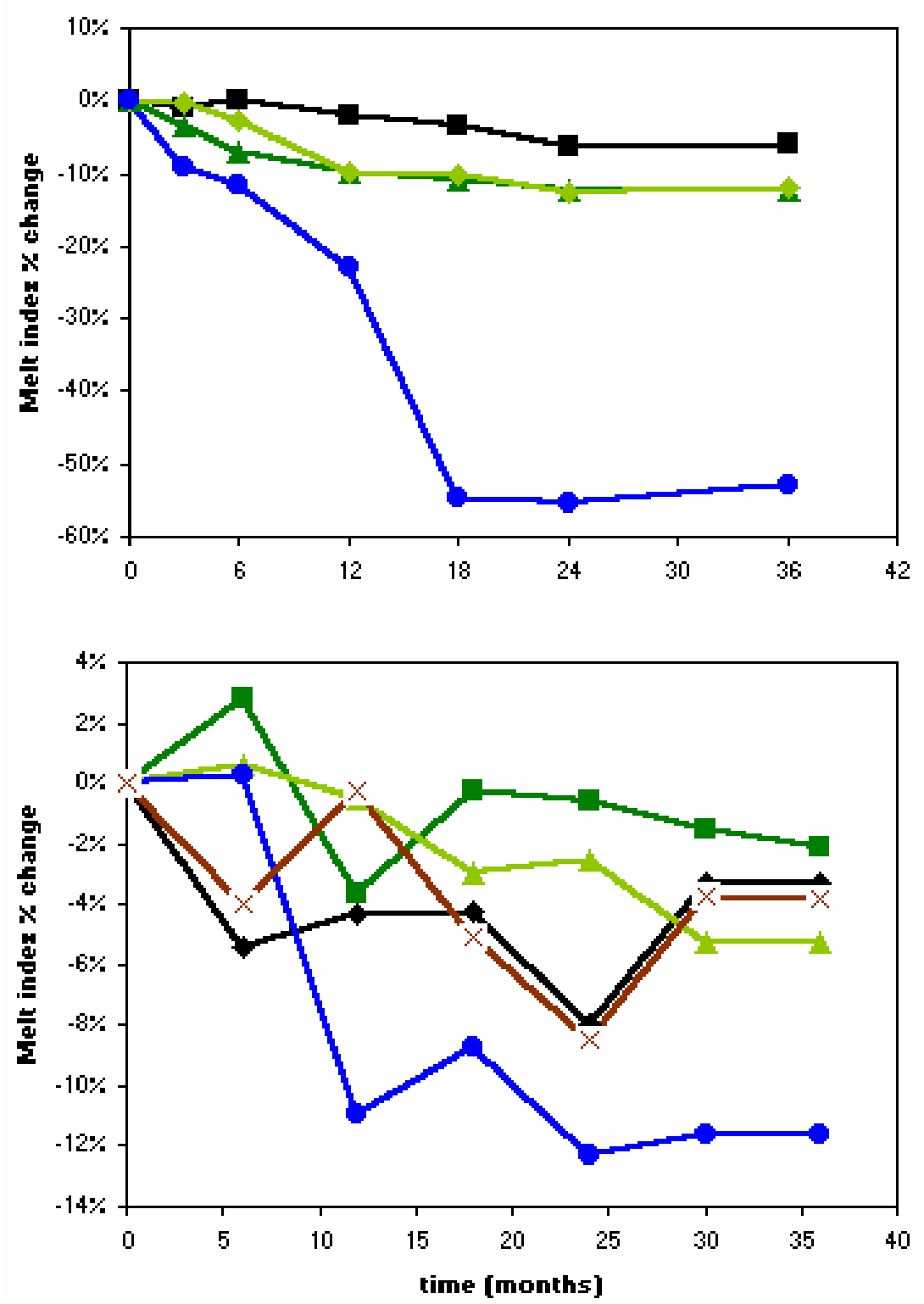

Figure 4-13 Melt index profile comparison: 'W' (left), 'N' (right). Key: □, black; Δ, green; ◊, green 'FA'; ○, blue; x, brown

Generally, a decrease was observed in melt index, elongation, and impact strength, and an increase in density during degradation (Figure 4-14). In some instances, however, the trends shown are in opposite directions for the same property. The clearest example of this is in the case of the elongation profile of the 'W' samples, where the black samples show an increase as opposed to the usual decrease. Opposite trends like this are most likely caused by competing degradation mechanisms as with the case of the tensile properties. The effect of the carbon black UV-absorber seems to have a dramatic effect on the type of degradation happening in PE.

4.2.3 Ash

As expected, ash content did not change much with exposure time. But comparing the ash content of samples of the same color can show how closely their resin formulations match in terms of residuals of non-polymeric material. This is another method to determine the validity of combining data. These non-polymeric residuals usual provide strong chromophores for initiation of oxidation, thus different concentrations of ash would cause different rates of oxidation. The Ash content measurements for both 'W' and 'N' are presented in Figure 4-15. From these graphs, the difference in ash content is shown to be minimal for all colors, thus further validating the combination of colors.

4.2.4 Arrhenius Modeling of Mechanical Properties

The mechanical/physical property profiles of the polyethylene samples exhibit little linear behavior. Many of the property data profiles over time, however, follow the same typical model discussed in Section 2: a period of slow degradation (incubation), followed by a dramatic change (acceleration), until a limit is reached (stabilization). An

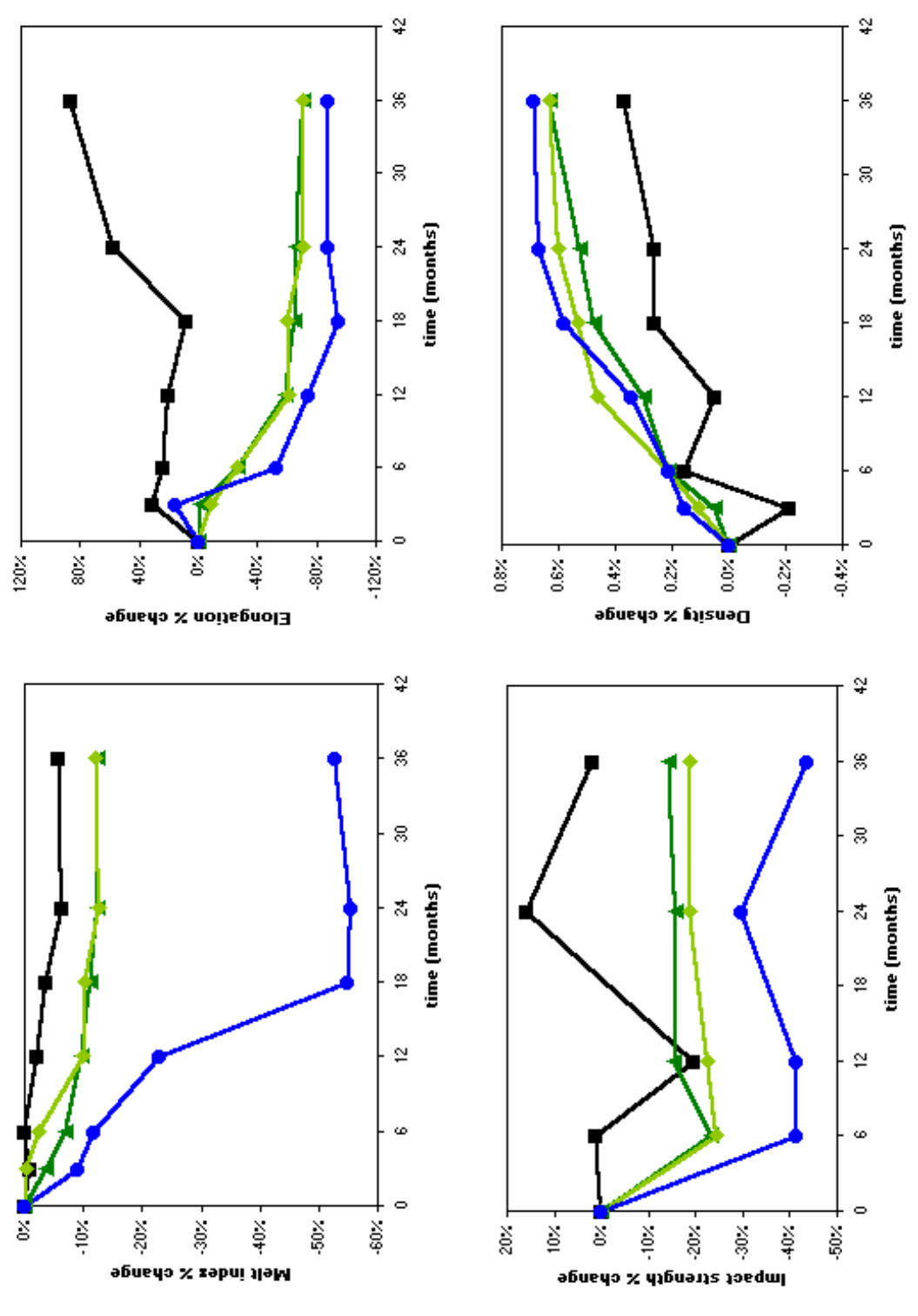

Figure 4-14 'W' profiles. Key: □, black; △, green; ◇, green 'FA'; ○, blue

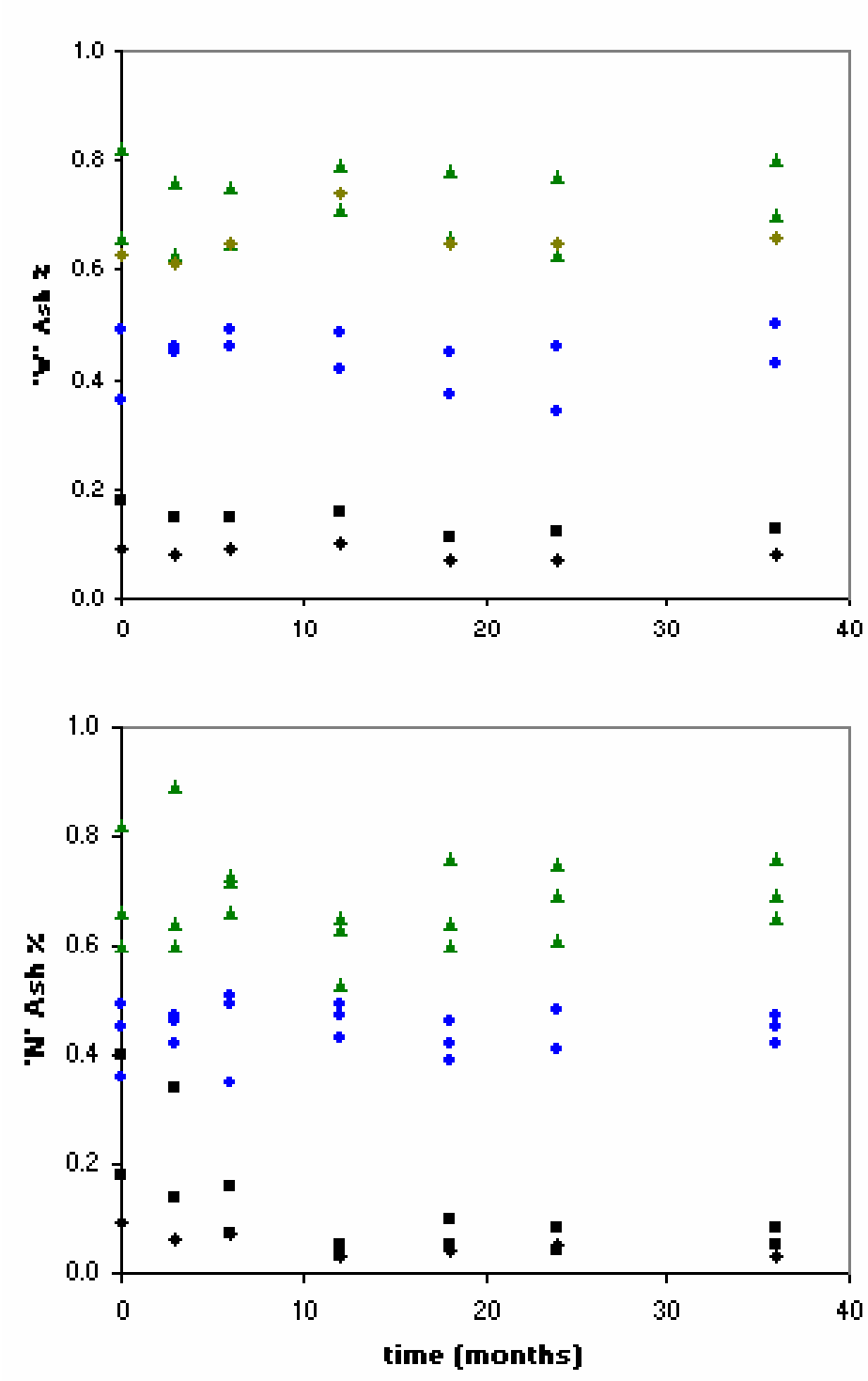

Figure 4-15 Ash Content of: 'W' (left), 'N' (right). Key: □, black; Δ, green; ◊, green 'FA'; ○, blue

example of this pattern, the elongation profile for the green 'W' (WOM) samples, is shown in Figure 4-16.

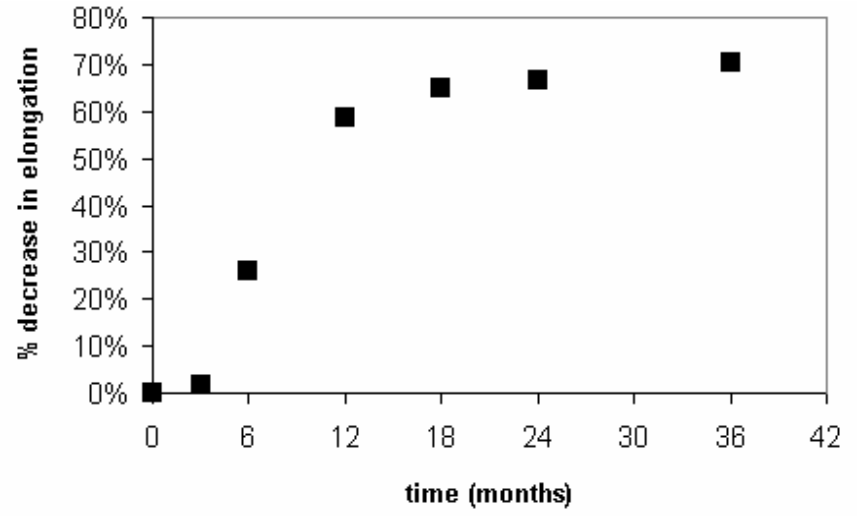

Figure 4-16 Percent increase in elongation: 'W' green

As these property changes are induced by chemical reactions, this pattern of property change profiles understandably agrees with reaction modeling by the Arrhenius equation. As Arrhenius equation modeling has successfully represented this pattern in previous modeling, its application was attempted with the PE property profiles. Referring back to Bruijn's version of the Arrhenius Equation (Equation 2-6):

$$K = k_0 \cdot e^{(-E_a / R \cdot T)} \cdot I^{\alpha} \qquad \textbf{(4-1)}$$

For the typical pattern of oxidation described in Section 2, a stabilization or limit of oxidation implies samples that the reaction rate has decreased until reaching zero. For a profile showing a property change over time, as in Figure 4-16, the property under examination cannot be correlated to a time-profile of *K* (reaction rate) because the

property reaches a limit when the rate approaches 0. The slope of the time-profile of the property can be interpreted as *K,* however. If the fraction of the original value either gained or lost is defined as the property change, *y*:

$$y = 1 - \frac{P}{P_0} \tag{4-2}$$

Then the profile of *y* as a function of time [*y(t)*] is the function represented in the typical degradation profile of any property in this study (Figure 4-16). If the slope of this function is the reaction rate at any time, *t*:

$$K(t) = \frac{d}{dt} y(t) \tag{4-3}$$

Then the property change at time *t* is the integral of the reaction rate at time *t*:

$$y(t) = \int K(t) dt \tag{4-4}$$

The integration of the reaction rate requires the nomination of what variables change with time of exposure and which do not. *R* and k_0 remain constant with time. Although many weather acceleration studies have employed an elevated temperature or temperature cycles to increase the chemical reaction rate, the oxidation rate has shown to depend on other factors much more than temperature (Bruijn 1996) when varied over a range of 8 ˚C. Therefore, temperature changes will be assumed to be a constant as a long-term average, even in outdoor weathering environments where the temperature fluctuates based on diurnal and seasonal cycles.

The activation energy of all the reaction kinetics involved is suspected to decrease with time, as the propagation of free radicals continues to accelerate the oxidation. So a simple inverse relationship is proposed:

$$E_a(t) = \frac{1}{t} \tag{4-5}$$

The UV intensity, *I*, is a constant over the exposure time by its definition (irradiance normalized by time). But α most likely changes over time of exposure, as the stability of the polymer decreases with time due to rapid chromophore generation in oxidation and the consumption/migration of additives discussed in Section 2-5. The value of α has been reported to vary between 0.5 for non-UV stabilized plastics and 1 for stabilized plastics (Vink 1983). If the stability decreases with time, then the value of α is also inversely proportional to time. For integration simplicity, the UV intensity and α were combined as a function of *t* squared, to show greater dependence on time than the activation energy:

$$I^{\alpha(t)} = \frac{C}{t^2} \tag{4-6}$$

C represents a constant based on the UV intensity and the initial value of α. Substituting these functions of time into Equation 4-1 provides the proposed relationship of reaction rate to time of exposure:

$$K(t) = k_0 \cdot e^{(-1/t \cdot R \cdot T)} \cdot \frac{C}{t^2} \tag{4-7}$$

y(t) is the integral of this function:

$$y(t) = \int k_0 \cdot e^{(-1/t \cdot R \cdot T)} \cdot \frac{C}{t^2} dt \qquad \textbf{(4-8)}$$

Moving the constants out of the integral and rearrangement of the variables yields:

$$y(t) = k_0 \cdot C \int \frac{e^{(-1/t \cdot R \cdot T)}}{t^2} dt \qquad \textbf{(4-9)}$$

Integration of this function with respect to *t*:

$$y(t) = -k_0 \cdot C \cdot R \cdot T \cdot e^{(-1/t \cdot R \cdot T)} \qquad \textbf{(4-10)}$$

If the constants outside of the exponent are combined into one constant for the purposes of modeling:

$$A = -k_0 \cdot C \cdot R \cdot T \qquad \textbf{(4-11)}$$

And the constants inside the exponent as another constant:

$$B = \frac{-1}{R \cdot T} \qquad \textbf{(4-12)}$$

Then the function for the property change at any time, *t*, of exposure is:

$$y(t) = A \cdot e^{(-B/t)} \qquad \textbf{(4-13)}$$

This variation of the Arrhenius equation was used to model all the property data by using Excel's "solver" function to minimize the square of the residuals (SOR) between *y(t)* at a given exposure time and the corresponding property measurement. To facilitate comparison between each other and the EDS data, the direction of any

decreasing trends in property changes (y) was reversed in all subsequent profiles. In other words, the negative trends (downward) in melt index, elongation, impact strength and tensile strength were all reversed to show the degree of property change as opposed to the absolute property change. All fits of the data, including the constants A and B, the sum of residuals, and the graphed profile for each data set are included in Appendix C.

The fits were particularly good for the 'W' data for melt index, elongation, and density. Figure 4-17 shows an example: the elongation data for 'W'-green. This is the same data as shown in Figure 4-16, only the change is represented as a fraction instead of a percentage. The 'W' impact strength data showed less goodness of fit because of the unusual profiles of initial dramatic increases, followed by a slow decrease (Figure 4-18). The tensile data was difficult to fit because of the lack of any trends. The 'N' data showed comparative lack of fit for the impact and tensile data, and good fits for the rest. The 'L' data does not show much goodness of fit because of the extreme lack of any trends to model.

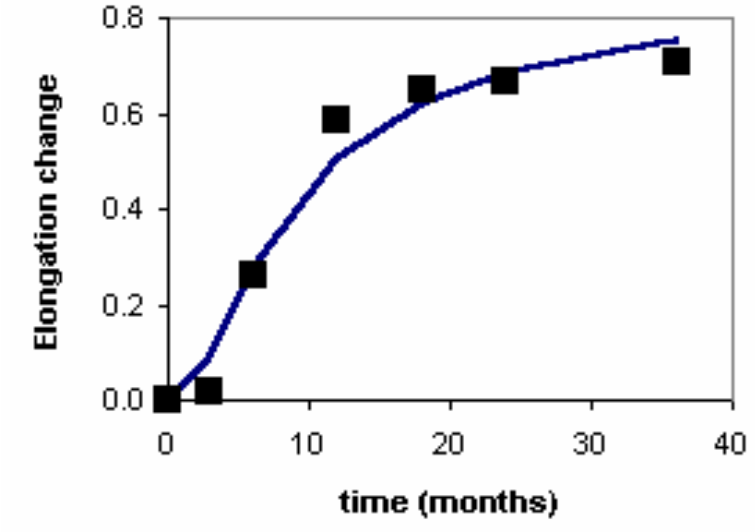

Figure 4-17 'W' green elongation data and fit

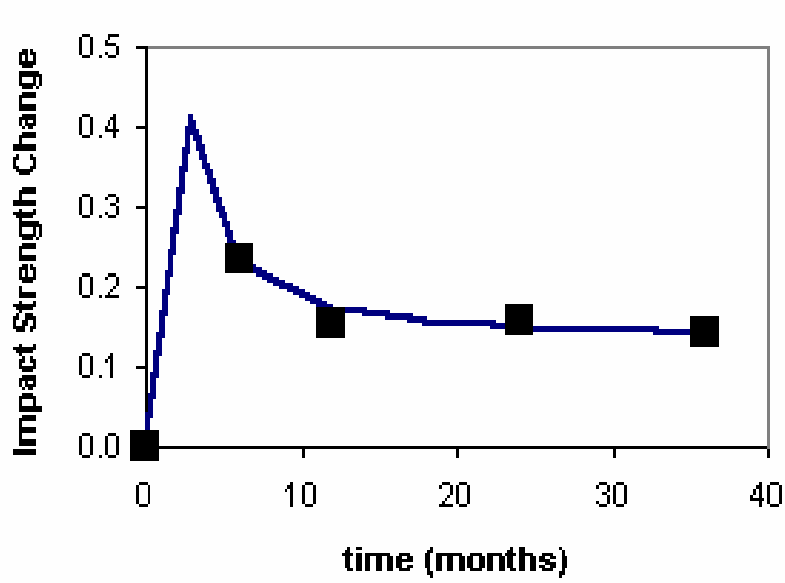

Figure 4-18 'W' green impact strength data and fit

4.3 Energy Dispersive Spectroscopy: Polyethylene

Once again, the need for repeats as well as a standard basis for comparison prompted the combination of data for all cart-sizes by colors. The Wilcoxon signed-rank tests were performed on the EDS data to test the assumption that the degradation profiles for EDS O-percent do not change with cart size. The results are presented in Table 4-2 as null hypothesis confidence percent (confidence that there is a significant difference). The 'N' confidence percentages are again presented as the average of the test between the three pairings of sizes.

The data showed low confidence in difference between the sample sets for all the colors except for the 'W' black data (87% confidence of a significant difference). This can be attributed to the small sample set size. These sample sets consist only of the measurements from each of the six exposure-time periods. Without the five or four

Table 4-2 Confidence (%) for PE-EDS color combination

Set	Black	Green	Blue
W	87	12	37
N	58	16	64

(tensile strength exclusion) sets of property data to build sample sets from for comparison as were done with the mechanical/physical data comparisons, a correlation will be difficult to detect. With the confidence in similarity from the Wilcoxon test, the EDS O-percent data for all cart sizes was combined by color.

The data was then profiled over time and is shown in Figure 4-19. Induction time, acceleration, and stabilization can be seen in the 'W' profiles of oxidation. Black is not surprisingly the slowest to oxidize, and the other colors oxidize at comparable rates. The 'W' samples therefore suggest fulfillment of the primary objective of this study: to establish EDS analysis as a method of characterization of the oxidation in plastics. The regular increasing trends provide compliance with the first evaluation requirement listed in Section 1. And the matching Arrhenius behavior of the O-percent profiles and the mechanical property profiles suggests compliance with the second evaluation requirement.

The 'N' data shows similar profiles for all colors, but no regular increase as would be predicted. The spike at 30 months is discussed with the Arrhenius modeling of the data (next section). The absence of clear trends in 'L' is readily apparent.

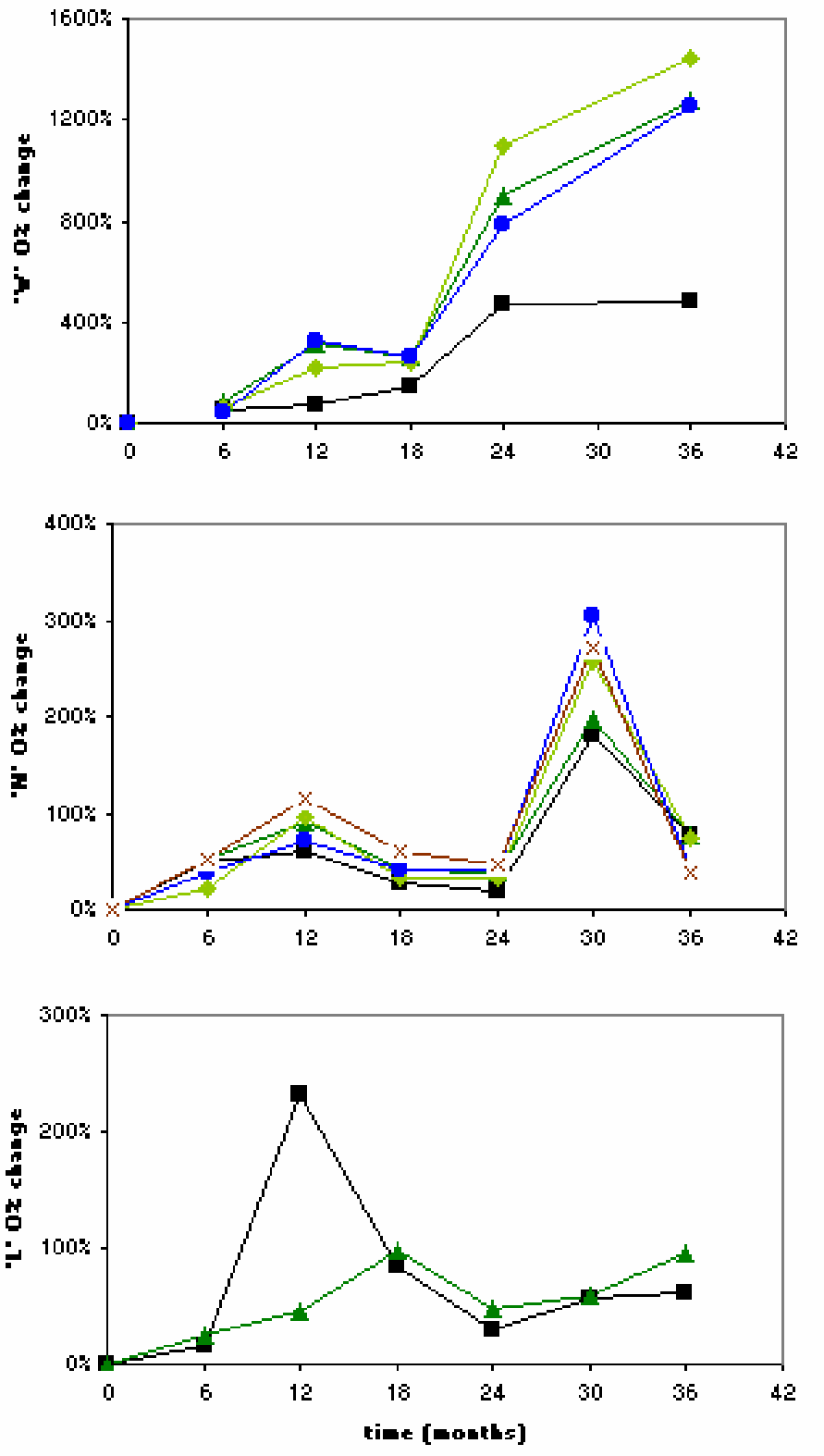

Figure 4-19 EDS O-percent profiles for: 'W' (top), 'N' (middle), 'L' (bottom). Key: □, black; Δ, green; ◊, green 'FA'; ○, blue; x, brown

4.3.1 C/O Ratios

Assuming that disregarding the other elements does not significantly effect the C/O profiles, the O-percent was subtracted from unity (100 percent) to determine the carbon atomic percentage, and the C/O ratios were subsequently calculated. The previous study analyzing C/O ratios reported decreasing linear profiles of those ratios with exposure time (Onyiriuka 1993). This study's C/O ratio profiles do indeed show linear behavior for the polyethylene samples. The linear behavior is especially evident in the "W" samples. The "N" and "L" samples exhibit more residual error from a linear fit, but still show a linear trend. This ordered profile of increasing oxidation further suggests compliance with the first requirement listed in Section 1.

A linear function (Equation 4-14) was fit to the data for each polyethylene cart color (Figure 4-20).

$$y = m \cdot x + b \qquad \textbf{(4-14)}$$

y represents the decrease in C/O ratio over time in months, which is plotted on the *x*-axis. For the "W" samples, the slope (*m*) and intercept (*b*) were nearly constant for all colors, with an average slope of –1.33 and intercept of 43.2. The "N" samples showed similar regularity, with an average slope and intercept of –0.57 and 46.1, respectively. The laboratory-weathered samples ('W') thus exhibit a slope 2.3 times as steep as the naturally weathered samples ('N'), indicating that the acceleration factor is 2.3x for oxidation of the polyethylene samples in this experimental setup. This agrees with the 2.5x acceleration for oxygen uptake reported by Gijsman, Hennekens and Janssen (1996).

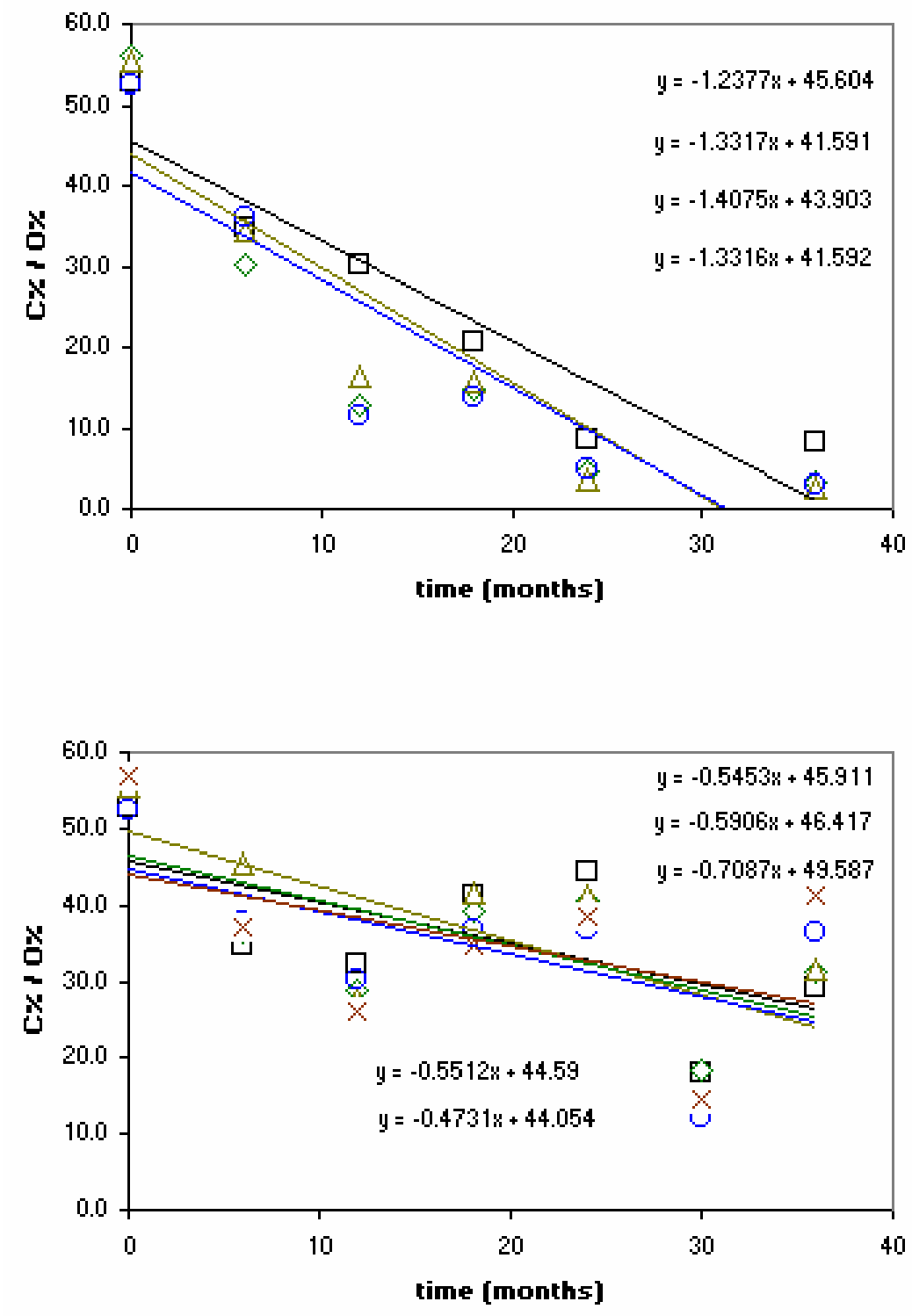

Figure 4-20 C/O Ratio decrease and linear fits for PE: 'W' (top), 'N' (bottom). Key: □, black; Δ, green; ◊, green 'FA'; ○, blue; x, brown

A noteworthy trend in the linear fits is that the slopes for the black and brown carts' data is always the least in magnitude (slightly closer to zero) of the colors, suggesting that the linear profile and the corresponding acceleration factor change with photosensitivity, the most sensitive materials having the steepest slopes and largest acceleration.

4.3.2 Arrhenius Modeling of EDS Data

The EDS O-percent profiles of the polyethylene samples also follow the same typical model discussed in Section 2 and illustrated in Figure 4-16. The Arrhenius variation (Equation 4-13) was used to model all the EDS data by the same method as with the mechanical properties, and the fits are presented along with the mechanical data in Appendix C.

The 'W' profiles show good fits (with the exception of black), and exhibit some linear behavior after 18 months (Figure 4-21).

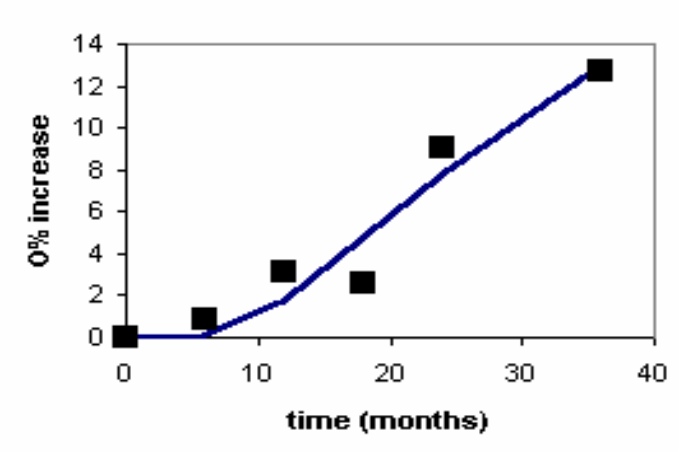

Figure 4-21 EDS O-percent profile and fit for 'W' green

The ‘N’ profiles show unusually high O-percent measurements at time 5 (30 months). ‘N’ green is shown in Figure 4-22 as an example. Whether this is due to a genuine weathering increase in oxidation (and subsequent lowering afterwards) or EDS bias is unknown, but the lack of accompanying spikes in the mechanical data at 30 months, and the uniformity of the spike across all ‘N’ carts at 30 months suggests that this is data skewed somehow by the EDS metric.

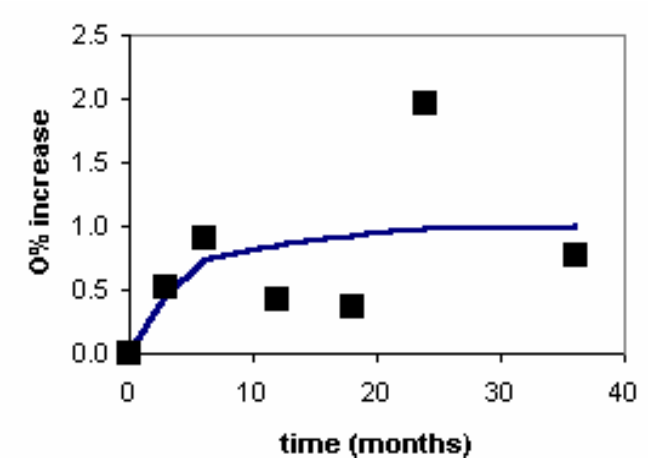

Figure 4-22 EDS O-percent profile and fit for ‘N’ green.

4.3.3 Oxidation on Unexposed Sides

An interesting phenomenon in data not reported with the oxidation data of the exposed surfaces is the minimal increase in EDS O-percent shown by the unexposed sides of the polyethylene samples (Figure 4-23).

Slow surface oxidation on the side opposite to that exposed in UV-degradation experiments has been described in the literature as the effects of limited UV transmission combined with easy oxygen diffusion (Gijsman, Meijers and Vitarelli 1999). Polyolefins do not absorb UV light with wavelength greater than 290 nm. Therefore, the UV light

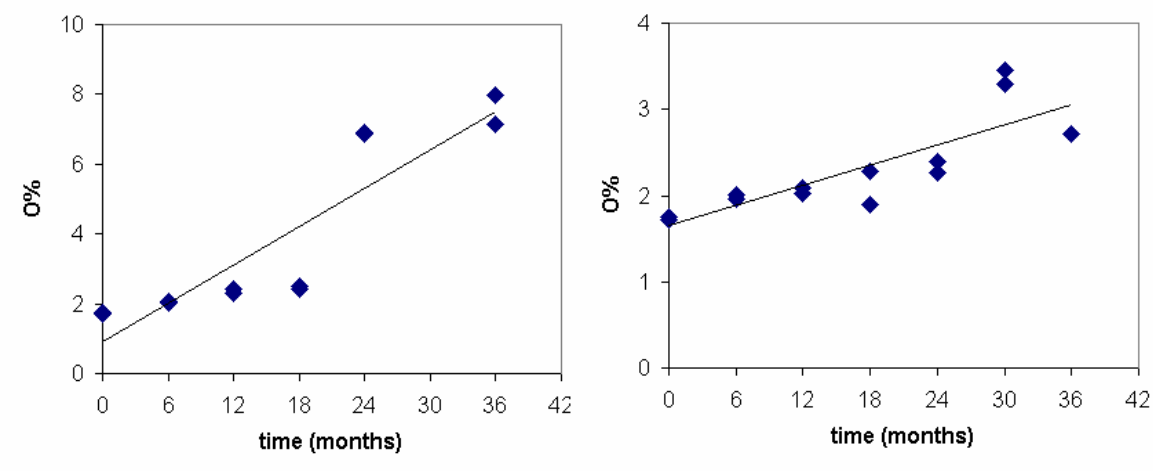

Figure 4-23 O-percent of unexposed surfaces: 'W' black (left), 'N' black (right)

will pass through the substance and degrade both the front and backsides of PE, being limited by oxygen diffusion on either side. The backside oxidation will, of course, be less than on the exposed side because of the higher energy, low wavelength radiation that reaches only the exposed surface. In this case, the unexposed sides are suspected to have degraded a small amount from this limited UV transmission and available oxygen, and not from oxidation by other means besides UV acceleration.

4.4 Correlation: Polyethylene

4.4.1 Service Lifetime Prediction

If Equation 4-13 is solved for *t*, the resulting equation is the function of the time of degradation to any property change, *y*:

$$t(y) = \frac{-B}{\ln(y/A)} \qquad \textbf{(4-15)}$$

With this function, the time to 50% change in a property (the critical degradation extent discussed in Section 2-6) can be predicted based upon the fit. This was done for all property data (Table 4-3), but the melt index, density, and tensile strength show understandable degradation limits before this kind of decrease can be accomplished by oxidation, and are thus not included. The impact strength profiles could not model this property change for some of the data sets as well (shown by "NA").

Table 4-3 Time (months) to 50% property change for PE samples

Set	Color	Elongation	Impact strength	O-percent
W	black	24.6	NA	29.9
W	green	11.7	2.6	8.5
W	green FA	11.1	1.8	8.9
W	blue	7.6	2.3	8.9
N	black	56.4	NA	34.3
N	green	40.0	NA	6.9
N	green FA	149.1	47.5	10.8
N	blue	91.7	PA	10.7
N	brown	88.5	PA	5.4

4.4.2 Acceleration Factors

By dividing the time to 50% change for the 'N' samples by the 'W' samples, the acceleration factor for accelerated exposure time to natural exposure time for this experimental setup (PE, Los Angeles outdoors: WOM) was calculated. This was done for both elongation and extent of oxidation (O-percent). The factors are presented by color in Table 4-4.

Table 4-4 Acceleration factors for PE: elongation and O-percent

Color	Elongation	O-percent
black	2.29	1.15
green	3.41	0.80
green FA	13.39	1.21
blue	12.10	1.20
Average	**7.80**	**1.09**

The great range in acceleration factor for elongation is perplexing, but agrees with the confusion associated with reported acceleration factors throughout the literature. An average of 7.8x for elongation of PE agrees with the 6-8x reported by Gijsman, Hennekens and Janssen (1996).

The extent of oxidation shows a much smaller range. The average of 1.1 denotes nearly equal rates of oxidation in both the WOM and naturally weathered samples. The oxygen uptake for PE demonstrated an acceleration factor of 2.5x in the same by Gijsman, Hennekens and Janssen (1996). The low multiplier calculated in this study is equally as perplexing as the variation in the elongation acceleration factor.

4.4.3 Other Correlations

In hopes of finding a regular method of correlating the mechanical property degradation to the EDS O-percent profile, the constants *A* and *B* (from Equation 4-13) for the O-percent fits were compared against the same constants for the mechanical property fits. Ratios of the EDS constants to the mechanical property constants were calculated for each mechanical property and color; *A* for the EDS fit was divided by *A* of the same color for each mechanical property and this was repeated for *B*.

The ratios are listed for all of the mechanical properties in Appendix D, and Table 4-5 illustrates an example – that of the black samples. In Table 4-5, the constants *A* and *B* from the fits of both the EDS and elongation profiles are presented for both the accelerated-weathered ('W') and naturally weathered ('N') data. The ratio of the constant, from the EDS data to the elongation data, is presented, as well as the average of the two ratios.

Table 4-5 Fit constants *A* and *B*, and ratio comparisons between EDS and elongation: Black PE

	(*A*)		
	W	N	
EDS	3.26E+05	3.26E+05	
elongation	2.952	1.028	average
ratio	**1.10E+05**	**3.17E+05**	**2.14E+05**
	(*B*)		
	W	N	
EDS	399.978	459.150	
elongation	43.746	40.629	average
ratio	**9.143**	**11.301**	**10.222**

As seen in the example in Table 4-5, the ratios are comparable between weathering modes, i.e. the ratios are nearly the same for a given mechanical property across all the data for 'W', and 'N'. Although not the case with the black samples, the similarities in constant-ratios often applied to the 'L' samples as well. This has great implications: no matter what rate of weathering occurs on a plastic product, the oxidation will still correlate in a repeatable way to mechanical property degradation. In other words, the correlation between the accelerated weathering and natural weathering can be made without the need for an accepted acceleration factor. Predictions of mechanical

property degradation in natural service environments for other PE black samples may be made with only a few EDS measurements, and without any additional mechanical testing.

Table 4-6 shows the average of all of the ratios, including all 'W' and 'N' samples. Visual inspection shows that another comparison can be made even across the constant-ratios for the green, green FA, and blue samples, suggesting that similar colors show the same repeatable correlation.

Table 4-6 EDS/property ratios of modeling constants *A* and *B*

Property	Constant	black	green	green FA	blue	brown
Melt Index	*A*	5.2E+06	136.76	139.53	23.97	10.32
	B	-161.20	4.39	2.35	1.80	-0.28
Elongation	*A*	2.1E+05	19.34	26.33	15.38	0.53
	B	10.31	2.56	3.15	2.89	-0.02
Impact Energy	*A*	3.6E+06	132.11	129.86	52.60	8.6E+05
	B	-39.76	-5.22	-10.71	-26.32	0.02
Density	*A*	3.6E+07	2345.86	2995.26	2103.88	80.91
	B	14.58	1.97	2.98	2.29	-0.05
Tensile Strength	*A*	1.22	1.0E+07	954.30	73.95	-26.78
	B	0.33	-0.70	-10.83	0.61	-0.08

By exposing any PE product with similar color to a short duration of accelerated weathering, the profiles of natural oxidation can be projected from the fit constants, and then the mechanical property degradation profile can be plotted based on the ratios of the fit constants.

For example, if a PE trash cart of a color similar to green or blue were to be evaluated for service life, a high irradiance weathering device could be used to rapidly oxidize a small sample from the surface of the product. After a few months, enough EDS data could be collected (at regular time intervals of exposure) to model the data based on Equation 4-16 (repeated from Equation 4-13):

$$y(t) = A \cdot e^{(-B/t)} \quad \textbf{(4-16)}$$

The fitted constants, *A* and *B*, could then be divided by the ratios listed in Table 4-6 to find the constants needed to plot the material property degradation profiles through a high extent of degradation. And this could be available without ever having to do mechanical testing on the sample and without reliance on a questionable acceleration factor.

To understand how widely this correlation can be applied requires further testing of the mechanical property degradation and O-percent for PE samples of a variety of colors and weathering rates.

Another method of correlation is that used by Carrasco and others (2001) and mentioned in Section 2-6: linear plots of the property change against the extent of oxidation. This is an indication that the profiles are similar, i.e. that the induction, acceleration, and stabilization stages happen at the same time in both the mechanical property profile and the oxidation profile. If the slope of the profiled change in a mechanical property is the same at a given time as the slope of the corresponding profiled change in oxidation, plotting the data points directly against each other should yield a linear graph.

Figure 4-24 shows the profiles of melt index, elongation, impact strength and density against the change in O-percent, for all 'W' samples. Results show some linear behavior, but not as much as the previous study (Carrasco and others 2001). What linearity is shown was already present in the profiles against time (Figure 4-14), i.e. the

profiles against change in O-percent shown in Figure 4-24 mirror the profiles against time seen in Figure 4-14.

4.5 Impact Strength Properties: ABS

The normalized data for the impact strength properties measured in the ABS samples after QUV exposure was taken as the average of all repeats for each time period and property and profiled against time as the percent change. The resultant profiles are presented in Figure 4-25.

4.5.1 Failure Mode Variation

A challenge encountered in the Dynatup impact testing of the ABS samples was the dual behavior of both ductile and brittle behavior. The transition from ductile failure to brittle failure in impact testing over the course of degradation has been documented (Schoolenberg 1988a). Brittle materials require little energy to initiate and propagate surface cracks, eventually leading to shatter-type failure. Ductile materials do not shatter upon impact failure but rather by puncture and require higher energy to initiate and propagate the crack. Typical impact test load/energy profiles over time are presented in Figure 4-26 for brittle and ductile materials, as well as materials exhibiting a combination of both brittle and ductile behavior.

The unoxidized (control) ABS samples varied greatly in mechanism of failure. The majority of the samples showed failure by “extrusion” (ductile puncture) around the tup, while the others showed brittle fracture into pieces at failure. Brittle and ductile extremes were seen in the data:

- Normalized energy to maximum load: ~10 to 152 ($ft \cdot lbs/in^2$)

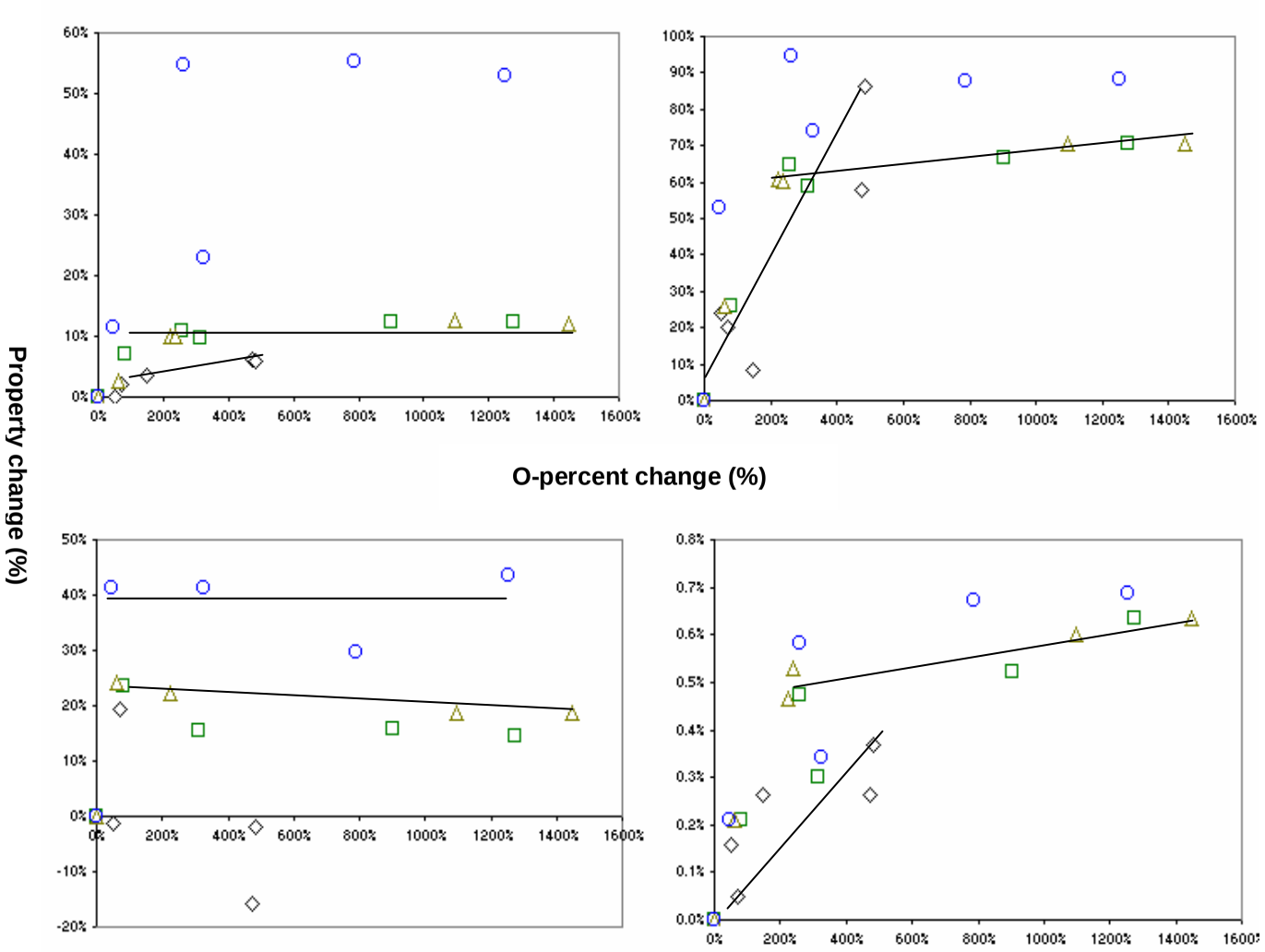

Figure 4-24 'W' property change vs. change in O-percent: melt index (top-R), elongation (top-L), impact strength (bottom-L), and density (bottom-R). Key: □, black; Δ, green; ◊, green 'FA'; ○, blue; x, brown

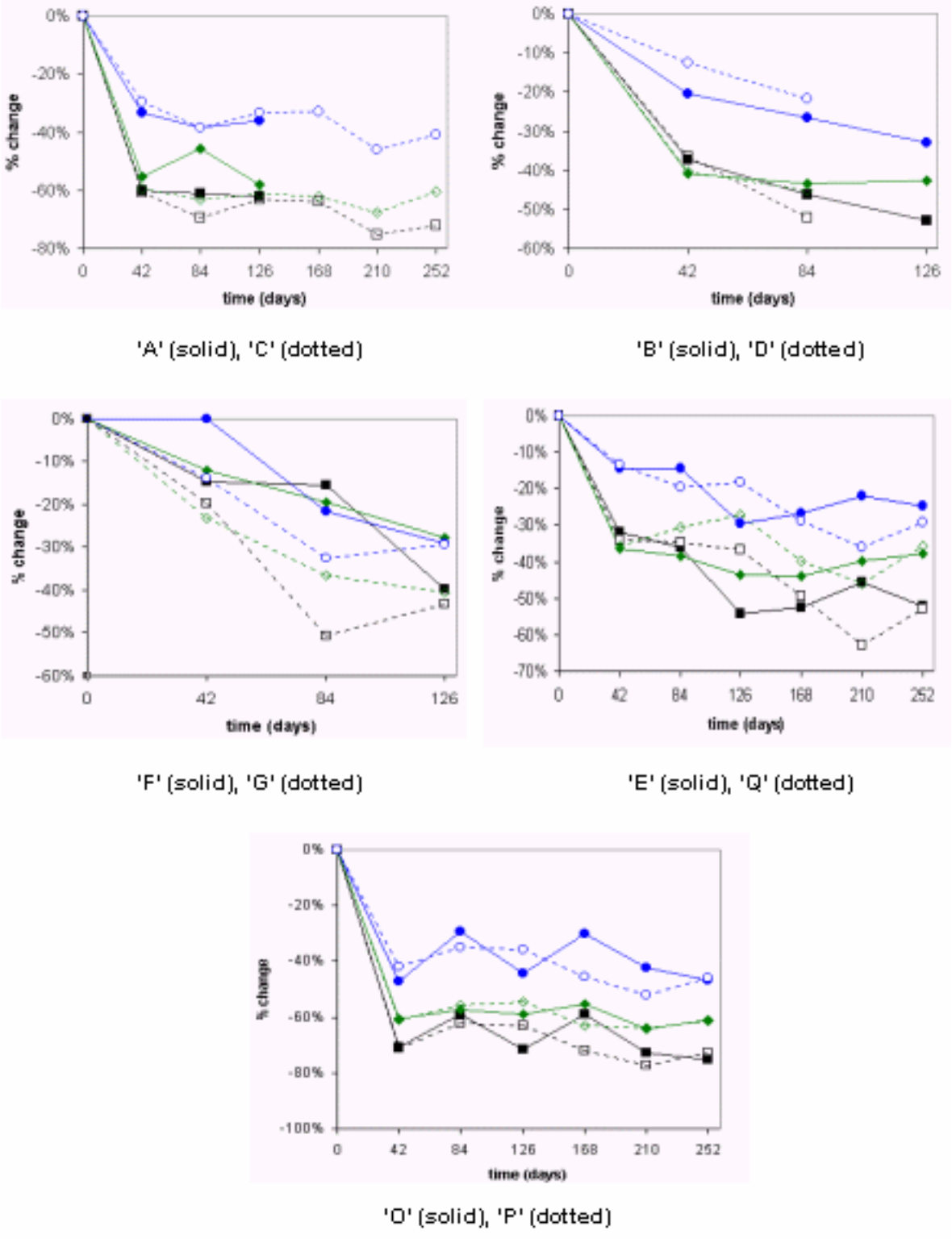

Figure 4-25 ABS normalized impact data. Key: □, EML; ◊, TE; ○, ML

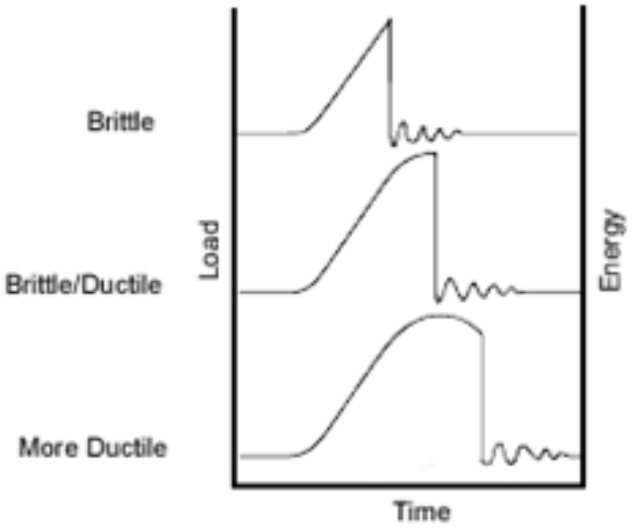

Figure 4-26 Impact testing failure modes

- Normalized total energy: ~ 10 to 180 ($ft \cdot lbs/in^2$)
- Normalized maximum load: ~ 900 to 8000 (lbs/in^2)

This suggests separating the samples according to failure mode to compare data. This would be difficult because of the dual nature of failure for many of the samples – showing a combination of brittle and ductile behavior, as illustrated in the combination profile in Figure 4-26. Many sample failures would thus be hard to separate into one mode or the other. Also, the distribution in each mode cannot be expected to stay constant. The confidence in comparative analysis is reduced when the sample size of each subset changes throughout the experiment. Therefore, no attempts at data categorization according to failure mode were made. However, with a focus on service life, failure mechanism is not significant in the eyes of the customer or manufacturer. As with the polyethylene samples, all that matters is when it actually fails. The average of all data, both for brittle and ductile behavior, hopefully characterizes the aging effects on an average ABS product exposed to similar irradiance.

The problem was alleviated with time. As the samples were oxidized under UV exposure, the expected embrittlement occurred and the failure mechanism shifted to mostly brittle failure by only 42 days of exposure (time period 1). This showed a positive effect on the variation of the impact strength data, as it was no longer polarized around two extremes.

A test for normalized distribution around the mean was performed on all data subsets (n=10 for controls, n=6 for all other time periods) to see how normally distributed the data is for each time period. The percent confidence in normality was taken as an average for all time periods to compare normality between formulations and is presented in Table 4-7.

Table 4-7 Percent confidence in normality for ABS impact data

	With controls			Without controls		
Formula	Energy to Max Load	Total Energy	Max Load	Energy to Max Load	Total Energy	Max Load
A	71.5	65	61	76.3	74.3	74.3
B	55.3	67	45.8	57.7	65	51
C	46	45.3	33.4	50.5	45.7	36.7
D	45	56.7	42.7	34	75.5	49
E	47.4	58.3	64.9	54	53.8	63.8
F	51	72.5	30	63.7	66.3	37.7
G	49.8	53.8	46.8	37.7	53.7	53
O	61.7	61	41.7	63.5	66.5	46.7
P	45.4	55.3	46	43.2	52.2	46.5
Q	51	62	50.4	48.5	58.2	56.5

All ABS formulations show little normalization of data; the average confidence in normality for all subsets is only about 50%, prompting the use of nonparametric tests in any statistical analysis. The dual failure mode is suspected to contribute to the limited

confidence in normality of the ABS impact strength data. This was confirmed by taking the average of the percent confidence in normality for each formulation again, but this time excluding the control percent confidence in normality. Because embrittlement caused the failure mode to become more unilaterally brittle-failure for all samples after the control samples, the percent confidence in normality should increase when excluding the polar distribution of data from the controls. This is indeed the case as a slight rise in most of the percent confidence values is seen (also in Table 4-7) after this exclusion.

4.5.2 Formula Exclusions

As mentioned in Section 3, no EDS analysis was performed on the ABS samples of formulations ‘B’, ‘C’, ‘D’, ‘P’, or ‘Q’. SEM and EDS analysis was only performed on formulas ‘A’, ‘E’, ‘F’, ‘G’, and ‘O’, due to the lack of statistical difference in the property profiles.

After collecting all of the impact property data and profiling it over time, obvious similarities in the profiles of the formulations were considered. Similar formulations were evaluated with statistics to determine if the profiles for various pairs of formulations were similar enough to not waste any further resources in their evaluation.

As seen in Table 4-7, the data even without the control samples included are (as with the PE data) non-parametric. Therefore, to test for a significant difference between the sample sets of paired formulations, the Wilcoxon signed-ranks test is used again, instead of the paired samples t-test.

The first possible exclusion evaluated was either ‘O’ or ‘P’. These two late-purchased sheets are both white and have similar additive packages. As seen in Figure 4-25, the profiles for each property are remarkably similar when paired for these two

formulations. Table 4-8 shows the Wilcoxon null hypothesis confidence perrcent for the comparison between the two paried sample sets.

Table 4-8 Null confidence (%) of 'O', 'P', and 'Q'

Comparison	Energy to max load	Total energy	Max load
O vs. P	44	16	44
O vs. Q	97	97	97

For all three properties, there is no significant difference between the profiles for 'O' and 'P', and thus separate analysis of their profiles will not provide any benefit over analyzing only one or the other. For comparison, 'O' and 'Q' should have very different degradation profiles due to the white/black color difference and do indeed show a significant difference with 97% confidence for all properties. Because 'O' has more normalized data than 'P' (Refer Table 4-7), 'P' was excluded.

'O' was then compared against 'C', the other white sheet with an additive package. The Wilcoxon null hypothesis returned similar results showing that there was no significant difference. Table 4-9 shows the Wilcoxon null hypothesis confidence percentages for all remaining significant comparisons. Because 'O' once again shows more normalization, 'C' was excluded, leaving 'O' as the lone white sheet with a UV-stabilizer package. 'A' was included, although white, because of the difficulty in proving statistical similarity with other profiles due to few data points (only three time periods).

For the black samples, 'D' was excluded because of the lack of data (pulled from chamber after 84 days to make way for the new sheets) and its lack of statistical difference from 'E', the other stabilized black sheet. 'Q', the later-purchased, UV-

Table 4-9 Null confidence (%) of remaining comparisons

Comparison	Energy to max load	Total energy	Max load
A vs. C	75	75	75
C vs. O	0	84	44
E vs. B	50	50	75
E vs. D	50	50	0
E vs. Q	16	78	56

stabilized black sheet showed little statistical difference from 'E', showed slightly less normalization, and was excluded. 'B', the non-stabilized black sheet, showed little statistical difference from 'E' either (even with similarly few data points as with 'A'), suggesting that the additives used in the black sheets did not improve their UV stability, and that the stability shown (when compared to the white sheets) is due to the carbon black and not the UV additives. Since 'B' has only three time periods of exposure, and is less normalized than 'E', it was excluded and 'E' remained as the only black formulation.

The competitor samples, being gray and brown, with highly different profiles from the other formulations, were both included. This left 'A', 'E', 'F', 'G', and 'O' as the only formulations to continue profiling and analyze with EDS.

4.5.3 Arrhenius Modeling of Impact Properties

As with the PE samples, the mechanical/physical property data of the ABS samples exhibits very little linear behavior (apart from the horizontal plateaus). The data is represented well by the Arrhenius variation (Equation 4-13), including the limit (horizontal plateau) at the tail ends of the profiles (Figure 4-27).

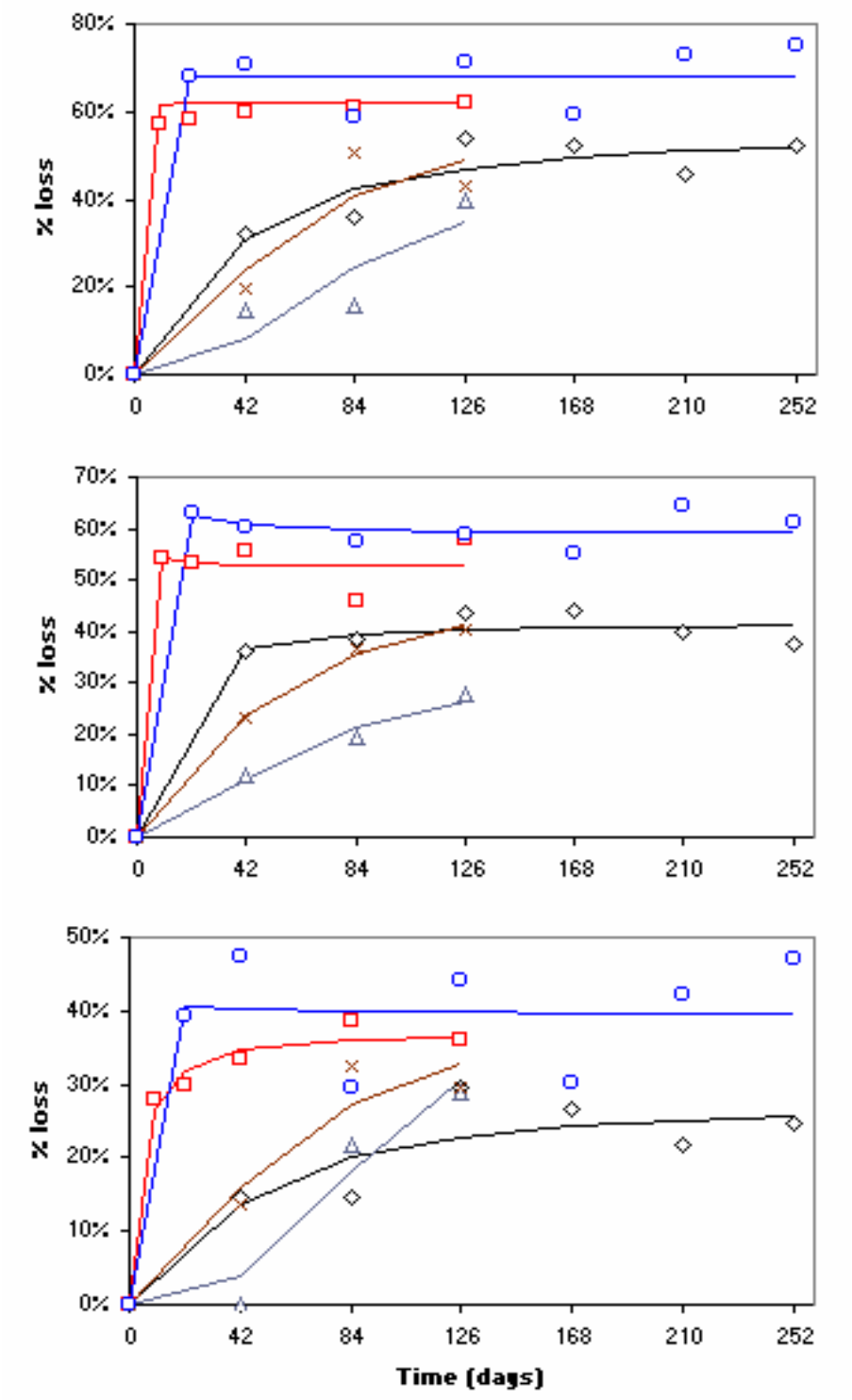

Figure 4-27 ABS impact data and fits: Energy to max load (top), total energy (middle), max load (bottom). Key: □, 'A'; ◊, 'E'; Δ, 'F'; x, 'G'; ○, 'O'

"F", "G", and "E" do not exhibit a horizontal limit in impact property changes over the 252 days of exposure. "E" appears to be approaching its limit in all cases (may already be reached at 126 days for total energy), but "F" and "G" still have relatively steep slopes at the end of the 126 days of their exposure, suggesting that the horizontal limit would not be reached for some time.

Unlike the PE samples, incubation periods were not recognizable from the data. This is most likely due to the plentitude of chromophores existent in the polymer structure's functional groups, allowing much faster rates of oxidation than with PE. There may still be an induction time in the photooxidation of ABS, but much shorter time periods would be required to detect any early trends of this nature.

This is especially true for the white formulations ('A' and 'O'), for which detection of induction times is not the only possible benefit of shorter time periods of evaluation. The white samples' mechanical property profiles show immediate sharp increases and then immediate leveling off (by 42 days) at horizontal plateaus for all mechanical properties (energy to maximum load, total energy, and maximum load) (Figure 4-28). With only min/max data, the profile of change over time in the mechanical properties and oxidation is impossible to determine without analysis of shorter times of exposure.

4.5.4 Challenge of Outdoor Tables

All ABS samples failed the 50% retention of impact properties test too soon to be considered as candidates for outdoor tables. This was known after only 84 days of testing. Therefore, the three new sheets ('O', 'P', and 'Q') were purchased from the same

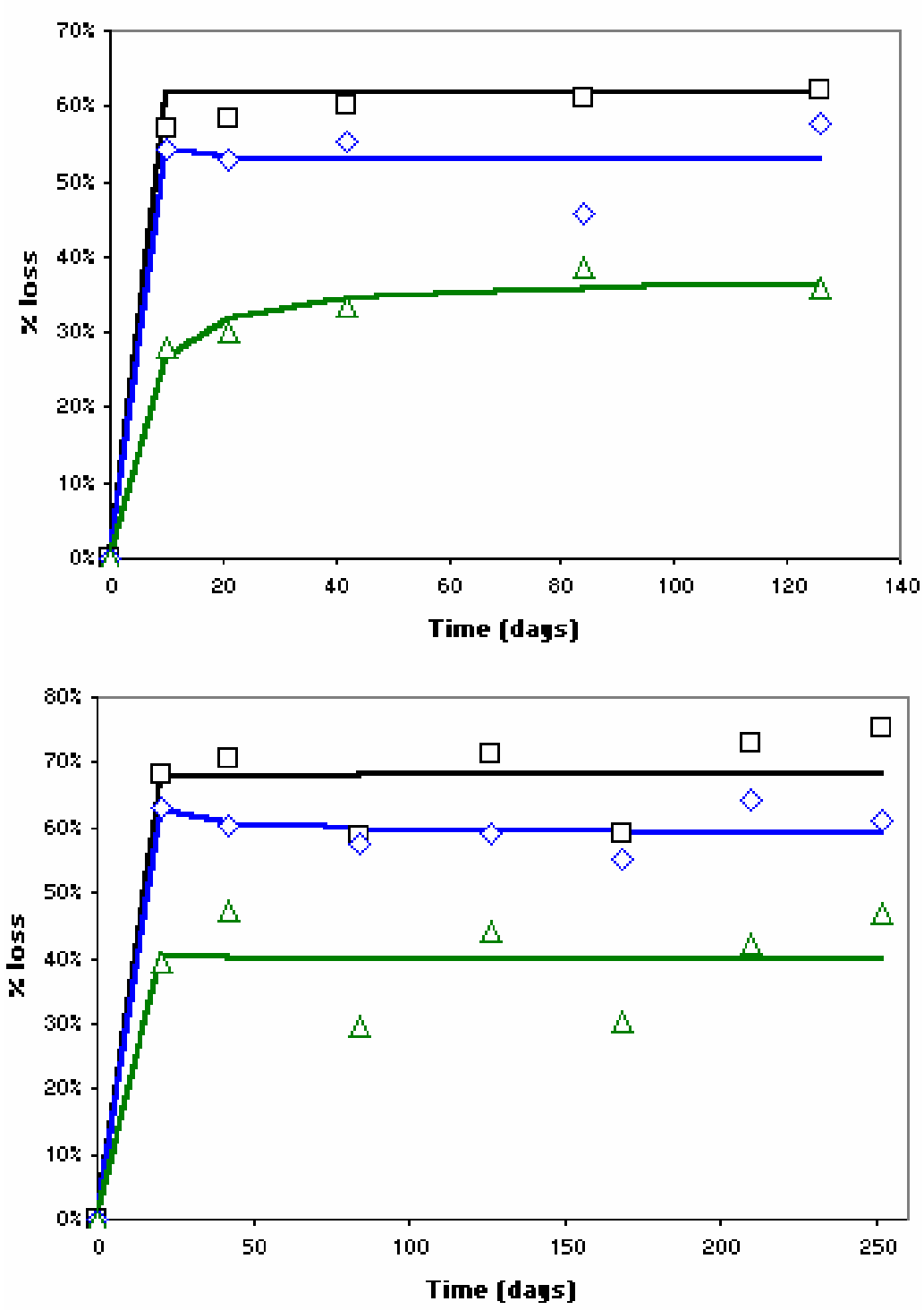

Figure 4-28 ABS impact data and fits: A (top), O (bottom). Key: □, energy to max load; ◊, total energy; Δ, max load

manufacturer with claims that these new formulations might perform better. Testing was abandoned of 'D' at that point (84 days) to create enough room in the UV chamber to begin testing the new samples. But these new samples faired just as poorly.

As this became apparent, it was suggested to Mity-Lite that there may not be a significantly functional anti-oxidant/UV-absorber package in any of the formulations purchased. The relative UV instability of ABS to other plastics due to the BR-portion double bonds (Piton and Rivaton 1997) was mentioned in Section 2-5, but additives should be able to make the material more stabilized than what was seen in this study. Mity-Lite confirmed that their own testing had shown the absence of or less of the UV-stabilizers specified in the additives packages. The competitor formulations 'F' and 'G' did not perform much better, and began with low impact strength properties initially when compared to the sheets purchased by Mity-Lite. The stabilization of ABS for outdoor products thus remains a daunting task.

4.6 Energy Dispersive Spectroscopy: ABS

4.6.1 C/O Ratios

The C/O ratio profiles for ABS do not exhibit linear behavior, as shown in Figure 4-29. However, all formulations of ABS show a horizontal plateau (limit) after 42 days of exposure. A data point was added at 21 days for "O" and 10 and 21 days for "A" to try to elucidate the profiles before the limit is reached, and the resultant profiles could be linear before this limit. These early data points are profiled in Figure 4-17 as well. But the slope of the curves is leveling off fast even at these time periods, prompting the need to look at

even shorter durations of exposure (under 2 weeks) to understand the pre-limit profiles and prove linear character of the C/O ratios.

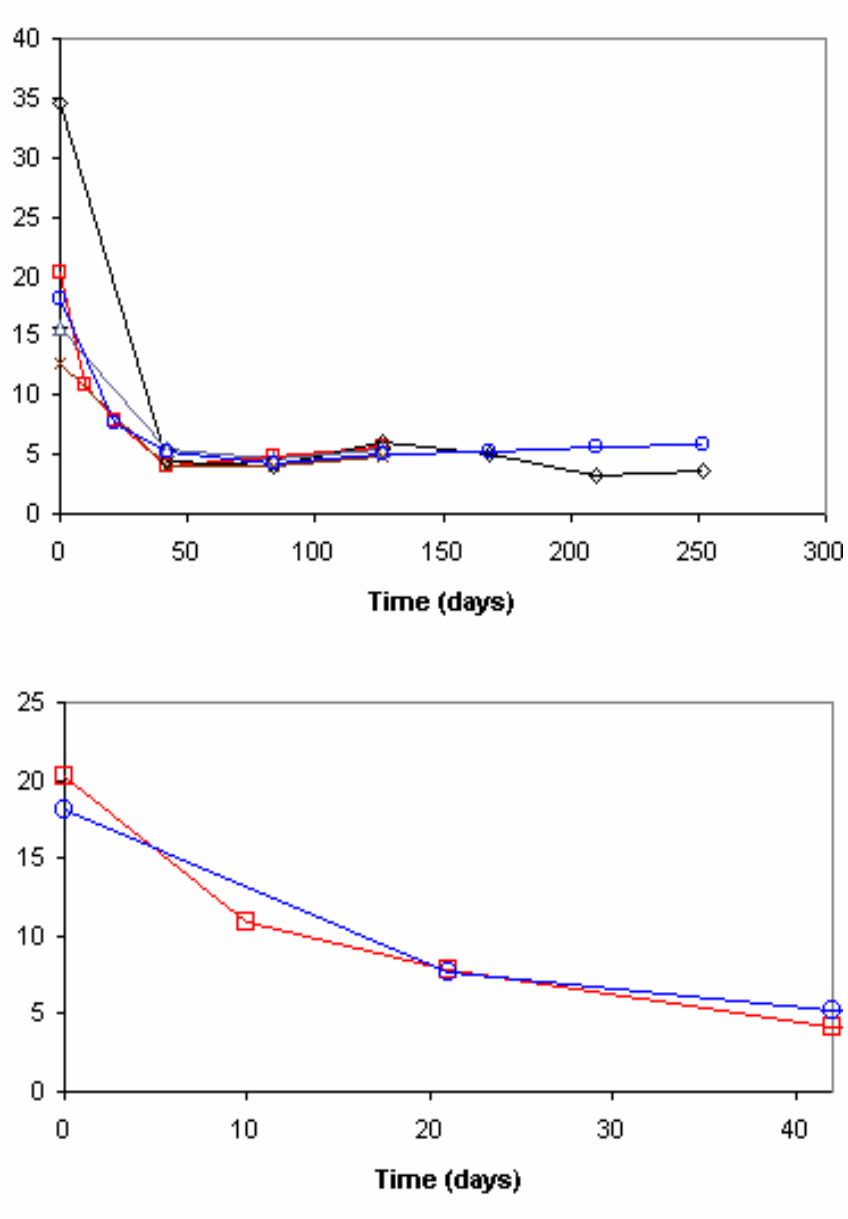

Figure 4-29 ABS C/O ratios: all exposure periods (top), 42 days and under (bottom). Key: □, 'A'; ◊, 'E'; Δ, 'F'; x, 'G'; ○, 'O'

4.6.2 Arrhenius Modeling of EDS Data

As with the C/O ratios for the ABS data, the O-percent profiles also reach a horizontal plateau after 42 days for exposure for all ABS formulations. As already mentioned, the "A" and "O" formulations' mechanical properties have all reached a horizontal plateau by 42 days as well – suggesting that without further oxidation the impact properties do not continue to decrease. This agrees with the stabilization reported by Yakimets, Lai and Guigon (2004) and mentioned in Section 2, and suggests Arrhenius character. The increasing oxidation and Arrhenius behavior correlation to the mechanical properties once again suggest compliance with the requirements listed in Section 1. The O-percent profiles, along with their modeled fits according to Equation 4-13 are presented in Figure 4-30.

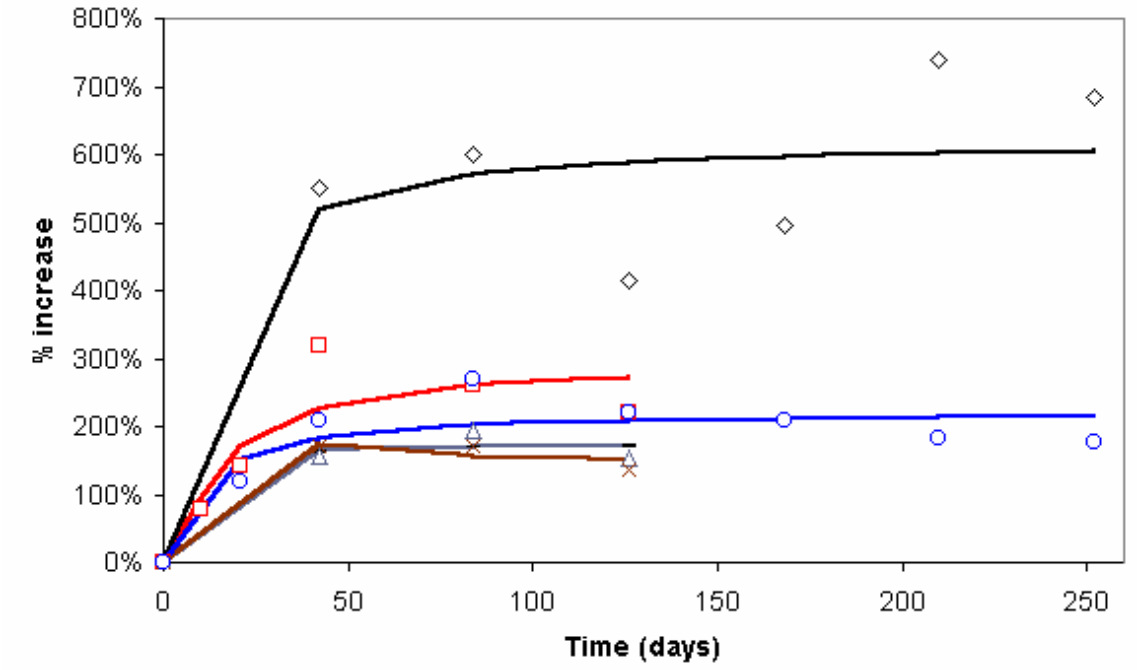

Figure 4-30 ABS O-percent data and fits. Key: □, 'A'; ◊, 'E'; Δ, 'F'; x, 'G'; ○, 'O'

In contrast, “F”, “G”, and “E” don’t exhibit this agreement between oxidation limit and mechanical properties, as none of these formulations showed any horizontal limits in impact property changes over the 252 days of exposure. The further decrease in mechanical properties even after surface oxidation has ceased could be due to deeper oxidation past an oxygen-saturated surface. This could be tested by future experimentation with higher EDS beam energy (15 kV) to increase sample depth penetration, or by performing similar EDS on the samples after microtoming the surface layers off as done by Gulmine and others (2003).

4.7 Correlation: ABS

4.7.1 Service Lifetime Prediction

Using Equation 4-15 with the fitted constants, the time to 50% loss was calculated for all properties and is presented in Table 4-10. The maximum load profiles show limits to degradation that prevent them from reaching a loss of 50%, and are not listed. The same applies to the total energy profiles for all samples except for ‘A’ and ‘O’. The profiles for these two formulations barely get past the 50% degradation plateau by 42 days, but then exhibit negative slopes and therefore cannot predict times according to their fits.

The negative slope of the O-percent fit for ‘G’ prevents this function to predict times as well. But the graphed profile of ‘G’ shows a close match to the profile for ‘F’ at a 50% increase in O-percent, so the time can be inferred to be the same as for ‘F’, or 2.4 months.

Table 4-10 Time (months) to 50% decrease in energy to max load and 50% increase in oxygen content: ABS

Formulation	Energy to Max Load	Oxygen Content
A	0.1	6.6
E	183.9	3.1
F	243.3	2.4
G	132.8	N/A
O	0.4	5.6

4.7.2 Other Correlations

As done with the PE fit constants (*A* and *B*), the ABS mechanical property fit constants were compared to the EDS fit constants as ratios. 'E', 'F', and 'G' were not expected to correlate well to the EDS data because of the disagreement in saturation time (at what point does the limit happen). Table 4-11 shows all the fitted constants and the EDS/property ratios of the fitted constants.

Table 4-11 Fit constants *A* and *B*, and ratio comparisons between EDS and impact properties: ABS

	Energy to Max Load		Total Energy		Max Load		EDS	
Sheet	*A*	*B*	*A*	*B*	*A*	*B*	*A*	*B*
'A'	0.619	0.023	0.527	-0.272	0.375	3.366	3.00	11.8
ratio:	4.85	519.57	5.70	-43.42	8.01	3.50		
'E'	0.576	26.110	0.421	5.662	0.293	31.824	6.25	7.79
ratio:	10.85	0.30	14.84	1.38	21.38	0.24		
'F'	0.732	92.581	0.412	55.433	0.853	129.718	1.76	3.08
ratio:	2.41	0.03	4.29	0.06	2.07	0.02		
'G'	0.703	45.326	0.544	35.202	0.468	45.223	1.40	-9.23
ratio:	1.98	-0.20	2.57	-0.26	2.98	-0.20		
'O'	0.681	0.120	0.590	-1.235	0.396	-0.533	2.23	8.31
ratio:	3.27	69.01	3.78	-6.73	5.63	-15.58		

There is no natural-weathering ABS data to compare the ratios across weathering modes, as done with the PE data. However, some interesting trends are apparent. The black sheet ('E') shows the highest ratios in *A* (the linear scalar factor in Equation 4-13).

This agrees with the PE ratios where the black data shows extremely high *A*-ratios, showing agreement across materials and testing environments.

These ratios could be used in correlating mechanical to chemical degradation as well. With an ABS product of similar formulation (color and additives), the O-percent profile could be established and fit after only a few weeks of QUV exposure. The impact property profiles and service lifetime could then be predicted, without mechanical testing, by extrapolation with these ratios.

It seems that the ratios for each constant increase in linear proportion to each other from property to property within each formulation. This was quantified by dividing the ratios for total energy by those for energy to max load, and then dividing the ratios for max load by the ratios for energy to max load. These secondary ratios were noticed to be comparable at least for *A*, so the averages and their standard deviations were calculated as well. The results are presented in Table 4-12.

Table 4-12 Comparison of EDS : property ratios across properties

	Total Energy / Energy to Max Load		**Max Load / Energy to Max Load**	
Formulation	A	B	A	B
A	1.173	-0.084	1.651	0.007
E	1.368	4.612	1.970	0.820
F	1.777	1.670	0.858	0.714
G	1.294	1.288	1.503	1.002
O	1.156	-0.098	1.721	-0.226
Average	**1.354**	**1.478**	**1.541**	**0.463**
St Deviation	**0.252**	**1.924**	**0.417**	**0.539**

The data seems to be suitably distributed for *A*, as the standard deviations are ~20 to 25% of the mean. The standard deviations are greater than their corresponding means,

however, for *B*. As predicted, the data for 'E', 'F', and 'G' does not agree with each other in these EDS correlations as do 'A' and 'O'. The 'A' and 'O' ratios are in fact highly comparable. The averages for only the 'A' and 'O' data would be A=1.165 and B=-0.091 for the TE/EML ratio, and A=1.686 and B=-0.110 for the ML/EML ratio. This shows some correlation between the different impact properties measured.

The correlation method of Carrasco and others (2001) was again attempted with the ABS data. Figure 4-31 shows the profiles of the three impact properties against the change in O-percent. If the initial data points (control) are disregarded, linearity is seen for most profiles. However, this is once again already evident in the time profiles – linearity is shown after the first time period because of the limit in degradation reached.

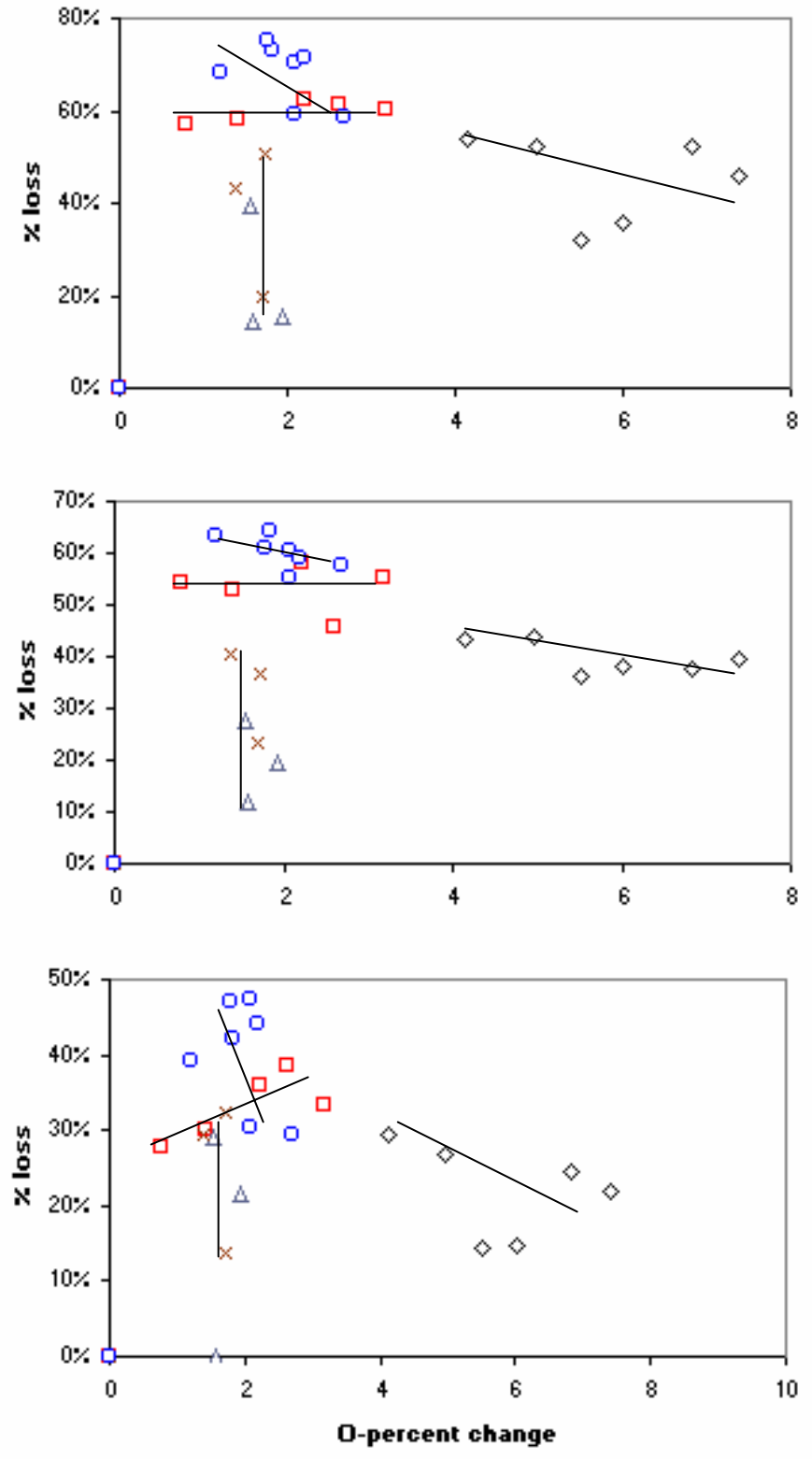

Figure 4-31 ABS property change vs. change in O-percent: energy to max load (top), total energy (middle), max load (bottom). Key: □, 'A'; ◊, 'E'; Δ, 'F'; x, 'G'; ○, 'O'

5 Conclusions and Recommendations

5.1 Evaluation of EDS Method

In accordance with the primary purpose of this study, as presented in Section 1, EDS analysis has proven to be a rapid, useful method of characterization of the oxidation in weathered plastic materials. The two requirements given in Section 1 for qualification of this method of analysis were:

1. Quantification of the extent of oxidation in a weathered plastic should yield clear profiles of increasing oxidation.
2. The profile of increasing oxidation should be able to be systematically correlated (matched up and agree) to the corresponding profiles of the mechanical properties of the weathered plastic.

Very good results were seen in respect to the first requirement. EDS analysis provided successful characterization of the extent of oxidation over time in the tested samples. The oxidation profiles (of most samples) yielded by the EDS method showed a clear increasing trend and even Arrhenius character agreeing with the usual profiles of chemical reaction-driven changes (incubation, acceleration, and stabilization phases).

Good results were also achieved in respect to the second requirement. Arrhenius-based modeling of the elongation in the PE samples, the impact strength of the ABS

samples, and the EDS oxygen content in both samples, produced similar profiles and provided a good understanding of the effects of photooxidative degradation on polyethylene and ABS over time. Modeling with a variation of the Arrhenius equation, of the oxygen content (O-percent) by EDS analysis provided similar profile trends to those seen in modeling of the mechanical property degradation. Incubation, acceleration and stabilization phases were all seen at similar time-of-exposure for both the oxygen content and the mechanical properties.

5.1.1 PE and ABS Comparison

As mentioned in Section 1, the effectiveness of EDS analysis was to be compared between moderately UV-sensitive materials (polyethylene) and highly sensitive ones (ABS). The effectiveness of the analysis is the degree to which it meets the two requirements listed above for establishment of the method. EDS analysis of the laboratory-weathered polyethylene samples ('W') shows high effectiveness. The samples produced increasing trends in oxidation, regular enough to show linear carbon-to-oxygen ratios over time (first requirement). The 'W' samples also show matching time-of-exposure for each stage of the Arrhenius behavior when compared to the mechanical property profiles (second requirement). The natural-weathered polyethylene samples ('L' and 'N') also show linear carbon-to-oxygen ratios, but do not exhibit regularly increasing oxidation profiles.

The ABS samples all show regular increasing trends in oxidation as well as Arrhenius behavior, but the pre-saturation (before the stabilization limit) oxidation curve is not well illustrated by this data because oxidation happened much faster than expected. To elucidate the pre-limit profiles and prove linear character of the carbon-to-oxygen

ratios requires further experimentation at even shorter durations of exposure (under 2 weeks).

The white ABS samples ('A' and 'O') showed stabilization at the same time-of-exposure as the mechanical properties (at 42 days). But the darker colored samples ('F', 'G', and 'E') did not correlate to their mechanical property profiles as well as the white samples or the polyethylene samples. The stabilization phase of the oxidation profile for these colors happened at earlier times-of-exposure than the projected stabilization time-of-exposure for the mechanical properties. This was attributed to deeper oxidation past an oxygen-saturated surface. This could also be tested by future experimentation, using higher EDS beam energy (15 kV) to increase sample depth penetration, or by performing similar EDS on the samples after microtoming the surface layers off.

In summary, the laboratory weathered polyethylene samples show the greatest effectiveness using EDS analysis, followed by the ABS samples, and then the natural weathered polyethylene samples.

5.2 Service Lifetime Prediction

The secondary objective of this study was to establish a method to predict the service lifetime of plastic materials in an outdoor environment. This was done by two methods. First, the modeled property change profile was projected to a certain degradation amount. Modeling of the elongation in the PE samples, the impact strength of the ABS samples, and the degree of oxidation in both allowed the extrapolation of the time-profiles to the point where oxidation is high enough to cause the mechanical properties to drop to a level that would be considered to be the end of the useful life of

the material. By this method, the service life of these plastics in the outdoor environment was predicted. For example, the time to a 50% drop in the elongation for the polyethylene samples is presented in Table 5-1, and the time to a 50% drop in the energy to maximum load in Dynatup impact testing for the ABS samples is presented in Table 5-2.

Table 5-1 Time (months) to 50% decrease in elongation for PE samples. Key: W, WOM (accelerated weathering); N, natural sunlight

Weathering Mode	Color	Time to 50% Elongation
W	black	24.6
W	green	11.7
W	green FA	11.1
W	blue	7.6
N	black	56.4
N	green	40.0
N	green FA	149.1
N	blue	91.7
N	brown	88.5

Table 5-2 Time (months) to 50% decrease in energy to maximum load (EML) for ABS samples by formulation

Formulation	Time to 50% EML
A	0.1
E	183.9
F	243.3
G	132.8
O	0.4

The second method of service lifetime prediction is one developed in this study and is based on correlating the EDS analysis of oxidation amounts to the previously determined relationship between oxidation and the degrading mechanical property. In this method, the time-of-exposure to a certain drop in a property is projected solely from EDS data and does not require mechanical testing. This is a valuable method because of the

comparatively non-destructive nature of the EDS testing as it only requires a small shaving off of the surface of the experimental samples.

This correlation was made by examining the fitted constants in the modified form of the Arrhenius Equation (Equation 4-13) that was used to model the data. The constants from the mechanical property profiles were related to the equivalent constants in the oxidation profiles and expressed as ratios between the two.

For the polyethylene samples, the ratios were found to be comparable between weathering modes, i.e. the ratios are nearly the same for a given mechanical property across all the data for 'W', and 'N'. The similarities oftentimes applied to the 'L' samples as well. This has great implications: no matter what rate of weathering occurs on a plastic product, the oxidation will still correlate in the same, repeatable way to mechanical property degradation. This provides a correlation that could be used for prediction of degradation and service life with only a few EDS measurements. By exposing any PE product with similar color to a short duration of accelerated weathering, the profiles of natural oxidation and mechanical property degradation can be extrapolated from EDS measurements of oxygen content.

To understand how widely this correlation can be applied requires further testing of the mechanical property degradation and O-percent for PE samples of a variety of colors and weathering rates.

5.3 Acceleration Factors

As discussed in Section 1, this study was not intended to evaluate the correlation of accelerated weathering devices to natural weathering. But due to the availability of

accelerated versus natural weathering data for the polyethylene samples in this study, the correlation between the two weathering modes was commented on for the purposes of further research into this area.

The time-profiles of property degradation were quickly "eyeballed" to determine a kind of acceleration factor by comparing the maximum percent property change. For example, the 'W' (WOM) blue carts' melt index data shows a maximum change of nearly 50% over the 3 years of exposure, whereas the 'N' (natural sunlight) blue carts only show a maximum change of about 12% over the same period of exposure, giving roughly a 4:1 ratio (4x). In similar fashion, the elongation and impact strength both show ~5:2 (2.5x) and density shows ~8:5 (1.6x). This does not show the typical acceleration factor however, which is based on the ratio of time to a certain change in a property. But it is a quick method to determine which properties will change the most.

By comparing the slopes of the carbon-to-oxygen ratio profiles over time, an acceleration factor for oxidation was produced. The laboratory-weathered samples ('W') exhibit a slope 2.3 times as steep as the naturally weathered samples ('N'), indicating that the acceleration factor is 2.3x for oxidation of the polyethylene samples in this experimental setup.

The most typically reported acceleration factors come from simply dividing the time of natural exposure to a given property change (often 50% decrease) by the time of accelerated exposure to the same property decrease. By dividing the time to 50% change for the 'N' samples by the 'W' samples, the acceleration factor for this experimental setup (PE, Los Angeles outdoors: WOM) was calculated. This was done for both

elongation (50% decrease) and extent of oxidation (O-percent)(50% increase). The factors are presented by color in Table 5-3 (repeated from Table 4-4).

Table 5-3 Acceleration factors for PE: elongation and extent of oxidation (based on 50% change)

Color	Elongation	O-percent
black	2.29	1.15
green	3.41	0.80
green FA	13.39	1.21
blue	12.10	1.20
Average	**7.80**	**1.09**

The great range in acceleration factor for elongation is perplexing, but agrees with the confusion associated with reported acceleration factors throughout the literature. An average of 7.8x for elongation of PE agrees with the 6-8x reported in the literature (Gijsman, Hennekens and Janssen 1996).

The extent of oxidation shows a much smaller range. The average of 1.1 denotes nearly equal rates of oxidation in both the WOM and naturally weathered samples. The oxygen uptake for PE demonstrated an acceleration factor of 2.5x in the same study by Gijsman, Hennekens and Janssen (1996). The low multiplier calculated in this study is equally as perplexing as the variation in the elongation acceleration factor.

5.4 ABS Outdoor Table Evaluation

All ABS samples lost 50% of their impact properties too soon to be considered as candidates for outdoor tables. The stabilization of ABS for outdoor products remains a challenge.

5.5 Summary and Future Experimentation

EDS is therefore presented as a viable means of monitoring the oxidation in a plastic-weathering system. But no comparisons were made in this study to other methods, suggesting further experimentation. EDS could further be tested as not only a viable means, but also the best means of oxidation-characterization by directly comparing the resultant oxidation profiles to the oxidation profiles provided by other commonly used characterization methods (e.g. FTIR-ATR and XPS) for the same weathering system. The oxidation profiles for all methods could then be matched to mechanical property profiles of the weathering system to see which method shows the best correlation (most agreement).

Further experimentation is also recommended to understand the time profiles of the oxidation of ABS. The oxidation of the ABS samples is not well illustrated by this data because oxidation happened much faster than expected. To apply the Arrhenius fit to the incubation and acceleration stages of the oxidation of ABS requires further experimentation at even shorter durations of exposure (under 2 weeks).

The last area of recommended future experimentation applies to the service-life prediction method using Arrhenius fit constants. A non-destructive method of service life prediction has been proposed based upon the behavior of the studied samples which does not require any testing other than EDS analysis. The correlation upon which this prediction method is based, however, requires further testing to determine its applicability. Testing should involve a variety of weathering environments (both natural and accelerated) as well as colors to determine how broadly the correlation may be applied.

References

Airaudo, C. B., A. Gayte-Sorbier, P. Aujoulat, and V. Mercier. "Thin-layer Chromatography of Amine Antioxidants and Antiozonants Used in Elastomers." *Journal of Chromatography* 437 (1988): 59-82.

Allen, N. S., ed. *Degradation and Stabilisation of Polyolefins.* London: Applied Science Publishers, 1983.

Allen, N. S., M. Edge, and M. Mohammadian. "UV and thermal Hydrolytic Degradation of Poly(ethylene terephthalate): Importance of Hydroperoxides and benzophenone end groups." *Polymer Degradation and Stability* 41 (1993): 191-196.

Allen, N. S., M. Edge, T. Corrales, M. Shah, D. Holdsworth, F. Catalina, C. Peinado, and E. P. Collar. "Thermal and Photooxidation of Polypropylene Influence of Long-term Ambient Oxidation: Spectroscopic, Thermal and Light Scattering Studies." *Polymer* 37, no. 12 (1996): 2323-2333.

Andrady, A. L. "Wavelength Sensitivity in Polymer Photodegradation." *Advances in Polymer Science* 128 (1997): 47-94.

"ASTM Reference Manual." Philadelphia: American Society for Testing and Materials, 2001.

Bataillard, P., L. Evangelista, and M. Thomas. "21: Analytics." In *Plastics Additives Handbook*, edited by H. Zweifel, and S. E. Amos. 5th ed. Cincinnati: Hanser Gardner Publications, 2001.

Bell, B., D. E. Beyer, N. L. Maecker, R. P. Papenfus, and D. B. Priddy. "Permanence of polymer stabilizers in hostile environments." *Journal of Applied Polymer Science* 54, no. 11 (1994): 1605-1612.

Billingham, N. C. "Physical Phenomena in the Oxidation and Stabilization of Polymers." In: *Oxidation Inhibition in Organic Materials, Vol. 2,* edited by J. Posposil and P. P. Klemchuk, 249-298. Boca Raton, FL: CRC Press (1990).

Bonekamp, J. E., N. L. Maecker. "The Permanence of UV Absorbers in a Rubber-modified Acrylic Film by UV/visible Spectrophotometry." *Journal of Applied Polymer Science* 54, no. 11 (1994): 1593-1604.

Brewis, D. M., R. H. Dahm, and I. Mathieson. "Electrochemical Pretreatment of Polymers with Dilute Nitric Acid Either Alone or in the Presence of Silver Ions." *Journal of Adhesion* 72 (2000): 373-386.

Bruijn, J. C. M. "Degradation Profiles of Thick High-Density Polyethylene Samples after Outdoor and Artificial Weathering." In *Polymer Durability: Degradation, Stabilization and Lifetime Prediction: Advances in Chemistry Series No. 249*, edited by R. L. Clough, N. C. Billingham, and K. T. Gillen, 599-620. Washington DC: American Chemical Society, 1996.

Budinski, K. G., and M. K. Budinski. *Engineering Materials: Properties and Selection*. 6th ed. Upper Saddle River, New Jersey: Prentice Hall, 1999.

Carey, F. A., and R. J. Sundberg. *Advanced Organic Chemistry, Part A: Structure and Mechanisms*. 3rd ed. New York: Plenum Press; 1990.

Carrasco, F.; P. Pagès, S. Pascual, and X. Colom. "Artificial Aging of High-density Polyethylene by Ultraviolet Irradiation." *European Polymer Journal* 37, no. 7 (July 2001): 1457-1464.

Celina, M., C. A. George, and N. C. Billingham. "Physical Spreading and Heterogeneity in Oxidation of Polypropylene." In *Polymer Durability: Degradation, Stabilization and Lifetime Prediction: Advances in Chemistry Series No. 249*, edited by R. L. Clough, N. C. Billingham, and K. T. Gillen, 159-174. Washington DC: American Chemical Society, 1996.

Conover, W. J. *Practical Nonparametric Statistics*. 3rd ed. New York: John Wiley & Sons, 1999.

Davis, A., and D. Sims. *Weathering of Polymers*. London: Applied Science, 1983.

Dorsey, J. G., W. T. Cooper, B. A. Siles, J. P. Foley, and H. G. Barth. "Liquid Chromatography: Theory and Methodology." *Analytical Chemistry* 68 (1996): 515R-568R.

Favez, D., D. G. Castner, B.D. Ratner, and H.J. Mathieu. "RF-plasma deposition and surface characterization of a biodegradable thin film coating." *European Cells and Materials* 3, Suppl. 1 (2002): 20-21.

Fechine, G. J. M., M. S. Rabello, R. M. Souto, and L. H. Catalani. "Surface Characterization of Photodegraded Poly(ethylene terephthalate). The Effect of Ultraviolet Absorbers." *Polymer* 45 (2004): 2303-2308.

Fujimoto, E., and T. Fujimaki. "Effects of pendant methyl groups and lengths of methylene segments in main-chains on photodegradation of aliphatic polyesters." *Polymer Journal: Society of Polymer Science* 31 (1999): 645-650.

Ghiggino, K. P. "Spectroscopic Methods in Polymer Studies." In: *The Effects of Radiation on High-Technology Polymers: ACS Symposium Series No. 381,* edited by E. Reichmanis and J. H. O'Donnell, 27-42. Washington DC: American Chemical Society, 1989.

Gijsman, P., J. Hennekens, and K. Janssen. "Comparison of UV Degradation of Polyethylene in Accelerated Test and Sunlight." In *Polymer Durability: Degradation, Stabilization and Lifetime Prediction: Advances in Chemistry Series No. 249*, edited by R. L. Clough, N. C. Billingham, and K. T. Gillen, 621-636. Washington DC: American Chemical Society, 1996.

Gijsman, P., G. Meijers, and G. Vitarelli. "Comparison of the UV-Degradation Chemistry of Polypropylene, Polyethylene, Polyamide 6 and Polybutylene Terephthalate." *Polymer Degradation and Stability* 65 (1999): 433-441.

Gillen, K. T., and R. L. Clough. "Models for Diffusion-Limited Oxidation." In *Radiation Effect on Polymers: ACS Symposium Series No. 475,* edited by R. L. Clough and S. W. Shalaby, 457-472. Washington DC: American Chemical Society, 1991.

Gillen, K. T., R. L. Clough, and J. Wise. "Prediction of Elastomer Lifetimes from Accelerated Thermal-Aging Experiments." In *Polymer Durability: Degradation, Stabilization and Lifetime Prediction: Advances in Chemistry Series No. 249*, edited by R. L. Clough, N. C. Billingham, and K. T. Gillen, 557-575. Washington DC: American Chemical Society, 1996.

Goldstein, J., D. Newbury, D. Joy, C. Lyman, P. Echlin, E. Lifshin, L. Sawyer, and J. Michael. *Scanning Electron Microscopy and X-Ray Microanalysis*. 3rd ed. New York: Kluwer Academic/Plenum, 2003.

Gulmine, J.V.; P. R. Janissek, H. M. Heise and L. Akcelrud. "Degradation Profile of Polyethylene After Artificial Accelerated Weathering." *Polymer Degradation and Stability* 79 (2003): 385-397.

Hackett, T. B., and K. D. Dillenbeck. "Characterization of Polyethylene as a Packaging Material for High Purity Process Chemicals." In: *Cost Effective Problem-Solving through Technical Creativity: Proceedings of the 39th Annual Technical Meeting of the Institute of Environmental Sciences Held in Las Vegas, Nevada, 2-7 May 1993,* 192-199. Rolling Meadows, IL: Institute of Environmental Sciences Press, 1993.

Hrdlovic, P. "Comparison of Photodegradation of some Common Polymers; Polyethylene, Polypropylene, Polyamide 6 and Polybutene Terephthalate." *Polymer News* 25, no. 8 (2000): 261-265.

Jahan, M. S., C. Wang, G. Schwartz, and J. A. Davidson. "Combined chemical and Mechanical Effects on Free-Radicals in UHMWPE joints during implantation". *Journal of Biomedical Materials Research* 25, no. 8 (1991): 1005-1017.

Kaczmarek, H. and C. Decker. “Photodegradation of Polystyrene and Polymethylmethacrylate Blends.” *Polymer Networks & Blends* 5 (1995): 1-10.

Kagiya, T., S. Nishimoto, Y. Watanabe, and M. Kato. “Importance of the Amorphous Fraction of Polypropylene in the Resistance to Radiation-induced Oxidative Degradation.” *Polymer Degradation and Stability* 12, no. 3 (1985): 261-275.

Karlsson, S., M. Hakkarainen, and A. Albertsson. “Dicarboxylic Acids and Ketoacids Formed in a Degradable Polyethylenes by Zip Depolymerization through a Cyclic Transition State.” *Macromolecules* 30 (1997): 7721-7728.

Kelly, C.T., J. R. White. “Photo-degradation of polyethylene and polypropylene at slow strain-rate.” *Polymer Degradation and Stability* 56, no. 3 (June 1997): 367-383.

Küpper, L., J. V. Gulmine, P. R. Janissek, and H. M. Heise. “Attenuated Total Reflection Infrared Spectroscopy for Micro-Domain Analysis of Polyethylene Samples after Accelerated Ageing within Weathering Chambers.” *Vibrational Spectroscopy* 34 (2004): 63-72.

Kurtz, S. M., O. K. Muratoglu, F. Buchanan, B. Currier, R. Gsell, K. Greer, G. Gualtieri, R. Johnson, S. Schaffner, K. Sevo, S. Spiegelberg, F. W. Shen, and S. S. Yau. “Interlaboratory Reproducibility of Standard Accelerated Aging Methods for Oxidation of UHMWPE.” *Biomaterials* 22 (2001): 1731-1737.

Kaczmarek, H. “Changes of Polymer Morphology Caused by U.V. Irradiation: 2. Surface Destruction of Polymer Blends.” *Polymer* 37, no. 4 (1996): 547-553.

Lee, S. H., and E. Ruckenstein. “Stability of Polymeric Surfaces Subjected to Ultraviolet Irradiation.” *Journal of Colloid and Interface Science* 117, no. 1 (May 1987): 172-179.

Lemaire, J., J. Gardette, J. Lacoste, P. Delprat, and D. Vaillant. “Mechanisms of Photooxidation of Polyolefins: Prediction of Lifetime in Weathering Conditions.” In *Polymer Durability: Degradation, Stabilization and Lifetime Prediction: Advances in Chemistry Series No. 249*, edited by R. L. Clough, N. C. Billingham, and K. T. Gillen, 577-598. Washington DC: American Chemical Society, 1996.

Lewis, C. J. “Quantifying the Effects of Aging on the Mechanical Properties of Medical Grade Polycarbonate and UV Cured Adhesives.” Master’s diss., Brigham Young University, 2004.

Maher, J. P., and D. H. Bank. “Development of a Methodology for Analysis of Full Field Strains in Thermoplastic Exterior Body panels Using Photoelastic Techniques.” In: *SAE Technical Paper Series, International Congress and Exposition Held in Detroit, Michigan 24-28 February 1992,* 299-308. Warrendale, Pennsylvania: SAE International, 1992.

Makowsik, M., S. Samuels, and A. Wagner. “Effect of Environmental Pollutants on the Discoloration of Polyolefins.” In *Proceedings of the 17th Annual International Conference on Advances in Stabilization and Degradation of Polymers Held in Luzern, Switzerland, June 1995,* edited by A. V. Patsis, 1-10. Basel: Technomic, 1995.

Marcato, B., C. Fantazzini, and F. Sevini. “Determination of Polymeric Hindered Amine Light Stabilizers in Polyolefins by High-performance Liquid Chromatography.” *Journal of Chromatography* 553 (1991): 415.

McKelvy, M. L., T. R. Britt, B. L. Davis, J. K. Gillie, L. A. Lentz, A. Leugers, R. A. Nyquist, and C. L. Putzig. “Infrared Spectroscopy.” *Analytical Chemistry* 68 (1996): 93R-160R.

Miller, M. A., and J. F. Maguire. “A Cumulant Expansion Approach to Predict the Service Lifetime of Polymers and Polymer Composites.” In: ASME International Congress and Exposition, 12-17 November 1995, edited by C. T. Sun, B.V. Sankar, and Y. D. S. Rajapakse, 63-66. Atlanta: ASME 1995.

Motyakin, M. V., J. L. Gerlock, and S. Schlick. “Electron Spin Resonance Imaging of Degradation and Stabilization Processes: Behavior of a Hindered Amine Stabilizer in UV-Exposed Poly(acrylonitrile-butadiene-styrene) Polymers.” *Macromolecules* 32 (1999): 5463-5467.

O'Donnell, B., J. R. White, and S. R. Holding. “Molecular Weight Measurement in Weathered Polymers.” *Journal of Applied Polymer Science* 52 (1994): 1607-1618.

Onyiriuka, E. C. “Effects of high-energy radiation on the surface chemistry of polystyrene: A mechanistic study.” *Journal of Applied Polymer Science* 47 (1993): 2187-2194.

Osawa, Z., S. Kuroda, S. Kobayashi, and F. Tanabe. “Photodegradation Mechanisms of Poly(*p*-phenylene sulfide) and Its Model Compounds.” In *Polymer Durability: Advances in Chemistry Series No. 249*, edited by R. L. Clough, N. C. Billingham, and K. T. Gillen, 127-138. Washington DC: American Chemical Society, 1996.

Piton, M., and A. Rivaton. “Photo-oxidation of ABS at long wavelengths ($\lambda > 300$ nm).” *Polymer Degradation and Stability* 55 (1997): 147-157.

Pospíšil, J. “Aromatic and Heterocyclic Amines in Polymer Stabilization.” In *Polysoaps/Stabilizers/Nitrogen-15 NMR*: *Advances in Polymer Science 124,* 87-189. Berlin: Springer, 1995.

Qayyum, M. M., and J. R. White. “Plastic Fracture in Weathered Polymers.” *Polymer* 28, no. 3 (1987): 469-476.

Qayyum, M. M., and J. R. White. “The Effect of Weathering on Residual Stresses and Mechanical Properties in Injection-Moulded Semi-Crystalline Polymers.” *Journal of Materials Science* 21, no. 7 (1986): 2391-2402.

Rabek, J. F. *Photostabilisation of Polymers*. London: Elsevier, 1990.

Rabello, M. S., and J. R. White. “Photodegradation of Polypropylene Containing a Nucleating Agent**.**” *Journal of Applied Polymer Science* 64 (1997): 2505-2517.

“Railway Gazette International.” Vol. 150, no. 9, 1450-1457. Sutton, England: Reed Business Publishing, 1994.

Ranby, B., and J. F. Rabek. *Photodegradation, Photo-oxidation and Photostabilisation of Polymers*. London: John Wiley & Sons, 1975.

Reich, L., and S. S. Stivala. *Elements of Polymer Degradation.* New York: McGraw-Hill, 1971.

Rodriguez, F. *Principles of Polymer Systems*. 4th ed. Washington DC: Taylor & Francis, 1989.

Sandilands, G. J., and J. R. White. “Effect of Aging on Internal Stress and Fatigue Fracture of Poly(4-Methel Pentene-1.” *Journal of Applied Polymer Science* 30, no. 12 (1985): 4771-4792.

Sawyer, L. C., and D. T. Grubb. *Polymer Microscopy*. 2nd ed. London: Chapman and Hall, 1996.

Schoolenberg, G. E. “A Fracture Mechanics Approach to the Effects of UV-Degradation on Polypropylene.” *Journal of Materials Science* 23 (1988): 1580-1590.

Schoolenberg, G. E. “A Study of the Ultra-violet Degradation Embrittlement of Polypropylene Polymer.” Ph.D. diss., Delft University of Technology, 1988.

Schoolenberg, G. E., and P. Vink. “Ultra-violet Degradation of Polypropylene: 1. Degradation Profile and Thickness of the Embrittled Surface Layer.” *Polymer* 32 (1991): 432-437.

Scoponi M., S. Cimmino, and M. Kaci. “Photo-stabilisation Mechanism Under Natural Weathering and Accelerated Photo-oxidative Conditions of LDPE Films for Agricultural Applications.” *Polymer* 41 (2000): 7969-7980.

Sherman, E. S., A. Ram, and S. Kenig. “Tensile Failure of Weathered Polycarbonate.” *Polymer Engineering Science* 22, no. 8 (1982): 457-465.

Shintani, H., and A. Nakamura. “Mechanism of Degradation and Crosslinking of Polyurethane When Irradiated by Gamma-Rays.” *Journal of Applied Polymer Science* 42 (1991): 1979-1987.

Srinivasan, R., B. Braren, and K. G. Casey. “Ultraviolet Laser Ablation and Decomposition of Organic Materials.” *Pure and Applied Chemistry* 62, no. 8 (1990): 1581-1584.

Stannet, V. “Chapter Two” In *Diffusion in Polymers,* edited by J. Crank, and G. S. Park, 41-73, London: Academic, 1968

Strong, A. B. “Los Angeles Public Report on Task Directive 10, Weatherometer testing for garbage cans.” Technical report, Brigham young University, 2002.

Strong, A. B. *Plastics Materials and Processing*. 3rd ed. Upper Saddle River, New Jersey: Prentice Hall, 2006.

Tavares, A. C., J. V. Gulmine, C. M. Lepiensk, and L. Akcelrud. “The Effect of Accelerated Aging on the Surface Mechanical Properties of Polyethylene.” *Polymer Degradation and Stability* 81, no. 2 (2003): 367-373.

Thompson, T., and P. P. Klemchuk. “Light Stabilization of Bisphenol A Polycarbonate.” In *Polymer Durability: Degradation, Stabilization and Lifetime Prediction: Advances in Chemistry Series No. 249*, edited by R. L. Clough, N. C. Billingham, and K. T. Gillen, 303-317. Washington DC: American Chemical Society, 1996.

Tidjani, A. “Comparison of Formation of Oxidation Products During Photooxidation of Linear Low Density Polyethylene Under Different Natural and Accelerated Weathering Conditions.” *Polymer Degradation and Stability* 68 (2000): 465-469.

Tidjani, A. “Photooxidation of polypropylene under natural and accelerated weathering conditions.” *Journal of Applied Polymer Science* 64 (1997): 2497-2503.

Vandenburg, H. J., A. A. Clifford, K. D. Bartle, J. Carroll, I. Newton, L. M. Garden, J. R. Dean, and C. T. Costley. “Critical Review: Analytical Extraction of Additives From Polymers.” *Analyst* 122 (1997): 101R-115R.

Vincent, J. A., J. M. Jansen, and J. J. Nijsten. “Reaction Kinetics in the Photooxidation of Polymers.” In *Proceedings of the 4th Annual International Conference on Advances in the Stabilization and Degradation of Polymers Held in Luzern, Switzerland June 1982,* edited by A. V. Patsis, 2-4. Basel: Technomic, 1982.

Vink, P. “The Photo-Oxidation of Polyolefins – Structural and Morphological Aspects.” In *Degradation and Stabilisation of Polyolefins,* edited by N. S. Allen, 213-246. London: Applied Science, 1983.

Vink, P. “Degradation and Stabilisation of Materials.” In *Journal of Applied Polymer Science: Applied Polymer Symposium No. 35*, 265-275. New York: John Wiley & Sons, 1979.

Winslow, F. H. “Recent Studies of Polymer Degradation and Stabilization.” *Die Makromolekulare Chemie* 2, no. S19791 (supplement) (1979): 27-34.

Wu, Q., B. Qu, Y. Xu, and Q. Wu, "Surface Photo-oxidation and Photostabilisation of Photocross-linked Polyethylene." *Polymer Degradation and Stability* 68, no. 1 (2000): 97-102.

Yakimets, I., D. Lai, and M. Guigon. "Effect of Photo-oxidation Cracks on Behaviour of Thick Polypropylene Samples." *Polymer Degradation and Stability* 86 (2004): 59-67.

Zielnik, A. F. "Weather Testing." *Plastics Technology* 50, no. 3 (March 2004): 52-57.

APPENDICES

Appendix A. SEM Images

SEM images: Polyethylene (Los Angeles)

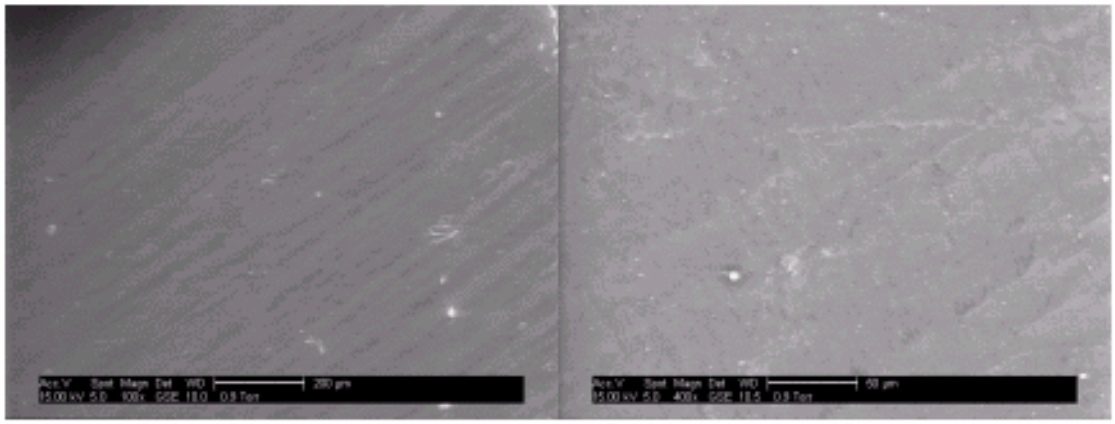

Initial sample 9 – 100x

Initial sample 9 – 400x

GREEN

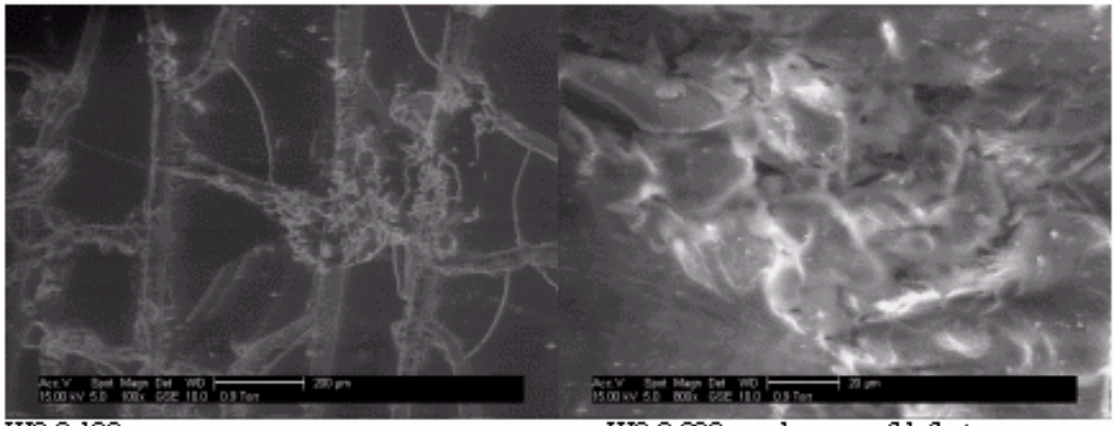

W3-3 100x

W3-3 800x – close-up of defect area

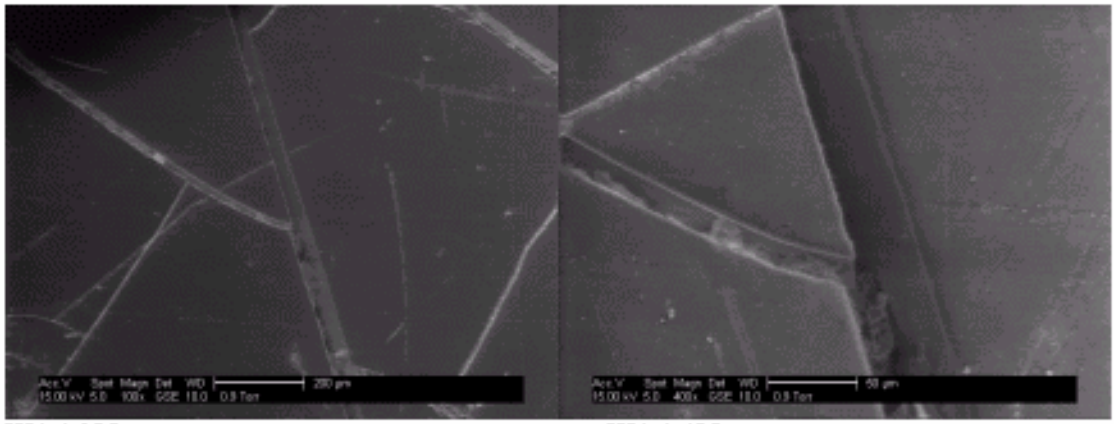

W4-4 100x

W4-4 400x

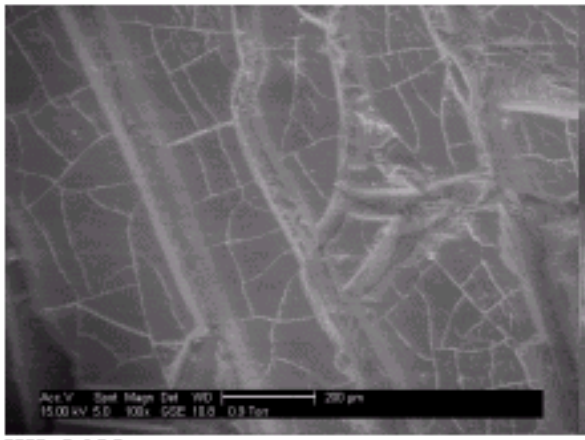

W3-5 100x

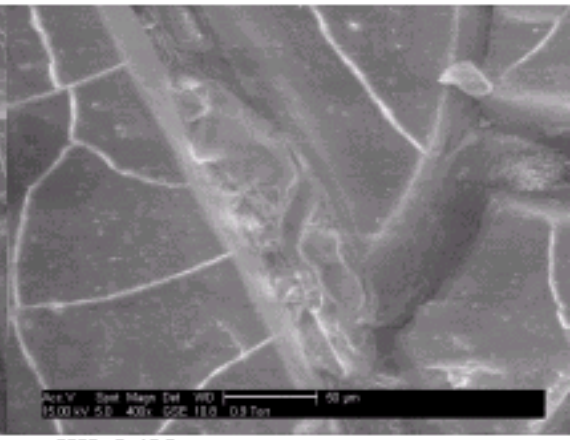

W3-5 400x

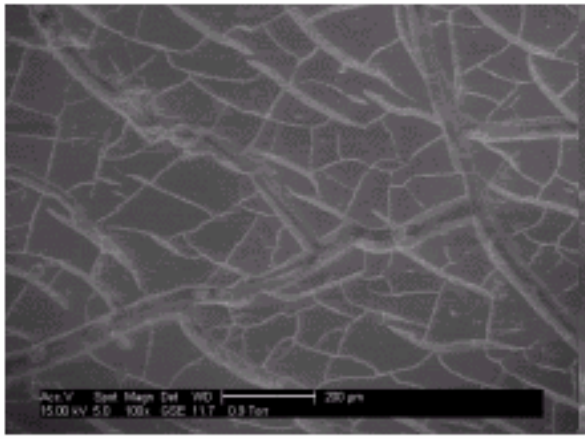

W3-6 100x

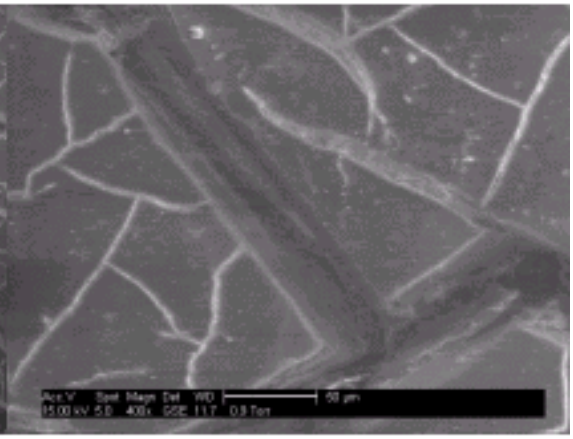

W3-6 400x

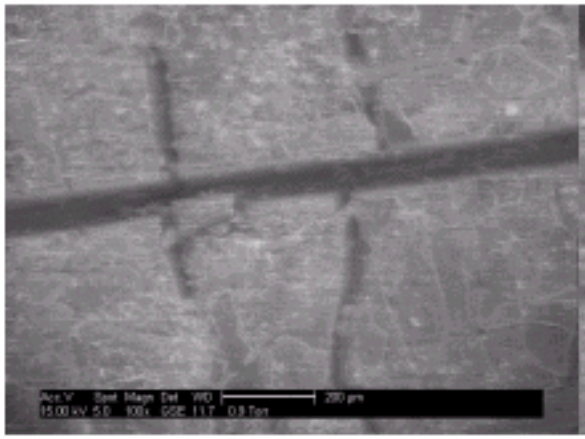

WS-6 100x very fine mottling

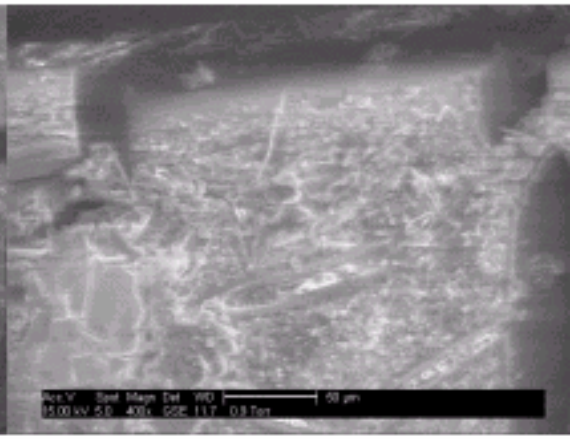

WS-6 400x

BLUE

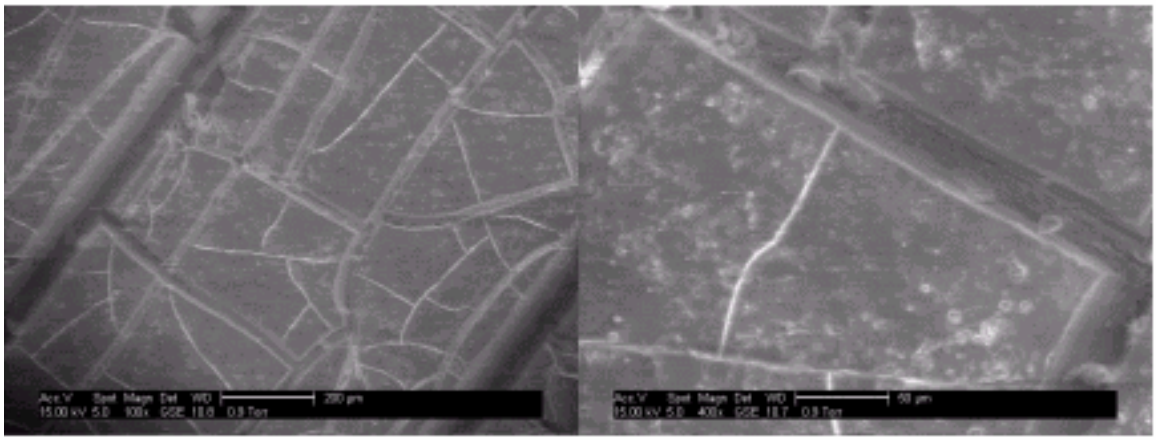

W6-S 100x

W6-S 400x

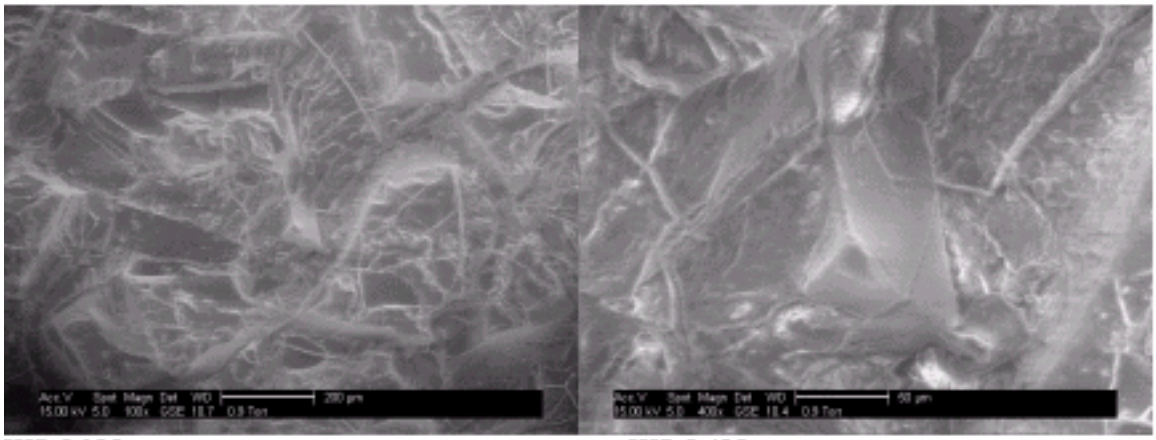

W7-S 100x

W7-S 400x

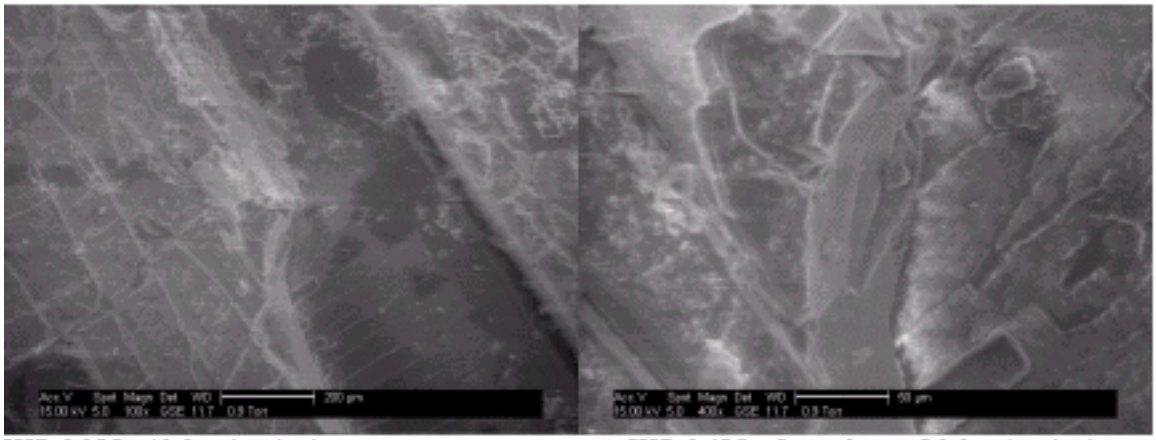

W7-6 100x (delamination)

W7-6 400x (boundary of delamination)

BLACK

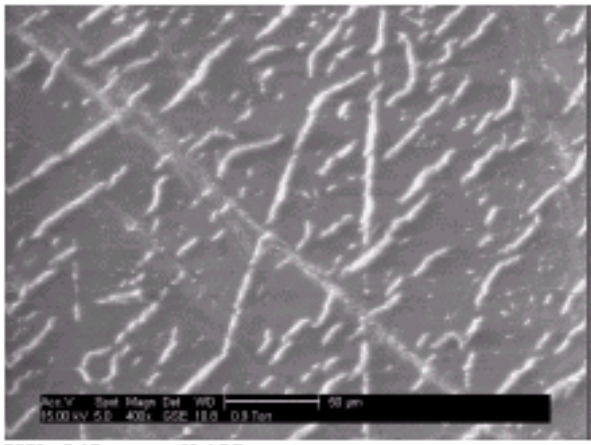

W1-5 "bottom" 400x

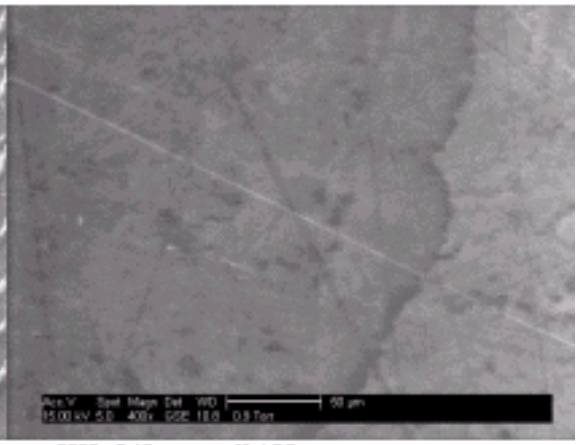

W2-5 "bottom" 400x

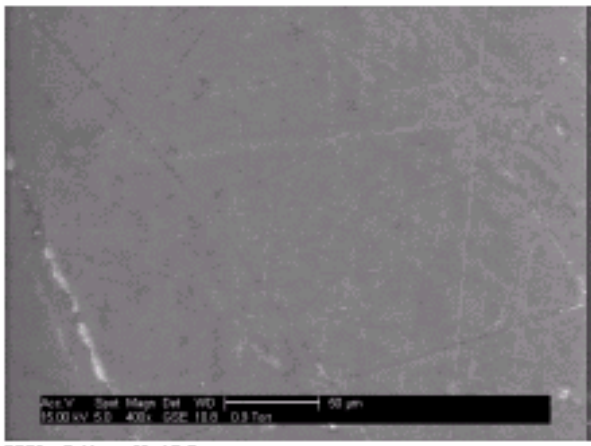

W1-5 "top" 400x

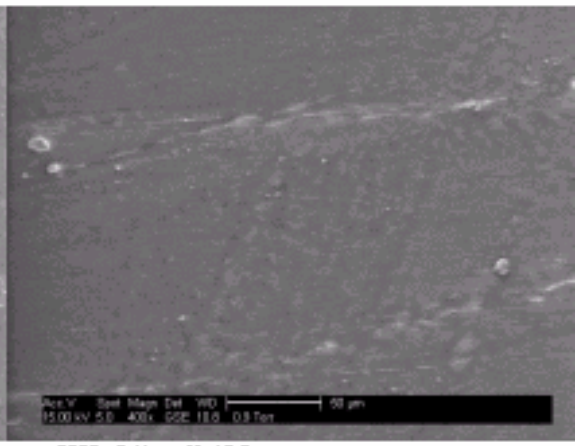

W2-5 "top" 400x

L green

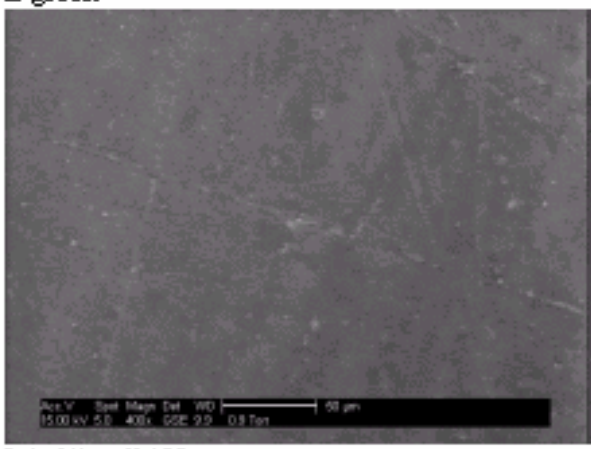

L4-6 "top" 400x

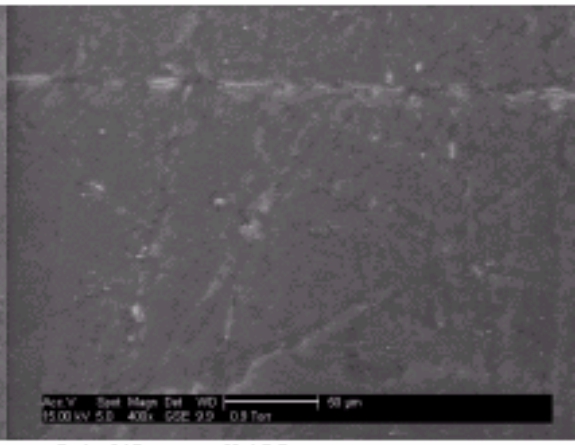

L4-6 "bottom" 400x

L black

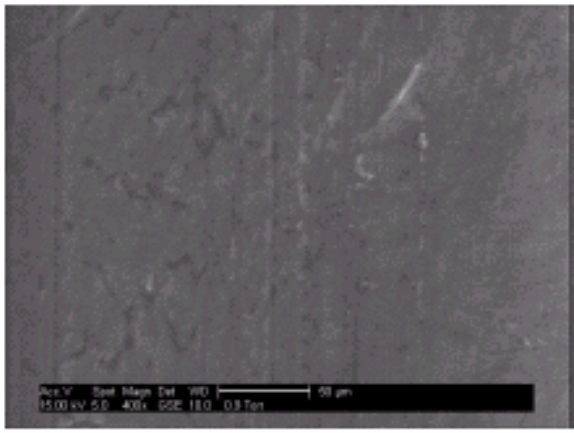

L1-5 "bottom" 400x

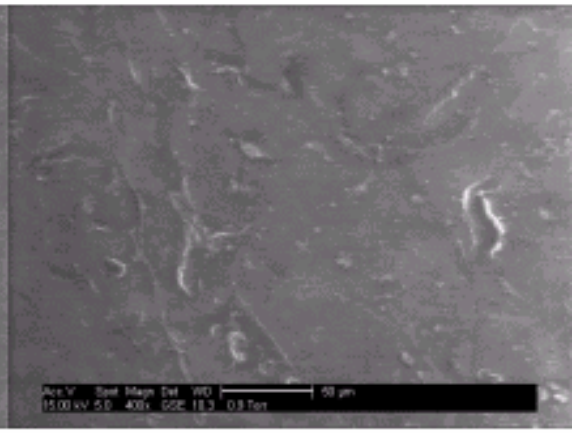

L1-6 "bottom" 400x

N - blue

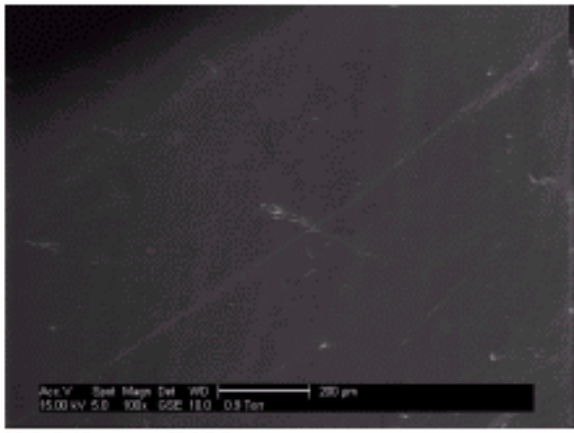

N6-2 "bottom" 100x

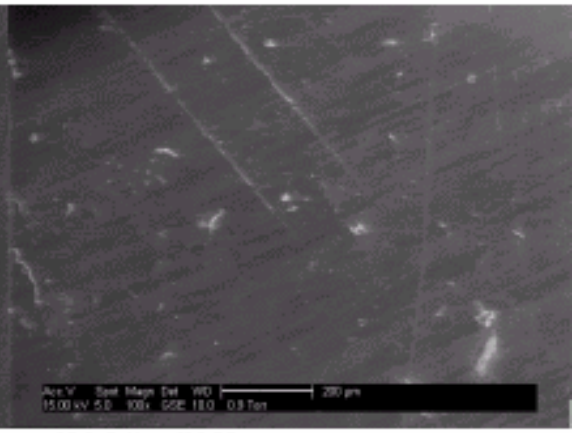

N6-2 "top" 100x

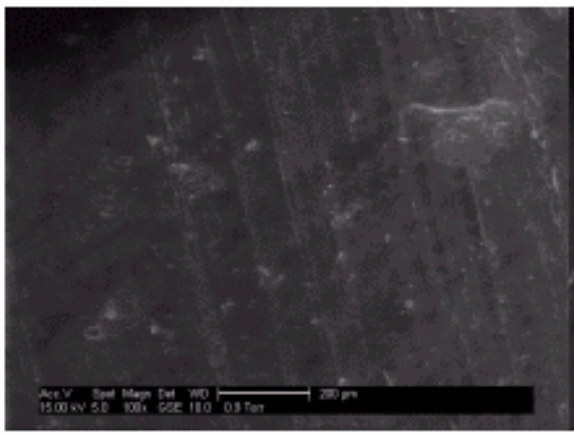

N7-2 "bottom" 100x

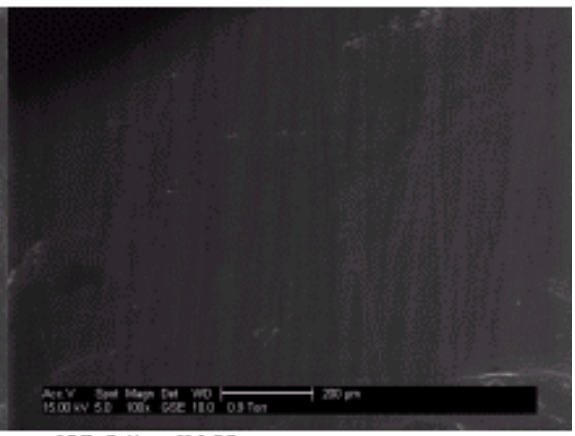

N7-2 "top" 100x

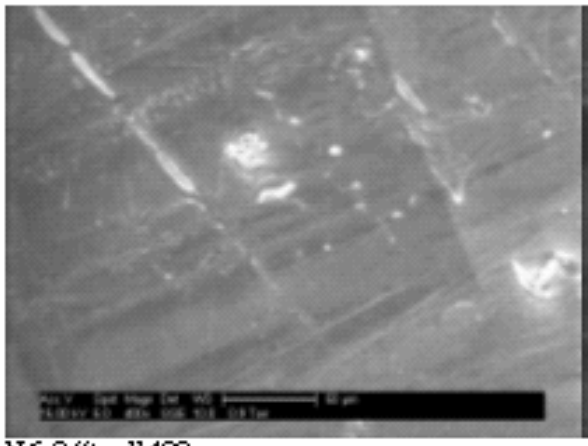

N6-2 "top" 400x

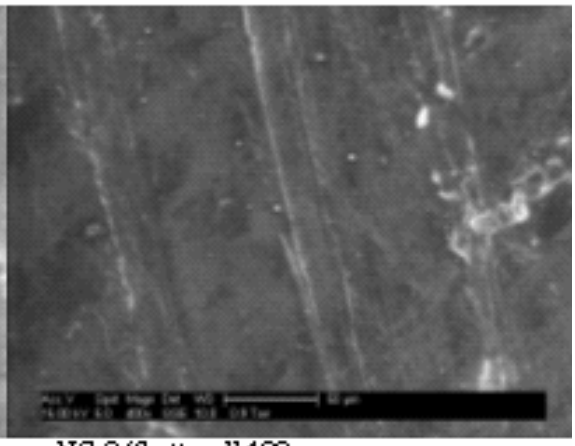

N7-2 "bottom" 400x

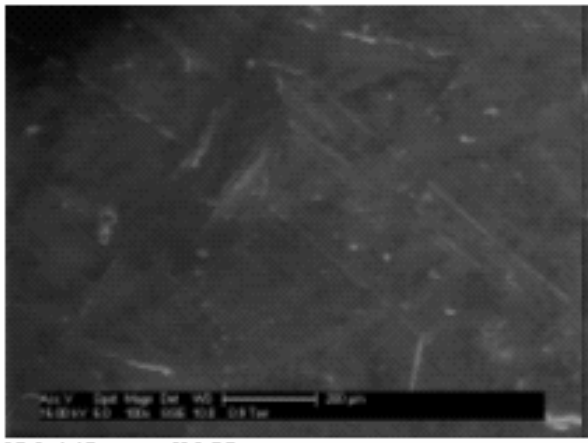

N6-4 "bottom" 100x

N6-4 "bottom" 400x

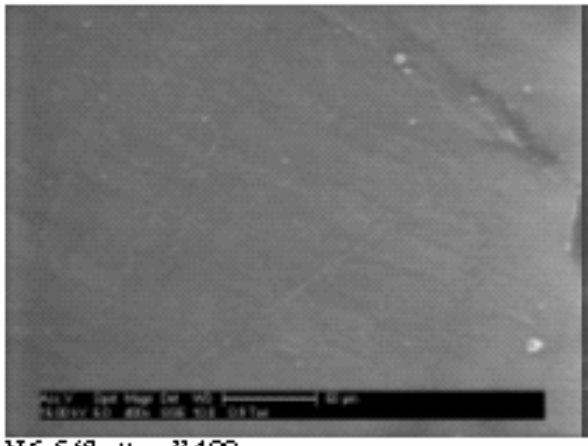

N6-5 "bottom" 400x

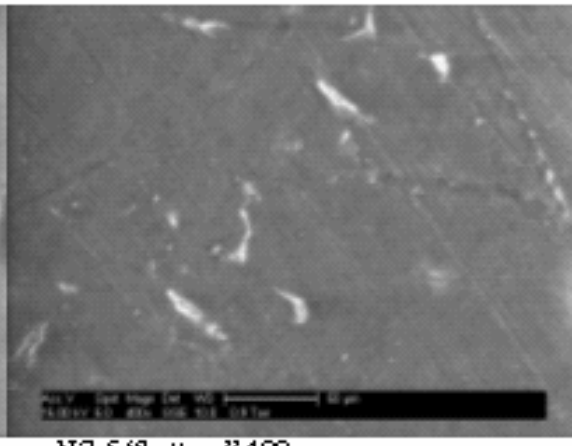

N7-5 "bottom" 400x

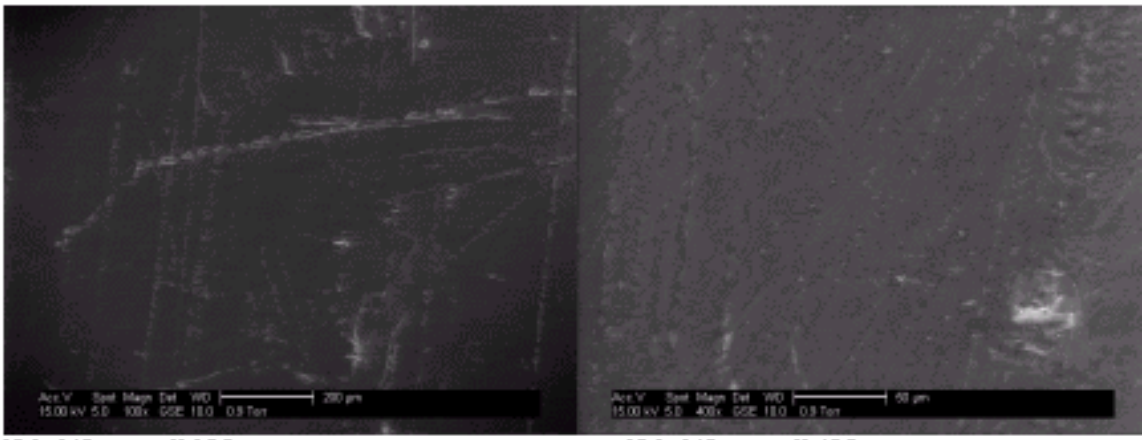

N6-6 "bottom" 100x N6-6 "bottom" 400x

N-black

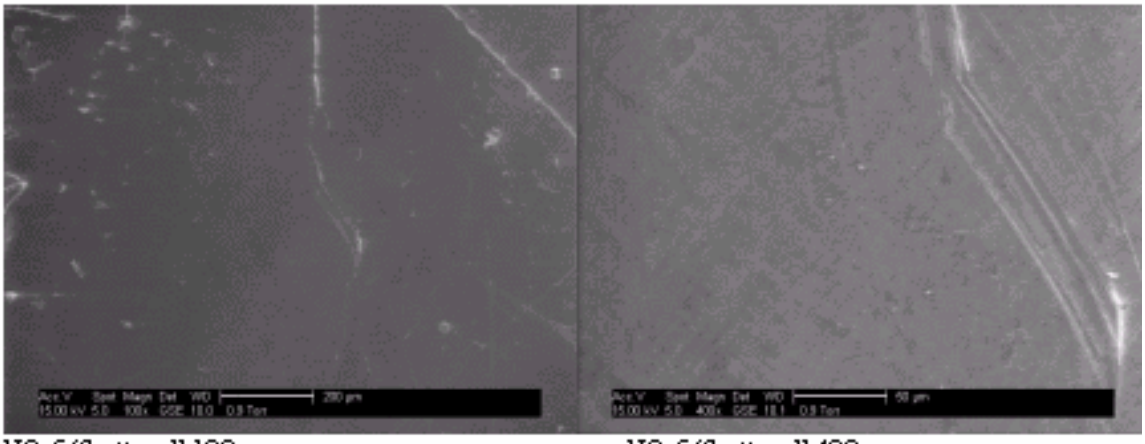

N2-5 "bottom" 100x N2-5 "bottom" 400x

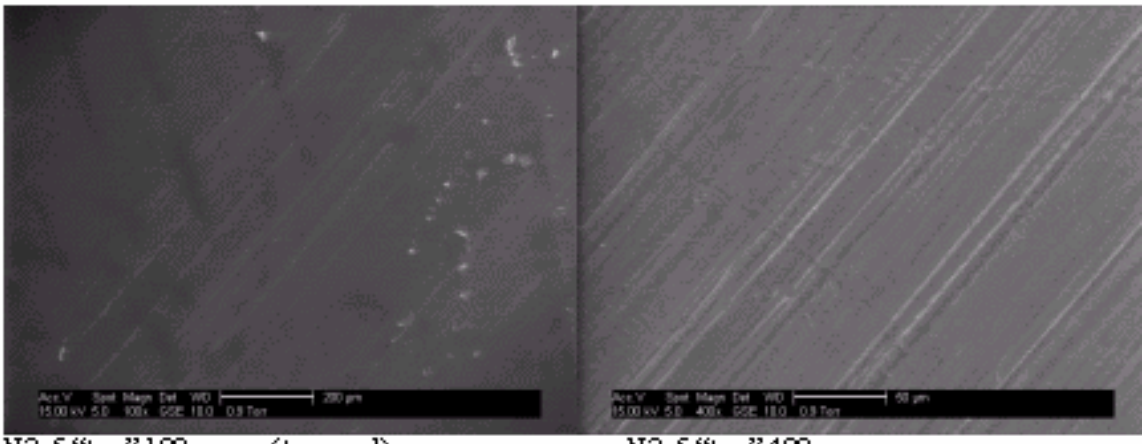

N2-5 "top" 100x (top used) N2-5 "top" 400x

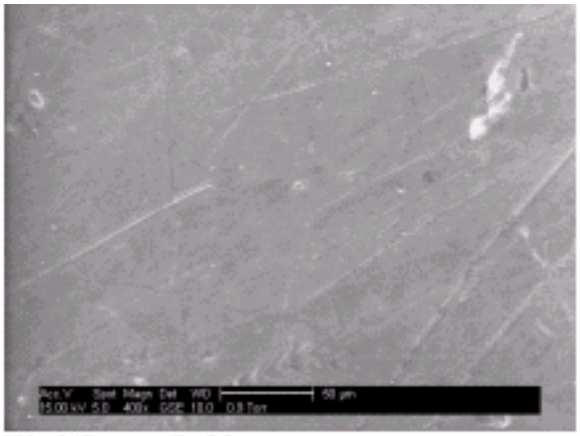

N1-6 "bottom" 400x

N Green

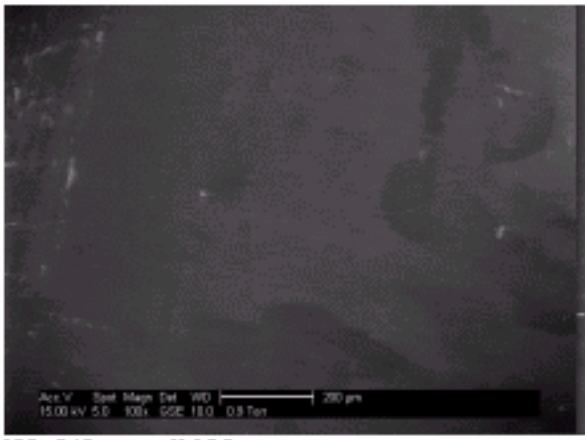

N3-5 "bottom" 100x

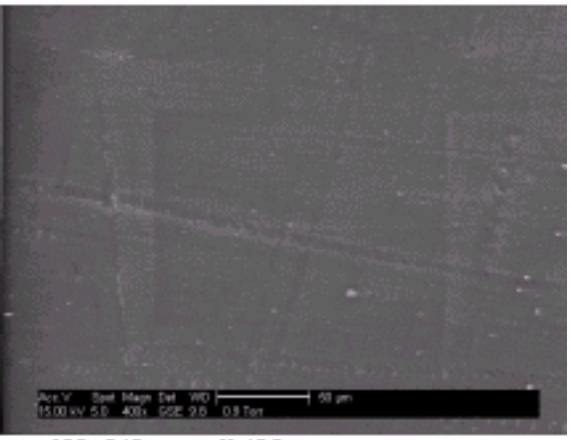

N3-5 "bottom" 400x

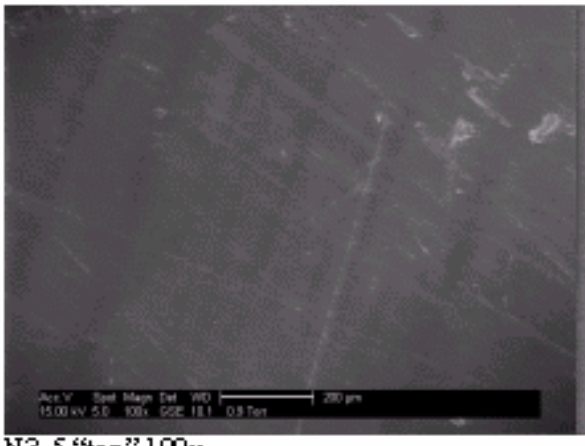

N3-5 "top" 100x

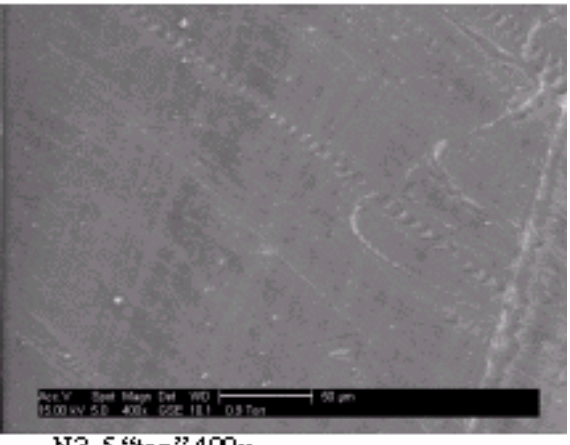

N3-5 "top" 400x

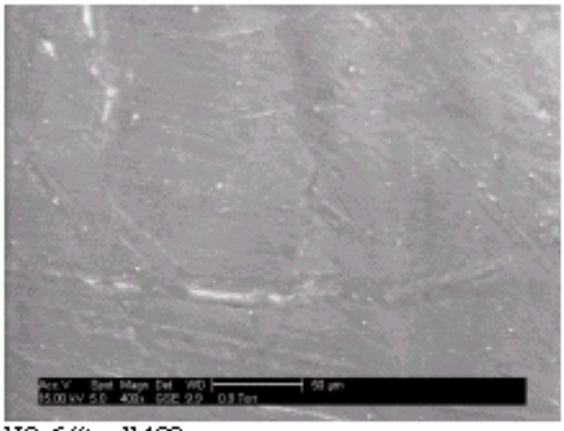

N3-6 "top" 400x

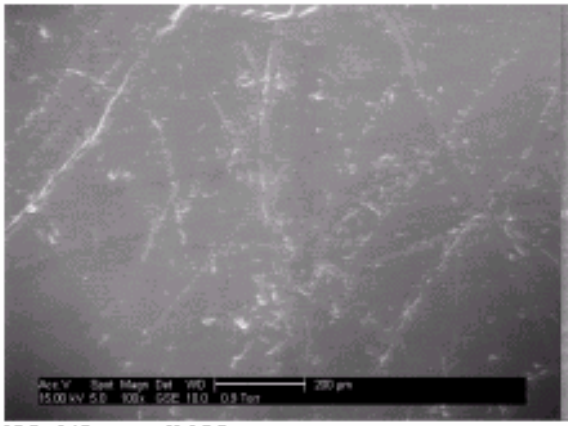

N5-6 "bottom" 100x

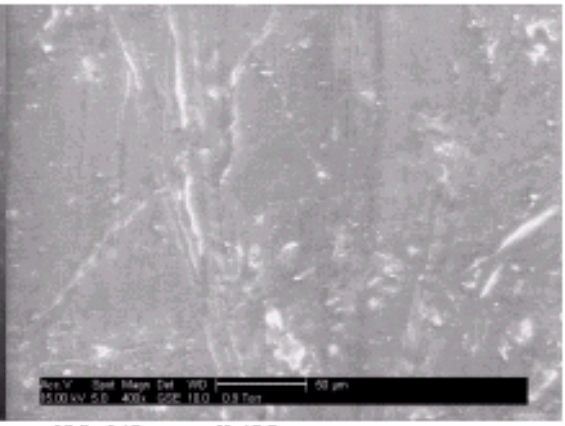

N5-6 "bottom" 400x

SEM images: ABS (Mity-Lite)

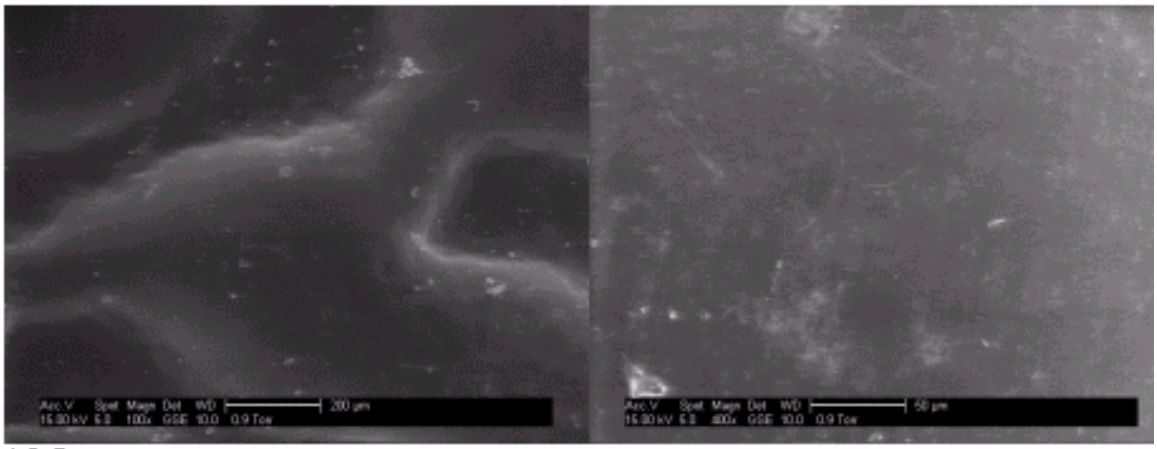

A0-7

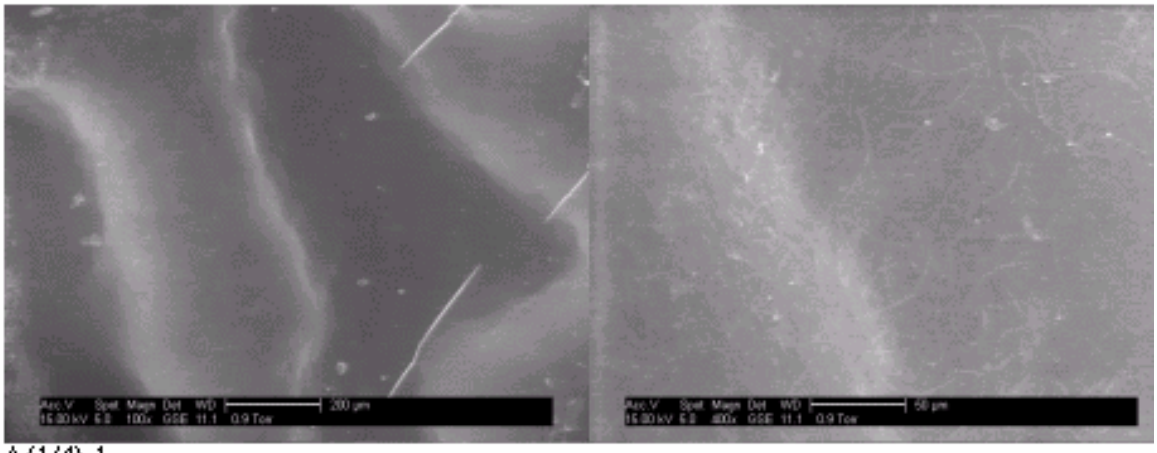

A(1/4)-1

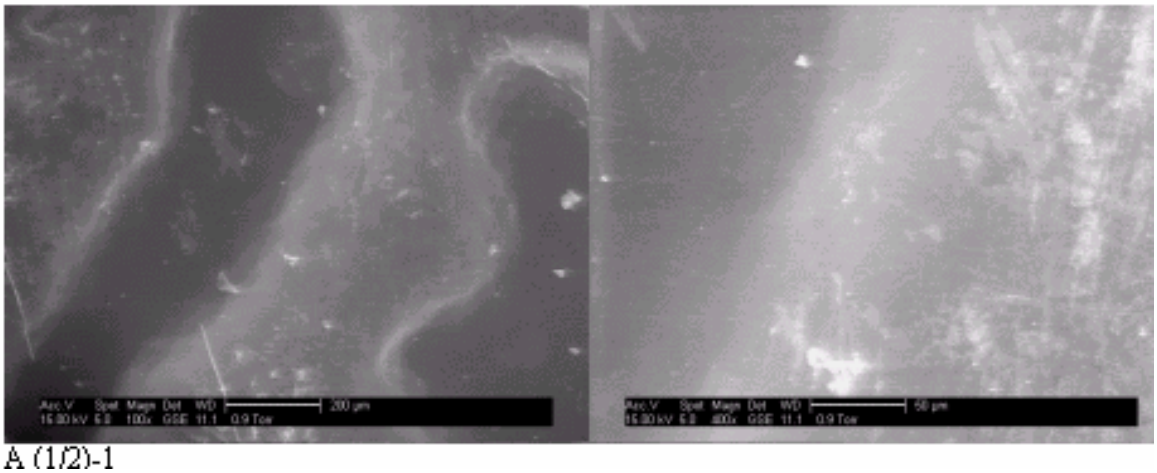

A (1/2)-1

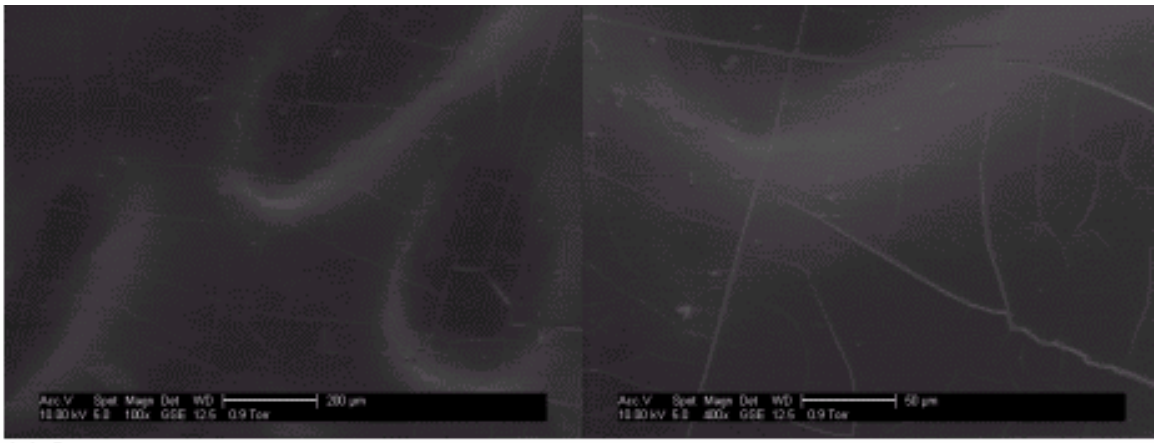

A1-2

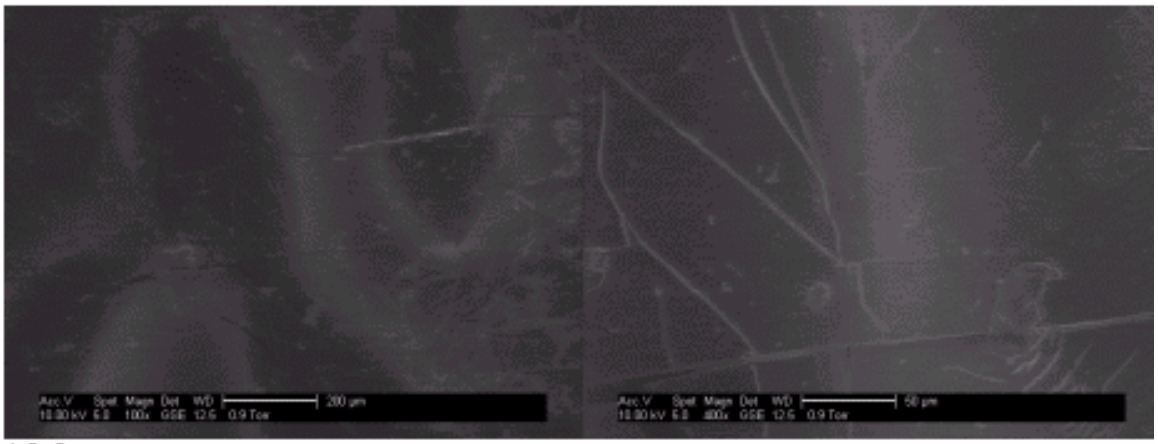

A2-5

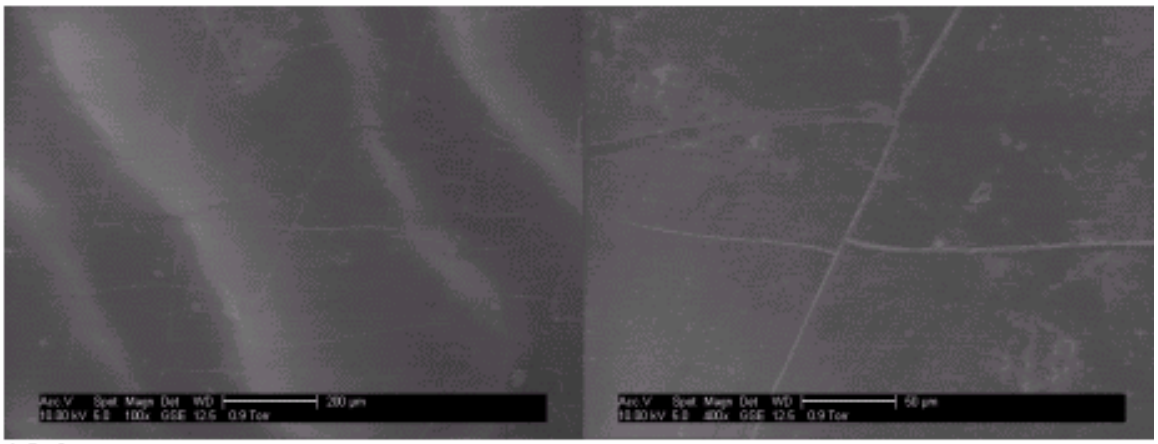

A3-6

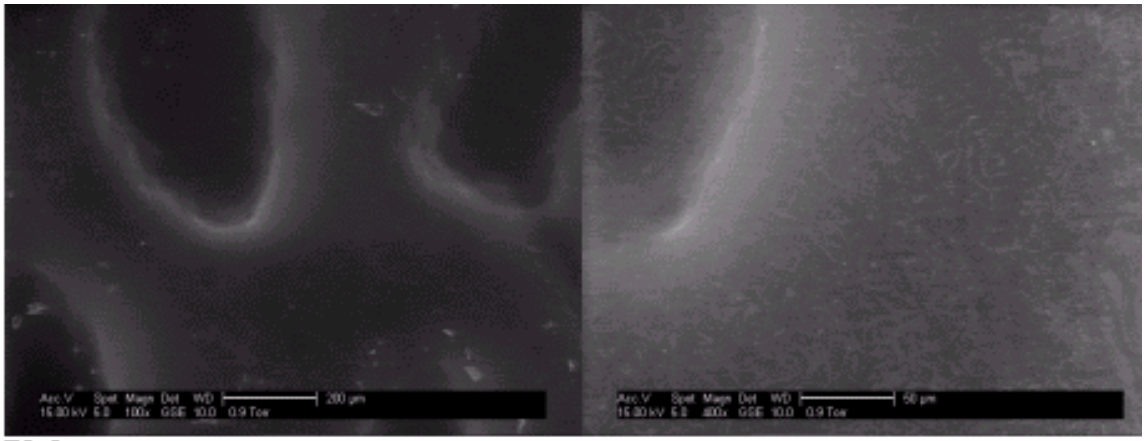

E0-5

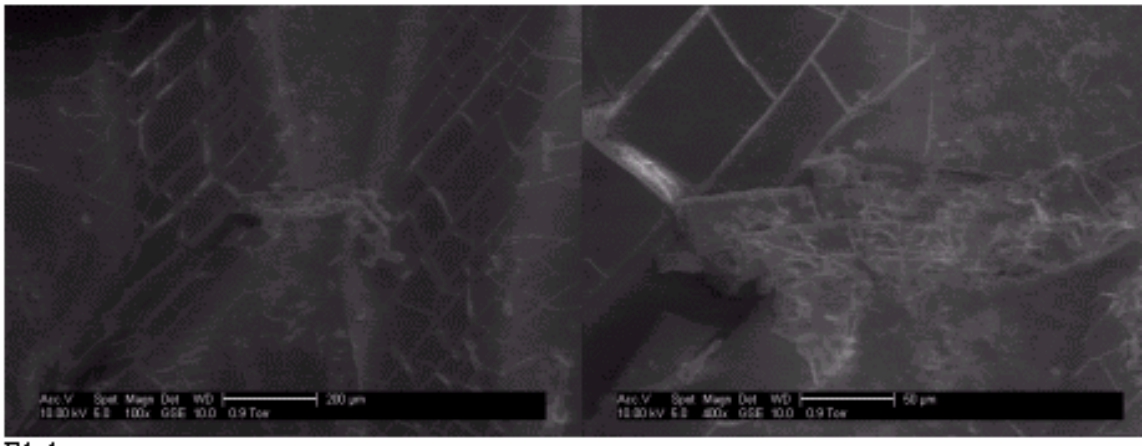

E1-1

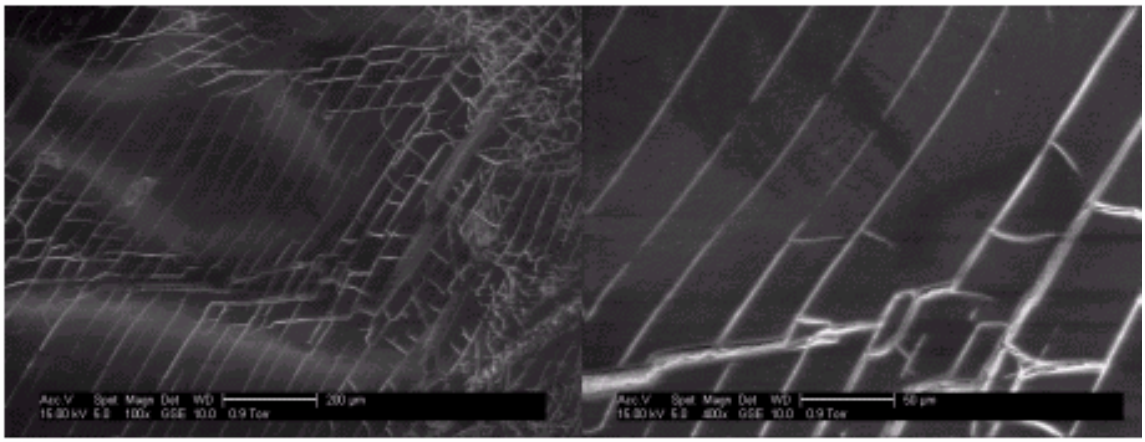

E2-6

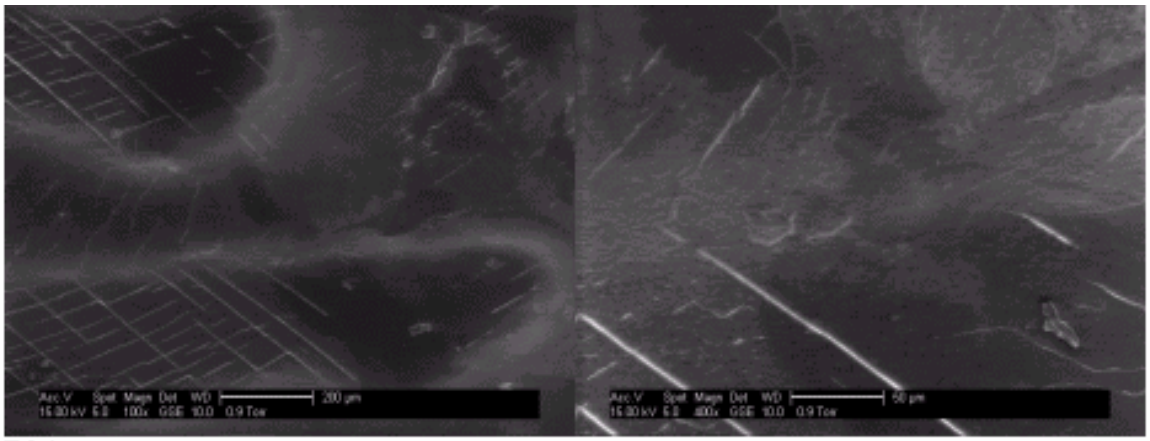

E6-1

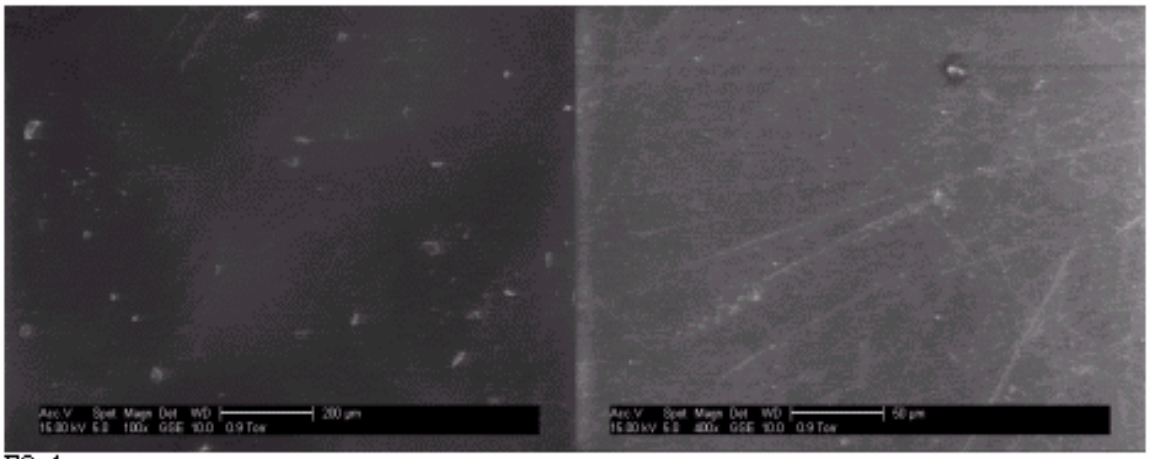

F0-4

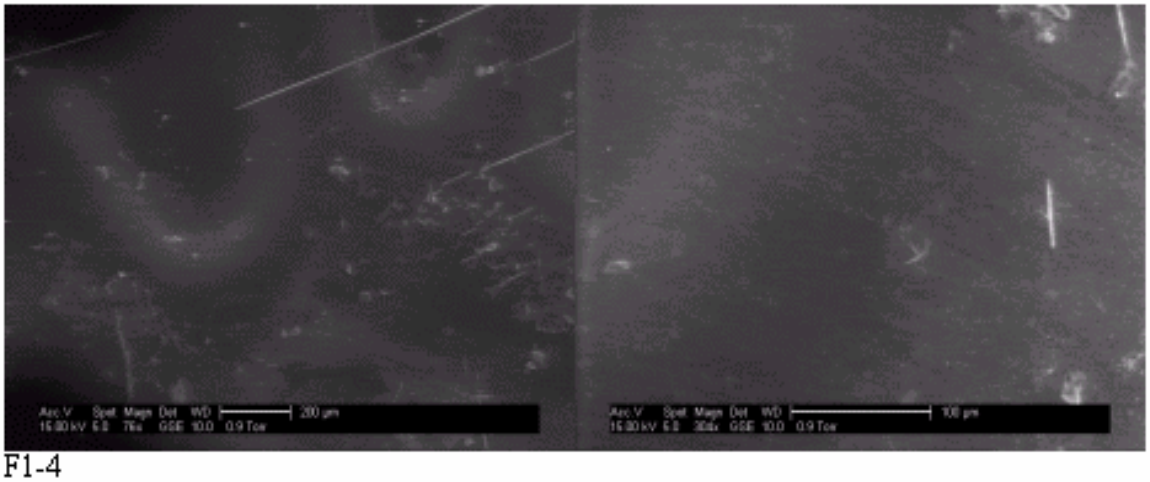

F1-4

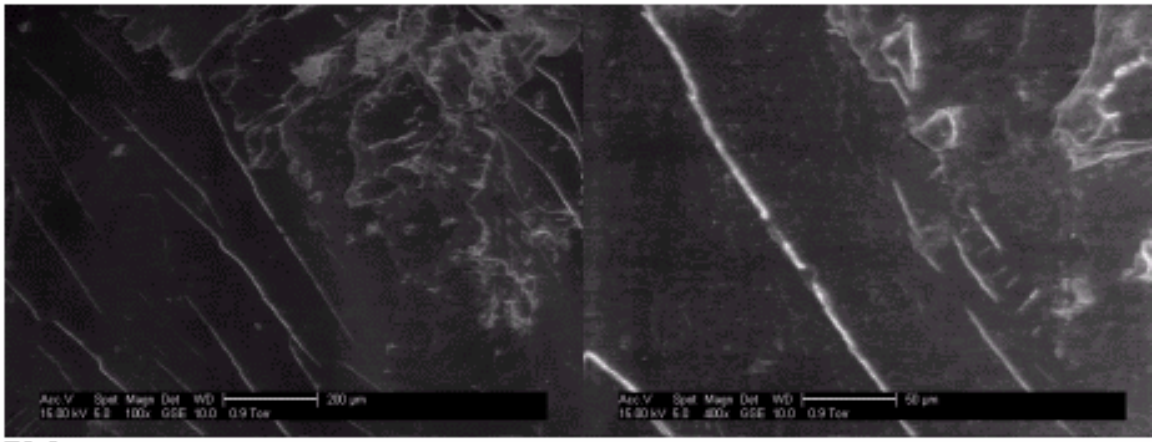

F2-3

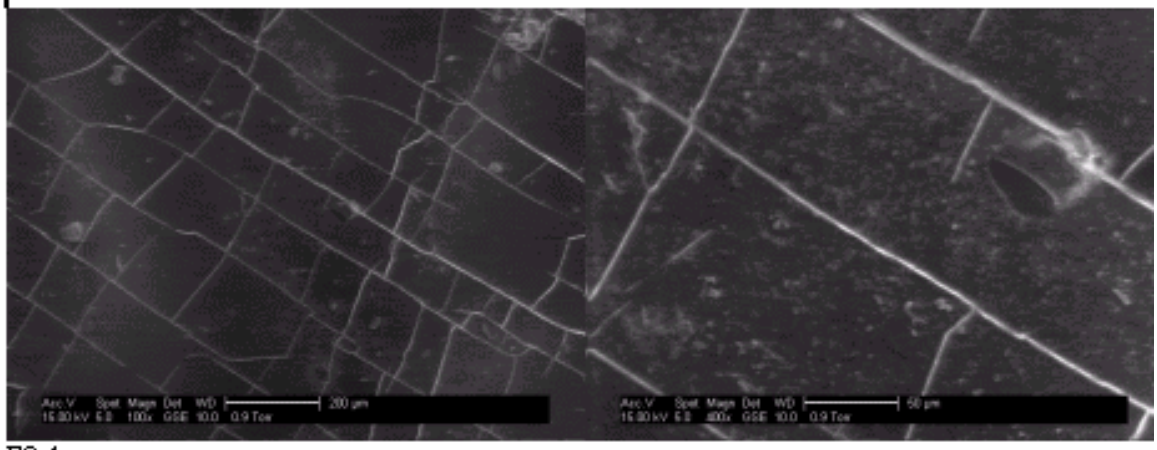

F3-1

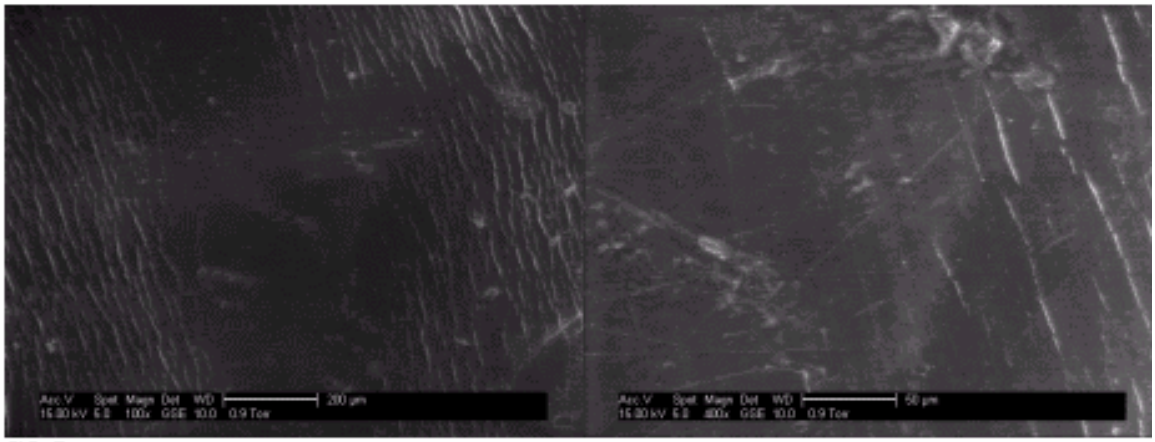

G0-7

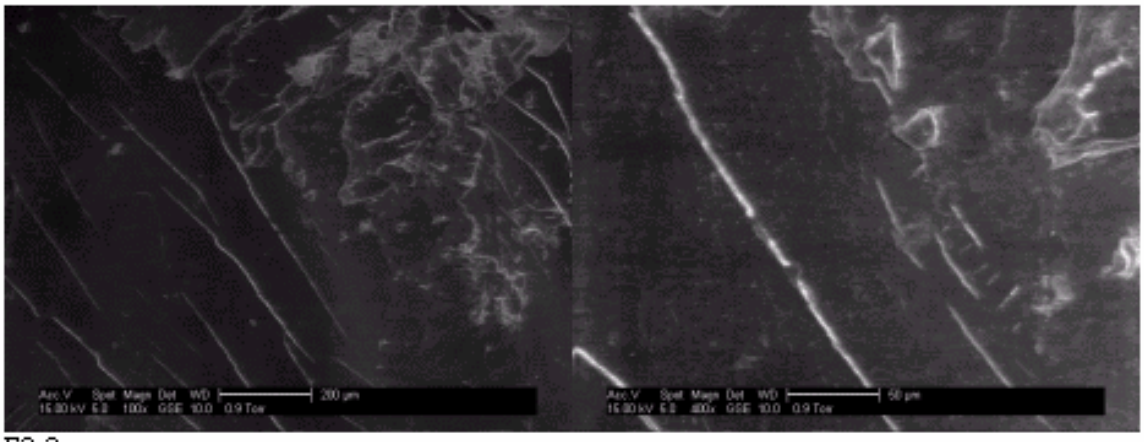

F2-3

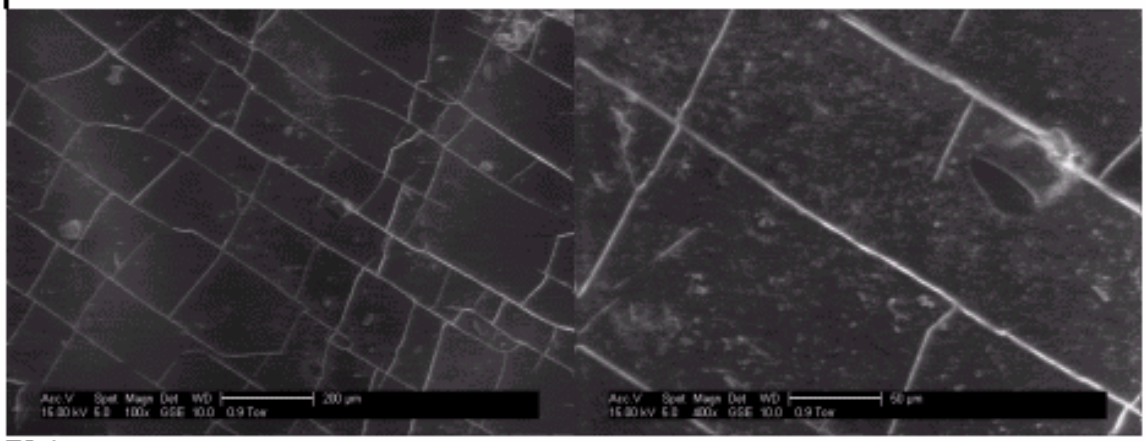

F3-1

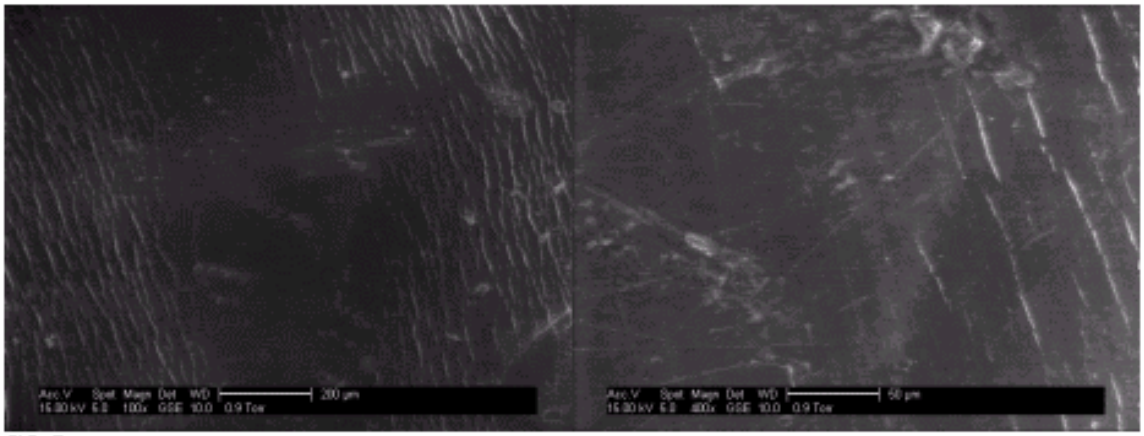

G0-7

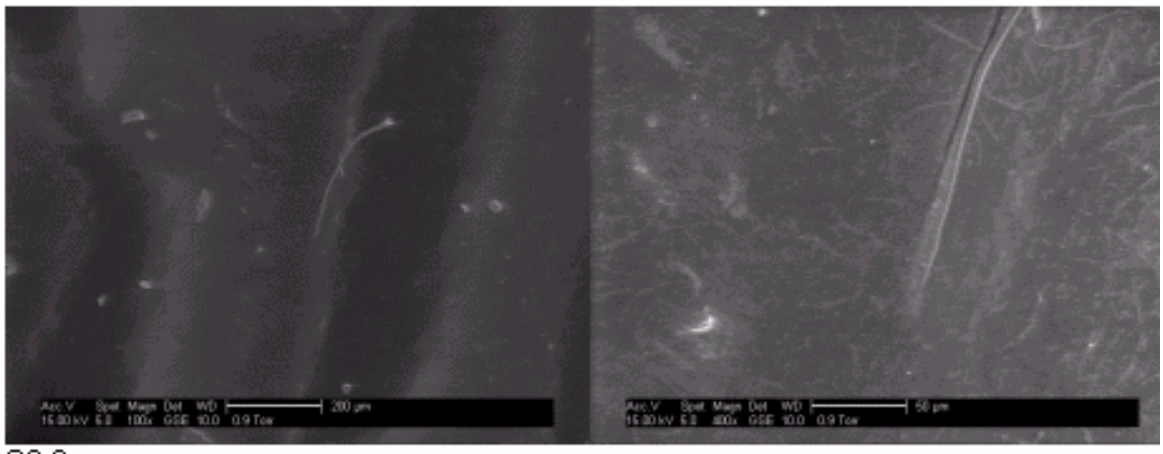

O0-3

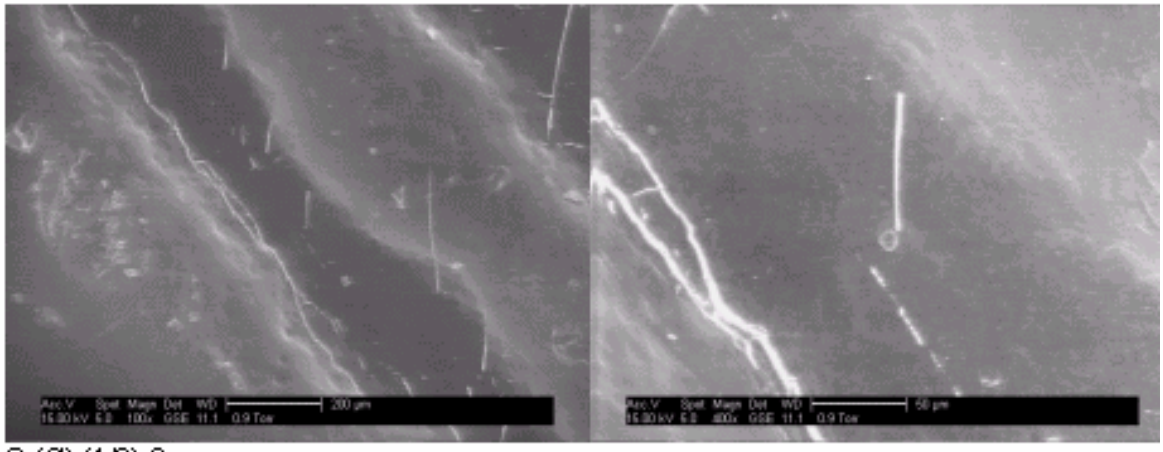

O (C) (1/2)-2

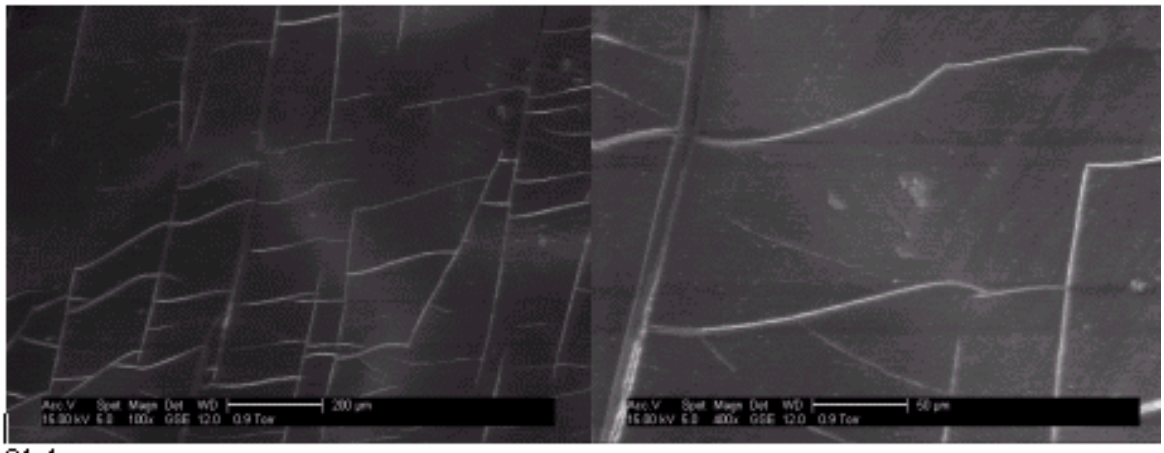

01-1

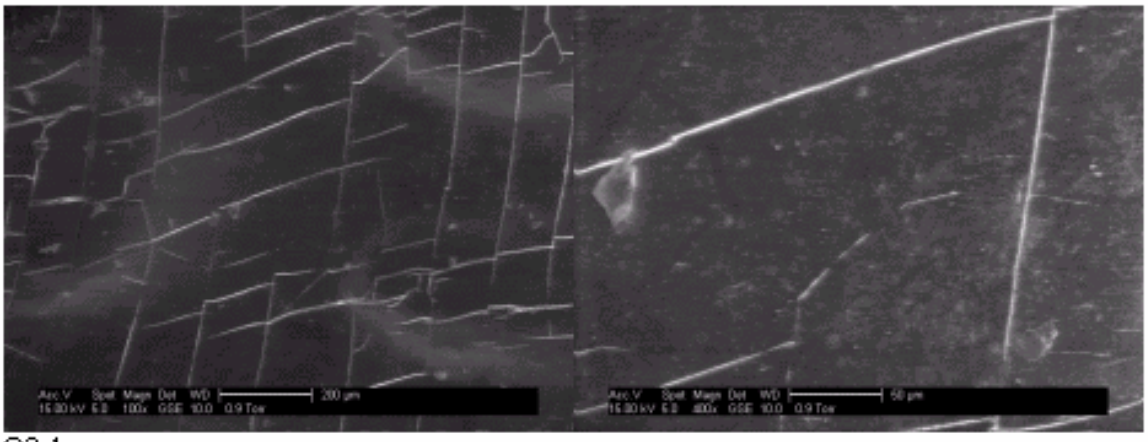

O2-1

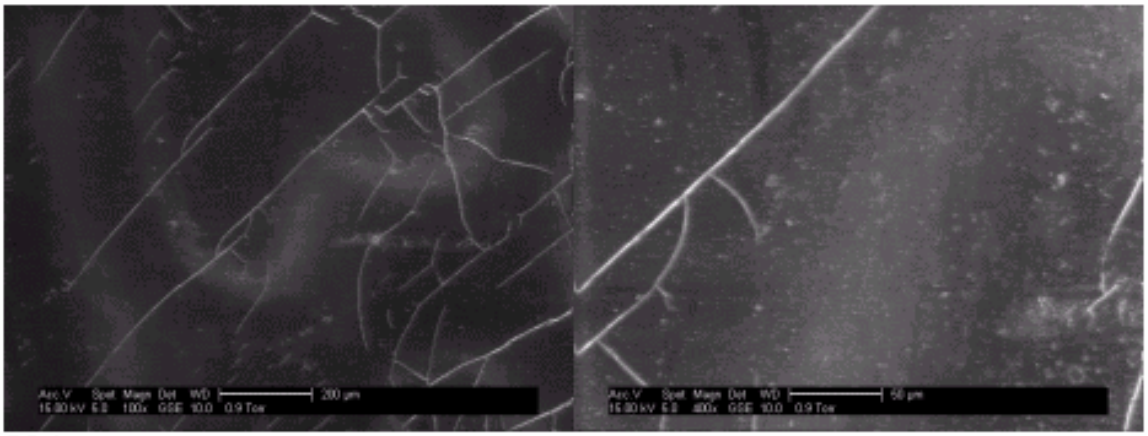

O3-1

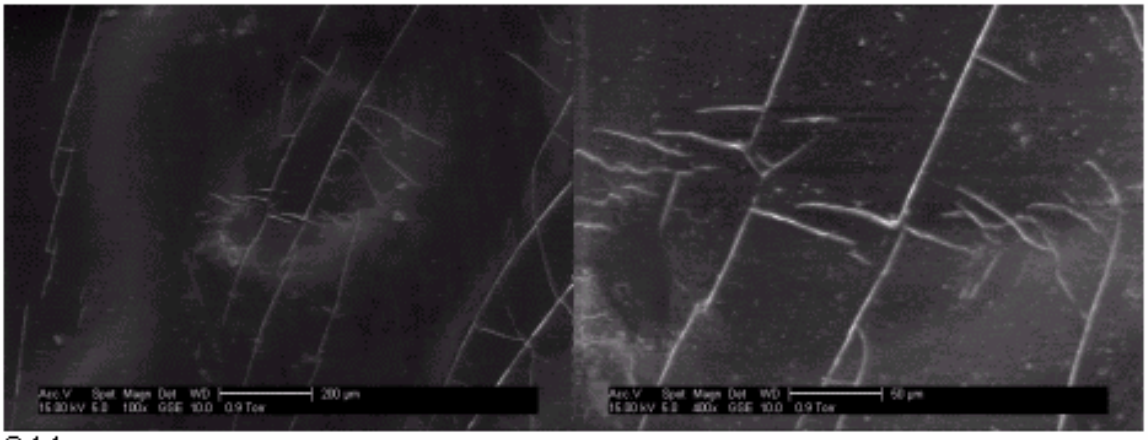

O4-1

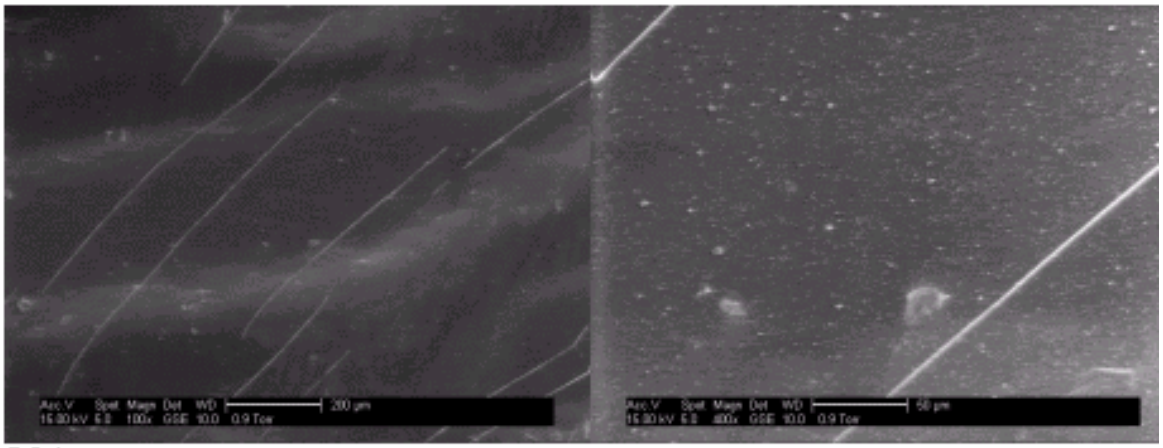

O5-1

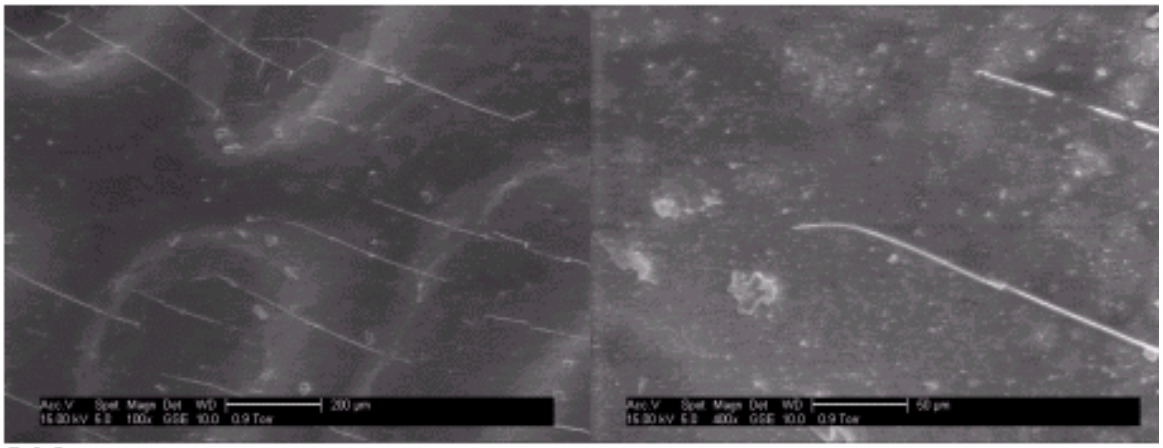

O6-2

Appendix B. Polyethylene Mechanical Test Data

Sample ID	Expo Time	Date sampled	Size	Color	% Ash	Melt Index	Izod Impact	Tensile Strength	Total Elong	Density
Initial 1	0	3/11/03	65	Black	0.09	7.44	1.56	3430	379	0.949
2	0	2/20/03	95	Black	0.18	6.48	1.31	3167	319	0.952
3	0	2/20/03	65	Green	0.82	6.67	1.26	3107	359	0.949
4	0	2/20/03	95	Green	0.66	6.82	1.30	3054	517	0.946
5	0	2/24/03	95	Green	0.63	6.36	1.58	3115	515	0.946
6	0	2/24/03	65	Blue	0.36	6.80	1.22	3087	512	0.945
7	0	2/24/03	95	Blue	0.49	6.34	1.36	3333	369	0.947
8	0	2/20/03	35	Black	0.40	6.66	1.14	3266	397	0.952
9	0	2/20/03	35	Green	0.60	5.23	1.21	3435	340	0.951
10	0	2/24/03	35	Blue	0.45	7.56	1.10	3259	378	0.948
11	0	2/20/03	65	Brown	0.40	5.35	1.62	3362	308	0.947
Control C1-1	3mo	8/8/03	65	Black	0.06	7.54	None	3318	409	0.949
C2-1	3mo	8/8/03	95	Black	0.10	6.41	None	3302	310	0.951
C3-1	3mo	8/8/03	65	Green	0.74	6.79	None	3231	484	0.950
C4-1	3mo	8/8/03	95	Green	0.64	6.86	None	3077	483	0.948
C5-1	3mo	8/8/03	95	Green	0.66	6.52	None	3133	537	0.948
C6-1	3mo	8/8/03	65	Blue	0.41	6.65	None	3040	443	0.945
C7-1	3mo	8/8/03	95	Blue	0.47	6.22	None	3351	416	0.948
Spl Ctrl SC1-1	3mo	8/8/03	65	Black	0.04	7.34	None	3262	387	0.946
SC2-1	3mo	8/8/03	95	Black	0.13	6.71	None	3241	364	0.948
SC3-1	3mo	8/8/03	65	Green	0.73	6.71	None	3187	403	0.948
SC4-1	3mo	8/8/03	95	Green	0.58	7.08	None	3121	326	0.947
SC5-1	3mo	8/8/03	95	Green	0.60	6.34	None	3079	456	0.946
SC6-1	3mo	8/8/03	65	Blue	0.40	6.85	None	3025	592	0.944
SC7-1	3mo	8/8/03	95	Blue	0.45	6.16	None	3232	572	0.945
Weather W1-1	3mo	8/8/03	65	Black	0.08	7.49	None	3236	473	0.947
W2-1	3mo	8/8/03	95	Black	0.15	6.33	None	3126	438	0.950
W3-1	3mo	8/8/03	65	Green	0.76	6.34	None	3111	420	0.948
W4-1	3mo	8/8/03	95	Green	0.63	6.67	None	2986	412	0.948
W5-1	3mo	8/8/03	95	Green	0.61	6.34	None	2964	473	0.947
W6-1	3mo	8/8/03	65	Blue	0.45	6.12	None	2876	572	0.945
W7-1	3mo	8/8/03	95	Blue	0.46	5.84	None	3321	438	0.950
No Load N1-1	6mo	8/27/03	65	Black	0.06	6.41	1.27	3182	272	0.948
N2-1	6mo	8/27/03	95	Black	0.14	6.32	1.25	3203	289	0.950
N3-1	6mo	8/27/03	65	Green	0.89	6.79	1.27	3031	582	0.949
N4-1	6mo	8/27/03	95	Green	0.64	7.28	1.23	3134	389	0.947
N5-1	6mo	8/27/03	95	Green	0.63	6.40	1.59	3103	533	0.947
N6-1	6mo	8/27/03	65	Blue	0.42	6.88	1.06	2955	537	0.945
N7-1	6mo	8/27/03	95	Blue	0.46	6.25	1.24	3242	387	0.947
N8-1	6mo	8/27/03	35	Black	0.34	6.64	1.08	3116	435	0.952
N9-1	6mo	8/27/03	35	Green	0.60	5.24	1.19	3322	343	0.950

N10-1	6mo	8/27/03	35	Blue	0.47	7.64	1.06	3190	472	0.945
N11-1	6mo	8/27/03	65	Brown	0.41	5.14	1.60	3355	289	0.948
Fld-Lded L1-1	6mo	8/29/03	65	Black	0.07	6.87	1.74	3046	347	0.946
L4-1	6mo	8/29/03	95	Green	0.71	7.03	1.34	3035	484	0.949
Control C1-2	6mo	11/8/03	65	Black	0.09	7.27	1.29	3205	354	0.950
C2-2	6mo	11/8/03	95	Black	0.16	6.42	1.27	3200	312	0.952
C3-2	6mo	11/8/03	65	Green	0.78	6.70	1.31	3104	368	0.950
C4-2	6mo	11/8/03	95	Green	0.65	6.95	1.24	3007	328	0.950
C5-2	6mo	11/8/03	95	Green	0.62	6.49	1.54	3154	471	0.949
C6-2	6mo	11/8/03	65	Blue	0.42	6.65	1.31	3030	392	0.946
C7-2	6mo	11/8/03	95	Blue	0.50	6.19	1.20	3343	440	0.949
Spl Ctrl SC1-2	6mo	11/8/03	65	Black	0.06	7.29	1.29	3366	430	0.950
SC2-2	6mo	11/8/03	95	Black	0.12	6.54	1.27	3456	400	0.951
SC3-2	6mo	11/8/03	65	Green	0.76	6.70	1.34	3186	333	0.949
SC4-2	6mo	11/8/03	95	Green	0.59	6.93	1.27	3009	364	0.948
SC5-2	6mo	11/8/03	95	Green	0.60	6.31	1.68	3082	428	0.948
SC6-2	6mo	11/8/03	65	Blue	0.42	6.86	1.26	3052	544	0.945
SC7-2	6mo	11/8/03	95	Blue	0.45	6.20	1.20	3253	409	0.947
Weather W1-2	6mo	11/10/03	65	Black	0.09	7.48	1.31	3333	424	0.952
W2-2	6mo	11/10/03	95	Black	0.15	6.45	1.28	3519	435	0.952
W3-2	6mo	11/10/03	65	Green	0.75	6.25	1.08	3334	295	0.950
W4-2	6mo	11/10/03	95	Green	0.65	6.29	0.90	3191	341	0.949
W5-2	6mo	11/10/03	95	Green	0.65	6.20	1.22	3168	380	0.948
W6-2	6mo	11/10/03	65	Blue	0.46	5.85	0.78	3069	258	0.946
W7-2	6mo	11/10/03	95	Blue	0.49	5.75	0.68	3378	161	0.950
No Load N1-21	1yr	3/5/04	65	Black	0.07	6.98	1.50	3131	330	0.950
N2-2	1yr	3/5/04	95	Black	0.16	6.14	1.25	3139	278	0.951
N3-2	1yr	3/5/04	65	Green	0.73	6.40	1.22	2997	409	0.950
N4-2	1yr	3/5/04	95	Green	0.66	6.80	1.21	3187	542	0.948
N5-2	1yr	3/5/04	95	Green	0.57	6.33	1.54	3125	309	0.946
N6-2	1yr	3/5/04	65	Blue	0.35	6.46	1.15	3109	539	0.947
N7-2	1yr	3/5/04	95	Blue	0.49	4.92	1.60	3361	331	0.949
N8-2	1yr	3/5/04	35	Black	0.07	6.55	1.08	3427	433	0.950
N9-2	1yr	3/5/04	35	Green	0.72	4.90	1.19	3508	279	0.950
N10-2	1yr	3/5/04	35	Blue	0.51	7.14	1.04	3210	527	0.949
N11-2	1yr	3/5/04	65	Brown	0.42	5.34	1.64	3362	266	0.949
L1-2	1yr	3/5/04	65	Black	0.09	6.54	1.62	3302	263	0.948
L4-2	1yr	3/5/04	95	Green	0.73	6.70	1.33	3196	505	0.951
Control C1-3	1yr	5/17/04	65	Black	0.11	7.33	1.88	3193	423	0.949
C2-3	1yr	5/17/04	95	Black	0.16	5.89	1.85	3270	275	0.951
C3-3	1yr	5/17/04	65	Green	0.79	6.49	1.72	3213	372	0.949
C4-3	1yr	5/17/04	95	Green	0.58	6.77	1.46	2988	434	0.948
C5-3	1yr	5/17/04	95	Green	0.64	6.26	2.14	3108	597	0.948
C6-3	1yr	5/17/04	65	Blue	0.43	6.61	1.82	2951	572	0.946
C7-3	1yr	5/17/04	95	Blue	0.54	7.12	1.19	3108	500	0.947
Spl Ctrl SC1-3	1yr	5/17/04	65	Black	0.07	6.97	2.18	3010	310	0.948
SC2-3	1yr	5/17/04	95	Black	0.13	6.25	1.93	3076	313	0.950
SC3-3	1yr	5/17/04	65	Green	0.73	6.51	1.63	3024	436	0.947
SC4-3	1yr	5/17/04	95	Green	0.72	6.82	1.32	2981	360	0.947
SC5-3	1yr	5/17/04	95	Green	0.63	6.37	1.88	2993	504	0.945
SC6-3	1yr	5/17/04	65	Blue	0.40	6.62	1.78	2991	449	0.945
SC7-3	1yr	5/17/04	95	Blue	0.55	5.88	1.47	3249	391	0.947
Weather W1-3	1yr	5/17/04	65	Black	0.10	7.47	1.55	3220	417	0.951
W2-3	1yr	5/17/04	95	Black	0.16	6.18	1.60	3242	414	0.951
W3-3	1yr	5/17/04	65	Green	0.79	5.84	1.46	3183	183	0.951
W4-3	1yr	5/17/04	95	Green	0.71	6.34	1.14	3040	163	0.950

W5-3	1yr	5/17/04	95	Green	0.74	5.73	1.56	3101	201	0.950
W6-3	1yr	5/17/04	65	Blue	0.42	4.86	0.79	2973	196	0.948
W7-3	1yr	5/17/04	95	Blue	0.48	5.23	0.98	3270	51	0.950
No Load N1-3	1.5yr	8/27/04	65	Black	0.03	7.05	1.27	3150	378	0.950
N2-3	1.5yr	8/27/04	95	Black	0.05	5.99	1.35	3171	322	0.951
N3-3	1.5yr	8/27/04	65	Green	0.63	6.39	1.29	3138	353	0.948
N4-3	1.5yr	8/27/04	95	Green	0.53	7.25	1.25	3078	517	0.948
N5-3	1.5yr	8/27/04	95	Green	0.64	6.17	1.46	2929	734	0.947
N6-3	1.5yr	8/27/04	65	Blue	0.43	6.32	1.09	3058	502	0.946
N7-3	1.5yr	8/27/04	95	Blue	0.49	5.59	1.19	3278	346	0.948
N8-3	1.5yr	8/27/04	35	Black	0.03	6.66	1.13	3054	617	0.947
N9-3	1.5yr	8/27/04	35	Green	0.65	5.09	1.25	3320	284	0.951
N10-3	1.5yr	8/27/04	35	Blue	0.47	6.99	1.00	3079	602	0.947
N11-3	1.5yr	8/27/04	65	Brown	0.39	5.08	1.62	3429	260	0.948
L1-3	1.5yr	8/27/04	65	Black	0.04	6.73	1.51	3378	312	0.948
L4-3	1.5yr	8/27/04	95	Green	0.68	6.49	1.16	3175	607	0.950
Control C1-4	1.5yr	12/22/04	65	Black	0.07	6.25	None	3197	344	0.946
C2-4	1.5yr	12/22/04	95	Black	0.16	6.14	None	3139	326	0.951
C3-4	1.5yr	12/22/04	65	Green	0.74	6.36	None	3238	455	0.948
C4-4	1.5yr	12/22/04	95	Green	0.64	6.67	None	3060	365	0.948
C5-4	1.5yr	12/22/04	95	Green	0.63	6.24	None	3090	625	0.948
C6-4	1.5yr	12/22/04	65	Blue	0.42	6.66	None	3005	556	0.946
C7-4	1.5yr	12/22/04	95	Blue	0.55	6.60	None	3231	470	0.948
Spl Ctrl SC1-4	1.5yr	12/22/04	65	Black	0.09	6.21	None	3158	318	0.947
SC2-4	1.5yr	12/22/04	95	Black	0.13	6.20	None	3179	324	0.951
SC3-4	1.5yr	12/22/04	65	Green	0.72	6.39	None	3235	429	0.948
SC4-4	1.5yr	12/22/04	95	Green	0.69	6.63	None	3065	452	0.948
SC5-4	1.5yr	12/22/04	95	Green	0.64	6.29	None	3083	399	0.948
SC6-4	1.5yr	12/22/04	65	Blue	0.42	6.72	None	2982	548	0.945
SC7-4	1.5yr	12/22/04	95	Blue	0.53	5.64	None	3318	482	0.948
Weather W1-4	1.5yr	12/22/04	65	Black	0.07	7.42	None	3286	418	0.953
W2-4	1.5yr	12/22/04	95	Black	0.11	6.03	None	3335	340	0.953
W3-4	1.5yr	12/22/04	65	Green	0.78	5.81	None	3190	149	0.953
W4-4	1.5yr	12/22/04	95	Green	0.66	6.20	None	3033	148	0.951
W5-4	1.5yr	12/22/04	95	Green	0.65	5.72	None	2979	204	0.951
W6-4	1.5yr	12/22/04	65	Blue	0.37	3.08	None	2957	27	0.950
W7-4	1.5yr	12/22/04	95	Blue	0.45	2.86	None	3340	21	0.953
No Load N1-4	2yr	3/1/05	65	Black	0.04	6.89	1.88	3229	317	0.949
N2-4	2yr	3/1/05	95	Black	0.10	5.89	1.75	3232	323	0.952
N3-4	2yr	3/1/05	65	Green	0.76	6.81	1.55	3097	394	0.950
N4-4	2yr	3/1/05	95	Green	0.64	7.15	1.50	3071	373	0.950
N5-4	2yr	3/1/05	95	Green	0.67	6.20	1.78	3083	497	0.949
N6-4	2yr	3/1/05	65	Blue	0.39	6.11	1.56	3031	557	0.947
N7-4	2yr	3/1/05	95	Blue	0.42	5.29	1.52	3372	361	0.948
N8-4	2yr	3/1/05	35	Black	0.05	6.15	1.76	3196	646	0.950
N9-4	2yr	3/1/05	35	Green	0.60	4.78	1.50	3311	352	0.952
N10-4	2yr	3/1/05	35	Blue	0.46	6.79	1.29	3097	659	0.947
N11-4	2yr	3/1/05	65	Brown	0.37	4.90	2.00	3388	337	0.950
L1-4	2yr	3/5/05	65	Black	0.05	6.32	1.92	3139	247	0.948
L4-4	2yr	3/5/05	95	Green	0.70	6.51	1.67	3050	582	0.950
Control C1-5	2yr	6/23/05	65	Black	0.07	6.23	1.34	3132	335	0.948
C2-5	2yr	6/23/05	95	Black	0.16	6.26	1.51	3249	518	0.951
C3-5	2yr	6/23/05	65	Green	0.70	6.40	1.32	3320	434	0.950
C4-5	2yr	6/23/05	95	Green	0.62	6.71	1.18	3046	515	0.948
C5-5	2yr	6/23/05	95	Green	0.62	6.17	1.56	3037	761	0.948
C6-5	2yr	6/23/05	65	Blue	0.36	6.55	1.17	3002	488	0.947

C7-5	2yr	6/23/05	95	Blue	0.53	6.42	1.02	3255	486	0.948
Spl Ctrl SC1-5	2yr	6/23/05	65	Black	0.05	6.21	1.27	2862	350	0.948
SC2-5	2yr	6/23/05	95	Black	0.11	6.13	1.35	3103	376	0.951
SC3-5	2yr	6/23/05	65	Green	0.67	6.25	1.40	3045	443	0.948
SC4-5	2yr	6/23/05	95	Green	0.53	6.59	1.18	2867	537	0.948
SC5-5	2yr	6/23/05	95	Green	0.51	6.13	1.74	2819	578	0.947
SC6-5	2yr	6/23/05	65	Blue	0.36	6.48	1.39	2864	528	0.944
SC7-5	2yr	6/23/05	95	Blue	0.39	5.75	1.20	3211	421	0.948
Weather W1-5	2yr	6/23/05	65	Black	0.07	7.37	1.56	3319	597	0.952
W2-5	2yr	6/23/05	95	Black	0.12	5.72	1.60	3298	505	0.954
W3-5	2yr	6/23/05	65	Green	0.77	5.66	1.10	3126	164	0.953
W4-5	2yr	6/23/05	95	Green	0.63	6.17	1.03	3000	111	0.952
W5-5	2yr	6/23/05	95	Green	0.65	5.56	1.34	2959	152	0.952
W6-5	2yr	6/23/05	65	Blue	0.34	3.09	0.89	2809	58	0.952
W7-5	2yr	6/23/05	95	Blue	0.46	2.78	0.79	3196	50	0.953
No Load N1-5	2.5 Y	3/1/05	65	Black	0.05	7.09	1.40	3364	329	0.949
N2-5	2.5 Y	3/1/05	95	Black	0.08	5.99	1.36	3359	479	0.951
N3-5	2.5 Y	3/1/05	65	Green	0.75	6.71	1.41	3229	372	0.950
N4-5	2.5 Y	3/1/05	95	Green	0.69	6.99	1.29	3153	498	0.949
N5-5	2.5 Y	3/1/05	95	Green	0.63	6.03	1.40	3022	639	0.949
N6-5	2.5 Y	3/1/05	65	Blue	0.41	6.15	1.20	3016	505	0.947
N7-5	2.5 Y	3/1/05	95	Blue	0.48	5.30	1.11	3346	412	0.950
N8-5	2.5 Y	3/1/05	35	Black	0.04	6.81	1.12	3206	593	0.949
N9-5	2.5 Y	3/1/05	35	Green	0.61	4.83	1.20	3391	323	0.952
N10-5	2.5 Y	3/1/05	35	Blue	0.48	6.88	1.05	3121	588	0.950
N11-5	2.5 Y	3/1/05	65	Brown	0.41	5.15	1.71	3462	409	0.951
Loaded L1-5	2.5 Y	3/5/05	65	Black	0.05	6.38	1.56	3191	256	0.947
L4-5	2.5 Y	3/5/05	95	Green	0.69	6.51	1.18	3119	718	0.950
No Load N1-6	3yr	2/27/06	65	Black	0.03	7.09	1.32	3238	419	0.949
N2-6	3yr	2/27/06	95	Black	0.05	5.99	1.31	3270	443	0.951
N3-6	3yr	2/27/06	65	Green	0.76	6.71	1.27	3158	518	0.949
N4-6	3yr	2/27/06	95	Green	0.69	6.87	1.31	3083	515	0.949
N5-6	3yr	2/27/06	95	Green	0.64	6.03	1.38	3080	598	0.949
N6-6	3yr	2/27/06	65	Blue	0.42	6.15	1.15	2956	791	0.947
N7-6	3yr	2/27/06	95	Blue	0.45	5.30	1.27	3505	420	0.950
N8-6	3yr	2/27/06	35	Black	0.08	6.81	1.08	3249	577	0.950
N9-6	3yr	2/27/06	35	Green	0.65	4.83	1.17	3466	351	0.952
N10-6	3yr	2/27/06	35	Blue	0.47	6.88	1.04	3129	617	0.949
N11-6	3yr	2/27/06	65	Brown	0.40	5.15	1.66	3357	320	0.950
Loaded L1-6	3yr	2/28/06	65	Black	0.04	6.79	1.54	3242	405	0.948
L4-6	3yr	2/28/06	95	Green	0.65	6.77	1.16	3076	547	0.950
Weather W1-6	3yr	6/26/06	65	Black	0.08	7.35	1.30	3259	605	0.954
W2-6	3yr	6/26/06	95	Black	0.13	5.79	1.44	3228	678	0.954
W3-6	3yr	6/26/06	65	Green	0.80	5.63	1.06	3224	120	0.954
W4-6	3yr	6/26/06	95	Green	0.70	6.20	0.88	3044	132	0.953
W5-6	3yr	6/26/06	95	Green	0.66	5.60	1.28	3082	152	0.952
W6-6	3yr	6/26/06	65	Blue	0.43	3.20	0.60	2786	98	0.952
W7-6	3yr	6/26/06	95	Blue	0.50	2.99	0.63	3097	17	0.953
Control C1-6	3yr	6/26/06	65	Black	0.05	6.26	1.25	3192	336	0.947
C2-6	3yr	6/26/06	95	Black	0.19	6.16	1.20	3264	316	0.951
C3-6	3yr	6/26/06	65	Green	0.79	6.55	1.57	3289	527	0.948
C4-6	3yr	6/26/06	95	Green	0.61	6.59	1.22	3188	566	0.948
C5-6	3yr	6/26/06	95	Green	0.64	6.23	1.52	3126	614	0.946
C6-6	3yr	6/26/06	65	Blue	0.39	6.31	1.03	3072	610	0.944
C7-6	3yr	6/26/06	95	Blue	0.55	6.47	0.89	3259	503	0.947
Spl Ctrl SC1-6	3yr	6/26/06	65	Black	0.02	6.02	1.45	3175	318	0.947

SC2-6	3yr	6/26/06	95	Black	0.09	5.96	1.48	3163	314	0.952
SC3-6	3yr	6/26/06	65	Green	0.74	6.36	0.57	3211	428	0.949
SC4-6	3yr	6/26/06	95	Green	0.58	6.35	1.22	3054	493	0.949
SC5-6	3yr	6/26/06	95	Green	0.64	6.06	1.63	3112	568	0.947
SC6-6	3yr	6/26/06	65	Blue	0.47	6.56	1.27	2979	481	0.945
SC7-6	3yr	6/26/06	95	Blue	0.48	6.55	1.19	3290	476	0.948

Appendix C. Polyethylene Arrhenius Fits

Melt Index

black		a	0.1117
		b	19.2183
	Arr-k	MI	residuals
0	0.0000	0.0000	0
3	0.0002	0.0079	5.953E-05
6	0.0045	-0.0010	3.017E-05
12	0.0225	0.0205	4.149E-06
18	0.0384	0.0355	8.461E-06
24	0.0502	0.0626	0.0001552
36	0.0655	0.0587	4.591E-05
		sum	0.0003035

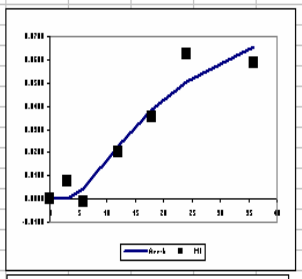

green		a	0.1410
		b	4.1547
	Arr-k	MI	residuals
0	0.0000	0.0000	0
3	0.0353	0.0361	6.46E-07
6	0.0705	0.0706	7.27E-09
12	0.0997	0.0974	5.461E-06
18	0.1119	0.1102	2.988E-06
24	0.1186	0.1239	2.866E-05
36	0.1256	0.1237	3.732E-06
		sum	4.15E-05

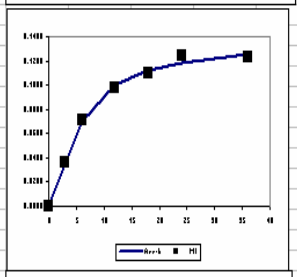

green FA		a	0.1689
		b	8.7955
	Arr-k	MI	residuals
0	0.0000	0.0000	0
3	0.0090	0.0038	2.735E-05
6	0.0390	0.0256	0.0001789
12	0.0811	0.0989	0.0003135
18	0.1036	0.1011	6.516E-06
24	0.1171	0.1259	7.773E-05
36	0.1323	0.1199	0.0001529
		sum	0.0007568

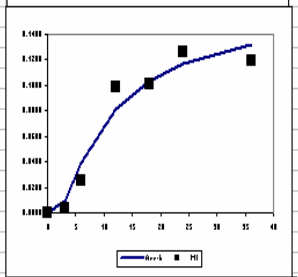

blue		a	0.7962
		b	10.6890
	Arr-k	MI	residuals
0	0.0000	0.0000	0
3	0.0226	0.0894	0.0044602
6	0.1341	0.1162	0.0003208
12	0.3267	0.2300	0.0093582
18	0.4396	0.5479	0.0117114
24	0.5100	0.5533	0.0018784
36	0.5916	0.5288	0.00395
		sum	0.0316791

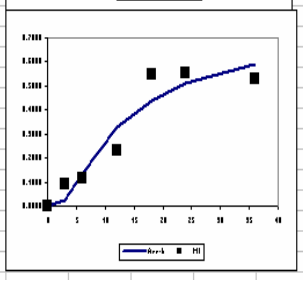

Elongation

black		a	2.9520
		b	43.7465
	Arr-k	Elong	residuals
0	0.0000	0.0000	0
3	0.0000	0.3105	0.0964286
6	0.0020	0.2412	0.0572037
12	0.0771	0.1990	0.0148756
18	0.2598	0.0844	0.0307742
24	0.4770	0.5791	0.0104359
36	0.8757	0.8608	0.0002216
		sum	0.2099395

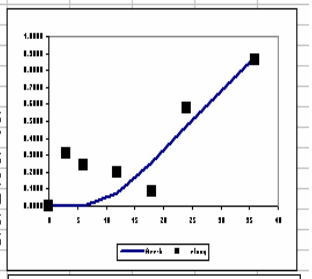

green		a	0.9175
		b	7.1126
	Arr-k	Elong	residuals
0	0.0000	0.0000	0
3	0.0857	0.0166	0.0047757
6	0.2804	0.2593	0.0004433
12	0.5072	0.5875	0.0064424
18	0.6180	0.6493	0.0009814
24	0.6822	0.6642	0.0003222
36	0.7530	0.7052	0.0022857
		sum	0.0152506

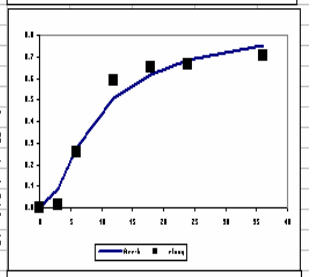

green FA		a	0.8967
		b	6.5044
	Arr-k	Elong	residuals
0	0.0000	0.0000	0
3	0.1026	0.0816	0.000442
6	0.3033	0.2621	0.0016935
12	0.5215	0.6097	0.0077799
18	0.6248	0.6039	0.0004366
24	0.6838	0.7049	0.0004413
36	0.7485	0.7049	0.0019052
		sum	0.0126985

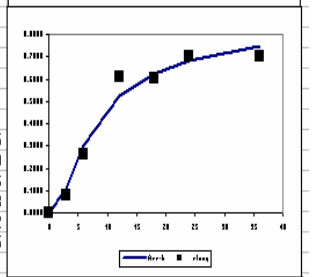

blue		a	1.1977
		b	6.6173
	Arr-k	Elong	residuals
0	0.0000	0.0000	0
3	0.1319	-0.1521	0.0806761
6	0.3975	0.5299	0.0175181
12	0.6900	0.7395	0.0024468
18	0.8293	0.9452	0.0134358
24	0.9091	0.8756	0.0011212
36	0.9966	0.8813	0.0133041
		sum	0.128502

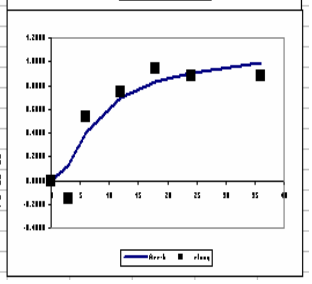

Arrhenius fits of PE: ‘W’ – melt index and elongation

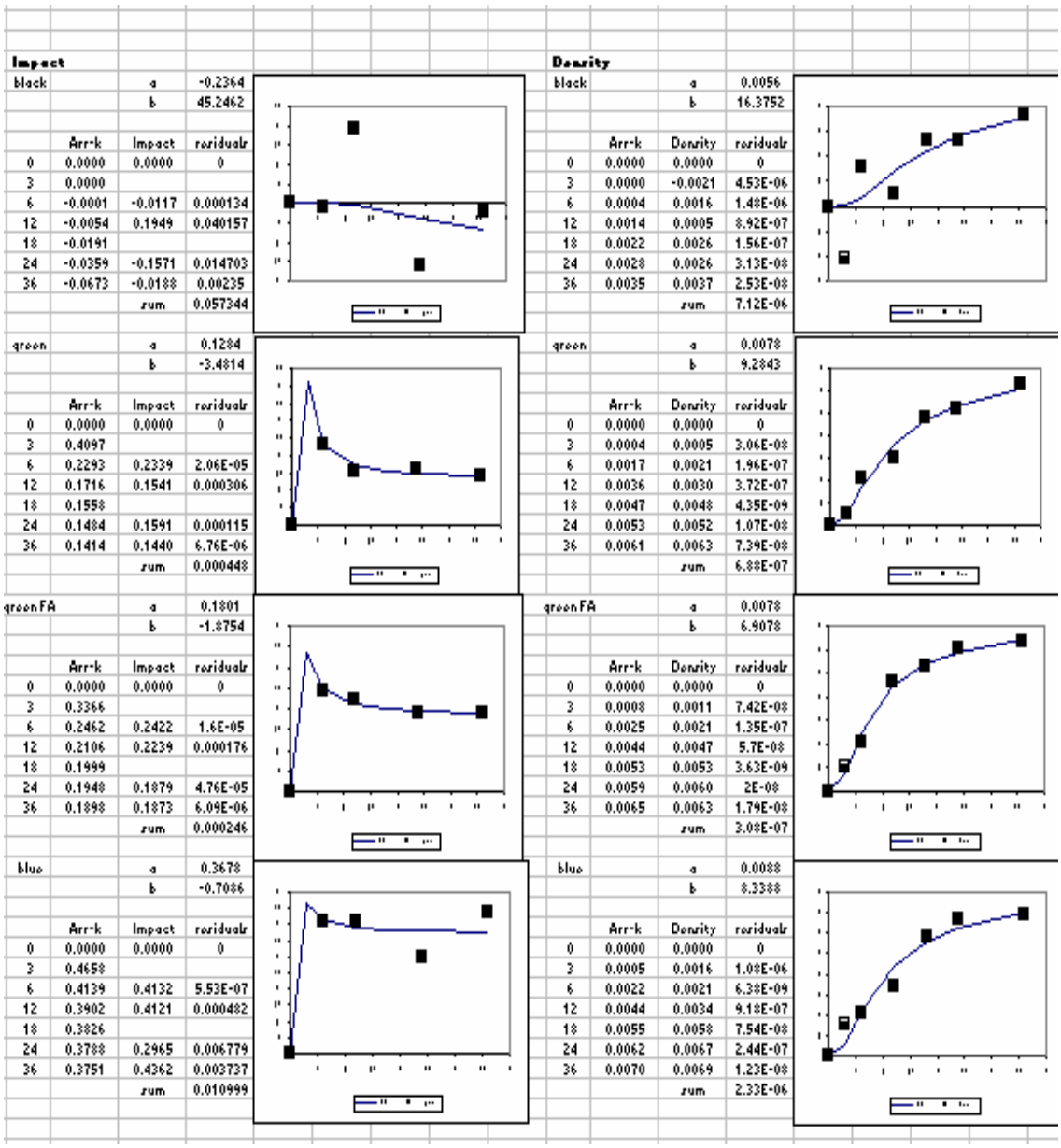

Impact			
black		a	-0.2364
		b	45.2462
	Arr-k	Impact	residualr
0	0.0000	0.0000	0
3	0.0000		
6	-0.0001	-0.0117	0.000134
12	-0.0054	0.1949	0.040157
18	-0.0191		
24	-0.0359	-0.1571	0.014703
36	-0.0673	-0.0188	0.00235
		sum	0.057344
green		a	0.1284
		b	-3.4814
	Arr-k	Impact	residualr
0	0.0000	0.0000	0
3	0.4097		
6	0.2293	0.2339	2.06E-05
12	0.1716	0.1541	0.000306
18	0.1558		
24	0.1484	0.1591	0.000115
36	0.1414	0.1440	6.76E-06
		sum	0.000448
greenFA		a	0.1801
		b	-1.8754
	Arr-k	Impact	residualr
0	0.0000	0.0000	0
3	0.3366		
6	0.2462	0.2422	1.6E-05
12	0.2106	0.2239	0.000176
18	0.1999		
24	0.1948	0.1879	4.76E-05
36	0.1898	0.1873	6.09E-06
		sum	0.000246
blue		a	0.3678
		b	-0.7086
	Arr-k	Impact	residualr
0	0.0000	0.0000	0
3	0.4658		
6	0.4139	0.4132	5.53E-07
12	0.3902	0.4121	0.000482
18	0.3826		
24	0.3788	0.2965	0.006779
36	0.3751	0.4362	0.003737
		sum	0.010999

Density			
black		a	0.0056
		b	16.3752
	Arr-k	Density	residualr
0	0.0000	0.0000	0
3	0.0000	-0.0021	4.53E-06
6	0.0004	0.0016	1.48E-06
12	0.0014	0.0005	8.92E-07
18	0.0022	0.0026	1.56E-07
24	0.0028	0.0026	3.13E-08
36	0.0035	0.0037	2.53E-08
		sum	7.12E-06
green		a	0.0078
		b	9.2843
	Arr-k	Density	residualr
0	0.0000	0.0000	0
3	0.0004	0.0005	3.06E-08
6	0.0017	0.0021	1.96E-07
12	0.0036	0.0030	3.72E-07
18	0.0047	0.0048	4.35E-09
24	0.0053	0.0052	1.07E-08
36	0.0061	0.0063	7.39E-08
		sum	6.88E-07
greenFA		a	0.0078
		b	6.9078
	Arr-k	Density	residualr
0	0.0000	0.0000	0
3	0.0008	0.0011	7.42E-08
6	0.0025	0.0021	1.35E-07
12	0.0044	0.0047	5.7E-08
18	0.0053	0.0053	3.63E-09
24	0.0059	0.0060	2E-08
36	0.0065	0.0063	1.79E-08
		sum	3.08E-07
blue		a	0.0088
		b	8.3388
	Arr-k	Density	residualr
0	0.0000	0.0000	0
3	0.0005	0.0016	1.08E-06
6	0.0022	0.0021	6.38E-09
12	0.0044	0.0034	9.18E-07
18	0.0055	0.0058	7.54E-08
24	0.0062	0.0067	2.44E-07
36	0.0070	0.0069	1.23E-08
		sum	2.33E-06

Arrhenius fits of PE: ‘W’ – impact strength and density

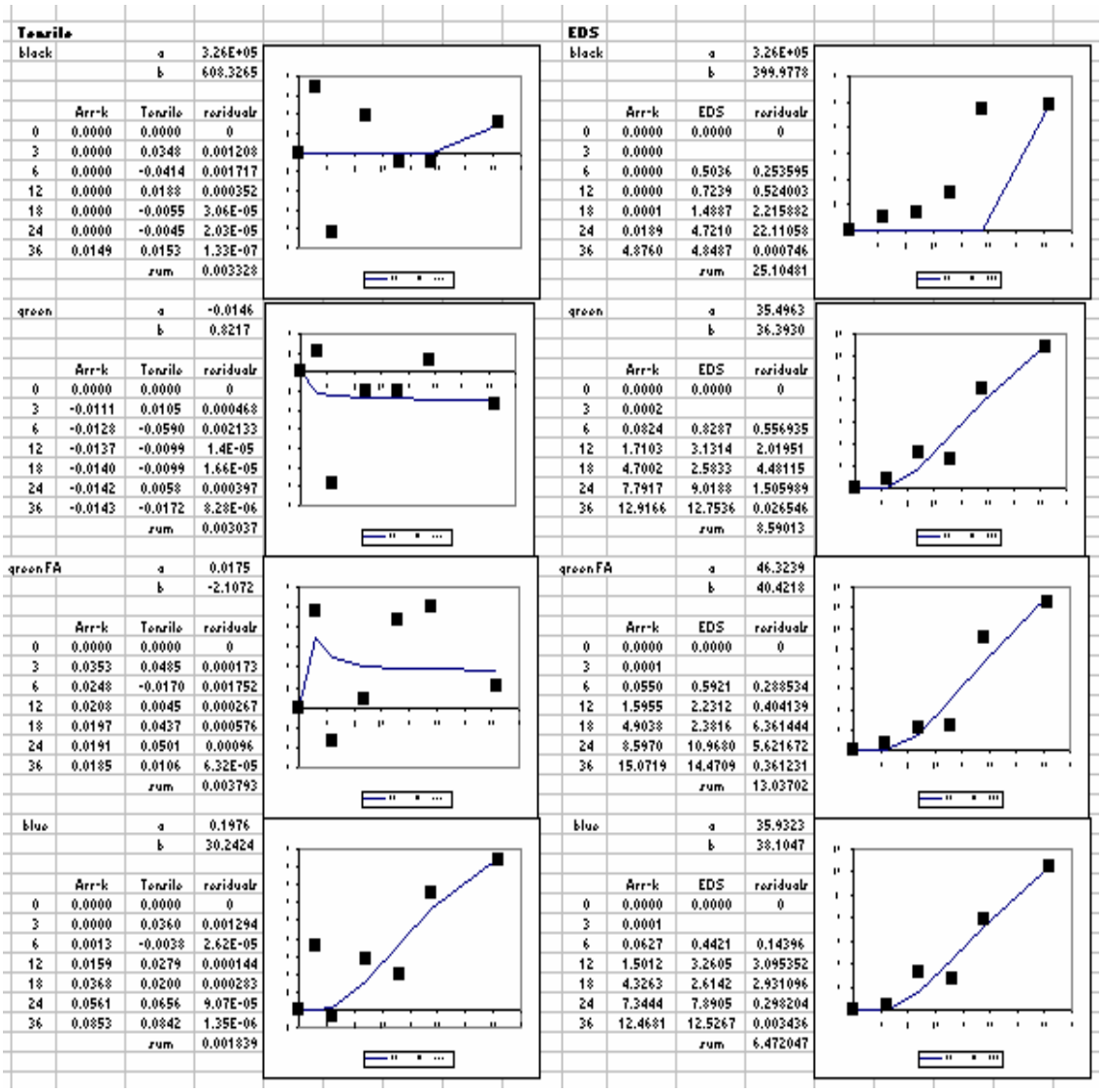

Tensile			
black		a	3.26E+05
		b	608.3265
	Arr-k	Tensile	residualr
0	0.0000	0.0000	0
3	0.0000	0.0348	0.001208
6	0.0000	-0.0414	0.001717
12	0.0000	0.0188	0.000352
18	0.0000	-0.0055	3.06E-05
24	0.0000	-0.0045	2.03E-05
36	0.0149	0.0153	1.33E-07
		sum	0.003328
green		a	-0.0146
		b	0.8217
	Arr-k	Tensile	residualr
0	0.0000	0.0000	0
3	-0.0111	0.0105	0.000468
6	-0.0128	-0.0590	0.002133
12	-0.0137	-0.0099	1.4E-05
18	-0.0140	-0.0099	1.66E-05
24	-0.0142	0.0058	0.000397
36	-0.0143	-0.0172	8.28E-06
		sum	0.003037
greenFA		a	0.0175
		b	-2.1072
	Arr-k	Tensile	residualr
0	0.0000	0.0000	0
3	0.0353	0.0485	0.000173
6	0.0248	-0.0170	0.001752
12	0.0208	0.0045	0.000267
18	0.0197	0.0437	0.000576
24	0.0191	0.0501	0.00096
36	0.0185	0.0106	6.32E-05
		sum	0.003793
blue		a	0.1976
		b	30.2424
	Arr-k	Tensile	residualr
0	0.0000	0.0000	0
3	0.0000	0.0360	0.001294
6	0.0013	-0.0038	2.62E-05
12	0.0159	0.0279	0.000144
18	0.0368	0.0200	0.000283
24	0.0561	0.0656	9.07E-05
36	0.0853	0.0842	1.35E-06
		sum	0.001839

EDS			
black		a	3.26E+05
		b	399.9778
	Arr-k	EDS	residualr
0	0.0000	0.0000	0
3	0.0000		
6	0.0000	0.5036	0.253595
12	0.0000	0.7239	0.524003
18	0.0001	1.4887	2.215882
24	0.0189	4.7210	22.11058
36	4.8760	4.8487	0.000746
		sum	25.10481
green		a	35.4963
		b	36.3930
	Arr-k	EDS	residualr
0	0.0000	0.0000	0
3	0.0002		
6	0.0824	0.8287	0.556935
12	1.7103	3.1314	2.01951
18	4.7002	2.5833	4.48115
24	7.7917	9.0188	1.505989
36	12.9166	12.7536	0.026546
		sum	8.59013
greenFA		a	46.3239
		b	40.4218
	Arr-k	EDS	residualr
0	0.0000	0.0000	0
3	0.0001		
6	0.0550	0.5921	0.288534
12	1.5955	2.2312	0.404139
18	4.9038	2.3816	6.361444
24	8.5970	10.9680	5.621672
36	15.0719	14.4709	0.361231
		sum	13.03702
blue		a	35.9323
		b	38.1047
	Arr-k	EDS	residualr
0	0.0000	0.0000	0
3	0.0001		
6	0.0627	0.4421	0.14396
12	1.5012	3.2605	3.095352
18	4.3263	2.6142	2.931096
24	7.3444	7.8905	0.298204
36	12.4681	12.5267	0.003436
		sum	6.472047

Arrhenius fits of PE: ‘W’ – tensile strength and EDS O-percent

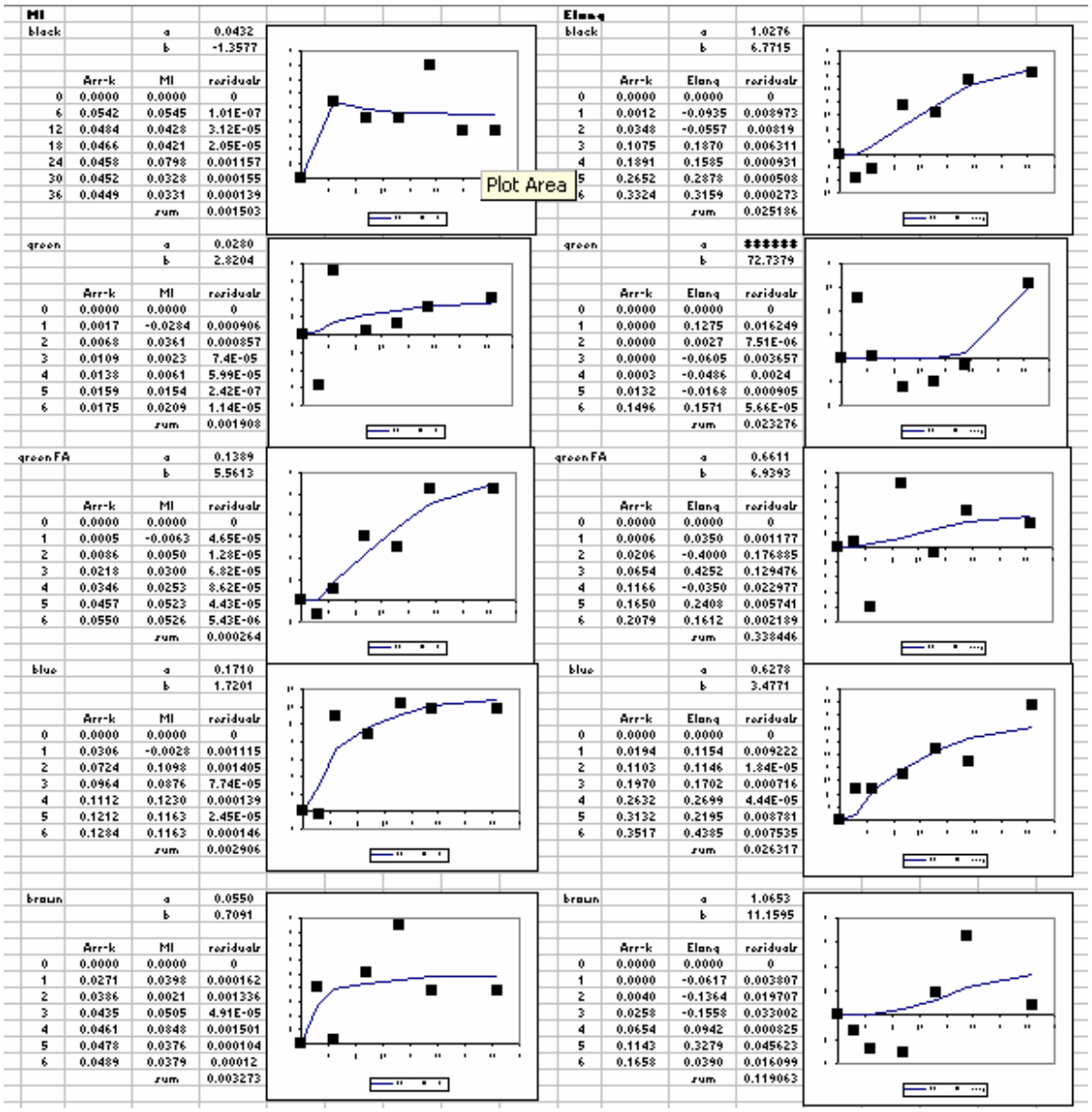

Arrhenius fits of PE: ‘N’ – melt index and elongation

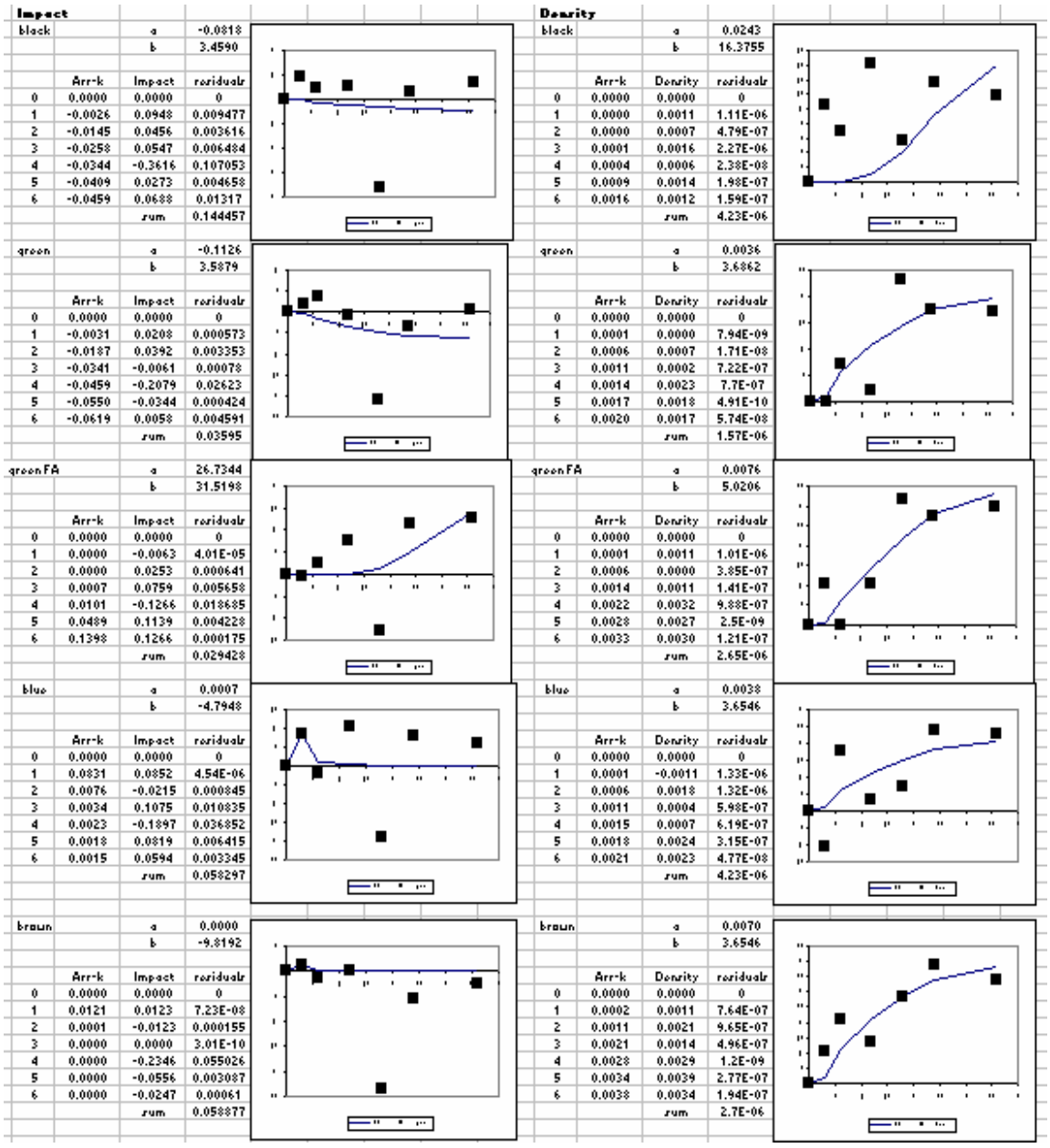

Impact

black		a	-0.0818
		b	3.4590

	Arr-k	Impact	residualr
0	0.0000	0.0000	0
1	-0.0026	0.0948	0.009477
2	-0.0145	0.0456	0.003616
3	-0.0258	0.0547	0.006484
4	-0.0344	-0.3616	0.107053
5	-0.0409	0.0273	0.004658
6	-0.0459	0.0688	0.01317
		sum	0.144457

green		a	-0.1126
		b	3.5879

	Arr-k	Impact	residualr
0	0.0000	0.0000	0
1	-0.0031	0.0208	0.000573
2	-0.0187	0.0392	0.003353
3	-0.0341	-0.0061	0.00078
4	-0.0459	-0.2079	0.02623
5	-0.0550	-0.0344	0.000424
6	-0.0619	0.0058	0.004591
		sum	0.03595

greenFA		a	26.7344
		b	31.5198

	Arr-k	Impact	residualr
0	0.0000	0.0000	0
1	0.0000	-0.0063	4.01E-05
2	0.0000	0.0253	0.000641
3	0.0007	0.0759	0.005658
4	0.0101	-0.1266	0.018685
5	0.0489	0.1139	0.004228
6	0.1398	0.1266	0.000175
		sum	0.029428

blue		a	0.0007
		b	-4.7948

	Arr-k	Impact	residualr
0	0.0000	0.0000	0
1	0.0831	0.0852	4.54E-06
2	0.0076	-0.0215	0.000845
3	0.0034	0.1075	0.010835
4	0.0023	-0.1897	0.036852
5	0.0018	0.0819	0.006415
6	0.0015	0.0594	0.003345
		sum	0.058297

braun		a	0.0000
		b	-9.8192

	Arr-k	Impact	residualr
0	0.0000	0.0000	0
1	0.0121	0.0123	7.23E-08
2	0.0001	-0.0123	0.000155
3	0.0000	0.0000	3.01E-10
4	0.0000	-0.2346	0.055026
5	0.0000	-0.0556	0.003087
6	0.0000	-0.0247	0.00061
		sum	0.058877

Density

black		a	0.0243
		b	16.3755

	Arr-k	Density	residualr
0	0.0000	0.0000	0
1	0.0000	0.0011	1.11E-06
2	0.0000	0.0007	4.79E-07
3	0.0001	0.0016	2.27E-06
4	0.0004	0.0006	2.38E-08
5	0.0009	0.0014	1.98E-07
6	0.0016	0.0012	1.59E-07
		sum	4.23E-06

green		a	0.0036
		b	3.6862

	Arr-k	Density	residualr
0	0.0000	0.0000	0
1	0.0001	0.0000	7.94E-09
2	0.0006	0.0007	1.71E-08
3	0.0011	0.0002	7.22E-07
4	0.0014	0.0023	7.7E-07
5	0.0017	0.0018	4.91E-10
6	0.0020	0.0017	5.74E-08
		sum	1.57E-06

greenFA		a	0.0076
		b	5.0206

	Arr-k	Density	residualr
0	0.0000	0.0000	0
1	0.0001	0.0011	1.01E-06
2	0.0006	0.0000	3.85E-07
3	0.0014	0.0011	1.41E-07
4	0.0022	0.0032	9.88E-07
5	0.0028	0.0027	2.5E-09
6	0.0033	0.0030	1.21E-07
		sum	2.65E-06

blue		a	0.0038
		b	3.6546

	Arr-k	Density	residualr
0	0.0000	0.0000	0
1	0.0001	-0.0011	1.33E-06
2	0.0006	0.0018	1.32E-06
3	0.0011	0.0004	5.98E-07
4	0.0015	0.0007	6.19E-07
5	0.0018	0.0024	3.15E-07
6	0.0021	0.0023	4.77E-08
		sum	4.23E-06

braun		a	0.0070
		b	3.6546

	Arr-k	Density	residualr
0	0.0000	0.0000	0
1	0.0002	0.0011	7.64E-07
2	0.0011	0.0021	9.65E-07
3	0.0021	0.0014	4.96E-07
4	0.0028	0.0029	1.2E-09
5	0.0034	0.0039	2.77E-07
6	0.0038	0.0034	1.94E-07
		sum	2.7E-06

Arrhenius fits of PE: 'N' – impact strength and density

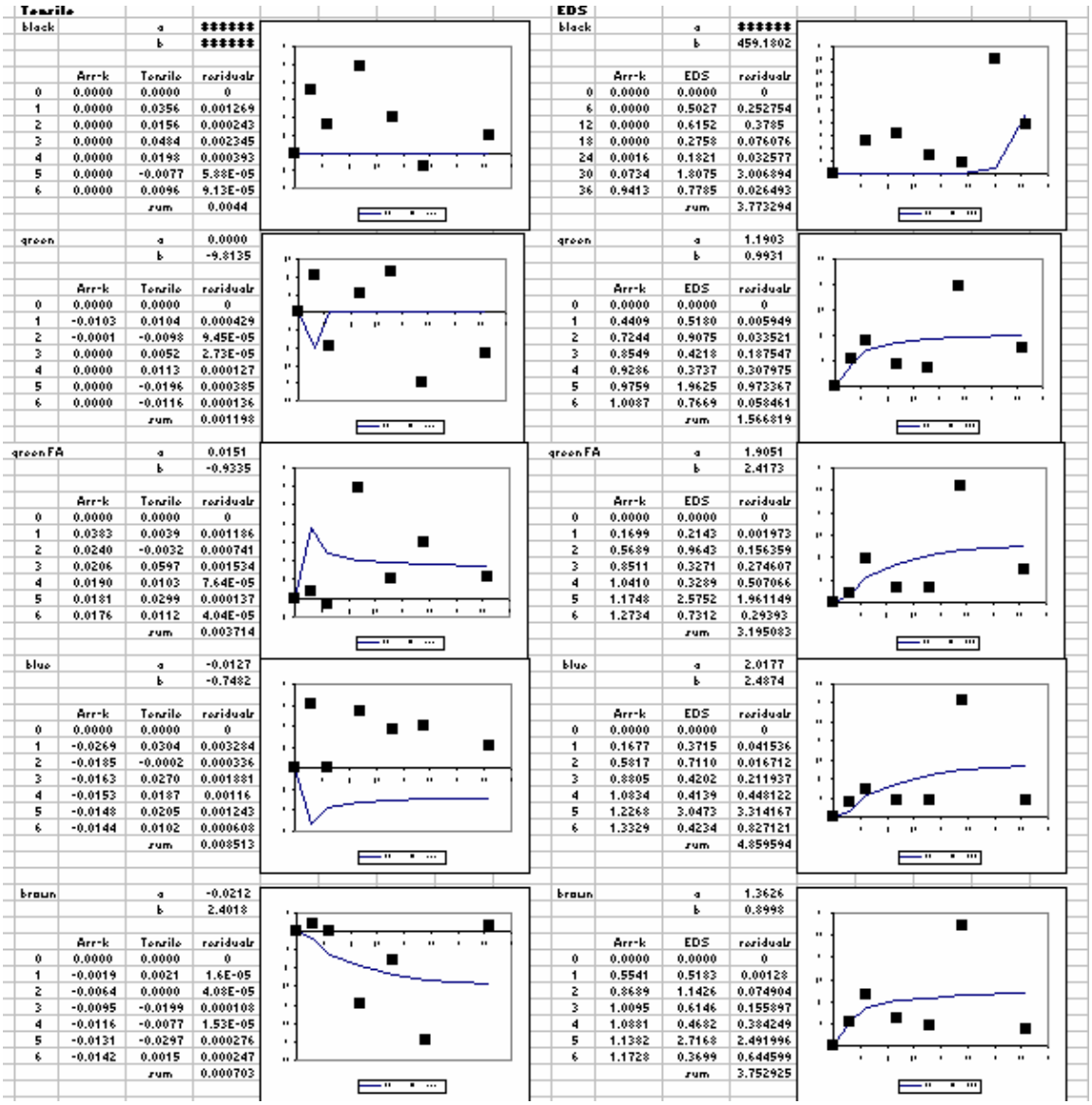

Tensile

black		a	######
		b	######
	Arr-k	Tensile	residualr
0	0.0000	0.0000	0
1	0.0000	0.0256	0.001269
2	0.0000	0.0156	0.000243
3	0.0000	0.0484	0.002345
4	0.0000	0.0198	0.000393
5	0.0000	-0.0077	5.88E-05
6	0.0000	0.0096	9.13E-05
		sum	0.0044

green		a	0.0000
		b	-9.8135
	Arr-k	Tensile	residualr
0	0.0000	0.0000	0
1	-0.0103	0.0104	0.000429
2	-0.0001	-0.0098	9.45E-05
3	0.0000	0.0052	2.73E-05
4	0.0000	0.0113	0.000127
5	0.0000	-0.0196	0.000385
6	0.0000	-0.0116	0.000136
		sum	0.001198

greenFA		a	0.0151
		b	-0.9335
	Arr-k	Tensile	residualr
0	0.0000	0.0000	0
1	0.0383	0.0039	0.001186
2	0.0240	-0.0032	0.000741
3	0.0206	0.0597	0.001534
4	0.0190	0.0103	7.64E-05
5	0.0181	0.0299	0.000137
6	0.0176	0.0112	4.04E-05
		sum	0.003714

blue		a	-0.0127
		b	-0.7482
	Arr-k	Tensile	residualr
0	0.0000	0.0000	0
1	-0.0269	0.0304	0.003284
2	-0.0185	-0.0002	0.000336
3	-0.0163	0.0270	0.001881
4	-0.0153	0.0187	0.00116
5	-0.0148	0.0205	0.001243
6	-0.0144	0.0102	0.000608
		sum	0.008513

braun		a	-0.0212
		b	2.4018
	Arr-k	Tensile	residualr
0	0.0000	0.0000	0
1	-0.0019	0.0021	1.6E-05
2	-0.0064	0.0000	4.08E-05
3	-0.0095	-0.0199	0.000108
4	-0.0116	-0.0077	1.53E-05
5	-0.0131	-0.0297	0.000276
6	-0.0142	0.0015	0.000247
		sum	0.000703

EDS

black		a	######
		b	459.1802
	Arr-k	EDS	residualr
0	0.0000	0.0000	0
6	0.0000	0.5027	0.252754
12	0.0000	0.6152	0.3785
18	0.0000	0.2758	0.076076
24	0.0016	0.1821	0.032577
30	0.0734	1.8075	3.006894
36	0.9413	0.7785	0.026493
		sum	3.773294

green		a	1.1903
		b	0.9931
	Arr-k	EDS	residualr
0	0.0000	0.0000	0
1	0.4409	0.5180	0.005949
2	0.7244	0.9075	0.033521
3	0.8549	0.4218	0.187547
4	0.9286	0.3737	0.307975
5	0.9759	1.9625	0.973367
6	1.0087	0.7669	0.058461
		sum	1.566819

greenFA		a	1.9051
		b	2.4173
	Arr-k	EDS	residualr
0	0.0000	0.0000	0
1	0.1699	0.2143	0.001973
2	0.5689	0.9643	0.156359
3	0.8511	0.3271	0.274607
4	1.0410	0.3289	0.507066
5	1.1748	2.5752	1.961149
6	1.2734	0.7312	0.29393
		sum	3.195083

blue		a	2.0177
		b	2.4874
	Arr-k	EDS	residualr
0	0.0000	0.0000	0
1	0.1677	0.3715	0.041536
2	0.5817	0.7110	0.016712
3	0.8805	0.4202	0.211937
4	1.0834	0.4139	0.448122
5	1.2268	3.0473	3.314167
6	1.3329	0.4234	0.827121
		sum	4.859594

braun		a	1.3626
		b	0.8998
	Arr-k	EDS	residualr
0	0.0000	0.0000	0
1	0.5541	0.5183	0.00128
2	0.8689	1.1426	0.074904
3	1.0095	0.6146	0.155897
4	1.0881	0.4682	0.384249
5	1.1382	2.7168	2.491996
6	1.1728	0.3699	0.644599
		sum	3.752925

Arrhenius fits of PE: 'N' – tensile strength and EDS O-percent

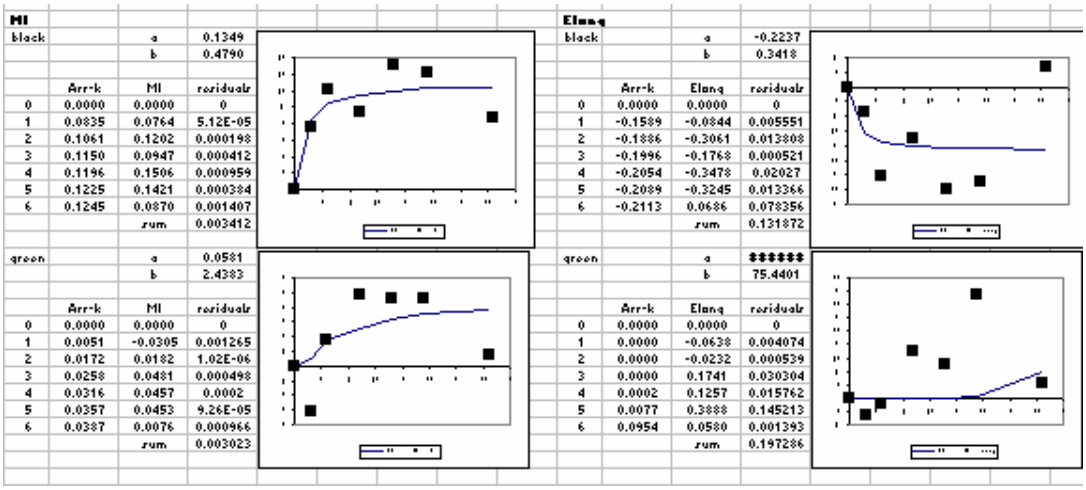

MI

black		a	0.1349
		b	0.4790
	Arr-k	MI	residualr
0	0.0000	0.0000	0
1	0.0835	0.0764	5.12E-05
2	0.1061	0.1202	0.000198
3	0.1150	0.0947	0.000412
4	0.1196	0.1506	0.000959
5	0.1225	0.1421	0.000384
6	0.1245	0.0870	0.001407
		sum	0.003412
green		a	0.0581
		b	2.4383
	Arr-k	MI	residualr
0	0.0000	0.0000	0
1	0.0051	-0.0305	0.001265
2	0.0172	0.0182	1.02E-06
3	0.0258	0.0481	0.000498
4	0.0316	0.0457	0.0002
5	0.0357	0.0453	9.26E-05
6	0.0387	0.0076	0.000966
		sum	0.003023

Elong

black		a	-0.2237
		b	0.3418
	Arr-k	Elong	residualr
0	0.0000	0.0000	0
1	-0.1589	-0.0844	0.005551
2	-0.1886	-0.3061	0.013808
3	-0.1996	-0.1768	0.000521
4	-0.2054	-0.3478	0.02027
5	-0.2089	-0.3245	0.013366
6	-0.2113	0.0686	0.078356
		sum	0.131872
green		a	######
		b	75.4401
	Arr-k	Elong	residualr
0	0.0000	0.0000	0
1	0.0000	-0.0638	0.004074
2	0.0000	-0.0232	0.000539
3	0.0000	0.1741	0.030304
4	0.0002	0.1257	0.015762
5	0.0077	0.3888	0.145213
6	0.0954	0.0580	0.001393
		sum	0.197286

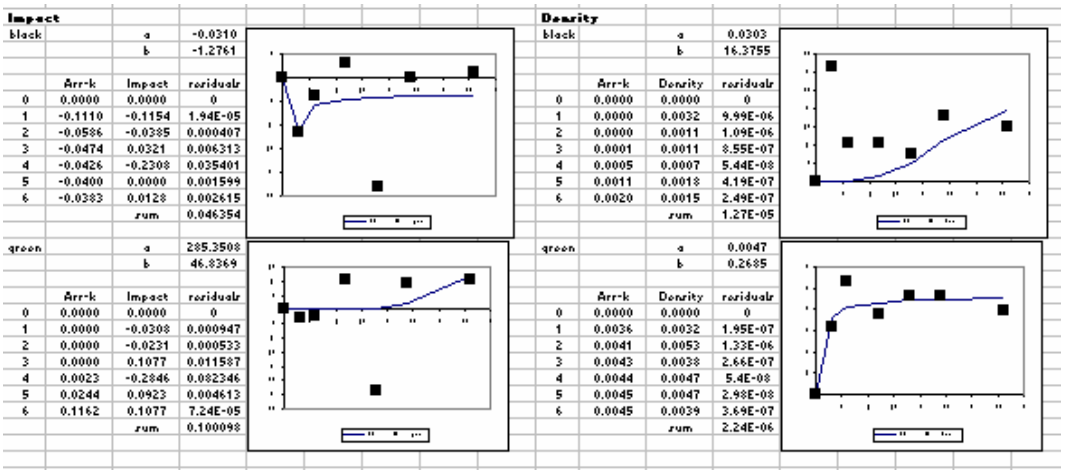

Impact

black		a	-0.0310
		b	-1.2761
	Arr-k	Impact	residualr
0	0.0000	0.0000	0
1	-0.1110	-0.1154	1.94E-05
2	-0.0586	-0.0385	0.000407
3	-0.0474	0.0321	0.006313
4	-0.0426	-0.2308	0.035401
5	-0.0400	0.0000	0.001599
6	-0.0383	0.0128	0.002615
		sum	0.046354
green		a	285.3508
		b	46.8369
	Arr-k	Impact	residualr
0	0.0000	0.0000	0
1	0.0000	-0.0308	0.000947
2	0.0000	-0.0231	0.000533
3	0.0000	0.1077	0.011587
4	0.0023	-0.2846	0.082346
5	0.0244	0.0923	0.004613
6	0.1162	0.1077	7.24E-05
		sum	0.100098

Density

black		a	0.0303
		b	16.3755
	Arr-k	Density	residualr
0	0.0000	0.0000	0
1	0.0000	0.0032	9.99E-06
2	0.0000	0.0011	1.09E-06
3	0.0001	0.0011	8.55E-07
4	0.0005	0.0007	5.44E-08
5	0.0011	0.0018	4.19E-07
6	0.0020	0.0015	2.49E-07
		sum	1.27E-05
green		a	0.0047
		b	0.2685
	Arr-k	Density	residualr
0	0.0000	0.0000	0
1	0.0036	0.0032	1.95E-07
2	0.0041	0.0053	1.33E-06
3	0.0043	0.0038	2.66E-07
4	0.0044	0.0047	5.4E-08
5	0.0045	0.0047	2.98E-08
6	0.0045	0.0039	3.69E-07
		sum	2.24E-06

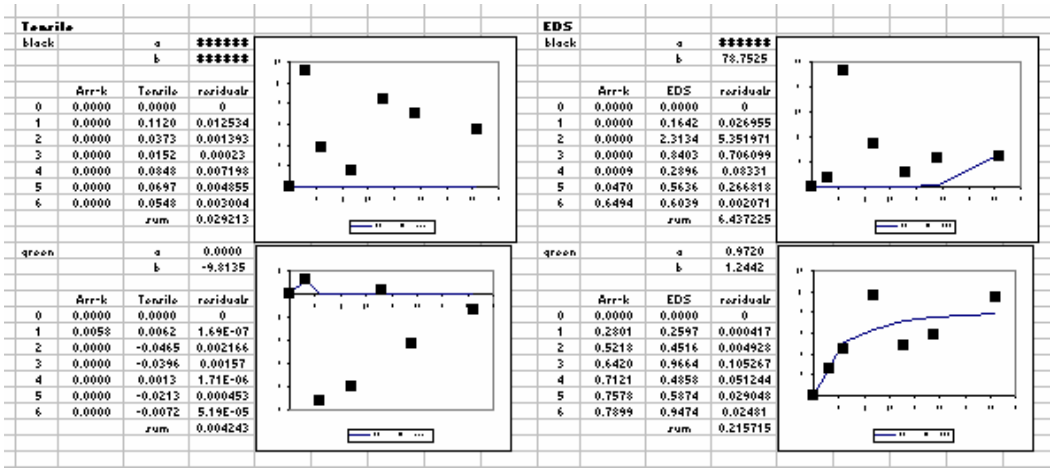

Tensile

black		a	######
		b	######
	Arr-k	Tensile	residualr
0	0.0000	0.0000	0
1	0.0000	0.1120	0.012534
2	0.0000	0.0373	0.001393
3	0.0000	0.0152	0.00023
4	0.0000	0.0848	0.007198
5	0.0000	0.0697	0.004855
6	0.0000	0.0548	0.003004
		sum	0.029213
green		a	0.0000
		b	-9.8135
	Arr-k	Tensile	residualr
0	0.0000	0.0000	0
1	0.0058	0.0062	1.69E-07
2	0.0000	-0.0465	0.002166
3	0.0000	-0.0396	0.00157
4	0.0000	0.0013	1.71E-06
5	0.0000	-0.0213	0.000453
6	0.0000	-0.0072	5.19E-05
		sum	0.004243

EDS

black		a	######
		b	78.7525
	Arr-k	EDS	residualr
0	0.0000	0.0000	0
1	0.0000	0.1642	0.026955
2	0.0000	2.3134	5.351971
3	0.0000	0.8403	0.706099
4	0.0009	0.2896	0.08331
5	0.0470	0.5636	0.266818
6	0.6494	0.6039	0.002071
		sum	6.437225
green		a	0.9720
		b	1.2442
	Arr-k	EDS	residualr
0	0.0000	0.0000	0
1	0.2801	0.2597	0.000417
2	0.5218	0.4516	0.004928
3	0.6420	0.9664	0.105267
4	0.7121	0.4858	0.051244
5	0.7578	0.5874	0.029048
6	0.7899	0.9474	0.02481
		sum	0.215715

Arrhenius fits of PE: ‘L’ – all properties

Appendix D. PE Fit Constants and Ratio Comparisons

V	Melt Index			Elongation			Impact Energy			Density			Tensile			EDS		
w-bla	A	B	SOR	A	B	SOR	A	B	SOR	A	B	SOR	A	B	SOR	A	B	SOR
constants	0.112	19.218	0.0003	2.952	43.746	0.2099	-0.236	45.246	0.0573	0.006	16.375	7.12E-06	3.26E+05	608.3265	0.0033	3.26E+05	399.978	25.10
EDS x	2.92E+06	2.08E+01		1.10E+05	9.14E+00		-1.38E+06	8.84E+00		5.87E+07	2.44E+01		1.00E+00	6.58E-01		A		
w-gre	A	B	SOR	A	B	SOR	A	B	SOR	A	B	SOR	A	B	SOR	a	B	SOR
constants	0.141	4.155	0.0000	0.918	7.113	0.0153	0.128	-3.481	0.0004	0.008	9.284	6.88E-07	-0.015	0.822	0.0030	35.496	36.393	8.59
EDS x	2.52E+02	8.76E+00		3.87E+01	5.12E+00		2.76E+02	-1.05E+01		4.52E+03	3.92E+00		-2.42E+03	4.43E+01				
w-gfa	A	B	SOR	A	B	SOR	A	B	SOR	A	B	SOR	A	B	SOR	A	B	SOR
constants	0.169	8.795	0.0008	0.897	6.504	0.0127	0.180	-1.875	0.0002	0.008	6.908	3.08E-07	0.017	-2.107	0.0038	46.324	40.422	13.04
EDS x	2.74E+02	4.60E+00		5.17E+01	6.21E+00		2.57E+02	-2.16E+01		5.90E+03	5.85E+00		2.65E+03	-1.92E+01				
w-blu	A	B	SOR	A	B	SOR	A	B	SOR	A	B	SOR	A	B	SOR	A	B	SOR
constants	0.796	10.689	0.0317	1.198	6.617	0.1285	0.368	-0.709	0.0110	0.009	8.339	2.33E-06	0.198	30.242	0.0018	35.932	38.105	6.47
EDS x	4.51E+01	3.56E+00		3.00E+01	5.76E+00		9.77E+01	-5.38E+01		4.08E+03	4.57E+00		1.82E+02	1.26E+00				

N	Melt Index			Elongation			Impact Energy			Density			Tensile			EDS		
w-bla	A	B	SOR	A	B	SOR	A	B	SOR	A	B	SOR	A	B	SOR	A	B	SOR
constants	0.0432	-1.3576	0.0015	1.0276	40.6291	0.0252	-0.0818	20.7541	0.1445	0.0243	98.2531	4.23E-06	2.25E+05	3.26E+10	0.0044	3.26E+05	459.1504	3.77
EDS x	7.53E+06	-3.38E+02		3.17E+05	1.13E+01		-3.98E+06	2.21E+01		1.34E+07	4.67E+00		1.45E+00	1.41E-08				
w-gre	A	B	SOR	A	B	SOR	A	B	SOR	A	B	SOR	A	B	SOR	A	B	SOR
constants	0.0280	16.9227	0.0019	2.75E+04	436.4274	0.0233	-0.1126	21.5273	0.0359	0.0036	22.1175	1.57E-06	0.0000	-58.8812	0.0012	1.1903	5.9586	1.57
EDS x	4.25E+01	3.52E-01		4.32E-05	1.37E-02		-1.06E+01	2.77E-01		3.28E+02	2.69E-01		-2.11E+06	-1.01E-01				
w-gfa	A	B	SOR	A	B	SOR	A	B	SOR	A	B	SOR	A	B	SOR	A	B	SOR
constants	0.1389	33.3679	0.0003	0.6611	41.6357	0.3384	26.7344	189.1186	0.0294	0.0076	30.1235	2.65E-06	0.0151	-5.6008	0.0037	1.9051	14.5039	3.20
EDS x	1.37E+01	4.35E-01		2.88E+00	3.48E-01		7.13E-02	7.67E-02		2.49E+02	4.81E-01		1.27E+02	-2.59E+00				
w-blu	A	B	SOR	A	B	SOR	A	B	SOR	A	B	SOR	A	B	SOR	A	B	SOR
constants	0.1710	10.3206	0.0029	0.6278	20.8624	0.0263	0.0007	-28.7687	0.0583	0.0038	21.9279	4.23E-06	-0.0127	-4.4895	0.0085	2.0177	14.9247	4.86
EDS x	1.18E+01	1.45E+00		3.21E+00	7.15E-01		2.93E+03	-5.19E-01		5.30E+02	6.81E-01		-1.59E+02	-3.32E+00				
w-bro	A	B	SOR	A	B	SOR	A	B	SOR	A	B	SOR	A	B	SOR	A	B	SOR
constants	0.0550	4.2549	0.0033	1.0653	66.9572	0.1191	0.0000	-58.9151	0.0589	0.0070	21.9279	2.70E-06	-0.0212	14.4108	0.0007	1.3626	5.3988	3.75
EDS x	2.48E+01	1.27E+00		1.28E+00	8.06E-02		2.07E+06	-9.16E-02		1.94E+02	2.46E-01		-6.42E+01	3.75E-01				

L	Melt Index			Elongation			Impact Energy			Density			Tensile			EDS		
w-bla	A	B	SOR	A	B	SOR	A	B	SOR	A	B	SOR	A	B	SOR	A	B	SOR
constants	0.1349	2.8737	0.0034	-0.2237	2.0510	0.1319	-0.0310	-1.2761	0.0464	0.0303	98.2529	1.27E-05	2.25E+05	3.26E+10	0.0292	3.26E+05	472.5147	6.44
EDS x	2.41E+06	1.64E+02		-1.46E+06	2.30E+02		-1.05E+07	-3.70E+02		1.08E+07	4.81E+00		1.45E+00	1.45E-08				
w-gre	A	B	SOR	A	B	SOR	A	B	SOR	A	B	SOR	A	B	SOR	A	B	SOR
constants	0.0581	14.6300	0.0030	2.75E+04	452.6407	0.1973	285.3508	46.8369	0.1001	0.0047	1.6110	2.24E-06	0.0000	-58.8812	0.0000	0.9720	7.4653	0.22
EDS x	1.67E+01	5.10E-01		3.53E-05	1.65E-02		3.41E-03	1.59E-01		2.06E+02	4.63E+00		3.06E+06	-1.27E-01				

Polyethylene Fit Constants *A* and *B*, and Ratio Comparisons Between EDS and Mechanical Properties